Linear Multiblock Copolymers: Synthesis and Characterisation

Dissertation zur Erlangung des Grades
„Doktor der Naturwissenschaften“
im Promotionsfach Chemie

am Fachbereich Chemie, Pharmazie und Geowissenschaften der
Johannes Gutenberg-Universität Mainz

vorgelegt von

Eduard Grune

en in Nowos

Mainz

JOHANNES GUTENBERG UNIVERSITÄT MAINZ

MATERIALS IN MAINZ SCIENCE

Dekan:

1. Berichterstatter:

2. Berichterstatter:

Tag der mündlichen Prüfung: 13.12.2018

Die als Dissertation vorgelegte Arbeit wurde in der Zeit von Juli 2015 bis November 2018 am Institut für Organische Chemie der Johannes Gutenberg-Universität Mainz im Arbeitskreis von Herrn Univ.-Prof. Dr. Holger Frey angefertigt.

Hiermit versichere ich gemäß § 10 Abs. 3d der Promotionsordnung vom 24.07.2007
a) Ich habe die jetzt als Dissertation vorgelegte Arbeit selbst angefertigt und alle benutzten Hilfsmittel (Literatur, Apparaturen, Material) in der Arbeit angegeben.
b) Ich habe oder hatte die jetzt als Dissertation vorgelegte Arbeit nicht als Prüfungsarbeit für eine staatliche oder andere wissenschaftliche Prüfung eingereicht.
c) Ich hatte weder die jetzt als Dissertation vorgelegte Arbeit noch Teile davon bei einer anderen Fakultät bzw. einem anderen Fachbereich als Dissertation eingereicht.

_____

Eduard Grune

Für

meine Eltern

"The greatest challenge to any thinker is stating the problem in a way that will allow a solution."

—Bertrand Russell

Danksagung

Table of contents

Motivation and Objectives

Block copolymers represent a highly important specialty polymer class, with manifold applications ranging from footwear to asphalt modifiers. This development was made possible by the discovery of the living anionic polymerization in 1956, which enabled the preparation of highly defined block copolymers on a large scale for the first time. Until today, for synthetic polymers the carbanionic polymerization offers an unreached level of control of the polymer architecture, enabling the preparation of high molecular weight block copolymers with very narrow molecular weight distributions. The major drawback of this polymerization technique is the high sensitivity of the living chain end towards protic impurities, leading to demanding synthesis procedures. Especially the preparation of block copolymers bears a high risk of unintended termination due to impurities introduced during every intrusion in the living polymer solution.

Nevertheless, the majority of block copolymers, particularly the materials actually used commercially, are still prepared by carbanionic polymerization. Especially triblock copolymers are the most common type of block copolymers for applications requiring tough and resilient materials. In recent years block copolymers with block numbers exceeding three blocks have become the subject of various works, demonstrating their superior mechanical properties. The advantages of a large number of blocks are related to their domain bridging capability. Natural multiblock materials like silk gain their extraordinary resilience from an alternating array of amorphous and crystalline segments. This multiblock concept of alternating hard and soft segments can also be mimicked by high and low glass transition temperature segments like polyisoprene and polystyrene. However, the preparation of such structures is rather challenging.

Another current trend in polymer chemistry is bio-based materials. Due to the rise of environmental awareness, bio-based alternatives for already well-established petroleum-derived monomers become increasingly relevant, motivating the quest for suitable bio-monomers. Especially the terpene-based diene structure “myrcene” was the subject of several recent works, demonstrating its potential as a bio-based material. However, only little information about myrcene copolymerization kinetics

has been gathered to date. This lack of knowledge currently limits the applicability and potential of myrcene for the living anionic polymerization.

The objective of this thesis is to address these problems and to find a suitable solution. This thesis is subdivided in four major areas:

i. One-step block copolymer synthesis

Statistical (i.e., direct) copolymerization of monomers with highly diverging reactivities yields a block like structure in one step, due to the highly preferred incorporation of the more reactive monomer at first. The main challenge of this one-step block copolymer formation approach will be to identify a monomer combination with sufficiently different reactivities, albeit the capability of cross over propagation in both directions. Real-time NMR kinetic studies will enable to determine the reactivity ratios and to map the gradient structure of the resulting polymers. A detailed comparison of the mechanical properties with corresponding block copolymers prepared by sequential monomer addition will be essential to verify the blocky character of the one-step block copolymers.

ii. Preparation of linear multiblock copolymers

Linear alternating tapered multiblock copolymers of the $(AB)_n$ type may show superior mechanical properties to comparable ABA triblock copolymers due to multiple nanodomain bridging. At the same time, the few reports available for such materials show that elaborate synthesis approaches are required, limiting their potential. In this thesis, we target a suitable synthetic approach for well-defined $(AB)_n$ multiblock copolymers with high molecular weight segments and narrow dispersities.

iii. Correlation between polymer architecture and polymer properties

To examine the correlation between polymer architecture and mechanical response, profound investigations of the phase segregation behaviour and mechanical properties will be carried out by small angle scattering, transmission electron spectroscopy, tensile testing and dynamic mechanical analysis in cooperation with Prof. George Floudas (University of Ioannina) and Dr. Markus Gallei (Technische Universität Darmstadt).

iv. Potential and applicability of myrcene for the living anionic polymerization

Myrcene is a bio-based diene monomer that can be polymerised by carbanionic polymerization, providing flexible, polyisoprene-like materials that permit various post-polymerization modification reactions. To explore the potential of myrcene (Myr) as a bio-based monoterpene comonomer for styrenic monomers and to further examine its general applicability for the carbanionic copolymerization, real-time NMR kinetics studies with common monomers like isoprene, styrene and 4-methylstyrene will be carried out. Furthermore, a series of myrcene copolymers will be compared to the corresponding copolymers from isoprene to evaluate possible advantages of this diene monomer from biological sources.

Graphical Abstract

Chapter 2: One-step block copolymer synthesis

2.1 One-Step Block Copolymer Synthesis versus Sequential Monomer Addition: A Fundamental Study Reveals that one Methyl Group Makes a Difference

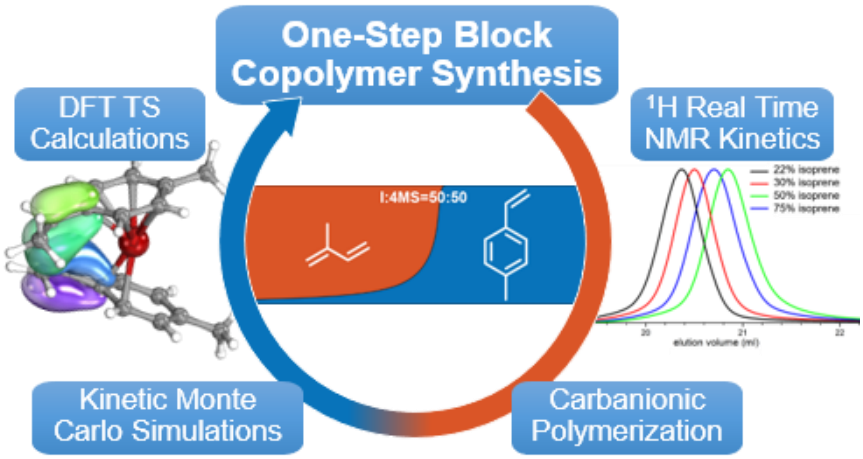

Chapter 3: Linear alternating $(AB)_n$ multiblock copolymers

3.1 Anionic Copolymerization Enables the Scalable Synthesis of Alternating $(AB)_n$ Multiblock Copolymers with High Molecular Weight in *n* Steps

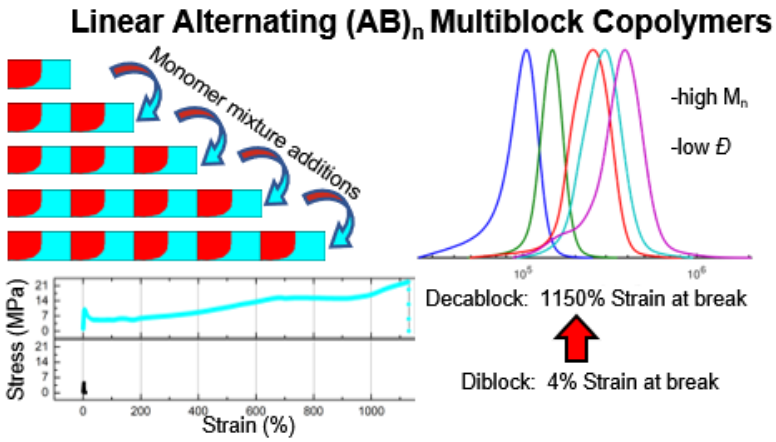

3.2 Tapered multiblock copolymers based on isoprene and 4-methylstyrene: Does a steep gradient make a difference?

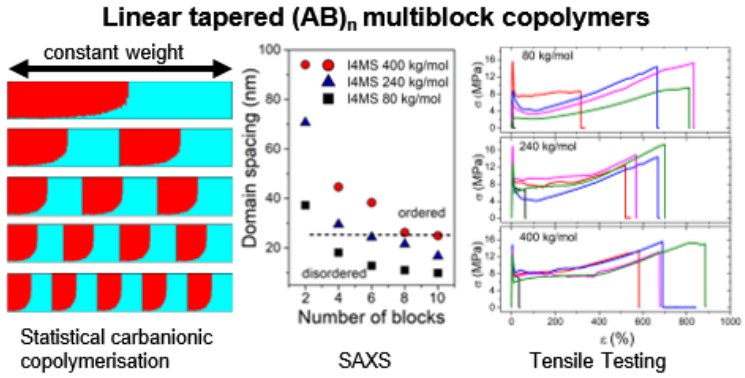

Chapter 4: Bio-based polymers

4.1 Towards bio-based tapered block copolymers: the behaviour of myrcene in the statistical anionic copolymerization

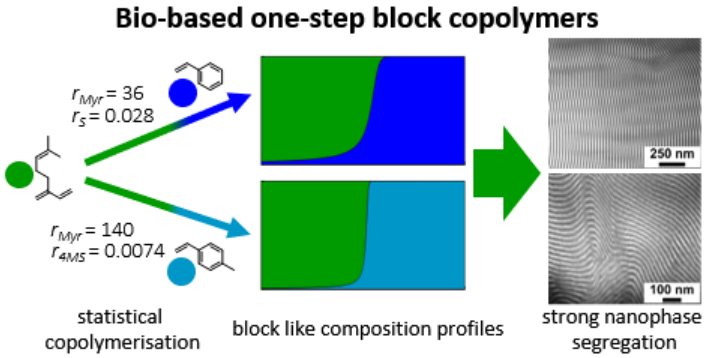

Abstract

This thesis deals with the preparation of linear alternating multiblock copolymers by living anionic copolymerization and the examination of their thermal behaviour, morphological and mechanical properties. Another major subject of this work is the examination of statistical carbanionic copolymerizations of dienes and styrenic monomers by *in-situ* ^{1}H NMR spectroscopy.

Chapter 1 introduces the field of living anionic polymerization and provides a theoretical base and the actual state of research regarding the copolymerization kinetics as well as synthesis and properties of block, gradient and multiblock copolymers.

In close collaboration with Tobias Johann the copolymerization kinetics of isoprene (I) and styrene (S), as well as isoprene and 4-methylstyrene (4MS), were examined by real-time ^{1}H NMR spectroscopy and evaluated by Monte-Carlo simulations in **Chapter 2**. Real-time monitoring of the copolymerization of isoprene and styrene permitted the calculation of the reactivity ratios, showing a good agreement with literature values and demonstrated the applicability of this method. Furthermore, it was possible to map the exact microstructure of I/S copolymers for the first time. *In-situ* kinetic studies of I/4MS revealed highly diverging reactivities and a more block like microstructure than I/S copolymers. The increased disparity of reactivities could be attributed to the electron donating effect of the methyl group of 4MS. Extensive Monte-Carlo simulation confirmed the block like structure of statistical I/4MS copolymers, concluding a one-step block copolymer formation. A detailed comparison of statistical and established sequential I/4MS copolymers revealed only minor differences between both copolymer types, confirming the block character of statistical I/4MS copolymers. Furthermore, the one-step block copolymers formation approach enabled the preparation of ultra high molecular weight block copolymers with extraordinary large domain sizes for photonic application (Chapter A2).

Chapter 3 deals with the synthesis and characterization of linear alternating $(AB)_n$ multiblock copolymers.

A rapid and scalable approach for the preparation of linear multiblock copolymers is described in **Chapter 3.1**. Based on the results of Chapter 2, the repetitive addition of a I/4MS mixture enabled to reduce the number of required steps and thus reduced the risk of unintended termination, yielding tapered $(AB)_n$ multiblock copolymers. This approach permitted the preparation of a first series of linear tapered multiblocks with high molecular weights and narrow molecular weight distributions. Due to the incompatibility of I and 4MS and the high molecular weights of the I and 4MS segments, all multiblocks undergo phase segregation, showing two separate glass transition temperatures. Stress-strain experiments revealed an extraordinary toughness for all multiblock samples and an increasing strain at break for an increasing number of blocks.

In **Chapter 3.2** the correlation between polymer architecture and mechanical and morphological properties was investigated in close collaboration with Prof. George Floudas (University of Ioannina) and Dr. Markus Gallei (TU Darmstadt). Using the synthetical approach described in Chapter 3.1, several series of linear tapered $(AB)_n$ multiblock copolymers with constant molecular weights and varying number of blocks were prepared and examined by tensile testing, dynamic scanning calorimetry (DSC), dynamic mechanical analysis (DMA), transmission electron microscopy (TEM) and small angel X-ray scattering (SAXS). Stress-strain experiments showed strongly enhanced toughness for increasing molecular weights and increasing number of blocks. At the same time, SAXS measurements revealed decreasing domain sizes and enhanced mixing of the I and 4MS segments for increasing block numbers.

Chapter 4 presents detailed kinetic studies of the statistical carbanionic copolymerization of the bio-based monomer myrcene (Myr). Real-time ^{1}H NMR kinetic measurements were used to examine the copolymerizations of Myr/I, Myr/S and Myr/4MS and to determine the reactivity ratios and microstructure for each monomer combination. While the copolymerization of Myr/I yielded a gradient copolymer with a long tapered section, the copolymerizations of Myr/S and Myr/4MS resulted in block like structures. Furthermore, a terpolymerization of Myr/I/4MS revealed that myrcenes high reactivity lowers the incorporation rate of 4MS in the diene segment, altering the composition profile to an even more block copolymer like

structure. Due to the block like structure of Myr/S, Myr/4MS and Myr/I/4MS copolymers, all samples undergo phase segregation, showing two separate glass transitions and forming lamellar morphologies with long range orders.

The appendix chapters present the results of further collaborative efforts that led to publications.

Chapter A1 describes the adjustment of the polymer microstructure in an emulsion copolymerization of two aziridines by altering the monomer concentration in the continuous phase. Due to different solubility, one monomer was preferably soluble in the continuous phase, while the other was preferably located in the droplets. Changing the monomer concentration in the continuous phase effected the monomer diffusion into the droplets and therefore the monomer feed during the copolymerization. Real-time ^{1}H NMR spectroscopy permitted to monitor the monomer incorporation and to map the microstructure for various monomer feeds, proving a change from a random to an adjustable gradient microstructures.

Chapter A2 deals with the preparation and characterization of ultrahigh molecular weight block copolymers via statistical copolymerization. Based on the results of Chapter 2, the one-step block copolymer formation approach was used to prepare I/4MS block copolymers with molecular weight up to 2033 kg/mol. All samples showed excellent order and high periodicity of the lamellar and spherical morphologies. Furthermore, the high order, large domain sizes and different refractive indices of the I and 4MS segments provided excellent photonic properties for the bulk materials without the addition of solvents, salts or homopolymers.

Zusammenfassung

Die vorliegende Dissertation behandelt die Synthese von linearen alternierenden Multiblockcopolymeren mittels lebender anionischer Polymerisation sowie die Untersuchung ihres thermischen Verhaltens, sowie ihrer morphologischen und mechanischen Eigenschaften. Ein weiterer Schwerpunkt dieser Arbeit ist die kinetische Untersuchung der carbanionischen Copolymerisation von Dienen und Styrolderivaten in unpolaren Lösungsmitteln mittels *in-situ* ^{1}H-NMR-Kinetik.

Kapitel 1 ist eine Einführung in die lebende anionische Polymerisation und liefert die theoretischen Grundlagen sowie den aktuellen Stand der Forschung zu den Themenschwerpunkten: Copolymerisationskinetik, Synthese und Eigenschaften von Block-, Gradienten- und Multiblockcopolymeren.

In **Kapitel 2** wurde in Kooperation mit Tobias Johann die Kinetik der carbanionischen Copolymerisation sowohl von Isopren (I) und Styrol (S) als auch von Isopren und 4-Methylstyrol (4MS) mittels *in-situ* ^{1}H-NMR-Kinetik und Monte-Carlo-Simulationen untersucht. Eine Echtzeit ^{1}H-NMR-Kinetik der Copolymerisation von Isopren und Styrol ermöglichte neben der Berechnung der *r*-Parameter auch erstmalig die genaue Bestimmung der Gradientenstruktur von I/S Copolymeren. Eine analoge Messung von I/4MS ergab eine deutlich blockartigere Mikrostruktur, sowie einen größeren Unterschied der Reaktivitäten von Isopren und 4-Methylstyrol, hervorgerufen durch den +I Effekt der Methylgruppe von 4MS. Umfangreiche Monte-Carlo Simulationen unterstützen die Befunde der Kinetikmessungen und zeigten ebenfalls eine stark blockartige Mikrostruktur für statistische I/4MS Copolymere. Der starke Blockcharakter von statistischen I/4MS Copolymeren konnte in einem detaillierten Vergleich mit sequentiell hergestellten Blockcopolymeren bestätigt werden. Des Weiteren ermöglichte die einstufige Blockcopolymersynthese die Herstellung von ultrahochmolekularen Blockcopolymeren, deren hohe Ordnung und großen Domänengrößen einen photonischen Effekt hervorrufen (Kapitel A2).

Abschnitt 3 behandelt die Synthese und Charakterisierung von linearen alternierenden $(AB)_n$ Multiblock Copolymeren.

Aufbauend auf den Ergebnissen aus Kapitel 2 wird in **Kapitel 3.1** eine neue skalierbare Syntheseroute für lineare Multiblöcke beschrieben. Unter Ausnutzung der stark unterschiedlichen *r*-Parameter von I/4MS konnte die Anzahl der benötigten Zugabeschritte halbiert werden, wodurch das Risiko einer unkontrollierten Terminierung deutlich verringert wurde. Dies ermöglichte eine relativ einfache und schnelle Synthese von linearen alternierenden $(AB)_n$ Gradientenmultiblock Copolymeren mit hohen Molekulargewichten und engen Molekulargewichtsverteilungen. Eine erste $(AB)_n$ Multiblockreihe mit konstanten Blockgrößen und unterschiedlichen Molekulargewichten und Blockzahlen zeigte in Zug-Dehnungsversuchen eine enorme mechanische Belastbarkeit aller Proben, die mit steigender Blockzahl zunahm.

In Kooperation mit Prof. George Floudas (University of Ioannina) und Dr. Markus Gallei (TU Darmstadt) wurde in **Kapitel 3.2** die Korrelation zwischen Polymerarchitektur und mechanischen und morphologischen Eigenschaften untersucht. Unter Verwendung der in Kapitel 3.1 etablierten Syntheseroute wurden verschiedene Multiblockreihen mit konstantem Molekulargewicht und unterschiedlichen Blockzahlen hergestellt. Zug-Dehnungsversuche zeigten eine Zunahme der mechanischen Belastbarkeit mit steigendem Molekulargewicht und steigender Anzahl der Blöcke. Gleichzeitig konnte mittels SAXS Messungen eine Abnahme der Domänengrößen und somit eine verstärkte Vermischung der Isopren- und 4-Methylstyrolblöcke mit zunehmender Blockzahl beobachtet werden. Des Weiteren konnte ein grundlegendes Verständnis des Phasenseparationsverhaltens von Gradientenmultiblock Copolymeren erlangt werde.

Kapitel 4 behandelt die statistische carbanionische Copolymerisation des biobasierten Monomers Myrcen (Myr) in unpolaren Lösungsmitteln. In einer Reihe von Echtzeit Kinetikmessungen wurden die Copolymerisationen von Myr/I, Myr/S und Myr/4MS untersucht und für jedes Monomerpaar die *r*-Parameter sowie die Mikrostruktur berechnet. Während die Copolymerisation von Myr/I einen langen Gradienten aufwies, ergaben die Kombinationen Myr/S und Myr/4MS stark blockartige Mikrostrukturen. Zudem bewirkte die hohe Reaktivität von Myrcen, in einer Terpolymerisation von Myr/I/4MS, eine Verminderung der Einbaurate von

4-Methylstyrol in das Dien-Segment und erhöht dadurch den Blockcharakter des Copolymers. Durch die blockartige Struktur der Copolymere aus Myr/S, Myr/4MS und Myr/I/4MS zeigten alle Proben zwei Glasübergangstemperaturen und eine stark ausgeprägte lamellare Morphologie mit hoher Fernordnung.

In den Appendixkapiteln dieser Arbeit werden alle weiteren Zusammenarbeiten mit Kooperationspartnern in ihrer publizierten Form aufgeführt.

Kapitel A1 beschreibt die kontrollierte Einstellung der Mikrostruktur eines Copolymers in einer Emulsionspolymerisation von zwei Aziridinen durch eine Variation der Monomerkonzentration in der kontinuierlichen Phase. Auf Grund von unterschiedlichen Löslichkeiten der Aziridine, war ein Monomer überwiegend in der kontinuierlichen Phase (Dimethylsulfoxid (DMSO)) gelöst, während das andere Monomer nur in den Cyclohexantröpfchen vorzufinden war. Jede Änderung der Monomerkonzentration in der DMSO Phase beeinflusste auch die Monomerdiffusion in die Cylohexantröpfchen und somit die Einbaurate dieses Monomers. Echtzeit-Kinetik Messungen ermöglichten durch die Verfolgung des Monomereinbaus den Nachweis einer Veränderung der Mikrostruktur von alternierend bis hin zum einstellbaren Gradienten.

Kapitel A2 befasst sich mit der Synthese und Charakterisierung von ultrahochmelokularen Diblock Copolymeren mit Molekulargewichten von bis zu 2033 kg/mol. Aufbauend auf den Ergebnissen aus Kapitel 2 ermöglichten die stark unterschiedlichen Reaktivitäten von I/4MS die Synthese von ultrahochmolekularen Blockcopolymeren in nur einem Schritt. Alle Polymere zeigten eine sehr hohe Fernordnung und stark ausgeprägte Periodizität der lamellaren und sphärischen Morphologie. In Kombination mit den unterschiedlichen Brechungsindices der I und 4MS Segmente zeigten die ultrahochmolekularen Diblock Copolymere Bragg Streuung mit gitterabhängigen Reflexionsfarben ohne die Notwendigkeit von weiteren Additiven wie Lösungsmitteln, Salzen oder Homopolymeren.

Chapter 1: Introduction

1.1 Living anionic polymerization

1.1.1 Discovery of the living anionic polymerization

"Living Polymers" was the short and yet striking title of Michael Szwarcs' publication in 1956, that marked the beginning of a new research area (Figure 1).[1] Although the carbanionic polymerization was already used in industry since the early 20th century, Szwarc was the first to precisely describe the whole mechanism of this polymerization technique within just three sentences: "Polymeric molecules are born in an initiation process, they grow by a propagation process, and finally they 'die' in a termination process. […] A 'living' polymer does not grow indefinitely, nor does its molecular weight increase beyond certain limits. Any growth requires food, and the food for a growing polymer is monomer" (Figure 1).[1–3]

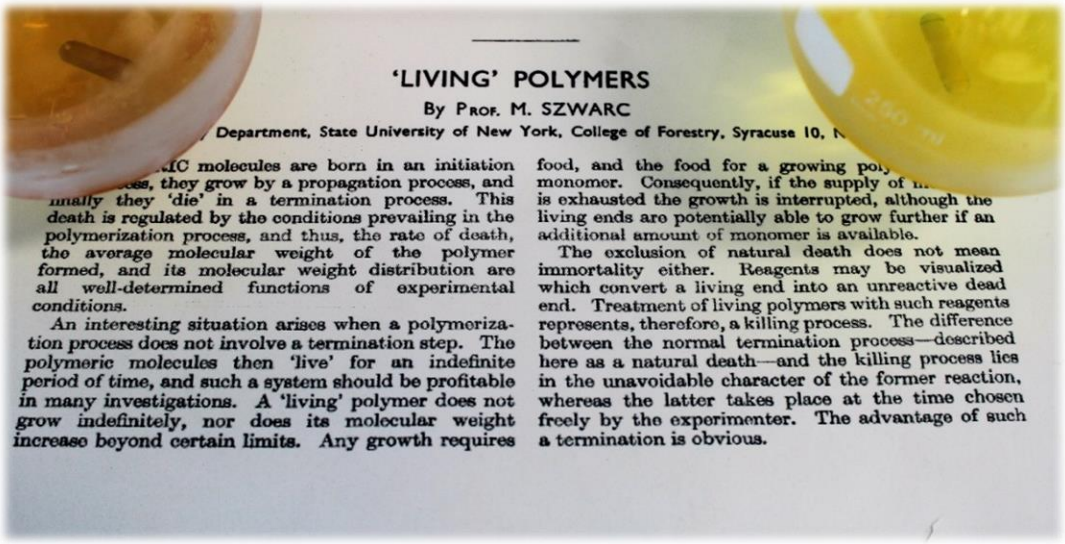

'LIVING' POLYMERS

By Prof. M. SZWARC

Department, State University of New York, College of Forestry, Syracuse 10, N

...IC molecules are born in an initiation ...ess, they grow by a propagation process, and ...nally they 'die' in a termination process. This death is regulated by the conditions prevailing in the polymerization process, and thus, the rate of death, the average molecular weight of the polymer formed, and its molecular weight distribution are all well-determined functions of experimental conditions.

An interesting situation arises when a polymerization process does not involve a termination step. The polymeric molecules then 'live' for an indefinite period of time, and such a system should be profitable in many investigations. A 'living' polymer does not grow indefinitely, nor does its molecular weight increase beyond certain limits. Any growth requires food, and the food for a growing poly... monomer. Consequently, if the supply of m... is exhausted the growth is interrupted, although the living ends are potentially able to grow further if an additional amount of monomer is available.

The exclusion of natural death does not mean immortality either. Reagents may be visualized which convert a living end into an unreactive dead end. Treatment of living polymers with such reagents represents, therefore, a killing process. The difference between the normal termination process—described here as a natural death—and the killing process lies in the unavoidable character of the former reaction, whereas the latter takes place at the time chosen freely by the experimenter. The advantage of such a termination is obvious.

Figure 1: Michael Szwarc publication in 1956.[4]

Originally Szwarc investigated the electron transfer from sodium naphthalide to styrene, when he accidentally discovered the living character of this reaction. He interpreted the colour change from the green naphthalide solution to the red polystyryllithium as "living polymers" due to the persistence of the red colour upon further styrene additions (Scheme 1).[5]

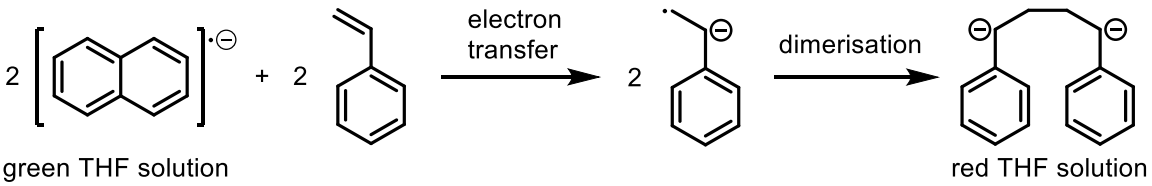

Scheme 1: Electron transfer from naphthalide to styrene, followed by dimerization of the styryl radical anion.

Furthermore, Szwarc recognized the potential of the living chain end and prepared the first highly defined triblock copolymers from isoprene and styrene.[6] Since then the carbanionic polymerization has become the most important method for the preparation of highly defined block copolymers with high molecular weights and narrow dispersities.[7] Nowadays triblock copolymers from styrene and isoprene or butadiene are the most relevant block copolymer types, and represent an important sector in the polymer industry, with manifold applications like footwear and adhesives.[8]

1.1.2 Mechanics and kinetics of the living anionic polymerization

Like the cationic and radical polymerization, the carbanionic polymerization belongs to the class of chain-growth reactions and consists of three main steps: (i) initiation, (ii) propagation and (iii) termination (Scheme 2).[9]

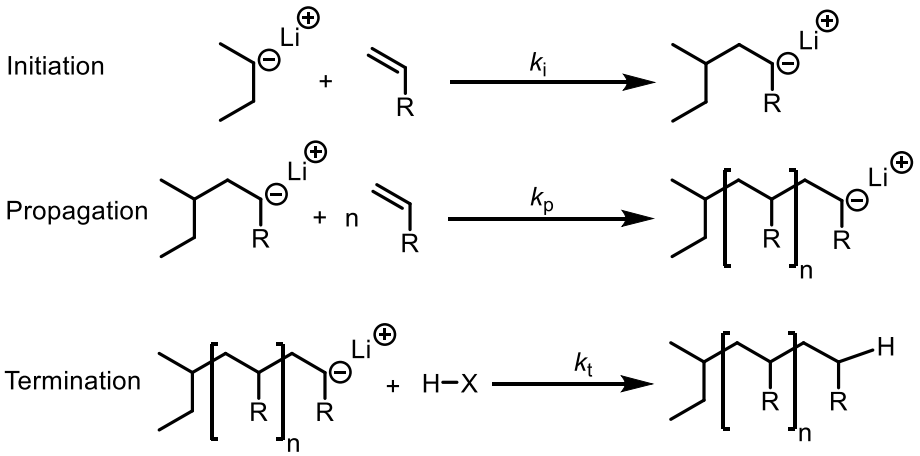

Scheme 2: The three elementary reactions of a carbanionic polymerization.

Typical initiators are organometallic compounds like *tert*-butyllithium and sodium naphthalide. In the case of sodium naphthalide, the initiation step is an electron transfer reaction to the monomer, forming radical anions that dimerise to dianions

(Scheme 1). Alkyl lithium compounds, on the other hand, react with the monomer in a nucleophilic addition, in which the carbanion is transferred to the α-carbon of the monomer (Scheme 2). Independent of the chosen initiator, the propagation is always a nucleophilic addition of monomers, passing the carbanion to the last added monomer unit (Scheme 2). Under ideal conditions, no side reactions, backbiting or termination occur, and the living chain end remains active even after full monomer consumption. Due to these unique characteristics, the carbanion concentration is constant and equals the initiator concentration. In combination with the concentration independence of the propagation rate, the monomer consumption of the carbanionic polymerization can be described by first order kinetics (1).

$$-\frac{d[M]}{dt} = k_p[M][M^-] = k_p[M][I^-] \qquad (1)$$

Furthermore, it is crucial that the initiation rate (k_I) is considerably higher than the propagation rate (k_p), so all polymer chains start to grow simultaneously.[10,11] In this case, the degree of polymerization ($\overline{P}_n$) can be described by equation (2), showing that $\overline{P}_n$ can be adjusted by the monomer-initiator ratio.

$$\overline{P}_n = \frac{[M]_0 - [M]_t}{[M^-]} = \frac{[M]_0 - [M]_t}{[I^-]} \qquad (2)$$

Another key parameter is the dispersity *Đ*, which is a measure of the distribution of molecular weights of a polymer sample. In the case of the living anionic polymerization, *Đ* is given by the Poisson distribution and converges to 1 for increasing molecular weights (3).[11,12]

$$Đ = \frac{M_w}{M_n} = \frac{P_w}{P_n} = 1 + \frac{1}{P_n} \qquad (3)$$

The narrow dispersities of a carbanionic polymerization result from its special characteristics. Since all polymer chains start to grow simultaneously, the concentration of active chains remains constant throughout the polymerization. The monomer addition is independent of previously added monomers. The frequency distribution of the degree of polymerization *x(P)* of a carbanionic polymerization is described by the Poisson distribution (4).[11]

$$x(P) = \frac{(v)^{P_i-1}}{(P_i-1)!}e^{-v} \tag{4}$$

In equation (4) the kinetic chain length *v* describes the average number of monomers added per chain and P_i is the degree of polymerization of polymer *i*. With the correlation (5)

$$w(P) = \frac{m(P)}{m} = \frac{x(P)M_0P_i}{(v+1)M_0} \tag{5}$$

$x(P)$ can be transformed to the weight distribution of the degree of polymerization, giving the weight fraction of a certain degree of polymerization P_i. (6)

$$w(P) = \frac{(v)^{P-1}P}{(P_i-1)!\,(v+1)}e^{-v} \tag{6}$$

Equation (6) enables to determine the weight and number average of the degree of polymerization (7), which are required to calculate the dispersity *Đ* (3).[9,12]

$$P_n = \frac{1}{\sum\frac{w_i(P)}{P_i}} \quad \text{and} \quad P_w = \sum w_i(P)P_i \tag{7}$$

The last step of a living anionic polymerization is the controlled termination by addition of terminating reagents like methanol. This final step can also be used to introduce functional groups at the chain end or to connect several polymer chains to star shaped polymers by coupling reagents (Scheme 3).

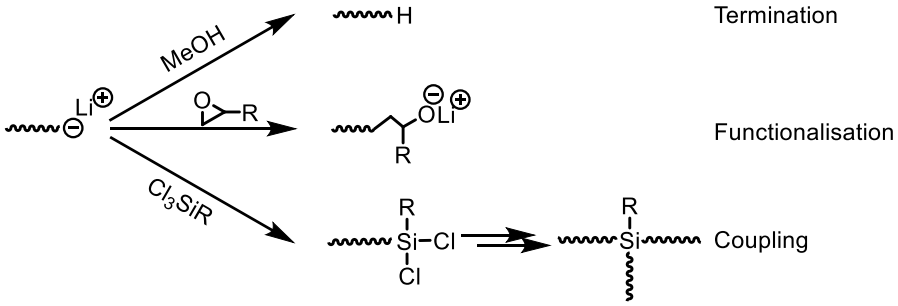

Scheme 3: Termination reactions of the living anionic polymerization.

The combination of all these unique characteristics enables the preparation of highly defined block copolymers with exceptional polymer architectures, narrow molecular weight distributions and high molecular weights.[13]

1.1.3 Monomers

Since the discovery of the living anionic polymerization in 1956 the scope of suitable monomers was continuously extended.[14–17] Nevertheless, common monomers like styrene, isoprene and butadiene still represent the majority of monomers used in industry and academia (Figure 2).[7]

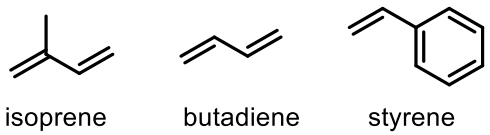

Figure 2: Common monomers used in the living anionic polymerization.

Due to the high reactivity of the living chain end, functionalised monomers such as vinylcatechols or vinylphenols require elaborate protective groups and the polymerization has to take place at low temperatures to maintain the living character.[7,18] However, various research groups, mainly Hirao et al., impressively demonstrated the polymerization of a variety of functionalised styrenic monomers. Compared to isoprene or butadiene, styrene offers more options for substitution. Hirao et al. developed a general procedure to functionalise styrene, most substituents being located in *para*-position (Figure 3).[7,19]

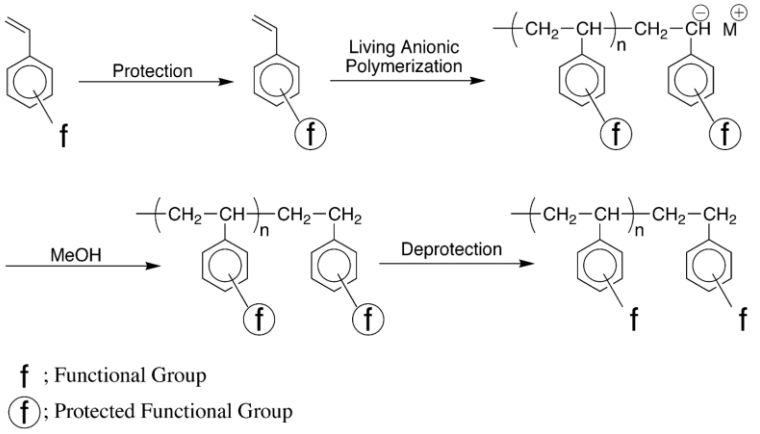

Figure 3: General procedure for the preparation and polymerization of functionalised styrenic monomers.[7,19]

The motivation behind this elaborate procedure is the possibility to change the polarity or the mechanical properties of polymers. Even the simplest substituents like methyl groups already result in a significant change in reactivity and properties.[20,21] Fetters and Morton substituted styrene with α-methylstyrene for the preparation of isoprene/α-methylstyrene triblock copolymers.[22] Due to the higher glass transition

temperature of the poly-α-methylstyrene block, the resulting polymers showed increased toughness, modulus and elongation at break in comparison to analogous triblock copolymers from isoprene and styrene.[22] This effect can be enhanced by larger substituents like *tert*-butyl or adamantyl groups, which provide even higher glass transition temperatures (T_g) than α-methylstyrene and therefore better mechanical properties.[23–25]

In recent years the raised awareness of the environmental impact of polymers from petrochemical sources has increased the interest for monomers from renewable and sustainable sources.[26–28] Among the numerous compounds, only a few are suitable for living anionic polymerization (Figure 4).[29]

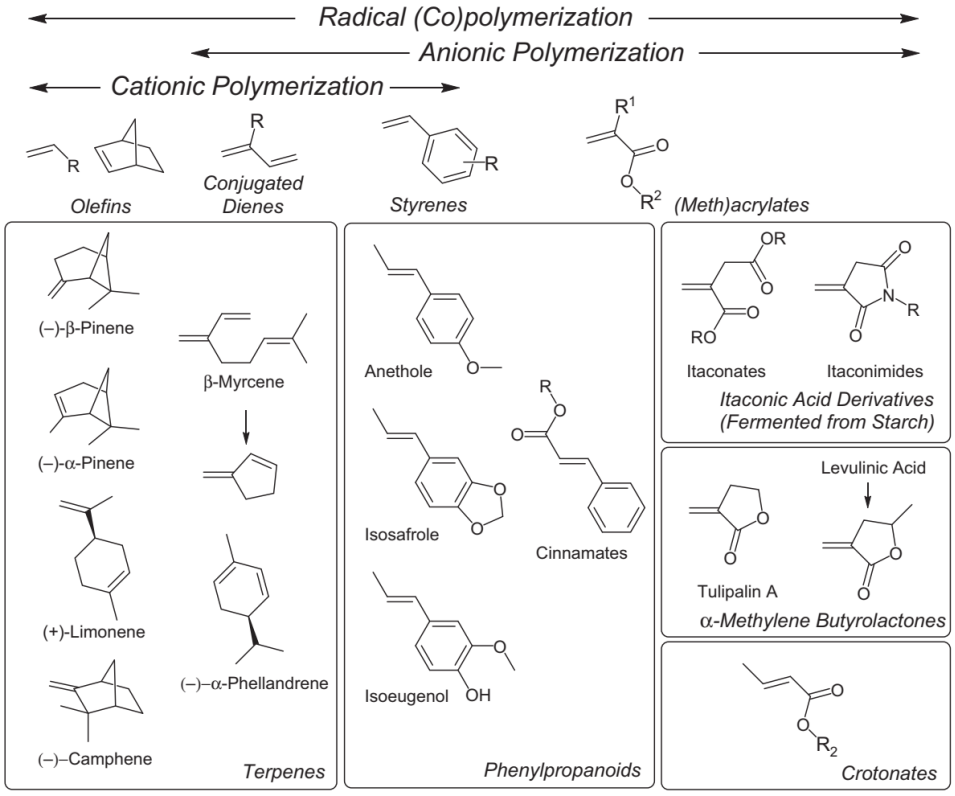

Figure 4: Monomers from sustainable/renewable sources.[29]

Especially myrcene has gained considerable interest in recent years.[30] Myrcene belongs to the class of monoterpenes and can be found in many plants like conifers, wild thyme and hops.[30,31] Commercially, myrcene is gathered in large scales by pyrolysis of β-pinene and recent developments in metabolically engineering enabled a microbial synthesis of myrcene.[30,32] Like isoprene and butadiene, myrcene can be polymerised at room temperature in apolar solvents using organolithium initiators, yielding a high content of 1,4 units.[29] This microstructure leads to a low glass

transition temperature and therefore good mechanical properties for corresponding elastomers.[33] Furthermore, the exterior double bond of polymyrcene enables various postmodificatios like thiol-ene click or epoxidation while preserving the low T_g backbone.[34,35]

1.2 Copolymerization kinetics

The combination of different monomers within one polymer chain offers almost infinite possibilities to adjust the mechanical properties of the resulting material. Besides sequential monomer addition, statistical (i.e., simultaneous) copolymerization of two different monomers can be used to achieve a particular microstructure. In this context, it is crucial to know the kinetics of the copolymerization in order to predict and control the chain architecture.

Every copolymerization of two monomers can be described by four reactions (Scheme 4) and two differential equations (8) and (9):

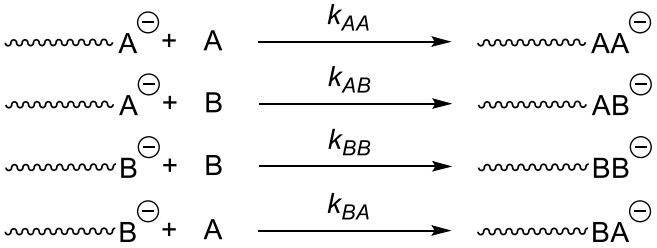

Scheme 4: Homopolymerization and cross-over reactions of a copolymerization.

$$-\frac{d[A]}{dt} = k_{AA}[A][A^-] + k_{BA}[A][B^-] \quad (8)$$

$$-\frac{d[B]}{dt} = k_{BB}[B][B^-] + k_{AB}[B][A^-] \quad (9)$$

In a carbanionic copolymerization termination and chain transfer reactions are absent, therefore the carbanion concentration does not change, and the decrease of the monomer concentration is equivalent to the amount of incorporated monomers. Thus, the simplified quotient of equations (8) and (9) gives the Mayo-Lewis equation (10), which describes the composition of the resulting polymer at any conversion.

$$\frac{d[A]}{d[B]} = \frac{[A]}{[B]} \cdot \frac{\frac{k_{AA}}{k_{AB}} \cdot [A] + [B]}{\frac{k_{BB}}{k_{BA}} \cdot [B] + [A]} \tag{10}$$

The reactivity ratios are defined as the ratio of the rates of the homopolymerization and cross-over reactions (11)[36].

$$\frac{k_{AA}}{k_{AB}} = r_A \qquad \frac{k_{BB}}{k_{BA}} = r_B \tag{11}$$

Depending on the combination of the reactivity ratios, every copolymerization can be classified into one of four classes, whereby each class has its specific microstructure and mechanical properties (Table 1).

Table 1: Classes of copolymerizations.[9]

class of copolymerization	r_A	r_B	$r_A r_B$
alternating	0	0	0
ideal	1	1	1
statistical	<0	<0	<0
compositional drift	<1 >1	>1 <1	≠1

The reactivity ratios of a monomer system highly depend on the polymerization technique and the polarity of the solvent (Figure 5). Especially in the carbanionic polymerization the polarity of the solvent has a strong effect on the copolymerization kinetics. Since the monomer addition to the living chains results from a nucleophilic attack of the carbanion, its aggregation state and counterion solvation have a strong impact on the propagation rate. In apolar solvents, carbanionic polydienes like polyisoprenyllithium usually form tetramers, while styrenic monomers usually are associated to dimers. However, in both cases, only the unimers are capable of monomer addition. Thus, prior to reaction with monomer complete dissociation of the aggregates is required.[37] Furthermore, apolar solvents enhance the counterion binding, resulting in further lowering of the propagation rate. In polar solvents, on the

other hand, all aggregates are dissolved and the counterion distance is enhanced, leading to very high propagation rates and mandatory low reaction temperatures.

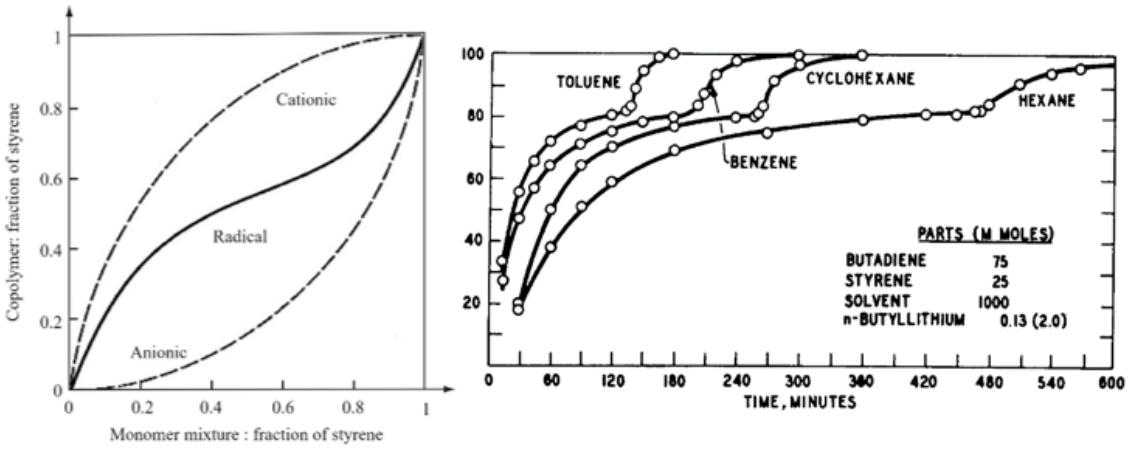

Figure 5: left: effect of the polymerization technique on the reactivity ratios of styrene and methyl methacrylate in the statistical copolymerization; right: effect of the solvent on the reactivity ratios of styrene and butadiene.[38,39]

Another possibility to influence the reactivity ratios is to alter the electron density of the reactive double bond by substitution of neighbouring atoms. This strategy is already well established for various organic reactions like free radical addition reactions, hydroboration and Diels-Alder reactions.[40–42] Furthermore, Dhami and Stothers observed a linear correlation between the ^{13}C NMR β-carbon shift and the electron density at the double bond.[43] Ishizone et al. transferred this concept to the living anionic copolymerization, revealing a correlation between the ^{13}C NMR β-carbon shift and the reactivity of the monomer and living chain end (Figure 6).[44]

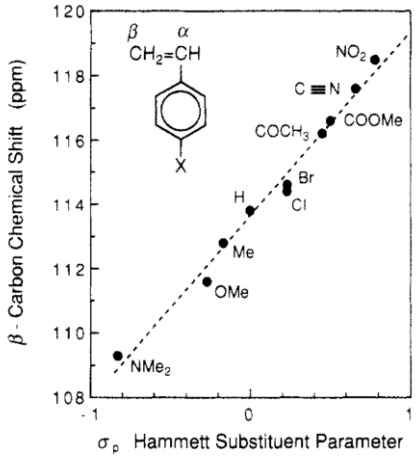

Figure 6: Correlation between ^{13}C NMR β-carbon shift and the reactivity of *para*-substituted styrene derivates.[44]

Hence, every electron withdrawing substituent lowers the electron density of the double bond, resulting in an enhanced monomer reactivity, but lower nucleophilicity of the chain end. Analogously, electron donating groups have a contrary effect.[44]

1.3 Determination of reactivity ratios

A copolymerization of two monomers can be completely described by its reactivity ratios. The calculation of these important parameters requires either the determination of the homopolymerization and cross-over rates or an alteration of the monomer concentrations during the copolymerization.[36,45] In both cases highly accurate measurements are required since already small errors lead to a strong deviation of the resulting reactivity ratios.

The most common methods for the evaluation of the reactivity ratios are the Fineman-Ross and Kelen-Tüdös methods.[46–48] Both methods compare the composition of the monomer feed $\left(\frac{M_A}{M_B}\right)$ with the polymer composition $\left(\frac{m_A}{m_B}\right)$ at different conversion and permit determination of the reactivity ratios through a linear application. In case of the Fineman-Ross equation (12) the slope represents r_A while the y intercept represents r_B (Figure 7).

$$\frac{M_A m_B}{M_B m_A}\left(\frac{m_A}{m_B} - 1\right) = r_A \left(\frac{M_A}{M_B}\right)^2 \frac{m_B}{m_A} - r_B \qquad (12)$$

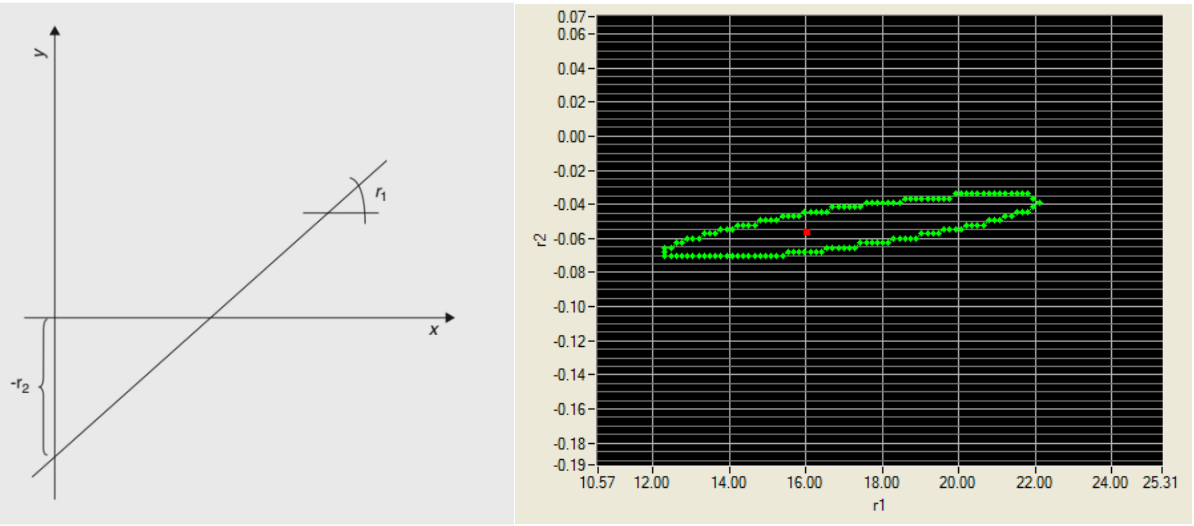

Figure 7: left: determination of reactivity ratios by Fineman-Ross; right: determination of reactivity ratios by contour, green circle: confidence interval, red dot: ideal values.[9]

Tidwell and Mortimer recognized that the Fineman-Ross method suffers from unequally weighted data, since extreme monomer compositions have a stronger effect on the slope and the *y* intercept than intermediate compositions and that the calculated reactivity ratios depend on which monomer is set as M_A.[49] To overcome these problems Kelen and Tüdös extended the Fineman-Ross equation by factor ε, giving the Kelen-Tüdös equation (13):

$$\frac{\frac{M_A m_B}{M_B m_A}\left(\frac{m_A}{m_B}-1\right)}{\varepsilon} = r_A \frac{\left(\frac{M_A}{M_B}\right)^2 \frac{m_B}{m_A}}{\varepsilon} - \frac{r_B}{\varepsilon} \quad \text{with} \quad \varepsilon = \alpha + \left(\frac{M_A}{M_B}\right)^2 \frac{m_B}{m_A} \tag{13}$$

Other nonlinear evaluation methods are the Mayo-Lowry and non-linear least square method (Figure 7).[50,51] Both methods require a lot more computational power but yield better and more reliable results.[52]

However, all methods require precise kinetic measurements to diminish the error of the resulting parameters. Historically, first kinetic experiments were carried out by terminating several copolymerization with different monomer ratios at low conversion, requiring a multitude of experiments for the observation of one copolymerization. Remarkably, in 1960 Worsfold and Bywater developed the first real-time monitoring method using all-glass reactors with ultraviolet-visible (UV) optical cells.[53] This technique enabled the exact determination of all rate constants and reactivity ratios within just a few experiments, leading to a fundamental understanding of the kinetics of a carbanionic polymerization.[37,53–56] Quinebèche et al. continued this approach by simplifying and extending the setup using a mid-infrared (MIR) probe (Figure 8).[57]

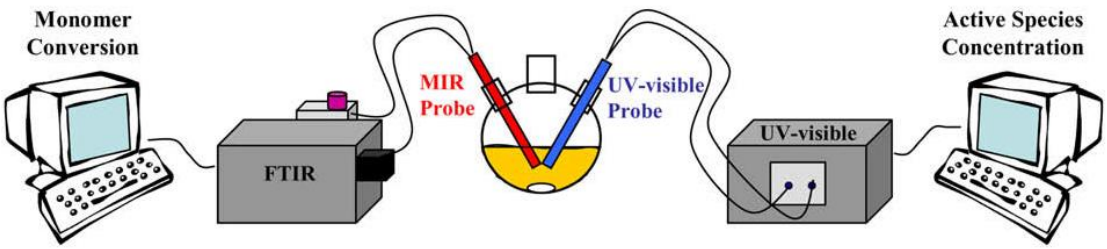

Figure 8: Setup for *in-situ* kinetic measurements of living anionic polymerizations.[57]

With this improved setup, Quinebéche et al. were able to determine the influence of temperature and solvent polarity on the homopolymerization and cross-over rates of

isoprene and styrene.[57] Although the combination of UV and MIR is a very versatile approach and suitable for various polymerization techniques, its major drawback is the necessity of special and expensive equipment. The newest approach for kinetic observation of living anionic copolymerizations is the *in-situ* ^{1}H NMR spectroscopy. In 2013 Natelello et al. accomplished the first carbanionic copolymerization in a NMR tube, demonstrating the capability of this method.[58,59] Although this rapid *in-situ* approach is strictly limited to monitoring the decrease of the monomer signals, the obtained results fully agree with previous data using more elaborate methods (Figure 9).[21]

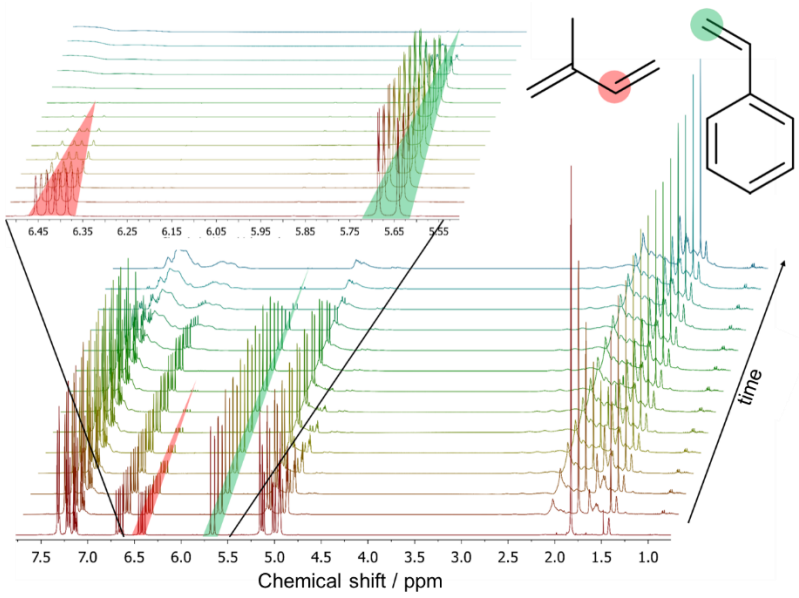

Figure 9: *In-situ* ^{1}H NMR spectroscopy of the copolymerization of isoprene and styrene in cyclohexane.

1.4 Block copolymers: phase separation and mechanical properties

Block copolymers consist of at least two different homopolymer segments, connected by covalent bonds. As a result, each homopolymer segment maintains its distinct properties, while the block copolymers' mechanical response is a combination of the individual properties of the segments. Block copolymers are usually prepared by sequential monomer addition. Therefore, only living polymerization techniques are suitable for the preparation of highly defined materials with narrow dispersities.[60] Since their first appearance in the early 1950s block copolymers have become the most important speciality polymers in industry and can be found in various applications ranging from footwear to adhesives.[8,61,62] The introduction of the living anionic polymerization finally enabled an economical grand scale production of block copolymers.[6] Block copolymers have found their way into high tech applications like light emitting diodes (LED's), semiconductor devices, nanolithography and nanoreactors (Figure 10).[63–65]

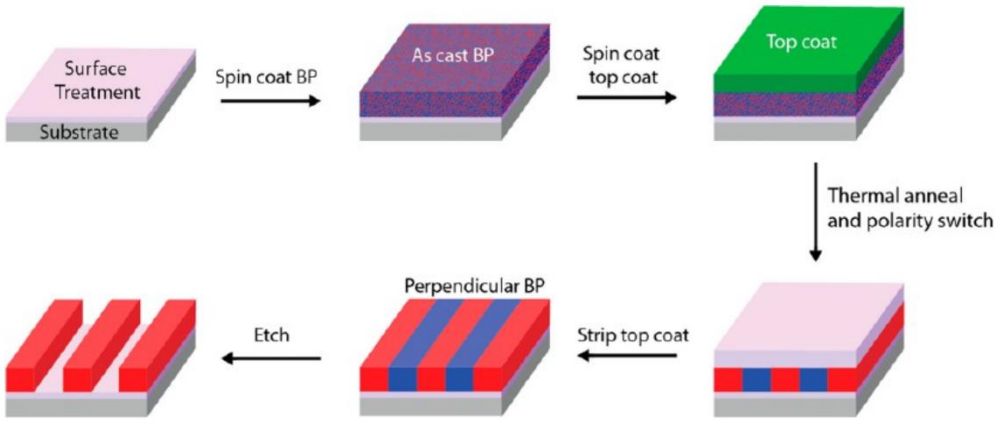

Figure 10: Orientation of block copolymer domains for nanolithography and nanoreactors.[63]

The main reason for the vast success and on the other hand the special mechanical properties of block copolymers is their capability to undergo phase separation on the nanometer scale. Due to the incompatibility of the blocks, each segment strives to minimize its interphase to the neighbouring segments. Unlike polymer blends, the covalent bonding of the homopolymer segments prevents macrophase separation, resulting in microphase separation.[66]

The phase separation behaviour of block copolymers can be described by the Flory-Huggins theory[67]:

$$\frac{\Delta G_m}{k_B T} = \frac{f_A}{N_A} ln f_A + \frac{f_B}{N_B} ln f_B + f_A f_B \chi_{AB} \quad (14)$$

ΔG_m represents the free energy, k_B the Boltzmann constant, T the temperature, f the volume fraction of monomer A or B, N the degree of polymerization and χ_{AB} the Flory-Huggins interaction parameter. The first two terms of equation (14) contribute to the entropy and therefore always favour phase mixing.[67] Since polymers usually have a large degree of polymerization, the entropy terms have only a minor effect on the phase separation. Thus, the enthalpy term or more specifically the Flory-Huggins interaction parameter (χ_{AB}) dominates the demixing of polymer blends. χ_{AB} describes the free energy cost per monomer and is defined as:

$$\chi_{AB} = \frac{Z}{k_B T}\left(\varepsilon_{AB} - \frac{\varepsilon_{AA} + \varepsilon_{BB}}{2}\right) \quad (15)$$

Here Z is the number of nearest neighbouring monomers to a copolymer configuration cell (confined periodic space in copolymer) and ε_{AB} is the interaction energy of monomers A and B.[68] Positive χ_{AB} indicates repulsion, while negative values indicate attraction of monomers A and B. Due to the inverse temperature dependency of χ_{AB}, phase separation can only occur at sufficiently low temperatures.[66] Depending on the composition of the copolymer the separated segments will form distinct morphologies (Figure 11).[69]

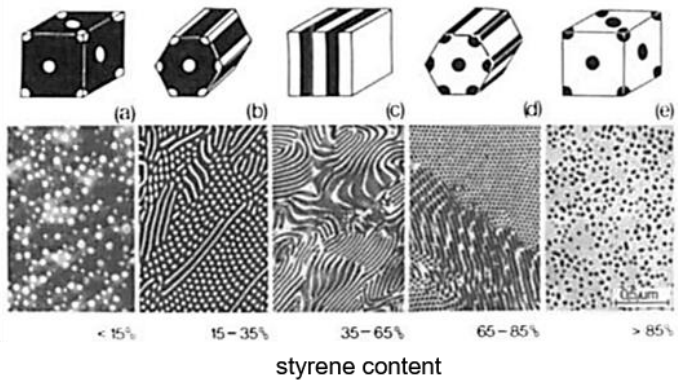

Figure 11: Morphologies of diblock copolymers from butadiene and styrene: a) styrene spheres in butadiene matrix; b) styrene cylinders in butadiene matrix; c) butadiene and styrene lamella; d) butadiene cylinders in styrene matrix; e) butadiene spheres in styrene matrix.[70]

Since the phase separation mainly depends on the composition, the degree of polymerization and the Flory-Huggins interaction parameter, it is possible to map all morphologies within a phase diagram (Figure 12).[66,71] The asymmetric shape of the phase diagram is caused by the unequal shape and densities of the monomers. Hence, every monomer system has its own phase diagram and varying ranges for every morphology, albeit the ordered phases are universal.

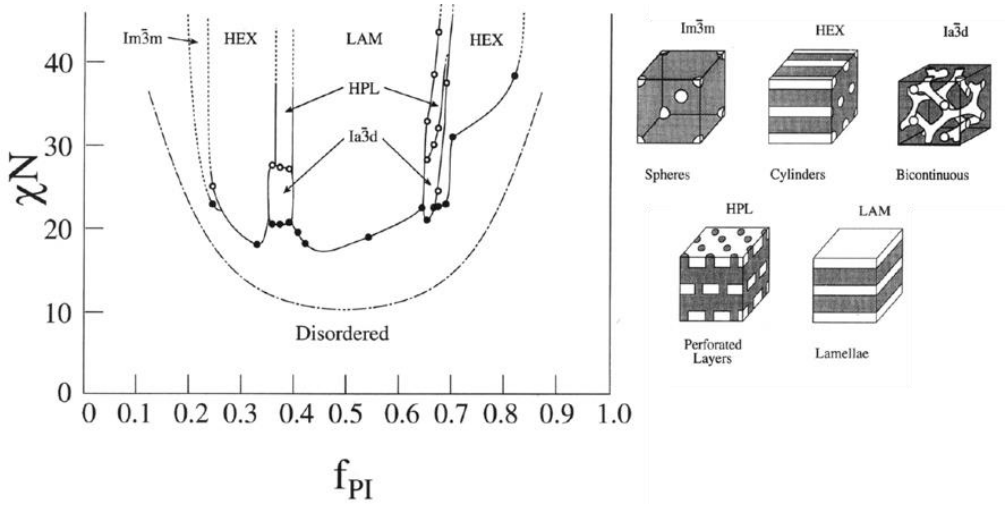

Figure 12: Morphologies and phase diagram of a diblock copolymer from isoprene and styrene.[69]

Most of these fundamental studies have been carried out on simple AB diblock copolymers. Unfortunately, diblock copolymers provide only poor mechanical properties, resulting in a strongly limited range of applications. On the other hand, ABA triblock copolymers, where A represents a glassy high T_g block and the central B block a flexible low T_g segment, form tough and resilient materials and represent the largest sector in block copolymer industry.[8] The most prominent example is Kraton D®, which is a SIS or SBS thermoplastic elastomer from styrene (S), isoprene (I) or butadiene (B).[72] Like AB diblocks, these structures undergo microphase separation, following the same general principles.[73] Hence, any change of the composition of ABA triblocks also results in a change of their phase segregation behaviour. Due to a strong correlation between microphase separation and mechanical properties, every compositional alteration alters morphology and mechanical response at the same time. Part of the great success of Kraton D® and other commercially relevant triblock copolymers can be attributed to this correlation, permitting a high level of customizability for the mechanical properties merely by

changing their composition, without the necessity of altering the monomer sequence or substituting monomers.[74]

To observe the mechanical response of a polymer material, tensile testing is the method of choice due to its easy applicability and strong explanatory power. In this experiment, the specimen is elongated unidirectionally, while the force required for extension is recorded (Figure 13).

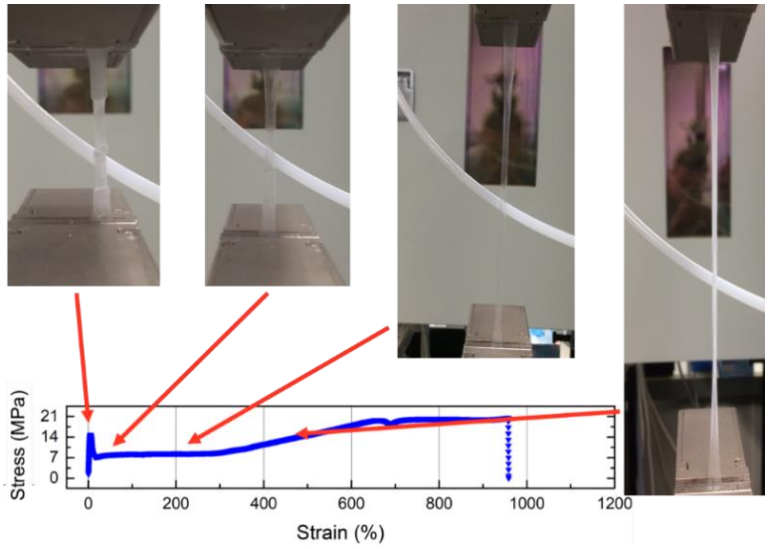

Figure 13: Stress-strain experiment of multiblock copolymer.

The shape of the resulting stress-strain curve mainly depends on molecular weight, composition and chain architecture of the material (Figure 14).[75]

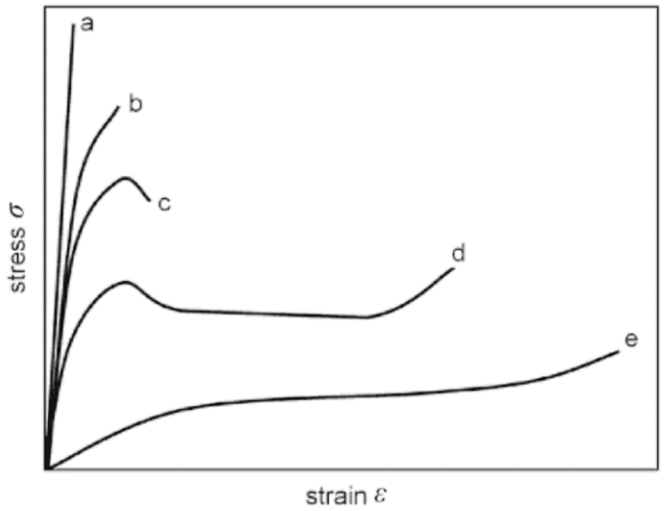

Figure 14: Stress-Strain curves of different polymer materials from brittle (a) to elastomeric (e).[75]

Figure 14 displays the stress-strain curves of different polymer types, varying from brittle (a) over ductile (c and d) to elastomeric (e). Every change of the slope of a stress-strain curve represents a specific mechanical response and the change of the slope indicates a change of the Young modulus.

While the slope of the linear section at the beginning of the curve represents the Young modulus, the integrated area under the curve represents the toughness of a material. The Young modulus is a measure of stiffness. The toughness is a measure for the energy a material can absorb before break. Very brittle polymers (Figure 14 a and b) show high stress and only low strain at break, resulting in a high Young modulus, but low toughness. Ductile polymers (Figure 14 c and d) show a lower Young modulus and yielding, enabling much stronger deformation of the polymer. The yield point is marked by a temporary drop of the stress, due to polymer yielding.[76] Any further strain of the sample upon this point causes irreversible (i.e., plastic) deformation. More elastic materials show necking after the yield point (Figure 13; Figure 14 d). The ensuing necking region is marked by nearly constant stress and thinning of the specimen. When the necking has propagated through the hole specimen, the stress increases again, caused by strain hardening (Figure 14 d).[77] Elastomeric or rubber like polymer possess low modulus and show elastic recovery even at high strain (Figure 14 e). Since these materials do not show a yield point, they sustain large deformation and high recoverability.[78]

As mentioned before, mechanical properties and microphase separation are strongly correlated in block copolymers. Therefore, every parameter affecting the morphology unavoidably has an impact on mechanical properties. As a result, the mechanical characteristics of a material mainly depend on the molecular weight, composition and polymer architecture. Yang et al. observed a linear correlation between molecular weight and mechanical properties, an increase of the molecular weight resulting in an enhancement of entanglements within the domains, providing a better mechanical response.[79,80] Another linear correlation could be observed between mechanics and composition. Qiao et al. and Diar et al. managed to isolate the effect of the morphology on the mechanical properties from any other parameter.[81,82] Both research groups observed a higher Young modulus and toughness for lamellar and double-gyroid morphologies, attributed to an enhanced connectivity of the glassy domains

(Figure 15). On the other hand, spherical and cylindrical morphologies of the glassy domains lead to a rubber like behaviour without a yield point (Figure 15).

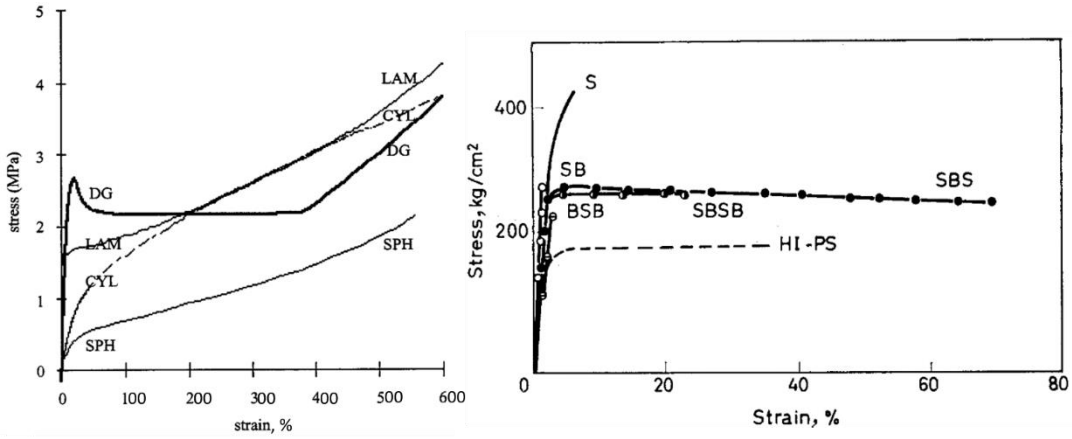

Figure 15: Stress-strain curves of left: SIS triblock copolymers from styrene (S) and isoprene (I) with varying morphologies; right: SBS triblock copolymers from styrene (S) and butadiene (B) with varying block sequences.[82]

Another important parameter to adjust the mechanical properties is the chain architecture. Matsuo et al. demonstrated that ABA triblock copolymers with a soft middle block and glassy outer blocks yield tough and resilient materials, while the opposite structure with a glassy middle block showed only poor mechanical properties (Figure 15 right). These results can be explained by the lower mobility of double tethered soft segments and a lack of crosslinking by vitrification of the outer glassy segments.[81]

1.5 Gradient copolymers

Gradient copolymers come in a variety of structures, each with its specific mechanical properties (Figure 16). Alteration of the length and shape of the taper enable to adjust various mechanical properties like morphology, domain spacing, glass transition temperature and order-disorder transition temperature.[84]

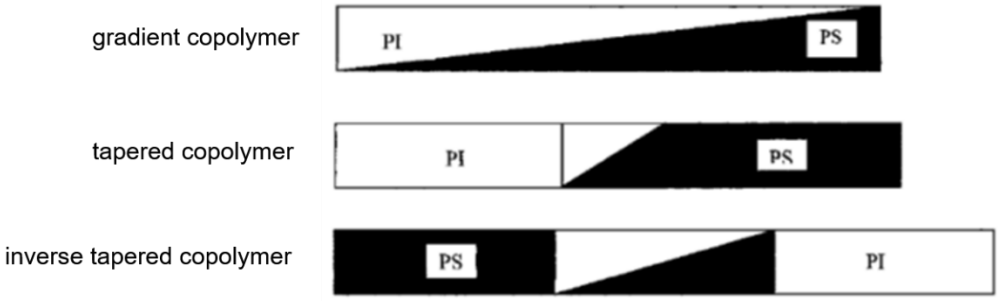

Figure 16: Different types of gradient copolymers.[85]

Gradient copolymers are usually prepared by statistical copolymerization of two monomers by controlled polymerization techniques, i.e. by living anionic polymerization or by controlled radical polymerization techniques.[86–88] During the statistical copolymerization, the more reactive monomer is incorporated preferentially. At the same time, its decreasing concentration increases the incorporation probability of the less reactive monomer, resulting in a gradual change of the composition. The shape and length of the tapered section highly depend on the disparity of the reactivity ratios. While similar reactivity ratios result in a long and shallow gradient, highly diverging reactivities yield block like tapered copolymers with a very steep taper.[21,89] Another possibility to prepare gradient copolymers is to control the monomer feed by automated pumps, providing complete control over polymer sequence, gradient length and shape.[90]

Independent of the chosen synthetic procedure, gradient copolymers show significant differences in their mechanical response, when compared to corresponding diblock copolymers. The tapered section of gradient copolymers acts as a compatibilizer between the polymer blocks, lowering the driving force for phase segregation.[91] The strength of the compatibilizing effect strongly depends both on the shape and length of the gradient.[92] Hadjichristidis et al. impressively demonstrated a linear correlation between the spinodal line and the gradient length for tapered copolymers

(Figure 17).[92] Inverted tapers show an even greater compatibilizing effect due to the increased interfacial area between the homopolymer segments.[92–94]

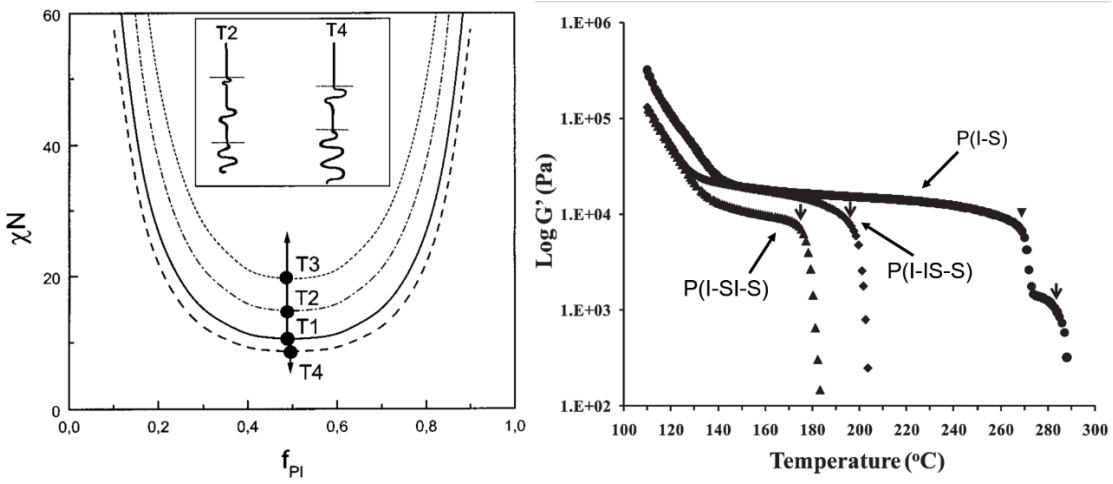

Figure 17: left: spinodal lines of gradient copolymers with increasing length of the tapered section (increases from T1 to T3); right: isochronal storage modulus (G') vs. temperature for diblock (P(I-S)), gradient copolymer (PI-IS-S)) and inverse tapered copolymer (P(I-SI-S)).[90,92]

Furthermore, the compatibilizing effect of the gradient also has an impact on the T_g and order-disorder transition temperature. In both cases the specific temperatures decrease with increasing volume fraction of the gradient, the effect being enhanced for inverse tapers (Figure 17).[90,92] Since the decrease of both temperatures only depends on the length and shape of the gradient, it can be used as a molecular weight and composition decoupling tool to tune morphology and mechanical response.[84]
Due to these unique characteristics, it is not surprising that gradient copolymers have found their way into commercial products. The two most prominent examples are Styroflex® and Styrolux®(Figure 18).[95,96]

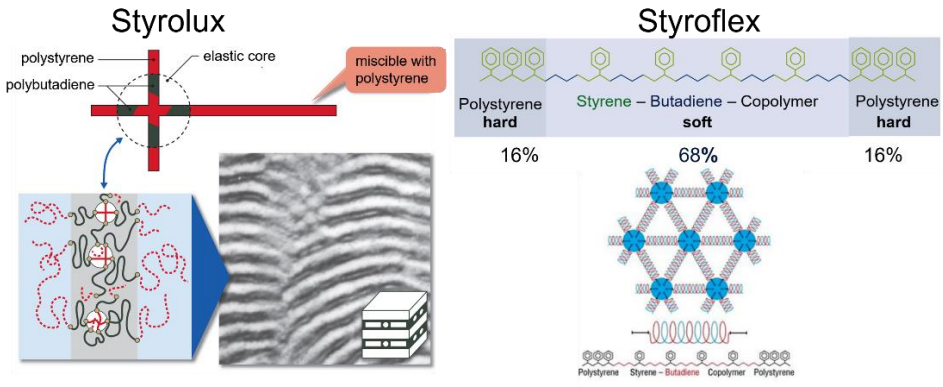

Figure 18: Structure and properties of Styrolux® and Styroflex®.[96]

Styrolux® is a star shaped multigradient copolymer with up to five asymmetric arms and an elastic polystyrene/polybutadiene gradient core. The preparation of Styrolux® includes multiple living anionic polymerization steps, starting with the preparation of the asymmetric polystyrene segments. The asymmetry provides enhanced miscibility with polystyrene or other polymers and prevents macrophase segregation of the polymer blends (Figure 18). The next two steps are (i) the addition of styrene/butadiene monomer mixtures to create the elastic core and (ii) finally the coupling of the asymmetric arms to generate a star copolymer. This peculiar polymer architecture improves the processability, making Styrolux® and its blends highly suitable for injection moulding.[95]

Styroflex®, on the other hand, is a symmetric triblock copolymer with a gradient middle block.[95,96] It is also prepared by living anionic polymerization and has a much larger elastic core than Styrolux®, providing high flexibility and enhanced interconnectivity of the middle blocks (Figure 18). Both materials, developed at BASF and now sold by the company INEOS Styrolution are used as packaging materials or as modifiers for other polymers like polystyrene or polymer blends with a worldwide production capacity exceeding 110000 t/a.[96] In both cases, the gradient serves multiple functions to improve processability and mechanical response: (i) due to the low order-disorder transition temperature (ODT) of the gradient, the processing temperature of this materials is lower than of comparable SBS triblock copolymers. (ii) The elastic tapered section enhances the strain at break and toughness of both materials. (iii) Since the gradient consists of a mixture of styrene and butadiene the overall diene content is much lower, resulting in improved thermal stability.[95] However, compared to competing products like Kraton D®, which represent perfect triblock copolymers, Styroflex® and Styrolux® show weaker phase segregation due to the compatibilizing effect of the gradient. Furthermore, classical SBS thermoplastic elastomers show higher elongation at break and yield points at lower stress, resulting in a better recoverability of the materials.

Nevertheless, the gradient structure of Styroflex® and Styrolux® permits a generally lower rubber content, while preserving similar elasticity as SBS triblock copolymers, providing a much higher impact strength and thermal stability.[95,96]

1.6 Multiblock copolymers

Nowadays, triblock copolymers, consisting of glassy outer blocks and rubbery middle blocks, represent the predominant polymer structure for a wide range of applications, due to their excellent mechanical characteristics.[97,98] Adding more blocks results in multiblock copolymers with even better extensibility and toughness than comparable triblock copolymers.[99–101] Due to the high potential of these materials, the interest in multiblock copolymers increased continuously, leading to an improved understanding of the consequences of this polymer architecture.[8,99]

The multiblock architecture can also be found in nature. Spider silk and silk from the silk worm are the most prominent example for natural multiblock copolymers. Both structures consist of an alternating sequence of hard and soft segments providing a high level of toughness and flexibility (Figure 19).[102–104]

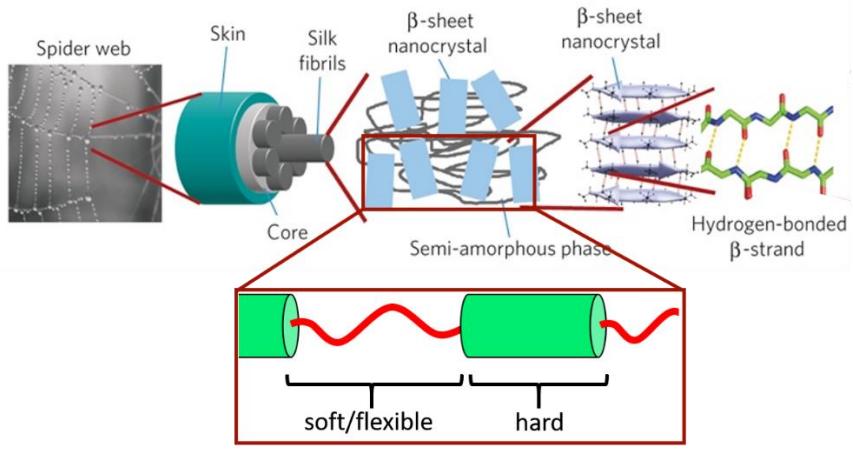

Figure 19: Structure of spider silk.[102]

This general concept of alternating flexible and rigid segments can also be reproduced in a biomimetic manner by copolymers consisting of low and high T_g blocks. The first attempt to prepare such a structure dates back to 1959 when Korotkov et al. used living anionic copolymerization to prepare the first linear multiblock copolymer from isoprene and styrene.[105] Corbin and Prud'Homme extended this approach by taking advantage of the different reactivities of isoprene and styrene, minimizing the number of steps required for the preparation of linear tapered multiblock copolymers.[106,107] However, Korotkov et al. carried out the synthesis of these elaborate structures at an early stage of development of the living anionic polymerization, lacking an appropriate set-up and analytical methods for the preparation and characterization of highly defined multiblock copolymers. In

consequence the resulting polymers showed broad molecular weight distributions and varying number of blocks due to uncontrolled terminations during every monomer addition step.[105]

The approach of Corbin and Prud'Homme, on the other hand, was far more advanced, yielding high molecular weight polymers with reasonable molecular weight distributions. Nonetheless, microstructure analysis revealed the formation of long gradients during every monomer addition, rendering these materials multi-gradient copolymers.[107,108]

The preparation of multiblock copolymers is still very challenging and many new approaches have been developed to tackle this problem. Especially controlled radical polymerization and catalytic precision polymerization approaches have been established as relevant synthetic pathways for multiblock structures in recent years. However, these techniques in most cases cannot provide highly defined copolymers with morphologically relevant block sizes, thus the carbanionic copolymerization remains the method of choice.[109–118]

Like in all other copolymer types the mechanical properties of multiblock copolymers strongly depend on the composition and length of the block segments. Their superior mechanical response is rooted in the block sequence and their special bulk conformations. Compared to a diblock copolymer, a multiblock structure possesses two end segments and several inner blocks. While a diblock copolymer is restricted to just one conformation, where each end block is located in its specific domain, the inner segments of a multiblock can form loops and bridges (Figure 20).[97,119–122] Every loop and bridge enhances domain interconnectivity, minimising possible failure in the bulk material, resulting in superior toughness and resilience of multiblock copolymers in comparison to diblock and triblock copolymers.

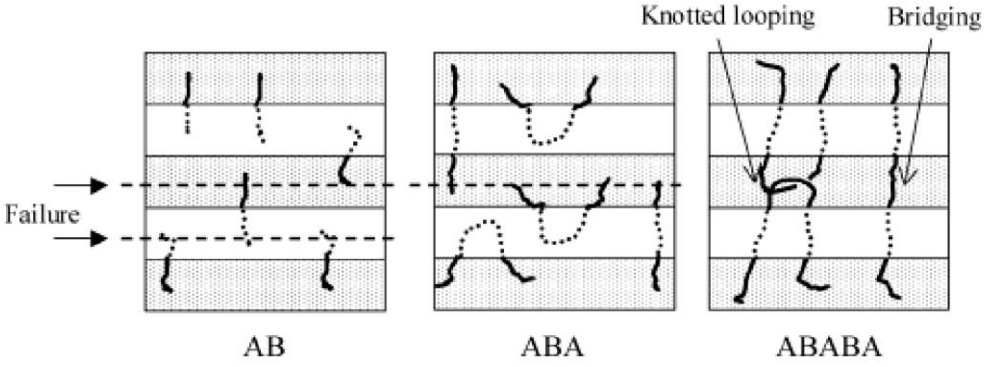

Figure 20: Bulk conformations of diblock, triblock and multiblock copolymers.[97]

The number of blocks also effects various other thermomechanical key properties like the domain sizes, glass transition and order disorder transitions temperatures, strain at break and toughness. This correlation enables to adjust all these parameters independent of block size and composition. It is well-known that increasing the number of blocks also increases the strain at break and toughness of a material due to the enhanced looping and bridging.[123–125] At the same time, a higher number of loops and bridges creates intermolecular constrains, lowering the free volume and immobilising the inner segments.[118,119,126] Since segment mobility is crucial for phase separation, the fraction of mixed interphase increases with the number of blocks, resulting in smaller domain sizes and converging glass transition temperature (Figure 21).[118,119,123,126]

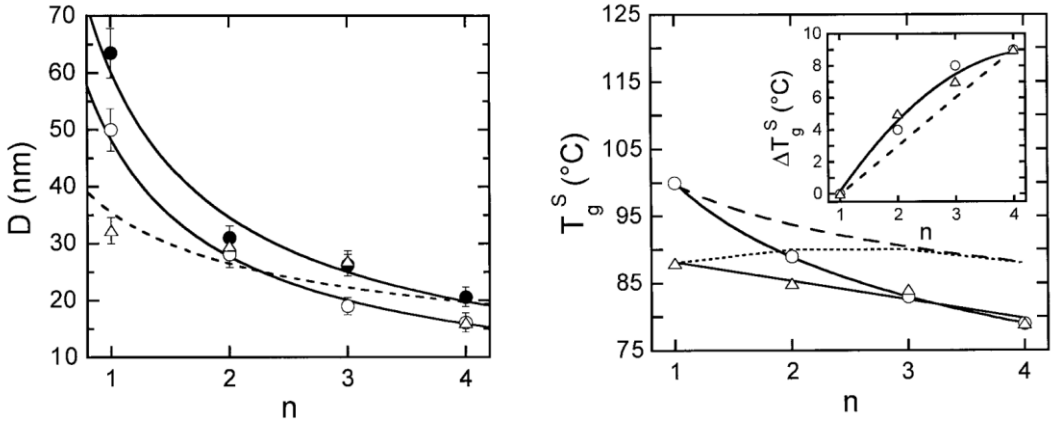

Figure 21: Correlation between domain sizes (left) and glass transition temperatures (right) and the number of blocks.[123]

At the same time reduced segment mobility enhances the melt relaxation times requiring higher temperatures to reach the disordered state (Figure 22).[127]

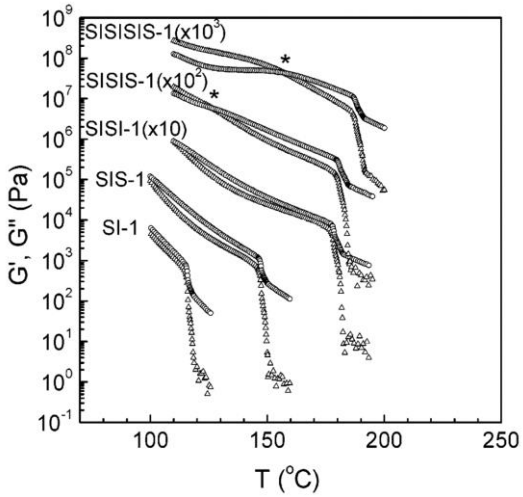

Figure 22: Correlation between order disorder transition temperature and number of blocks.[127]

In conclusion, multiblock copolymers offer superior mechanical properties and many options to adjust their mechanical response. However, the availability and applicability of these materials is currently limited by their challenging preparation, requiring a large number of steps and elaborate experimental set ups.

The focus of this dissertation is placed on the preparation and characterization of linear alternating multiblock copolymers. For this purpose, a one-step block copolymer formation approach has been developed, by taking advantage of the vigorously different reactivity ratios of dienes and styrenic monomers. In combination with sequential monomer addition it was possible to synthesise series of linear tapered alternating multiblock copolymers, varying in composition, molecular weight and number of blocks. These new materials have been characterised by a variety of methods to gain profound information regarding their mechanical and thermochemical properties and the correlation between polymer architecture and mechanical response.

In addition, in depth kinetics studies have been carried out on the living anionic copolymerization of myrcene to investigate its potential as a bio-based alternative for isoprene and its applicability for the preparation of multiblock copolymers and novel thermoplastic elastomers.

1.7 References

(1) Szwarc, M. 'Living' Polymers. *Nature* **1956**, *178*, 1168–1169.

(2) Harries, C. Über Kohlenwasserstoffe der Butadienreihe und über einige aus ihnen darstellbare künstliche Kautschukarten: I. Über Synthesen von Kohlenwasserstoffen der Butadienreihe. Über Isopren oder β-Methylbutadien. *Liebigs Ann. Chem.* **1911**, *383*, 157–227.

(3) Schlenk, W.; Appenrodt, J.; Michael, A.; Thal, A. Über Metalladditionen an mehrfache Bindungen. *Ber. Dtsch. Chem. Ges.* **1914**, *47*, 473–490.

(4) Leibig, D.; Morsbach, J.; Grune, E.; Herzberger, J.; Müller, A. H.E.; Frey, H. Die lebende anionische Polymerisation. *Chem. Unserer Zeit* **2017**, *51*, 254–263.

(5) Szwarc, M. Living polymers. Their discovery, characterization, and properties. *J. Polym. Sci. A Polym. Chem.* **1998**, *36*, ix–xv.

(6) Szwarc, M.; Levy, M.; Milkovich, R. Polymerization Initiated by Electron Transfer to Monomer. A New Method of Formation of Block Copolymers. *J. Am. Chem. Soc.* **1956**, *78*, 2656–2657.

(7) Hirao, A.; Loykulnant, S.; Ishizone, T. Recent advance in living anionic polymerization of functionalized styrene derivatives. *Prog. Polym. Sci.* **2002**, *27*, 1399–1471.

(8) Bates, C. M.; Bates, F. S. 50th Anniversary Perspective: Block Polymers Pure Potential. *Macromolecules* **2017**, *50*, 3–22.

(9) Koltzenburg, S.; Maskos, M.; Nuyken, O. *Polymere: Synthese, Eigenschaften und Anwendungen*; Imprint: Springer Spektrum: Berlin, Heidelberg, 2014.

(10) Baskaran, D.; Müller, A. H.E. Anionic vinyl polymerization-50 years after Michael Szwarc. *Prog. Polym. Sci.* **2007**.

(11) Gold, L. Statistics of Polymer Molecular Size Distribution for an Invariant Number of Propagating Chains. *J. Chem. Phys.* **1958**, *28*, 91–99.

(12) Tieke, B. *Makromolekulare Chemie: Eine Einführung*; Wiley-VCH: Weinheim, 2012.

(13) Hadjichristidis, N.; Iatrou, H.; Pitsikalis, M.; Mays, J. Macromolecular architectures by living and controlled/living polymerizations. *Prog. Polym. Sci.* **2006**, *31*, 1068–1132.

(14) Sweat, D. P.; Yu, X.; Kim, M.; Gopalan, P. Synthesis of poly(4-hydroxystyrene)-based block copolymers containing acid-sensitive blocks by living anionic polymerization. *J. Polym. Sci., Part A: Polym. Chem.* **2014**, *52*, 1458–1468.

(15) Leicht, H.; Göttker-Schnetmann, I.; Mecking, S. Stereoselective Copolymerization of Butadiene and Functionalized 1,3-Dienes. *ACS Macro Lett.* **2016**, *5*, 777–780.

(16) Kim, M.-J.; Yu, Y.-G.; Kang, N.-G.; Kang, B.-G.; Lee, J.-S. Precise Synthesis of Functional Block Copolymers by Living Anionic Polymerization of Vinyl Monomers Bearing Nitrogen Atoms in the Side Chain. *Macromol. Chem. Phys.* **2017**, *218*, 1600445.

(17) Tanaka, S.; Goseki, R.; Ishizone, T.; Hirao, A. Synthesis of Well-Defined Novel Reactive Block Polymers Containing a Poly(1,4-divinylbenzene) Segment by Living Anionic Polymerization. *Macromolecules* **2014**, *47*, 2333–2339.

(18) Leibig, D.; Müller, A. H. E.; Frey, H. Anionic Polymerization of Vinylcatechol Derivatives: Reversal of the Monomer Gradient Directed by the Position of the Catechol Moiety in the Copolymerization with Styrene. *Macromolecules* **2016**, *49*, 4792–4801.

(19) Nakahama, S.; Hirao, A. Protection and polymerization of functional monomers: Anionic living polymerization of protected monomers. *Prog. Polym. Sci.* **1990**, *15*, 299–335.

(20) Nakayama, M.; Hirohara, H.; Takaya, K.; Ise, N. Living anionic polymerizations of o- and p-methylstyrenes in 2-methyltetrahydrofuran. *J. Polym. Sci., Part A: Polym. Chem.* **1970**, *8*, 3653–3655.

(21) Grune, E.; Johann, T.; Appold, M.; Wahlen, C.; Blankenburg, J.; Leibig, D.; Müller, A. H. E.; Gallei, M.; Frey, H. One-Step Block Copolymer Synthesis versus Sequential Monomer Addition: A Fundamental Study Reveals That One Methyl Group Makes a Difference. *Macromolecules* **2018**, *51*, 3527–3537.

(22) Fetters, L. J.; Morton, M. Synthesis and Properties of Block Polymers. I. Poly-α-methylstyrene-Polyisoprene-Poly-α-methylstyrene. *Macromolecules* **1969**, *2*, 453–458.

(23) Chen, J. C.; Fetters, L. J. Structure-property relationships for thermoplastic block terpolymers containing poly(styrene-p-tert-butylstyrene) copolymer end segments. *Polym. Eng. Sci.* **1987**, *27*, 1300–1309.

(24) Kobayashi, S.; Matsuzawa, T.; Matsuoka, S.-i.; Tajima, H.; Ishizone, T. Living Anionic Polymerizations of 4-(1-Adamantyl)styrene and 3-(4-Vinylphenyl)-1,1‘-biadamantane. *Macromolecules* **2006**, *39*, 5979–5986.

(25) Kobayashi, S.; Kataoka, H.; Ishizone, T.; Kato, T.; Ono, T.; Kobukata, S.; Ogi, H. Synthesis and Properties of New Thermoplastic Elastomers Containing Poly[4-(1-adamantyl)styrene] Hard Segments. *Macromolecules* **2008**, *41*, 5502–5508.

(26) Ávila-Ortega, A.; Aguilar-Vega, M.; Loría Bastarrachea, M. I.; Carrera-Figueiras, C.; Campos-Covarrubias, M. Anionic synthesis of amine ω-terminated β-myrcene polymers. *J. Polym. Res.* **2015**, *22*, 8.

(27) Winnacker, M.; Rieger, B. Recent Progress in Sustainable Polymers Obtained from Cyclic Terpenes: Synthesis, Properties, and Application Potential. *ChemSusChem* **2015**, *8*, 2455–2471.

(28) Wilbon, P. A.; Chu, F.; Tang, C. Progress in Renewable Polymers from Natural Terpenes, Terpenoids, and Rosin. *Macromol. Rapid Commun.* **2013**, *34*, 8–37.

(29) Satoh, K. Controlled/living polymerization of renewable vinyl monomers into bio-based polymers. *Polym. J.* **2015**, *47*, 527–536.

(30) Behr, A.; Johnen, L. Myrcene as a Natural Base Chemical in Sustainable Chemistry: A Critical Review. *ChemSusChem* **2009**, *2*, 1072–1095.

(31) Sarkar, P.; Bhowmick, A. K. Synthesis, characterization and properties of a bio-based elastomer: Polymyrcene. *RSC Adv.* **2014**, *4*, 61343–61354.

(32) Kim, E.-M.; Eom, J.-H.; Um, Y.; Kim, Y.; Woo, H. M. Microbial Synthesis of Myrcene by Metabolically Engineered Escherichia coli. *J. Agric. Food. Chem.* **2015**, *63*, 4606–4612.

(33) Bolton, J. M.; Hillmyer, M. A.; Hoye, T. R. Sustainable Thermoplastic Elastomers from Terpene-Derived Monomers. *ACS Macro Lett.* **2014**, *3*, 717–720.

(34) Matic, A.; Schlaad, H. Thiol-ene photofunctionalization of 1,4-polymyrcene. *Polym. Int.* **2018**, *67*, 500–505.

(35) Zhou, C.; Wei, Z.; Jin, C.; Wang, Y.; Yu, Y.; Leng, X.; Li, Y. Fully biobased thermoplastic elastomers: Synthesis of highly branched linear comb poly(β-myrcene)- graft -poly(l -lactide) copolymers with tunable mechanical properties. *Polymer* **2018**, *138*, 57–64.

(36) Mayo, F. R.; Lewis, F. M. Copolymerization. I. A Basis for Comparing the Behavior of Monomers in Copolymerization; The Copolymerization of Styrene and Methyl Methacrylate. *J. Am. Chem. Soc.* **1944**, *66*, 1594–1601.

(37) Worsfold, D. J. Anionic copolymerization of styrene and isoprene in cyclohexane. *J. Polym. Sci., Part A: Polym. Chem.* **1967**, *5*, 2783–2789.

(38) Devaux, J.; Demoustier-Champagne, S. Chapter 2 Polymer Chemistry and Microstructure. *Molecular Characterization and Analysis of Polymers*; Comprehensive Analytical Chemistry; Elsevier, 2008; pp 13–755.

(39) Hsieh, H. L.; Glaze, W. H. Kinetics of Alkyllithium Initiated Polymerizations. *Rubber Chem. Technol.* **1970**, *43*, 22–73.

(40) Yasuda, M.; Harano, K.; Kanematsu, K. High peri- and regiospecificity of phencyclone: Kinetic evidence of the frontier-controlled cycloaddition reaction and molecular structure of the cycloadduct. *J. Org. Chem.* **1980**, *45*, 659–664.

(41) Walling, C.; Briggs, E. R.; Wolfstirn, K. B.; Mayo, F. R. Copolymerization. X. The Effect of meta- and para-Substitution on the Reactivity of the Styrene Double Bond. *J. Am. Chem. Soc.* **1948**, *70*, 1537–1542.

(42) Brown, H. C.; Kim, S. C. Hydroboration. 66. Addition of lithium triethylborohydride to substituted styrenes. A simple, convenient procedure for the Markovnikov hydroboration of aromatically conjugated olefins and the synthesis of unusual mixed trialkylboranes. *J. Org. Chem.* **1984**, *49*, 1064–1071.

(43) Dhami, K. S.; Stothers, J. B. 13C NMR Studies: Part III. Carbon-13 NMR Spectra of Substituted Acetophenones. *Can. J. Chem.* **1965**, *43*, 479–497.

(44) Ishizone, T.; Hirao, A.; Nakahama, S. Anionic polymerization of monomers containing functional groups. 6. Anionic block copolymerization of styrene derivatives para-substituted with electron-withdrawing groups. *Macromolecules* **1993**, *26*, 6964–6975.

(45) Wu, Z.-c.; Liu, Y.; Wei, W.; Chen, F.-s.; Qiu, G.-x.; Xiong, H.-m. Reaction kinetics in anionic copolymerization: A revisit on Mayo-Lewis equation. *Chin. J. Polym. Sci.* **2016**, *34*, 431–438.

(46) Fineman, M.; Ross, S. D. Linear method for determining monomer reactivity ratios in copolymerization. *J. Polym. Sci.* **1950**, *5*, 259–262.

(47) Kelen, T.; Tüdős, F. A new improved linear graphical method for determing copolymerization reactivity ratios. *React. Kinet. Catal. Lett.* **1974**, *1*, 487–492.

(48) Kelen, T.; TÜds, F. Analysis of the Linear Methods for Determining Copolymerization Reactivity Ratios. I. A New Improved Linear Graphic Method. *J. Macromol. Sci., Part A* **1975**, *9*, 1–27.

(49) Tidwell, P. W.; Mortimer, G. A. An improved method of calculating copolymerization reactivity ratios. *J. Polym. Sci., Part A: Polym. Chem.* **1965**, *3*, 369–387.

(50) Meyer, V. E.; Lowry, G. G. Integral and differential binary copolymerization equations. *J. Polym. Sci., Part A: Polym. Chem.* **1965**, *3*, 2843–2851.

(51) van Herk, A. M.; Dröge, T. Nonlinear least squares fitting applied to copolymerization modeling. *Macromol. Theory Simul.* **1997**, *6*, 1263–1276.

(52) Blankenburg, J.; Wagner, M.; Frey, H. Well-Defined Multi-Amino-Functional and Stimuli-Responsive Poly(propylene oxide) by Crown Ether Assisted Anionic Ring-Opening Polymerization. *Macromolecules* **2017**, *50*, 8885–8893.

(53) Bywater, S.; Worsfold, D. J. Anioninc Polynerization of Styrene Effect of Tetrahydrofuran. *Can. J. Chem.* **1962**, *40*, 1564–1570.

(54) Worsfold, D. J.; Bywater, S. Anionic Polymerization of Isoprene. *Can. J. Chem.* **1964**, *42*, 2884–2892.

(55) Johnson, A. F.; Worsfold, D. J. Anionic copolymerization of styrene and butadiene. *Makromol. Chem.* **1965**, *85*, 273–279.

(56) Bywater, S.; Worsfold, D. J. The Effect of Dielectric Constant on the Rate of Anionic Polymerization. *J. Phys. Chem.* **1966**, *70*, 162–166.

(57) Quinebèche, S.; Navarro, C.; Gnanou, Y.; Fontanille, M. In situ mid-IR and UV-spectroscopies applied to the determination of kinetic parameters in the anionic copolymerization of styrene and isoprene. *Polymer* **2009**, *50*, 1351–1357.

(58) Natalello, A.; Werre, M.; Alkan, A.; Frey, H. Monomer Sequence Distribution Monitoring in Living Carbanionic Copolymerization by Real-Time 1 H NMR Spectroscopy. *Macromolecules* **2013**, *46*, 8467–8471.

(59) Natalello, A.; Alkan, A.; Tiedemann, P. von; Wurm, F. R.; Frey, H. Functional Group Distribution and Gradient Structure Resulting from the Living Anionic Copolymerization of Styrene and para-But-3-enyl Styrene. *ACS Macro Lett.* **2014**, *3*, 560–564.

(60) Hadjichristidis, N.; Pitsikalis, M.; Iatrou, H. Synthesis of Block Copolymers. In *Block Copolymers I*; Abetz, V., Ed.; Springer Berlin Heidelberg: Berlin, Heidelberg, 2005; pp 1–124.

(61) Vaughn, T. H.; Suter, H. R.; Lundsted, L. G.; Kramer, M. G. Properties of some newly developed nonionic detergents. *J. Am. Oil Chem. Soc.* **1951**, *28*, 294–299.

(62) Mankowich, A. M. Micellar Molecular Weights of Selected Surface Active Agents. *J. Phys. Chem.* **1954**, *58*, 1027–1030.

(63) Bates, C. M.; Maher, M. J.; Janes, D. W.; Ellison, C. J.; Willson, C. G. Block Copolymer Lithography. *Macromolecules* **2013**, *47*, 2–12.

(64) Schacher, F. H.; Rupar, P. A.; Manners, I. Functional Block Copolymers: Nanostructured Materials with Emerging Applications. *Angew. Chem. Int. Ed. Engl.* **2012**, *51*, 7898–7921.

(65) Sinturel, C.; Bates, F. S.; Hillmyer, M. A. High χ–Low N Block Polymers: How Far Can We Go? *ACS Macro Lett.* **2015**, *4*, 1044–1050.

(66) Leibler, L. Theory of Microphase Separation in Block Copolymers. *Macromolecules* **1980**, *13*, 1602–1617.

(67) Hiemenz, P. C.; Lodge, T. P. *Polymer chemistry*, 2. ed.; CRC Press: Boca Raton u.a., 2007.

(68) Bates, F. S.; Fredrickson, G. H. Block Copolymers—Designer Soft Materials. *Physics Today* **1999**, *52*, 32–38.

(69) Khandpur, A. K.; Foerster, S.; Bates, F. S.; Hamley, I. W.; Ryan, A. J.; Bras, W.; Almdal, K.; Mortensen, K. Polyisoprene-Polystyrene Diblock Copolymer Phase Diagram near the Order-Disorder Transition. *Macromolecules* **1995**, *28*, 8796–8806.

(70) Schmitt, B. J. Polymerlegierungen – Struktur, Morphologie, Eigenschaften. *Angew. Chem.* **1979**, *91*, 286–309.

(71) Bates, F. S.; Fredrickson, G. H. Block copolymer thermodynamics: Theory and experiment. *Annu. Rev. Phys. Chem.* **1990**, *41*, 525–557.

(72) Miyamoto, T.; Kodama, K.; Shibayama, K. Structure and properties of a styrene–butadiene–styrene block copolymer. *J. Polym. Sci. A-2 Polym. Phys.* **1970**, *8*, 2095–2103.

(73) Fredrickson, G. H.; Bates, F. S. Dynamics of Block Copolymers: Theory and Experiment. *Annu. Rev. Mater. Sci.* **1996**, *26*, 501–550.

(74) Storey, R. F.; Chisholm, B. J.; Choate, K. R. Synthesis and Characterization of PS-PIB-PS Triblock Copolymers. *J. Macromol. Sci., Part A* **1994**, *31*, 969–987.

(75) Michler, G. H.; Baltá-Calleja, F. J. *Nano- and Micromechanics of Polymers*; Carl Hanser Verlag GmbH & Co. KG: München, 2012.

(76) Northholt, M. Yielding and hysteresis of polymer fibres. *Polymer* **1995**, *36*, 3485–3492.

(77) van Melick, H.G.H.; Govaert, L. E.; Meijer, H.E.H. On the origin of strain hardening in glassy polymers. *Polymer* **2003**, *44*, 2493–2502.

(78) Morton, M.; McGrath, J. E.; Juliano, P. C. Structure-property relationships for styrene-diene thermoplastic elastomers. *J. polym. sci., C Polym. symp.* **1969**, *26*, 99–115.

(79) McCormick, H. W.; Brower, F. M.; Kin, L. The effect of molecular weight distribution on the physical properties of polystyrene. *J. Polym. Sci.* **1959**, *39*, 87–100.

(80) Yang, A. C. M.; Kramer, E. J.; Kuo, C. C.; Phoenix, S. L. Craze fibril stability and breakdown in polystyrene. *Macromolecules* **1986**, *19*, 2010–2019.

(81) Qiao, L.; Leibig, C.; Hahn, S. F.; Winey, K. I. Isolating the Effects of Morphology and Chain Architecture on the Mechanical Properties of Triblock Copolymers. *Ind. Eng. Chem. Res.* **2006**, *45*, 5598–5602.

(82) Dair, B. J.; Honeker, C. C.; Alward, D. B.; Avgeropoulos, A.; Hadjichristidis, N.; Fetters, L. J.; Capel, M.; Thomas, E. L. Mechanical Properties and Deformation Behavior of the Double Gyroid Phase in Unoriented Thermoplastic Elastomers. *Macromolecules* **1999**, *32*, 8145–8152.

(83) Matsuo, M.; Ueno, T.; Horino, H.; Chujyo, S.; Asai, H. Fine structures and physical properties of styrene-butadiene block copolymers. *Polymer* **1968**, *9*, 425–436.

(84) Morris, M. A.; Gartner, T. E.; Epps III, T. H. Tuning Block Polymer Structure, Properties, and Processability for the Design of Efficient Nanostructured Materials Systems. *Macromol. Chem. Phys.* **2017**, *218*, 1600513.

(85) Hodrokoukes, P.; Pispas, S.; Hadjichristidis, N. Controlling Micellar Properties of Styrene/Isoprene Copolymers by Altering the Monomer Arrangement along the Chain. *Macromolecules* **2002**, *35*, 834–840.

(86) Tsukahara, Y.; Nakamura, N.; Hashimoto, T.; Kawai, H.; Nagaya, T.; Sugimura, Y.; Tsuge, S. Structure and Properties of Tapered Block Polymers of Styrene and Isoprene. *Polym. J.* **1980**, *12*, 455–466.

(87) Kuan, W.-F.; Roy, R.; Rong, L.; Hsiao, B. S.; Epps III, T. H. Design and Synthesis of Network-Forming Triblock Copolymers Using Tapered Block Interfaces. *ACS Macro Lett.* **2012**, *1*, 519–523.

(88) Zaremski, M. Y.; Kalugin, D. I.; Golubev, V. B. Gradient copolymers: Synthesis, structure, and properties. *Polym. Sci. Ser. A* **2009**, *51*, 103–122.

(89) Hashimoto, T.; Tsukahara, Y.; Tachi, K.; Kawai, H. Structure and properties of tapered block polymers. 4. "Domain-boundary mixing" and "mixing-in-domain" effects on microdomain morphology and linear dynamic mechanical response. *Macromolecules* **1983**, *16*, 648–657.

(90) Roy, R.; Park, J. K.; Young, W.-S.; Mastroianni, S. E.; Tureau, M. S.; Epps, T. H. Double-Gyroid Network Morphology in Tapered Diblock Copolymers. *Macromolecules* **2011**, *44*, 3910–3915.

(91) Spontak, R.; Williams, M. Thermodynamics of tapered styrene-butadiene block copolymers. *J. Macromol. Sci., Part B* **1989**, *28*, 1–24.

(92) Hodrokoukes, P.; Floudas, G.; Pispas, S.; Hadjichristidis, N. Microphase Separation in Normal and Inverse Tapered Block Copolymers of Polystyrene and Polyisoprene. 1. Phase State. *Macromolecules* **2001**, *34*, 650–657.

(93) Seo, Y.; Brown, J. R.; Hall, L. M. Effect of Tapering on Morphology and Interfacial Behavior of Diblock Copolymers from Molecular Dynamics Simulations. *Macromolecules* **2015**, *48*, 4974–4982.

(94) Luo, M.; Brown, J. R.; Remy, R. A.; Scott, D. M.; Epps III, T. H. Determination of Interfacial Mixing in Tapered Block Polymer Thin Films: Experimental and Theoretical Investigations. *Macromolecules* **2016**, *49*, 5213-5222.

(95) Knoll, K.; Nießner, N. Styrolux and styroflex from transparent high impact polystyrene to new thermoplastic elastomers. *Macromol. Symp.* **1998**, *132*, 231–243.

(96) Wagner, D.; Knoll, K. Styrol-Butadien-Blockcopolymere. *Kunststoffe* **2010**, *9*, 2371–2379.

(97) Mori, Y.; Lim, L. S.; Bates, F. S. Consequences of Molecular Bridging in Lamellae-Forming Triblock/Pentablock Copolymer Blends. *Macromolecules* **2003**, *36*, 9879–9888.

(98) Hermel, T. J.; Hahn, S. F.; Chaffin, K. A.; Gerberich, W. W.; Bates, F. S. Role of Molecular Architecture in Mechanical Failure of Glassy/Semicrystalline Block Copolymers: CEC vs CECEC Lamellae. *Macromolecules* **2003**, *36*, 2190–2193.

(99) Bates, F. S.; Hillmyer, M. A.; Lodge, T. P.; Bates, C. M.; Delaney, K. T.; Fredrickson, G. H. Multiblock Polymers: Panacea or Pandora. *Science* **2012**, *336*, 434–440.

(100) Ryu, C. Y.; Ruokolainen, J.; Fredrickson, G. H.; Kramer, E. J.; Hahn, S. F. Chain Architecture Effects on Deformation and Fracture of Block Copolymers with Unentangled Matrices. *Macromolecules* **2002**, *35*, 2157–2166.

(101) Hermel, T. J.; Wu, L.; Hahn, S. F.; Lodge, T. P.; Bates, F. S. Shear-Induced Lamellae Alignment in Matched Triblock and Pentablock Copolymers. *Macromolecules* **2002**, *35*, 4685–4689.

(102) Keten, S.; Xu, Z.; Ihle, B.; Buehler, M. J. Nanoconfinement controls stiffness, strength and mechanical toughness of beta-sheet crystals in silk. *Nat. Mater.* **2010**, *9*, 359–367.

(103) Heim, M.; Keerl, D.; Scheibel, T. Spider silk: From soluble protein to extraordinary fiber. *Angew. Chem. Int. Ed. Engl.* **2009**, *48*, 3584–3596.

(104) Yarger, J. L.; Cherry, B. R.; van der Vaart, A. Uncovering the structure–function relationship in spider silk. *Nat. Rev. Mater.* **2018**, *3*, 1–11.

(105) Korotkov, A. A.; Shibayev, L. A.; Pyrkov, L. M.; Aldoshin, V. G.; Frenkel', S.I. The synthesis and investigation of hybrid polymers — I. Styrene and isoprene block polymers formed by catalytic polymerization in solution under the action of butyl lithium. *Polym. Sci. USSR* **1960**, *1*, 157–170.

(106) Korotkov, A. A.; Chesnokova, N. N.; Trukhmanova, L. B. Polymerization of isoprene with a butyl lithium catalyst. *Polym. Sci. USSR* **1960**, *1*, 10–20.

(107) Corbin, N.; Prud'Homme, J. Multiblock copolymers of styrene and isoprene. I. Synthesis and characterization. *J. Polym. Sci. Polym. Chem. Ed.* **1976**, *14*, 1645–1659.

(108) Corbin, N.; Prud'Homme, J. Multiblock copolymers of styrene and isoprene. II. Microstructure and dilute solution properties. *J. Polym. Sci. Polym. Phys. Ed.* **1977**, *15*, 1937–1951.

(109) Hadjiantoniou, N. A.; Krasia-Christoforou, T.; Loizou, E.; Porcar, L.; Patrickios, C. S. Alternating Amphiphilic Multiblock Copolymers: Controlled Synthesis via RAFT Polymerization and Aqueous Solution Characterization. *Macromolecules* **2010**, *43*, 2713–2720.

(110) Soeriyadi, A. H.; Boyer, C.; Nyström, F.; Zetterlund, P. B.; Whittaker, M. R. High-order multiblock copolymers via iterative Cu(0)-mediated radical polymerizations (SET-LRP): Toward biological precision. *J. Am. Chem. Soc.* **2011**, *133*, 11128–11131.

(111) Zhang, Q.; Collins, J.; Anastasaki, A.; Wallis, R.; Mitchell, D. A.; Becer, C. R.; Haddleton, D. M. Sequence-Controlled Multi-Block Glycopolymers to Inhibit DC-SIGN-gp120 Binding. *Angew. Chem.* **2013**, *125*, 4531–4535.

(112) Takada, K.; Ito, T.; Kitano, K.; Tsuchida, S.; Takagi, Y.; Chen, Y.; Satoh, T.; Kakuchi, T. Synthesis of Homopolymers, Diblock Copolymers, and Multiblock Polymers by Organocatalyzed Group Transfer Polymerization of Various Acrylate Monomers. *Macromolecules* **2015**, *48*, 511–519.

(113) Simula, A.; Nikolaou, V.; Anastasaki, A.; Alsubaie, F.; Nurumbetov, G.; Wilson, P.; Kempe, K.; Haddleton, D. M. Synthesis of well-defined α,ω-telechelic multiblock copolymers in aqueous medium: In situ generation of α,ω-diols. *Polym. Chem.* **2015**, *6*, 2226–2233.

(114) Romain, C.; Zhu, Y.; Dingwall, P.; Paul, S.; Rzepa, H. S.; Buchard, A.; Williams, C. K. Chemoselective Polymerizations from Mixtures of Epoxide, Lactone, Anhydride, and Carbon Dioxide. *J. Am. Chem. Soc.* **2016**, *138*, 4120–4131.

(115) Radlauer, M. R.; Fukuta, S.; Matta, M. E.; Hillmyer, M. A. Controlled synthesis of ABCA' tetrablock terpolymers. *Polymer* **2017**, *124*, 60–67.

(116) Zhu, Y.; Radlauer, M. R.; Schneiderman, D. K.; Shaffer, M. S. P.; Hillmyer, M. A.; Williams, C. K. Multiblock Polyesters Demonstrating High Elasticity and Shape Memory Effects. *Macromolecules* **2018**, *51*, 2466–2475.

(117) Engelis, N. G.; Anastasaki, A.; Whitfield, R.; Jones, G. R.; Liarou, E.; Nikolaou, V.; Nurumbetov, G.; Haddleton, D. M. Sequence-Controlled Methacrylic Multiblock Copolymers: Expanding the Scope of Sulfur-Free RAFT. *Macromolecules* **2018**, *51*, 336–342.

(118) Zhang, J.; Deubler, R.; Hartlieb, M.; Martin, L.; Tanaka, J.; Patyukova, E.; Topham, P. D.; Schacher, F. H.; Perrier, S. Evolution of Microphase Separation with Variations of Segments of Sequence-Controlled Multiblock Copolymers. *Macromolecules* **2017**, *50*, 7380–7387.

(119) Smith, S. D.; Spontak, R. J.; Satkowski, M. M.; Ashraf, A.; Heape, A. K.; Lin, J. S. Microphase-separated poly(styrene-b-isoprene)n multiblock copolymers with constant block lengths. *Polymer* **1994**, *35*, 4527–4536.

(120) Spontak, R. J.; Fung, J. C.; Braunfeld, M. B.; Sedat, J. W.; Agard, D. A.; Ashraf, A.; Smith, S. D. Architecture-Induced Phase Immiscibility in a Diblock/Multiblock Copolymer Blend. *Macromolecules* **1996**, *29*, 2850–2856.

(121) Rasmussen, K.; Kober, E. M.; Lookman, T.; Saxena, A. Morphology and bridging properties of (AB)n multiblock copolymers. *J. Polym. Sci. Part B: Polym. Phys.* **2003**, *41*, 104–111.

(122) Faber, M.; Voet, V. S. D.; Brinke, G. ten; Loos, K. Preparation and self-assembly of two-length-scale A-b-(B-b-A)n-b-B multiblock copolymers. *Soft Matter* **2012**, *8*, 4479-4485.

(123) Spontak, R. J.; Smith, S. D. Perfectly-alternating linear (AB)n multiblock copolymers: Effect of molecular design on morphology and properties. *J. Polym. Sci. Part B: Polym. Phys.* **2001**, *39*, 947–955.

(124) Watanabe, H.; Matsumiya, Y.; Sawada, T.; Iwamoto, T. Rheological and Dielectric Behavior of Dipole-Inverted (SIS) p -Type Multiblock Copolymers: Estimates of Bridge/Loop Fractions for Respective I Blocks and Effect of Loops on High Extensibility of Bridges. *Macromolecules* **2007**, *40*, 6885–6897.

(125) Matsumiya, Y.; Watanabe, H.; Takano, A.; Takahashi, Y. Uniaxial Extensional Behavior of (SIS)p-Type Multiblock Copolymer Systems: Structural Origin of High Extensibility. *Macromolecules* **2013**, *46*, 2681–2695.

(126) Matsushita, Y.; Mogi, Y.; Mukai, H.; Watanabe, J.; Noda, I. Preparation and morphology of multiblock copolymers of the (AB)n type. *Polymer* **1994**, *35*, 246–249.

(127) Wu, L.; Cochran, E. W.; Lodge, T. P.; Bates, F. S. Consequences of Block Number on the Order−Disorder Transition and Viscoelastic Properties of Linear (AB) n Multiblock Copolymers. *Macromolecules* **2004**, *37*, 3360–3368.

Chapter 2: One-step block copolymer synthesis

2.1 One-Step Block Copolymer Synthesis versus Sequential Monomer Addition: A Fundamental Study Reveals that one Methyl Group Makes a Difference

Eduard Grune,[a,c,+] Tobias Johann,[a,d,+] Michael Appold,[b] Christian Wahlen,[a] Jan Blankenburg,[a,c] Daniel Leibig,[a,c] Axel H. E. Müller,*[,a] Markus Gallei,*[,b] Holger Frey*[,a]

[a] Institute of Organic Chemistry, Johannes Gutenberg-University, Duesbergweg 10-14, 55128 Mainz (Germany); E-mail: hfrey@uni-mainz.de

[b] Macromolecular Chemistry Department, Technische Universität Darmstadt, Alarich-Weiss-Str. 4, 64287 Darmstadt (Germany)

[c] Graduate School Material Science in Mainz, Staudingerweg 9, 55128, Mainz (Germany)

[d] Max Planck Graduate Center, Staudingerweg 9, 55128, Mainz (Germany)

[+]*The first two authors contributed equally*

Published in *Macromolecules* **2018**, 51, 3527−3537.

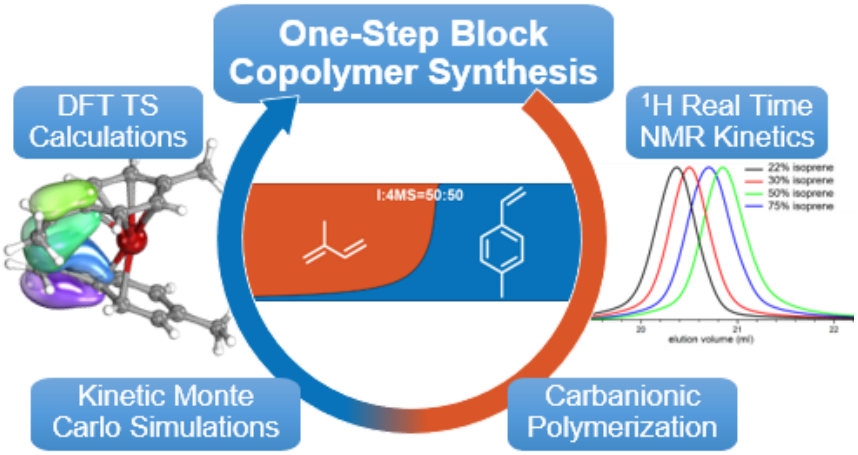

2.1.1 Abstract

Block copolymers of polyisoprene and polystyrene are key materials for polymer nanostructures as well as for several commercially established thermoplastic elastomers. In a combined experimental and kinetic Monte Carlo simulation study, the direct (i.e. statistical) living anionic copolymerization of a mixture of isoprene (I) and 4-methylstyrene (4MS) in non-polar media was investigated on a fundamental level. *In-situ* ^{1}H-NMR spectroscopy enabled to directly monitor gradient formation during the copolymerization and to determine the nature of the gradient. In addition, a precise comparison with the established copolymerization of isoprene and styrene (I/S) was possible. Statistical copolymerization in both systems leads to tapered block copolymers due to an extremely slow crossover from isoprene to the styrenic monomer. For the system I/4MS, the determination of the reactivity ratios shows highly disparate values with $r_{I} = 25.4$ and $r_{4MS} = 0.007$, resulting in a steep gradient of the comonomer composition. The rate constants determined from online NMR studies were used for a kinetic Monte Carlo simulation, revealing structural details, such as the distribution of the homopolymer sequences for both blocks, which are a consequence of the peculiar kinetics of the diene/styrene systems. DFT calculations were used to compare the established copolymerization of isoprene and styrene with the isoprene/4-methylstyrene system. A variety of gradient copolymers differing in molecular weight and monomer feed composition were synthesized, confirming strong microphase segregation as a consequence of the block like structure. The one-pot synthesis of such tapered block copolymers, avoiding high vacuum or break-seal techniques is a key advantage for the preparation of ultrahigh molecular weight block copolymers ($M_n > 1.5 \times 10^6$ g/mol) in one synthetic step. These materials show microphase-segregated bulk structures like diblock copolymers prepared by sequential block copolymer synthesis. Due to the living nature of the tapered block copolymer structures, a vast variety of complex structures is accessible by the addition of further monomers or monomer mixtures in subsequent steps.

2.1.2 Introduction

Living anionic polymerization is still state of the art for the preparation of highly defined block co- and terpolymers with low molecular weight dispersity and high

molecular weights, commonly by sequential addition of the monomers.[1,2] Block copolymer architectures play a key role in current polymer research for a vast variety of commercial and prospective applications that capitalize on their nanophase-segregated structures, such as thermoplastic elastomers, compatibilization of polymer blends, block copolymer lithography, nanomedicine, nano-reactors and highly ordered nanopatterns.[3-9] Eminent examples for block copolymers established on large technical scale are *Kraton*®, high impact polystyrene (HIPS) and more advanced, extremely elastic or tough thermoplastic materials like *Styroflex*® and *Styrodur*®.[10-12] The synthesis of block copolymers relies either on a living polymerization technique with consecutive addition of both monomers or highly efficient coupling reactions of prefabricated blocks.[13,14] In both cases several reaction steps are required, increasing the risk of irreversible termination, leading to homopolymer impurities. Thus, one-step strategies for the preparation of block copolymers are desirable. Direct, i.e. statistical copolymerization of a monomer pair using living anionic copolymerization can afford random or gradient monomer sequences,[15] depending on the reactivity ratios of the respective monomers. Early works in the 1960s regarding the direct carbanionic copolymerization of isoprene (I) and styrene (S) in hydrocarbon solvents already suggested a block copolymer like structure that was (erroneously) attributed to strongly differing monomer reactivities.[16] Johnson et al. observed a correlation between homopolymerization and crossover reaction, concluding that a gradual incorporation of the less reactive monomer occurred instead of a sharp transition between the blocks.[17,18] This type of block copolymer was designated “tapered block copolymer” and studied in several groundbreaking works, demonstrating the materials’ capability to undergo phase separation.[19,20]

Nevertheless, tapered copolymers of isoprene and styrene differ in their mechanical properties from the corresponding block copolymers prepared by sequential monomer addition. Hadjichristidis et al. demonstrated that both shape and length of the taper define the properties of the copolymers and can be used to precisely adjust mechanical properties like the glass transition, T_g, and the order-disorder transition temperature, T_{ODT}.[21,22] In elegant works of Epps and coworkers, deliberate manipulation of the tapered section was used to modify the nano-segregated morphologies both in bulk and in thin films.[23-26] Alteration of the monomer gradient

to manipulate the phase segregation and consequently, macroscopic materials properties requires the ability to adjust both length and shape of the gradient. Currently, there are three approaches to manipulate the tapered section of I/S gradient copolymers: (i) the use of traces of THF as a randomizer, (ii) sequential addition of the pure monomers or monomer mixtures and (iii) specific monomer addition protocols using automated syringes.[20,21,25]

In this work we introduce a chemical approach to lower the reactivity of styrene, capitalizing on simple methyl substitution, aiming at deliberate manipulation of the gradient. For a detailed understanding of the impact on copolymerization kinetics and resulting copolymer structures, we have also reinvestigated the well-known copolymerization of I/S by in-situ monitoring via ^{1}H-NMR spectroscopy to compare it with the copolymerization of isoprene and 4-methylstyrene (4MS). *In-situ* monitoring of a carbanionic copolymerization permits "mapping" the gradient structure of the growing copolymer chains. Especially near-infrared (NIR) and medium-infrared (MIR) in combination with UV-vis spectroscopy was employed for this purpose.[27,28]

In 2013 our group introduced real-time ^{1}H NMR kinetics studies as a key method to determine reactivity ratios in the living carbanionic polymerization of vinyl monomers.[29] Online monitoring of monomer consumption during the living polymerization in a sealed NMR tube enables the determination of the reactivity ratios by common evaluation methods like the Fineman-Ross, Kelen-Tüdös and Meyer-Lowry approaches.[30-32] The two reactivity ratios, r_1 and r_2 for a monomer pair define the relative rates of homopolymerization *vs*. crossover, i.e. copolymerization.[33] Since termination and transfer are absent in a living copolymerization, no compositional drift (non-homogeneity of first order) is observed for the polymer chains formed. Instead, the comonomer composition along the chain reflects the reactivity ratios (non-homogeneity of second order). Carbanionic copolymerization of isoprene and styrene (I/S) in a non-polar medium, such as cyclohexane, represents this type of monomer system with markedly different reactivity ratios (r_I = 12.8, r_S = 0.051).[18,27]

Here we present a fundamental study of the copolymerization of isoprene and 4-methylstyrene (4MS), with an in depth characterization of the tapered block copolymers formed, capitalizing on *in-situ* NMR kinetics, detailed kinetic calculations, kinetic Monte-Carlo simulation as well as DFT calculations. In this context, also the highly established monomer combination of isoprene and styrene is re-evaluated

from a fundamental perspective. The combination of methods employed also sheds light on differences in comparison to block copolymers generated by sequential addition of the monomers isoprene and 4MS, demonstrating that the peculiar kinetics of the diene/styrene copolymerization has to be considered also for sequential block copolymer synthesis, particularly with respect to the succession of the synthesis of the respective blocks.

2.1.3 Results and Discussion

2.1.3.1 Determination of reactivity ratios and propagation rate constants using real-time 1H-NMR

The determination of reactivity ratios for the statistical copolymerization commonly relies on terminating a series of polymerization reactions with different monomer feed at low conversion and characterization of the residual monomer concentration. Alternatively, samples can be withdrawn, while the polymerization proceeds.[33] Due to the high sensitivity of carbanions, this technique is not applicable to the living carbanionic copolymerization without irreversible termination of living chain ends.

Aiming at tapered block copolymers with a short gradient, we have studied the copolymerization of isoprene (I) with 4-methylstyrene (4MS), a readily available styrene derivative. For comparison, the reactivity ratios of copolymers of styrene (S) and isoprene were also determined in cyclohexane-d_{12}, using real-time ^{1}H-NMR spectroscopy with *s*ec-butyllithium as an initiator at 23 °C. The reactivity ratios determined from in-situ NMR for styrene and isoprene (r_I= 11.0, r_S = 0.049, see Supp. Inf., Figures S1, S2, Table S1) are in good agreement with literature values determined by other methods.[16,18] In case of copolymerization of 4MS, a styrene derivative with slightly enhanced electron density due to the methyl group, with isoprene highly divergent reactivity parameters (r_I = 25.4, r_{4MS} = 0.007) were observed (Supp. Inf., Figures S3, S4). For this monomer pair Figure 1 demonstrates the rapid incorporation of isoprene in the copolymers and formation of a second homopolymer block P4MS in the subsequent stage after full isoprene consumption.

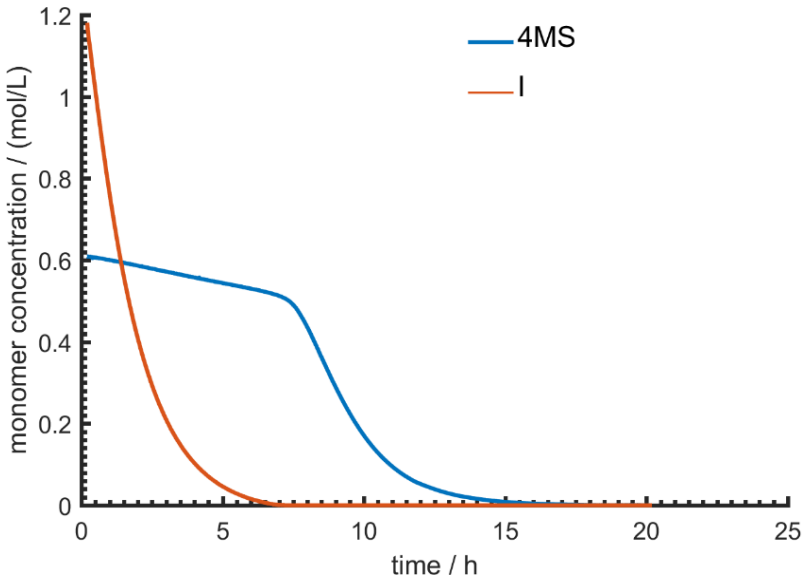

Figure 1: Plot of the single monomer concentrations versus time for the copolymerization of 4-methylstyrene (4MS, blue, c_0 = 0.61 mol/L) and isoprene (red, c_0 = 1.18 mol / L) in cyclohexane-d12 determined from in-situ NMR monitoring.

Besides the reactivity ratios r_1 and r_2, the homopolymerization rate constants play a crucial role in understanding the resulting gradient microstructure of the copolymers formed (*vide infra*). The homopolymerization rate constant of 4MS in cyclohexane-d_{12} was also determined by real-time ^{1}H-NMR spectroscopy in a sealed NMR tube at 23 °C. Taking into account that the P4MS chain ends are present as dimers, the propagation of 4MS can be described by the following kinetic equation in analogy to work of Fontanille *et al.*[27]

$$\frac{\mathrm{d}[4\mathrm{MS}]}{\mathrm{d}t} = k_{4\mathrm{MS}} \cdot [4\mathrm{MS}] \cdot [\mathrm{P4MSLi}]^{1/2} \qquad (1.1)$$

After fast initiation the polymerization follows pseudo first-order kinetics. Therefore, the apparent propagation rate constant, k, can be determined using a logarithmic representation of the measured values and linear regression (Figure S5, equations 1.1 and 1.2).

$$\ln\left(\frac{[4MS]_0}{[4\mathrm{MS}]_t}\right) = k_{4\mathrm{MS}} \cdot [\mathrm{BuLi}]_0^{1/2} \cdot t \qquad (1.2)$$

The apparent propagation rate constant of 4MS (k4MS = 1.26x10-3 (L/mol)1/2s-1) was determined as well. The homopolymerization rate constant of styrene in cyclohexane at 40 °C (kS,40°C = 2.4x10-2 (L/mol)1/2s-1) was reported by Fontanille et al.[27] Direct comparison of styrene and 4MS can be achieved by applying the Arrhenius equation using the reported activation energy and adjusting the rate constant of styrene k_S to 23°C (kS,23°C = 6.4x10-3 (L/mol)1/2s-1). Thus, the styrene homopolymerization rate is 5.1 times higher than the homopolymerization rate of 4MS. These different reactivities can be attributed to the small positive inductive effect of the methyl group in para position, which both decreases monomer reactivity and increases the reactivity of the living chain end. This will be discussed in detail below.

2.1.3.2 DFT calculations

To obtain theoretical insight into the effect of the *para*-methyl group on the reactivity of the styrene derivative 4MS, we performed DFT calculations of the polymerization pathway of styrene and 4MS. Since transition states are inaccessible for direct observation, e.g., by NMR spectroscopy, theoretical considerations by means of quantum chemical calculations can give valuable insight regarding the polymerization on a molecular level. In recent work, Morita and Van Beylen[34] reported an approach to model the total reaction pathway starting from polystyryllithium dimers to form a monomer-polystyryllithium precursor complex, the propagation transition state and finally the extended polymer product. Following this approach, we performed DFT calculations (B3LYP-D3-gCP/def2-TZVP//B3LYP-D3-gCP/def2-TZVP) to investigate the reaction pathway of the homopolymerization both for styrene and 4MS. Furthermore, the reactions of both monomers with H-Li were calculated to compare the resulting partial charges as a rough estimate of monomer reactivities.

In line with expectation, styrene exhibits a lower partial charge (-0.3686 e) at the vinyl β-carbon compared to 4MS (-0.3751 e). This position is attacked in the propagation step and can therefore be used for an assessment of monomer reactivity (Figure 2).

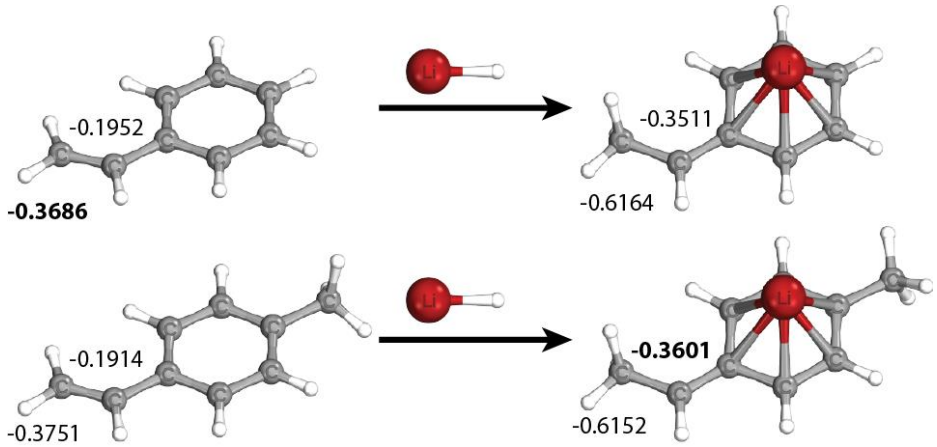

Figure 2: 3D representation of the reaction of styrene (top) and 4MS (bottom) with H-Li to form H-S-Li or H-4MS-Li respectively. The annotated values show the corresponding partial charge calculated by the NBO method.[35,36]

After addition of H-Li as a model compound for carbanionic propagation, H-4MS-Li shows higher partial charge (-0.3601 e) at the vinyl α-carbon compared to H-S-Li (-0.3511 e). From these calculations styrene can be expected to be more easily attacked by nucleophiles, resulting in higher reactivity as compared to 4MS. In contrast, poly(4-methylstyryl)lithium (P4MS-Li) chain ends can be expected to be more reactive than polystyryllithium chain (PS-Li) ends. These estimates can be further verified by investigating the reaction pathway for propagation of styrene and 4MS (Figure S6, Table S2). As expected, unimeric H-4MS-Li shows higher dissociation energy than the corresponding H-S-Li unimer. Even though propagation transition states show similar activation energies, the homopolymerization of 4MS (51.1 kJ/mol) requires slightly higher activation energy for propagation as compared to styrene (50.1 kJ/mol). One has to take into account that these calculated energies are electronic energies only and do not include entropic or solvent effects. In case of the free energy a difference of 5.8 kJ/mol was calculated, which translates to a rate constant ratio of styrene to 4MS of approximately 10. We note that these calculations are in good agreement with our experimentally determined differences of the reactivity of styrene and 4MS.

2.1.3.3 Comparison of the tapered microstructure of 4MS/I and S/I copolymers

The microstructure of 4MS/I and S/I copolymers, i.e., the shape and steepness of the taper plays a crucial role for the mechanical properties of the respective copolymers.[21-23] Real-time ^{1}H-NMR kinetics gives access to the mean microstructure by determination of the resulting rate constants and mean incorporation rates.

Direct comparison of the copolymerization rate constants (Table 1) reveals that the probability for crossover from polyisoprenyllithium (PI-Li) chain ends towards styrene in the I/S system is approximately double compared to PI-Li and 4MS. On the other hand, the crossover from PS-Li to isoprene is 40% less probable than from P4MS-Li chain ends. This explains that in case of the I/4MS monomer system the formation of long homosegments consisting of isoprene and 4MS, respectively, is more likely and therefore formation of a block copolymer with a steep monomer gradient (i.e., a short taper) can be expected.

Table 1: Reaction rate constants for the S/I and 4MS/I system determined from *in-situ* NMR

System	$10^{-4}\ k_{II}$ $(L/mol)^{1/4}s^{-1}$	$10^{-5}\ k_{I(4M)S}$ $(L/mol)^{1/4}s^{-1}$	$10^{-3}\ k_{(4M)S(4M)S}$ $(L/mol)^{1/2}s^{-1}$	$k_{(4M)SI}$ $(L/mol)^{1/2}s^{-1}$	r_I[b]	$r_{(4M)S}$[b]
I / S[a]	6.12	5.57	6.39	0.121	11.0	0.053
I / 4MS[b]	6.12	2.41	1.26	0.180	25.4	0.007

a: Values for styrene (k_{SS}) and isoprene (k_{II}) taken from Fontanille et al.[27] and corrected to 23°C; b: this work.

The different gradient structures of I/S and I/4MS can be directly derived from the real-time ^{1}H-NMR kinetic measurements (Figure 3, S1-4). The overall mean monomer composition, F, versus total conversion reveals that in the initial stages primarily isoprene is consumed, and following a steep gradient, a pure block of P4MS is formed. Compared to the I/S system the gradient of I/4MS copolymerization is considerably steeper (Figure 3, bottom).

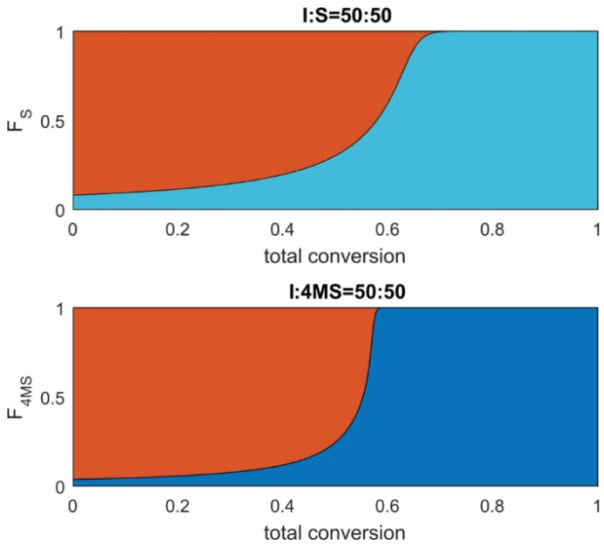

Figure 3: Reactivity ratios obtained from real-time ^{1}H-NMR measurements enable to simulate plots of the monomer incorporation profiles of isoprene (red) and styrene (light blue) or 4MS (blue) versus total conversion, reflecting the mean composition (F) of the polymer chains formed.

The determined reactivity ratios permit to simulate monomer incorporation profiles for any monomer feed composition (cf. Supp. Inf. S7, S8 for different initial monomer feeds).

2.1.3.4 Kinetic Monte-Carlo Simulation of the formation of tapered block copolymer chains

The real-time ^{1}H-NMR monitoring of copolymerization kinetics provides excellent access to the overall mean monomer composition in the polymer chains formed at any conversion. The Mayo-Lewis equation is a function of only two reactivity parameters and monomer concentrations.[33] From this globally derived equation no detailed insights regarding the monomer composition distribution can be extracted. The explicit sequence length distribution within the copolymers is not accessible with the currently available experimental methods. Broadbelt and coworkers developed a comprehensive kinetic Monte Carlo (KMC) model to describe the chemical composition distribution (CCD) and segment length distribution of copolymers by tracking the monomer-by-monomer sequence of each chain.[37] In particular, the segment length distribution can provide an excellent description of the gradient structure of copolymers. The KMC of the model of Broadbelt et al. was primarily

developed for radical polymerization, taking into account termination reactions, but no aggregation phenomena. In contrast, in an ideal anionic copolymerisiation no termination is present, but the copolymerization kinetics of isoprene with styrene derivatives is strongly dependent on the aggregation behavior of the living chain ends. Worsfold and Bywater proposed tetrameric aggregated PI-Li as the dominant species in non-polar solvents at not extremely low chain-end concentration. For PS-Li chain ends the presence of a dimeric species is widely accepted.[18] However, only unimeric chain ends, which form a dynamic equilibrium with their aggregated counterpart, are assumed to propagate. The following kinetic equations for copolymerization of 4MS and isoprene can be formulated in analogy to the equations for styrene and isoprene used by Fontanille et al. (Supp. Inf. Equation set S2).[27] To reveal the exact structure of the gradient and define the length of the tapered section both in the S/I and 4MS/I copolymers, we developed a KMC model based on the kinetic equations (Equation Sets S1 and S2). This permits to illustrate the monomer-by-monomer sequence of each chain, thus enabling evaluation of mean segment length and segment length distribution. Due to the influence of initiator concentration, degree of polymerization and monomer ratio, copolymers consisting of 200 units each of isoprene and styrene (or 4MS, respectively) were selected as a typical sample to elucidate the structure of the gradient.

Table 2: Calculated number-average ($\langle N \rangle_n$) and weight-average ($\langle N \rangle_w$) segment lengths for isoprene, styrene and 4MS monomer units obtained from Monte-Carlo simulation.

System	$\langle N_I \rangle_n$	$\langle N_I \rangle_w$	$\langle N_I \rangle_w / \langle N_I \rangle_n$	$\langle N_{4MS} \rangle_n$	$\langle N_{4MS} \rangle_w$	$\langle N_{4MS} \rangle_w / \langle N_{4MS} \rangle_n$
I / S	4.6	11.9	2.55	4.5	80.4	18.06
I / 4MS	7.8	23.9	3.06	7.4	141.3	19.22

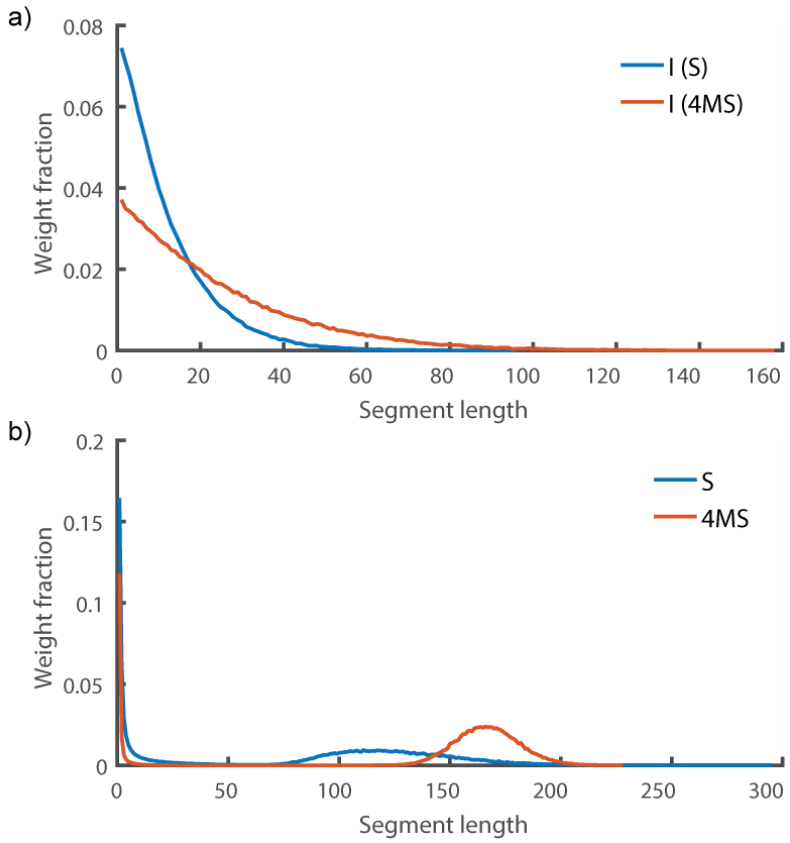

Figure 4: Plot of segment length weight distribution obtained from the KMC simulation for tapered copolymers of I/S (blue line) and I/4MS (red line); a) distribution for isoprene; b) distribution for styrene / 4MS. Simulation conditions: DP_n(I) = DP_n(S) = 200.

The segment length weight distribution is shown in Figure 4. The segment length is defined as the number of consecutive monomer units of one type without interruption by the other monomer unit. For both tapered block copolymers the non-interrupted isoprene homopolymer segments are rather small, i.e., below 50 (for I/S) or 100 (for I/4MS) units (Figure 5a) with a number average at 4.6 (I/S) and 7.8 (I/4MS) (Table 2). The mean weight average length of the isoprene segments is 11.9 for I/S and 23.9 for I/4MS. These segments are nearly exclusively interrupted by exactly one unit of S or 4MS (see bimodal distribution in Figure 5b with one maximum at $\langle N_{4MS} \rangle_w$ = 1). The reason for this high discrepancy between number and weight average is that at the beginning nearly all chains start with the largest isoprene segment (Figure 6). This is attributed to the ratio of the rates of isoprene

homopolymerization, R_{II}, versus crossover reaction rate, R_{I4MS}, (equation 2.1 and 2.2, same equations apply for styrene).

$$R_{II} = k_{II} \cdot [I] \cdot [PILi]^{1/4} \quad (2.1)$$

$$R_{I4MS} = k_{I4MS} \cdot [4MS] \cdot [PILi]^{1/4} \quad (2.2)$$

At the start of the reaction the monomer concentrations can be assumed to equal the initial feed. Therefore, in case of equivalent feed of comonomers, the initial segment length equals the reactivity ratio r_I (equation 2.3).

$$\frac{R_{II}}{R_{I4MS}} = \frac{k_{II}}{k_{I4MS}} = r_I \quad (2.3)$$

With increasing incorporation of isoprene, the average PI segment length decreases, leading to a gradient. Following the gradient part of the chain, a nearly pure block of P4MS (or PS, respectively) is formed, which is only rarely interrupted by isoprene residues. In case of styrene a mean weight-average of 80.4 and 141.3 units, respectively, for 4MS is calculated (Table 2). As shown in Figure 4b the segment length distribution of S and 4MS is split into two separated parts consisting of either one unit or a distribution with a maximum of 166 units for 4MS and 115 for S. This leads to the conclusion that 4MS or S is mainly distributed as one large block at the end of the chains or as single units that disrupt the isoprene block. The segment length distribution of the 4MS block is less broadened compared to styrene in the I/S system. Considering these results a shorter gradient and thus a highly block like copolymer is confirmed for the I/4MS system. Both the isoprene- and 4MS homosegments are larger and less frequently interrupted.

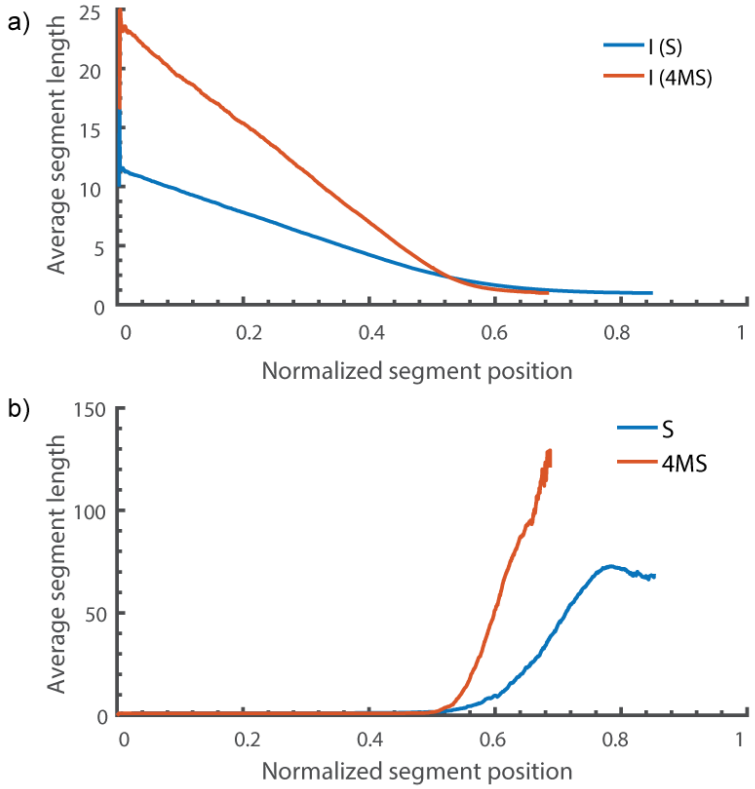

Figure 5: Plot of average segment length versus normalized segment position (relative position of the start of the segment) for I/S (blue lines) and I/4MS (red lines). a) plot for isoprene; b) plot for styrene (blue) and 4MS (red), respectively.

2.1.3.5 Synthesis of tapered and sequential block copolymers of isoprene and 4-methylstyrene

Based on the kinetics and simulation results, several series of copolymers were prepared both in statistical copolymerization reactions and by conventional sequential monomer addition. Our observations regarding the monomer sequence motivate the fundamental question, whether the tapered I/MS copolymers with the steep gradient determined by in-situ NMR kinetics may actually be viewed as block copolymers rather than gradient structures. Commonly an enhancement of phase mixing of two incompatible blocks is observed with increasing gradient length. Shortening the tapered intermediate segment results in a reduced compatibilization effect, diminishing the differences between block copolymers and tapered copolymers prepared by statistical copolymerization.[21,22,38] To elucidate the consequences of the block like nature of copolymers based on I/4MS, a comparison with

the corresponding block copolymers synthesized by sequential monomer addition in two steps is important. Several gradient and block copolymers varying in composition and molecular weight were prepared by anionic copolymerization and examined by SEC, ^{1}H-NMR and DSC (Table 3 and Supp. Inf.: Figures S9-S16 and Table S3). We emphasize that all polymers were prepared in a glovebox or in Schlenk flasks, avoiding high-vacuum or break-seal techniques. Except for the low molecular weight samples 10-12 all examined copolymers exhibit two glass transitions, indicating phase separation, regardless of their synthesis in a statistical one-pot or sequential (i.e., conventional) two-step copolymerization, as summarized in Table 3.

Table 3: One-step tapered block copolymers (-*co*-) and sequential block copolymers (-*b*-) based on isoprene (I) and 4-methylstyrene (4MS).

Entry	Polymer composition[a]	Isoprene content [mol-%]	Target M_n [kg/mol]	M_n (SEC)[b] [kg/mol]	$Đ = M_w/M_n$	v_I[c] [%]	T_g[d] (I/*4MS*) [°C]
1	P(I-*co*-4MS)	50	40	38.6	1.09	39	-50/86
2	PI-*b*-P4MS	50	40	46.5	1.09	41	-65/89
3	P(I-*co*-4MS)	30	60	76.3	1.12	24	-46/93
4	PI-*b*-P4MS	30	60	71.1	1.14	23	-70/97
5	P(I-*co*-4MS)	50	60	55.8	1.12	40	-51/102
6	PI-*b*-P4MS	50	60	76.6	1.10	39	-65/98
7	P(I-*co*-4MS)	50	400	360	1.07	40	-55/99
8	P(I-*co*-4MS)	60	130	133	1.09	50	-52/115
9	P(I-*co*-4MS)	90	1300	1250	1.32	86	-54/116
10	P(I-*co*-4MS)	50	2.5	4.4	1.20	29	26
11	PI-*b*-P4MS	50	2.5	3.8	1.12	30	-/-
12	P4MS-*b*-PI	50	2.5	2.4	1.06	40	20
13	P(I-*co*-4MS)	50	5	4.7	1.16	30	-15/21
14	PI-*b*-P4MS	50	5	5.4	1.09	36	-41/11
15	P4MS-*b*-PI	50	5	3.7	1.06	40	-47/6
16	P(I-*co*-4MS)	50	10	7.4	1.13	38	-31/16
17	PI-*b*-P4MS	50	10	8.6	1.09	39	-43/21
18	P4MS-*b*-PI	50	10	7.4	1.07	39	-43/23

[a] Polymer composition and preparation route with targeted isoprene and 4MS content: "*b*" sequential addition, "*co*" direct copolymerization; [b] Size exclusion chromatography (SEC) in THF at 25 °C, [c] calculated volume fractions based on densities from reference 39 [d] via differential scanning calorimetry (DSC).

2.1.3.6 Comparison of synthetic approaches for the preparation of I/4MS copolymers

As shown in Figure 6, the different synthetic approaches for the block copolymer synthesis lead to a significant effect on the resulting molecular weight distribution, leading to a distinct deviation from an ideal Poisson distribution (dashed line). Only when the P4MS block is prepared first, followed by consecutive addition of isoprene to generate P4MS-*b*-PI, low dispersities approaching the theoretical limit are obtained. Both for the direct copolymerization of isoprene with 4MS and for the sequential addition of 4MS to a living polyisoprenyllithium block broadening of the molecular weight distribution is observed. To shed light on these observations, we considered the initiation step of the second P4MS or PI block and the crossover reaction from an isoprene chain-end towards 4MS based on the kinetic equations, employing kinetic Monte Carlo simulation (*vide infra*).

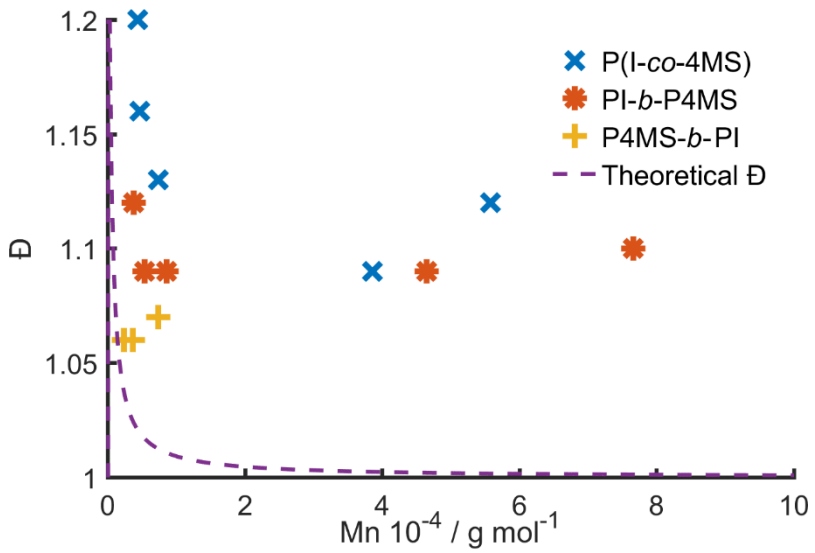

Figure 6: Dispersity *Đ* of prepared low to mid molecular weight (Mn < 105 g/mol) (block) copolymers with 50 mol-% isoprene content versus molecular weight of the polymer.

One key requirement for a narrow molecular weight distribution is that the initiation rate is considerably faster than the rate of chain propagation, as it was shown mathematically by Gold long ago.[40] Slow initiation leads to broadening of the molecular weight distribution, depending on the ratio k_i/k_p and the desired DP_n.

Considering the crossover rate constants versus the homopolymerization rate constants of isoprene and 4MS (Table 1), fast initiation of the second block only occurs for the crossover starting from a living P4MS-Li block to the isoprene monomer. In this case the rate of initiation is approximately 300 times faster than the propagation rate (k_{II}/k_{4MSI} = 294), ensuring conditions of a controlled polymerization for both blocks.

One has to consider that every direct copolymerization of two monomers with strongly differing reactivity ratios exhibits low crossover rates to the less favored monomer. Assuming reasonable propagation rates of both monomers on same order of magnitude, this inevitably leads to slow initiation rate compared to the propagation rate (k_{12}/k_{22}) (equation 3.1 and 3.2), thus hampering the controlled nature of an anionic polymerization.

$$r_1 = \frac{k_{11}}{k_{12}} \gg 1 \qquad \text{and} \qquad k_{11} \approx k_{22} \tag{3.1}$$

$$\frac{1}{r_1} = \frac{k_{12}}{k_{11}} \approx \frac{k_{12}}{k_{22}} \ll 1 \tag{3.2}$$

2.1.3.7 Monomer composition distribution

To further elaborate via theoretical approaches whether tapered block copolymers of isoprene and 4MS obtained by statistical copolymerization can be compared to block copolymers prepared by common sequential monomer addition, we utilized our developed KMC model to predict the monomer composition distribution. In addition, we aim at elucidating to which extent the polymerization of the second block is controlled. The simulated monomer compositions of the three different synthesis approaches are shown in Figure 7 and clearly demonstrate that the order of the monomer additions – diene or styrene derivative first - plays a crucial role. As expected, the 4MS-first approach produces a narrow molecular weight distribution of 4MS and isoprene with nearly invariable monomer composition (DP_n(I) / DP_n(total) ~ 0.5) (Figure 7a). The dispersity of the P4MS block calculated from the simulation displayed in Figure 7 is 1.02 for a sequential copolymerization, when the P4MS block is prepared first (rapid crossover).

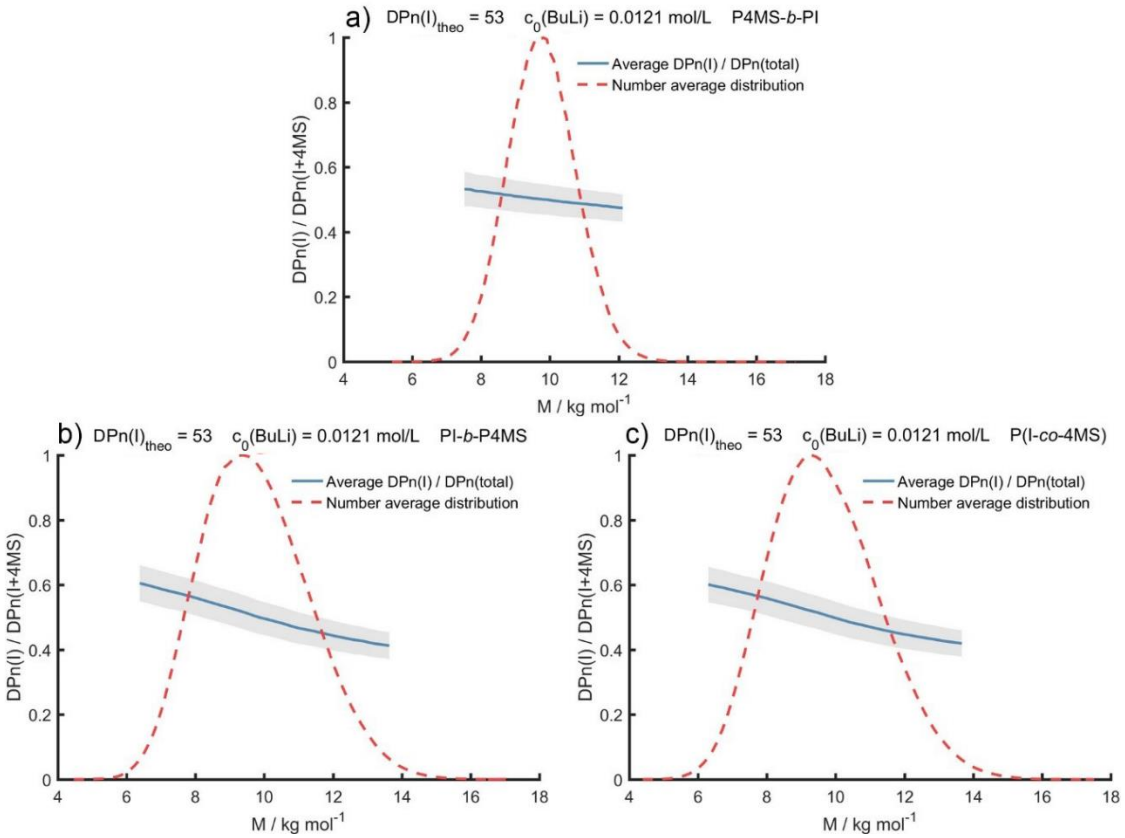

Figure 7: Average ratio of the degree polymerization of isoprene (DP_n(I)) to the total DP_n (blue) versus total molecular weight, simulated for the synthesized samples with molecular weight of 10 kg/mol (Table 3). The shaded area shows the standard deviation of the average DP_n(I) / DP_n(total) ratio. The red curve shows the normalized number-average distribution of the simulated copolymers. a) Sequential addition of (i) 4MS followed by (ii) isoprene; b) sequential addition of (i) isoprene followed by (ii) 4MS. c) Statistical copolymerization of 4MS and isoprene to form a tapered block copolymer.

However, if the PI block is generated first, the sequential approach leads to a simulated dispersity of 1.056 for the P4MS block. Remarkably, this is exactly the same result as obtained for the direct (statistical) copolymerization of the equimolar I/4MS mixture.

The mean isoprene content of the P4MS-*b*-PI block copolymer exhibits only a subtle change as a function of molecular weight. The ideal living anionic copolymerization should lead to an invariant mean monomer composition of the copolymer without any

dependence on the molecular weight. In this ideal case only, the arrangement of monomer units changes within the chain in dependence of the reactivity ratios. However, in both figures 7b and 7c broadened molecular weight distributions are observed, in agreement with the experimental results. A distinct drift of the chemical monomer composition over the molecular weight can be seen. It is remarkable that virtually no difference of the molecular weight distribution and the respective drift of the monomer composition between the statistical copolymerization of 4MS and isoprene and the sequential addition of 4MS to a PILi macroinitiator is detectable. Thus, the direct copolymerization of 4MS and isoprene may be considered to be initiated by a PILi macroinitiator, which is interrupted by 4MS in several places, but essentially follows the same kinetics as the conventional two-step approach. In both cases the crossover rate is rather slow (see Table 1). Therefore, not all chains start their growth at the same time to form the second P4MS block. This leads to inhomogeneous growth of the P4MS block, resulting in increased 4MS content at higher molecular weights. Due to statistics and mass conservation, some chains lack 4MS and therefore show increased isoprene content and lower molecular weights.

The compositional drift resulting from the slow crossover from PI-Li to 4MS can also be evaluated by comparing the distribution of isoprene and 4MS units to an ideal Poisson distribution (Figure 9). The distributions have been simulated for three synthesized polymers with a molecular weight of 2.5, 5 and 10 kg/mol according to the experimental conditions. In all cases isoprene polymerization affords a Poisson distribution. The distributions of 4MS are broader than the ideal Poisson distribution except for the case of P(4MS-*b*-I), leading to a broadened overall molecular weight distribution. This is also observed experimentally by slightly increased dispersity values (Figure 6 Table 3, see above) of these polymers. Comparing experimental values with simulation results, one has to consider that at higher molecular weights increased polydispersity indices are also influenced by impurities in addition to kinetic effects.

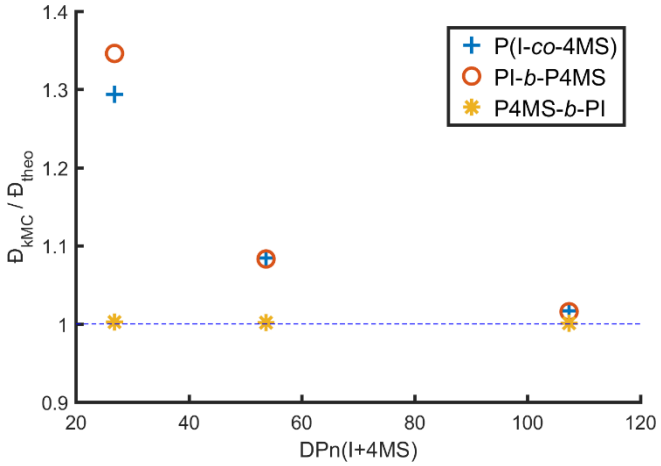

Figure 8: Comparison of the dispersity of the simulated monomer distribution ($Đ_{kMC}$) with ideal Poisson distribution ($Đ_{theo}$) versus degree of polymerization DPn according to the synthesized polymers with molecular weights of 2.5, 5 and 10 kg/mol (Table 3). A ratio of 1 equals the dispersity in an ideal living anionic polymerization.

2.1.3.8 Effect of the degree of polymerization on the molecular weight distribution

According to the Poisson distribution the dispersity of polymers made by a living polymerization decreases with increasing degree of polymerization. In our polymer syntheses we observed that especially at low molecular weights (Table 3 Entry 10, 13 and 16) the obtained molecular weight distributions are broader than expected, which we ascribe to the kinetic effects described above. To investigate the influence of the degree of polymerization on the dispersity we simulated the monomer composition of the statistical copolymerization of I/S and I/4MS, using the KMC model for different degrees of polymerization at an initial initiator concentration of 10^{-3} mol/L (see Figures S17, S18 for number average molecular weight distribution and average monomer composition in dependency of the molecular weight).

As expected, the simulated dispersity decreases with increasing molecular weight of the copolymers (Figure 9).

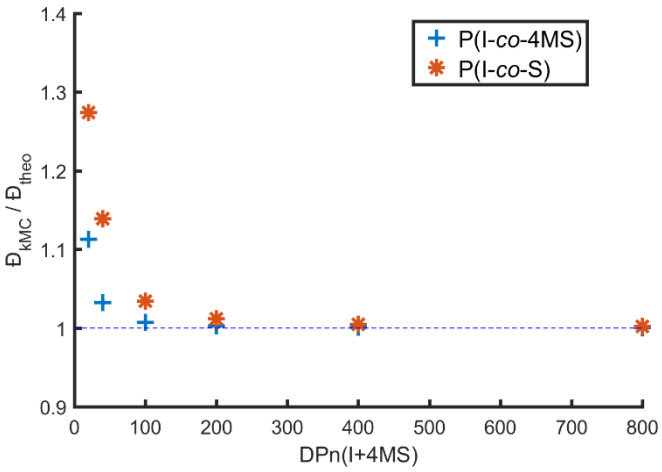

Figure 9: Comparison of simulated dispersities, $Đ_{KMC}$, with those of ideal Poisson distribution, $Đ_{theo}$, versus final degree of polymerization at an initial initiator concentration of 10^{-3} mol/L. A ratio of unity represents an ideal living anionic polymerization.

This is in good agreement with the experimental findings in Table 3 and Figure 8. In all considered cases the dispersity of copolymers of 4MS is superior to the dispersity obtained for those of styrene. In contrast to styrene in the I/S system, 4MS nearly approaches an ideal Poisson distribution at degrees of polymerization exceeding 200 (Figure 9). This can be rationalized by the lower homopolymerization rate constant of 4MS in comparison to styrene, thus increasing the controlled nature of the polymerization by the higher ratio of initiation rate versus propagation rate.

2.1.3.9 Influence of initiator and monomer concentration

During our kinetic simulations, we unexpectedly observed an influence of the initial initiator concentration on the resulting monomer composition distribution at a constant degree of polymerization. As shown in Figure 10, with increasing initial initiator concentration the deviation from an ideal Poisson distribution increases (Figure S19). Even though the overall deviation is rather small as compared to the influence of the targeted DP_n and the respective synthetic approach, as discussed before, the 4MS/I system shows a lower dependence on the concentration compared to the copolymerization of styrene with isoprene.

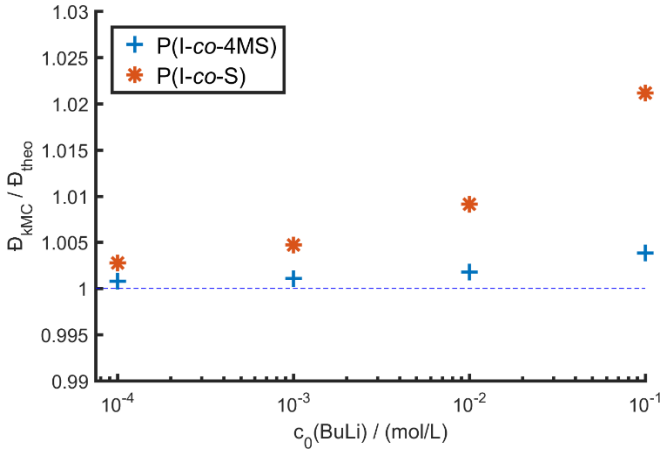

Figure 10: Comparison of simulated dispersity, $Đ_{kMC}$, to the ideal Poisson distribution versus initial initiator concentration (Simulation conditions: DP_n(I) = DP_n(4MS) = DP_n(S) = 200). A ratio of unity equals ideal living anionic polymerization. The concentration of 10^{-1} mol/L is only shown as a reference and cannot be obtained experimentally due to maximum bulk concentration.

We performed a mathematical derivation for the simplified case of sequential addition. The ratio of initiation from a PILi chain end as a macroinitiator and propagation rate of 4MS can be defined as $\alpha_{PILi \rightarrow 4MS} = R_{I4MS}/R_{4MS4MS}$. By simplifying the equations (see Supp. Inf., Equation Set S3 for the complete derivation) it can be shown that this ratio of initiation to propagation rate is independent of any monomer concentration:

$$\frac{\alpha_{PILi \rightarrow 4MS}([PILi]_1)}{\alpha_{PILi \rightarrow 4MS}([PILi]_2)} = \left(\frac{[PILi]_1}{[PILi]_2}\right)^{-1/4} \quad (4.1)$$

Consequently, with a 10-fold dilution the rate of initiation to propagation increases by approx. 1.7 times (Figure S20a). As a direct result the control over the polymerization of the second block is improved, leading to narrowing of the monomer distribution. The inverse approach of isoprene addition to a P4MSLi macroinitiator can be derived analogously (Figure S20b). In this case a 10-fold dilution decreases the ratio of initiation to propagation rate by a factor of approx. 0.6.

$$\frac{\alpha_{\mathrm{P4MSLi}\rightarrow\mathrm{I}}([\mathrm{P4MSLi}]_1)}{\alpha_{\mathrm{P4MSLi}\rightarrow\mathrm{I}}([\mathrm{P4MSLi}]_2)} = \left(\frac{[\mathrm{P4MSLi}]_1}{[\mathrm{P4MSLi}]_2}\right)^{1/4} \quad (4.2)$$

We emphasize that this scaling behavior is independent of reactivity ratios and monomer concentrations and is valid for every system where one chain end forms dimeric and the other forms tetrameric chain ends.

2.1.3.10 Consequences for the design of tapered block copolymers

The formation of tapered block copolymers is affected by various experimental parameters. As shown in this work, the small inductive effect of one methyl group on going from styrene to 4MS changes the system significantly. The ratio of initiation and propagation rates plays an important role to obtain chemically homogeneous, tapered block copolymers with narrow size distribution. However, this ratio is inherently low for monomers with divergent reactivity ratios. In the previous paragraphs we have demonstrated that high molecular weights and high dilution of the polymerization solutions are favorable to increase control of the copolymerization and to obtain well-defined tapered block copolymers. However, at very high dilution the presence of impurities may not be negligible, particularly when relying on carbanionic techniques. As a good starting point, an initiator concentration of 10^{-4} mol/L and a targeted degree of polymerization of at least 200 monomers per block is recommended, based on our simulation results. We believe that these fundamental results derived at the example of the I/4MS system are generally valid for the copolymerization of styrene derivatives with diene monomers like isoprene or butadiene.

2.1.3.11 Thermal properties and segregated morphologies of the tapered copolymers

A comparison of the glass transitions for block and gradient copolymers shows negligible differences for the higher glass transition temperature, $T_{g,4MS}$, as expected due to the homopolymer nature of this block in the tapered block copolymers. Larger differences are found for $T_{g,I}$. An increase of the T_g for the PI block in gradient

copolymers (-50 °C vs. -65 °C to -70 °C for PI homopolymer in sequential block copolymers) is attributed to the incorporation of the 4MS monomer in the PI segment, as already detailed in the simulations above.

We emphasize that in this work we do not present a comprehensive study of the morphology of all polymer samples prepared, but rather show some typical results obtained for selected samples to illustrate the potential of the I/4MS copolymerization. Microphase-segregated morphologies, well-known for I/S block copolymers, were obtained by varying the molecular weight and isoprene content (Figure 11 and Figure S21). Both parameters determine phase separation in the same manner as known for PI-*block*-PS diblock copolymers.[41] PI/P4MS can be reasonably assumed to exhibit a similar *Flory-Huggins* interaction parameter as PI/PS and thus a similar phase diagram. This behaviour supports the concept of a "one-pot block copolymer synthesis" put forward in this work for the I/4MS system. Detailed morphological characterization will be reported elsewhere.

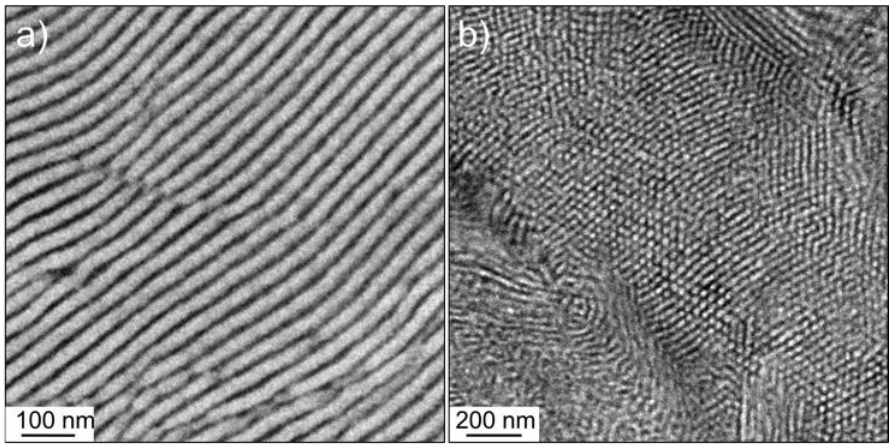

Figure 11: Typical TEM micrographs of I/4MS tapered block copolymers a) P(I-*co*-4MS) (entry 13 in Table S3), lamellae, lamellar distance 14.8 nm; b) P(I-*co*-4MS) (entry 3 in Table 3), hexagonal cylinder morphology, cylinder diameter 11.8 nm. PI was stained with OsO_4.

This also leads to the question whether there are advantages for a one-pot synthesis of block copolymers as opposed to the highly established sequential procedures. Obviously, the preparation of ultrahigh molecular weight block copolymers by sequential addition of monomers represents a difficult task, since the extremely low concentration of sensitive carbanionic chain ends does not permit to introduce a second monomer in the reaction vessel without significant chain termination,

necessitating a one-pot strategy. In this case direct statistical copolymerization like in the case of the I/4MS systems is highly favoured.

Tapered block copolymers featuring overall molecular weights as high as 1.25×10^6 g/mol were accessible as determined by SEC vs. PS standards (see Table 3 and Figure 12 a). First studies of the morphology of the tapered block copolymer with an overall number-average molecular weight of 1.25×10^6 g/mol, featuring a volume fraction of 86% I and 14% 4MS are given in Figure 12 (b-d). The spherical domains correspond to the P4MS blocks, while the dark matrix represents PI (staining with osmium tetroxide). It has to be mentioned that the observable P4MS spherical domains exhibit an average diameter of ca. 90 nm, which is larger than the thin slices prepared by ultramicrotomy (ca. 50 nm). For this reason, deformation of the spherical domains occurs during the cutting procedure, as seen in image 12d. However, all images evidence phase segregation into large spherical domains for the ultrahigh molecular weight block copolymers (UHMW BC). A detailed study of the properties of such systems is reported separately.[42]

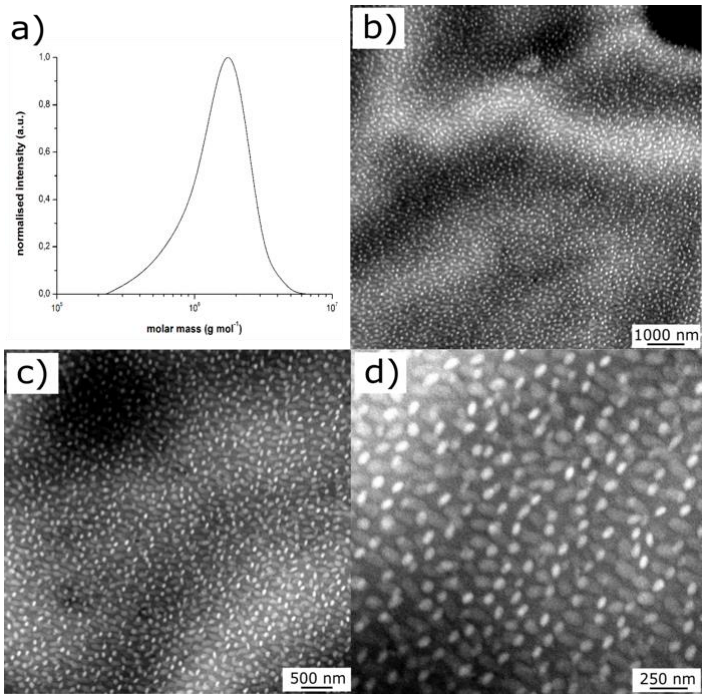

Figure 12: Molecular weight distribution of gradient block polymer P(I-*co*-4MS) with 14 wt-% 4MS (entry 9 in Table 3) obtained by SEC vs. PS standards. 12b-d: TEM micrographs showing spherical domains; PI was stained with OsO_4.

2.1.4 Conclusions

This combined experimental and simulation work introduces the one-step synthesis of tapered block copolymers from isoprene and 4-methylstyrene in cyclohexane by statistical living anionic copolymerization. Detailed understanding of the monomer gradient was achieved via real-time NMR kinetics, determined from the monomer consumption during copolymerization, DFT calculations and kinetic Monte Carlo simulation. To the best of our knowledge no example of a kinetic Monte Carlo model has been applied to the living carbanionic copolymerization to date, considering both the tetrameric polyisoprenyllithium and dimeric polystyryllithium chain ends. We demonstrate that for the I/4MS system in a statistical copolymerization a very short tapered midblock is formed as a consequence of the markedly different reactivity ratios (r_I = 25.4, r_{4MS} = 0.007). In all cases considered, the I/4MS system shows better controlled monomer distribution compositions and a shorter gradient structure in comparison to the established isoprene/styrene I/S copolymerization. The polyisoprene segments are less frequently interrupted by 4MS units, compared to the I/S copolymerization. The results emphasize the striking effect of a methyl group in para-position of styrene on the reactivity ratios in nonpolar media as well as its effect of significantly lowering the dispersity of the I/4MS copolymers in comparison to the I/S copolymers.

The potential of this one-pot strategy for block copolymer synthesis has been demonstrated at the example of a series of tapered block copolymers from low to ultrahigh molecular weight materials with molecular weights exceeding 10^6 g/mol. We emphasize that high-vacuum or break-seal techniques were avoided in all cases, thus the syntheses can be conveniently scaled up. For comparison, copolymers were also synthesized by the two possible sequential (i.e., conventional two-step) approaches starting both from 4MS and isoprene.

Finally, we emphasize the general nature of the results: we believe that the influence of both initiator concentration and targeted degree of polymerization are generally valid for every system combining a diene monomer like isoprene or butadiene and a styrene derivative. These monomer combinations play a key role for well-known and industrially established thermoplastic elastomers (TPEs). We emphasize that the direct copolymerization essentially follows the same kinetics as the two-step

approach, i.e., no significant difference can be detected in monomer composition distribution, thermal properties and phase segregation behaviour, if the flexible PI block is prepared first, since the slow crossover to the styrene monomer leads to broadening of the molecular weight distribution. It is obvious that the direct copolymerization of isoprene and 4-methylstyrene holds great promise for a large variety of complex polymer architectures, since the block structures formed remain living and permit further addition of monomers or monomer mixtures, greatly simplifying for instance for the synthesis of well-defined high molecular weight multiblock copolymers. The impact of the one-step method for a variety of complex block copolymer architectures and in particular for high molecular weight multiblock copolymers will be presented in a forthcoming work.

2.1.5 References

(1) Hadjichristidis, N.; Iatrou, H.; Pitsikalis, M.; Mays, J. Macromolecular architectures by living and controlled/living polymerisations. *Prog. Polym. Sci.* **2006**, *31*, 1068–1132.

(2) Tanaka, S.; Goseki, R.; Ishizone, T.; Hirao, A. Synthesis of Well-Defined Novel Reactive Block Polymers Containing a Poly(1,4-divinylbenzene) Segment by Living Anionic Polymerisation. *Macromolecules* **2014**, *47*, 2333–2339.

(3) Kim, H.-C.; Park, S.-M.; Hinsberg, W. D. Block Copolymer Based Nanostructures: Materials, Processes, and Applications to Electronics. *Chem. Rev.* **2010**, *110*, 146–177.

(4) Park, C.; Yoon, J.; Thomas, E. L. Enabling nanotechnology with self assembled block copolymer patterns. *Polymer* **2003**, *44*, 6725–6760.

(5) Bates, C. M.; Bates, F. S. 50th Anniversary Perspective: Block Polymers - Pure Potential. *Macromolecules* **2017**, *50*, 3–22.

(6) Stefik, M.; Mahajan, S.; Sai, H.; Epps, T. H.; Bates, F. S.; Gruner, S. M.; Disalvo, F. J.; Wiesner, U. Ordered three- and five-ply nanocomposites from ABC block terpolymer microphase separation with niobia and aluminosilicate sols. *Chem. Mater.* **2009**, *21*, 5466–5473.

(7) Schacher, F. H.; Rupar, P. A.; Manners, I. Functional Block Copolymers: Nanostructured Materials with Emerging Applications. *Angew. Chem. Int. Ed.* **2012**, *51*, 7898–7921.

(8) Ma, H.; Wang, Q.; Sang, W.; Han, L.; Liu, P.; Chen, J.; Li, Y.; Wang, Y. Synthesis of Bottlebrush Polystyrenes with Uniform, Alternating, and Gradient Distributions of Brushes Via Living Anionic Polymerisation and Hydrosilylation. *Macromol. Rapid Commun.* **2015**, *36*, 726–732.

(9) Lee, J. H.; Kim, Y.; Cho, J.-Y.; Yang, S. R.; Kim, J. M.; Yim, S.; Lee, H.; Jung, Y. S. In Situ Nanolithography with Sub-10 nm Resolution Realized by Thermally Assisted Spin-Casting of a Self-Assembling Polymer. *Adv. Mater.* **2015**, *27*, 4814–4822.

(10) Kraus, G.; Childers, C. W.; Gruver, J. T. Properties of random and block copolymers of butadiene and styrene. I. Dynamic properties and glassy transition temperatures. *J. Appl. Polym. Sci.* **1967**, *11*, 1581–1591.

(11) Knoll, K.; Nießner, N. Styrolux and styroflex from transparent high impact polystyrene to new thermoplastic elastomers. *Macromol. Symp.* **1998**, *132*, 231–243.

(12) Angelo, R. J.; Ikeda, R. M.; Wallach, M. L. Multiple glass transitions of block polymers. *Polymer* **1965**, *6*, 141–156.

(13) Lee, S.; Bluemle, M. J.; Bates, F. S. Discovery of a Frank-Kasper sigma phase in sphere-forming block copolymer melts. *Science* **2010**, *330*, 349–353.

(14) Ntaras, C.; Polymeropoulos, G.; Zapsas, G.; Ntetsikas, K.; Liontos, G.; Karanastasis, A.; Moschovas, D.; Rangou, S.; Stewart-Sloan, C.; Hadjichristidis, N.: E. L. Thomas, A. Avgeropoulos, Synthesis, characterization and self-assembly of well-defined linear heptablock quaterpolymers. *J. Polym. Sci. Part B: Polym. Phys.* **2016**, *54*, 1443–1449.

(15) Zaremski, M. Y.; Kalugin, D. I.; Golubev, V. B. Gradient copolymers: Synthesis, structure, and properties. *Polymer Science Series A* **2009**, *51*, 103–122.

(16) Zelinski, R.; Childers, C. W. Linear Elastomeric Block Polymers. *Rubber Chem. Technol.* **1968**, *41*, 161–181.

(17) van Beylen, M.; Bywater, S.; Smets, G.; Szwarc, M.; Worsfold, D. J. Developments in anionic polymerisation - A critical review. *Polysiloxane Copolymers/Anionic Polymerisation*; Springer, Berlin, Heidelberg: Berlin, Heidelberg, 1988; pp 87–143.

(18) Worsfold, D. J. Anionic copolymerisation of styrene and isoprene in cyclohexane. *J. Polym. Sci. Part A-1: Polym. Chem.* **1967**, *5*, 2783–2789.

(19) Hashimoto, T.; Tsukahara, Y.; Tachi, K.; Kawai, H. Structure and properties of tapered block polymers. 4. "Domain-boundary mixing" and "mixing-in-domain" effects on microdomain morphology and linear dynamic mechanical response. *Macromolecules* **1983**, *16*, 648–657.

(20) Hashimoto, T.; Shibayama, M.; Kawai, H. Domain-boundary structure of styrene-isoprene block copolymer films cast from solution. 4. Molecular-weight dependence of lamellar microdomains. *Macromolecules* **1980**, *13*, 1237–1247.

(21) Hodrokoukes, P.; Floudas, G.; Pispas, S.; Hadjichristidis, N. Microphase Separation in Normal and Inverse Tapered Block Copolymers of Polystyrene and Polyisoprene. 1. Phase State. *Macromolecules* **2001**, *34*, 650–657.

(22) Hodrokoukes, P.; Pispas, S.; Hadjichristidis, N. Controlling Micellar Properties of Styrene/Isoprene Copolymers by Altering the Monomer Arrangement along the Chain. *Macromolecules* **2002**, *35*, 834–840.

(23) Luo, M.; Brown, J. R.; Remy, R. A.; Scott, D. M.; Epps III, T. H. Determination of Interfacial Mixing in Tapered Block Polymer Thin Films: Experimental and Theoretical Investigations. *Macromolecules* **2016,** *49*, 5213–5222.

(24) Morris, M. A.; Gartner, T. E.; Epps III, T. H. Tuning Block Polymer Structure, Properties, and Processability for the Design of Efficient Nanostructured Materials Systems. *Macromol. Chem. Phys.* **2017**, *218*, 1600513.

(25) Roy, R.; Park, J. K.; Young, W.-S.; Mastroianni, S. E.; Tureau, M. S.; Epps, T. H. Double-Gyroid Network Morphology in Tapered Diblock Copolymers. *Macromolecules* **2011**, *44*, 3910–3915.

(26) Luo, M.; Epps III, T. H. Directed Block Copolymer Thin Film Self-Assembly: Emerging Trends in Nanopattern Fabrication. *Macromolecules* **2013**, *46*, 7567–7579.

(27) Quinebèche, S.; Navarro, C.; Gnanou, Y.; Fontanille, M. In situ mid-IR and UV-visible spectroscopies applied to the determination of kinetic parameters in the anionic copolymerisation of styrene and isoprene. *Polymer* **2009**, *50*, 1351–1357.

(28) Long, T. E.; Liu, H. Y.; Schell, B. A.; Teegarden, D. M.; Uerz, D. S. Determination of solution polymerisation kinetics by near-infrared spectroscopy. 1. Living anionic polymerisation processes. *Macromolecules* **1993**, *26*, 6237–6242.

(29) Natalello, A.; Werre, M.; Alkan, A.; Frey, H. Monomer Sequence Distribution Monitoring in Living Carbanionic Copolymerisation by Real-Time ^{1}H NMR Spectroscopy. *Macromolecules* **2013**, *46*, 8467–8471.

(30) Meyer, V. E.; Lowry, G. G. Integral and differential binary copolymerisation equations. *J. Polym. Sci. Part A: General Papers* **1965**, *3*, 2843–2851.

(31) Fineman, M.; Ross, S. D. Linear method for determining monomer reactivity ratios in copolymerisation. *J. Polym. Sci.* **1950**, *5*, 259–262.

(32) Kelen, T.; Tüdös, F. A new improved linear graphical method for determing copolymerisation reactivity ratios. *Reaction Kinetics and Catalysis Letters* **1974**, *1*, 487–492.

(33) Mayo, F. R.; Lewis, F. M. Copolymerisation. I. A Basis for Comparing the Behavior of Monomers in Copolymerisation; The Copolymerisation of Styrene and Methyl Methacrylate. *J. Am. Chem. Soc.* **1944**, *66*, 1594–1601.

(34) Morita, H.; van Beylen, M. New Vistas on the Anionic Polymerisation of Styrene in Non-Polar Solvents by Means of Density Functional Theory. *Polymers* **2016**, *8*, 371.

(35) Reed, A. E.; Weinstock, R. B.; Weinhold, F. Natural population analysis. *J. Chem. Phys.* **1985**, *83*, 735–746.

(36) Nikolaienko, T. Y.; Bulavin, L. A.; Hovorun, D. M. JANPA: An open source cross-platform implementation of the Natural Population Analysis on the Java platform. *Comput. Theor. Chem.* **2014**, *1050*, 15–22.

(37) Cho, A. S.; Broadbelt, L. J. Stochastic modelling of gradient copolymer chemical composition distribution and sequence length distribution. *Mol. Simul.* **2010**, *36*, 1219–1236.

(38) Tsukahara, Y.; Nakamura, N.; Hashimoto, T.; Kawai, H.; Nagaya, T.; Sugimura, Y.; Tsuge, S. Structure and Properties of Tapered Block Polymers of Styrene and Isoprene. *Polym J.* **1980**, *12*, 455–466.

(39) Wu, L.; Lodge, T. P.; Bates, F. S. Bridge to Loop Transition in a Shear Aligned Lamellae Forming Heptablock Copolymer. *Macromolecules* **2004**, *37*, 8184–8187.

(40) Gold, L. Statistics of Polymer Molecular Size Distribution for an Invariant Number of Propagating Chains. *J. Chem. Phys.* **1958**, *28*, 91–99.

(41) Khandpur, A. K.; Foerster, S.; Bates, F. S.; Hamley, I. W.; Ryan, A. J.; Bras, W.; Almdal, K.; Mortensen, K. Polyisoprene-Polystyrene Diblock Copolymer Phase Diagram near the Order-Disorder Transition. *Macromolecules* **1995**, *28*, 8796–8806.

(42) Appold, M.; Grune, E.; Frey, H.; Gallei, M. One-Step Anionic Copolymerisation Enables Formation of Linear Ultra-High Molecular Weight Block Copolymer Films Featuring Vivid Structural Colors in the Bulk State, *ACS Appl. Mater. & Interf.* **2018**, *10*, 18202-18212.

2.1.6 Supporting Information

2.1.6.1 Experimental Procedures

Materials: All chemicals and solvents were purchased from Acros Organics Co. and Sigma-Aldrich Co. Isopropyl alcohol and methanol were used as received without further purification. Cyclohexane was purified via distillation over sodium and degassed by three freeze-thaw cycles prior to use. Isoprene, styrene and 4-methylstyrene were purified by distillation over CaH_2 and degassed by three freeze-thaw cycles prior to use.

General polymerization procedure for one-step and sequential block copolymers: All copolymerizations were carried out in cyclohexane under argon atmosphere and room temperature in a glove box in 30 ml glass flasks equipped with septa. The degassed monomer/solvent (20 wt%) was initiated by *sec*-butyllithium (1.3 M in cyclohexane/hexane 92/8) via syringe. The solution was stirred over night to ensure full monomer conversion. The polymerization was terminated by adding 0.5 ml of degassed methanol via syringe. The polymers were precipitated in methanol, dried at reduced pressure and stored at -18 °C. For the preparation of block copolymers a mixture of isoprene/cyclohexane (10 wt%) was initiated by *sec*-butyllithium (1.3 M in cyclohexane/hexane 92/8). When full monomer conversion was achieved, 4-methylstyrene was added via syringe.

General polymerization procedure for ultrahigh molecular weight block copolymers:

P(I-*co*-4MS) (entry 17 in Table S3) ($PI_{20.310}$-*co*-$P4MSt_{2.240}$)

In an ampule equipped with a stir bar 320 mg (2.7 mmol) neat 4-methylstyrene and 1654 mg (24.29 mmol) isoprene were dissolved in 100 mL of dry cyclohexane inside a glove box. The polymerization was initiated by quick addition of 92 µL *sec*-butyllithium (0.0012 mmol, 0.013 M solution in hexane) with a syringe. The solution was stirred at room temperature for 1 week to ensure complete conversion. After adding a small amount of degassed methanol, the polymer was poured into a 10-fold excess of methanol. The polymer was collected by filtration, washed with

methanol, dried in vacuum and stored under argon or nitrogen at -18 °C (yield: 1170 mg, 97.5 %).

P(I-*co*-4MS) (entry 16 in Table S3) (PI_{690}-*co*-$P4MSt_{450}$)

In an ampule equipped with a stir bar, 826 mg (7 mmol) neat 4-methylstyrene and 714 mg (10.48 mmol) isoprene were dissolved in 50 mL dry cyclohexane inside a glove box. The polymerization was initiated by quick addition of 11 µL *sec*-butyllithium (0.0149 mmol, 1.4 M solution in hexane) with a syringe. The solution was stirred at room temperature for 1 day to ensure complete conversion. After adding a small amount of degassed methanol, the polymer was poured into a 10-fold excess of methanol. The polymer was collected by filtration, washed with methanol, dried in vacuum and stored under argon or nitrogen at -18 °C (yield: 1480 mg, 99.3 %).

^{1}H-NMR kinetics studies: The monomer/solvent mixtures (20 wt% in cyclohexane-d_{12}) were prepared in a glove box. All compounds were purified via distillation over CaH_2 prior to use. The mixtures were filled in conventional NMR tubes and sealed with rubber septa. A NMR spectrum of the mixture was measured prior to the initiation step. After the initiation with one drop of *sec*-butyllithium (1.3 M in cyclohexane/hexane 92/8) the NMR experiments were started without locking and shimming of the polymerization mixture. All spectra were measured with 4 scans at 400 MHz, and the time intervals between the spectra varied from 20 seconds to 1 minute due to the gradual decrease of the polymerization rate. The reaction temperature was kept constant at 23 °C. Typically, 150-250 ^{1}H NMR spectra were recorded and evaluated.

TEM Measurements: TEM experiments were carried out on a Zeiss EM 10 electron microscope operating at 60 kV. All images presented were recorded with a slow-scan CCD camera obtained from TRS (Tröndle) in bright field mode. Camera control was computer-aided using the ImageSP software from TRS.

Instrumentation: Additional NMR spectra were recorded on a Bruker Avance II 400 spectrometer working 400 MHz (^{1}H NMR). NMR chemical shifts are referenced

relative to tetramethylsilane. Standard SEC was performed with THF as the mobile phase (flow rate 1 mL min^{-1}) on a SDV column set from PSS (SDV 10^3, SDV 10^5, SDV 10^6) at 30 °C. Calibration was carried out using PS standards (from Polymer Standard Service, Mainz). For determining the thermal properties of the polymers differential scanning calorimetry (DSC) was performed with a Mettler Toledo DSC-1 in a temperature range of -100 °C to 150 °C with a heating rate of 10 K min^{-1}.

Determination of reactivity ratios: To determine the reactivity ratios by the Fineman-Ross[1], Kelen-Tüdös[2] and Meyer-Lowry[3] formalism, respectively, the proton signals at 5.54-5.64 ppm (4-methylstyrene), 5.6-5.7 ppm (styrene) and 6.34-6.44 ppm (isoprene) were used. In case of 4MS/I copolymerization the Meyer-Lowry formalism was used. Evaluation methods based on the differential form of the Mayo-Lewis equation did not perform well in case of 4MS/I copolymerization due to strongly curved composition shift, the incorporation determination by segmental linear fits is not sufficient. The integrated Meyer-Lowry equation can directly fit the composition shift during the copolymerization experiment and is superior to the differential version of the Mayo-Lewis equation. Relative errors of the reactivity ratios are not trivially determined for a non-linear fit with errors in both independent variables. The used Least Squares fit doesn't provide a concise prediction of the error structure.[4] Therefore, no errors for the reactivity ratios are indicated.

DFT: All DFT calculations have been performed using the ORCA 3.0.2 software suite.[5] Each geometry was optimized with the B3LYP DFT hybrid function with geometrical counterpoise correction (gCP) and dispersion correction (D3)[6,7] with def2-TZVP basis set.[8,9] To reduce the calculation effort the RIJCOSX approximation method was used.[10] For all ground states no imaginary frequency was detectable. For the transition state exactly one imaginary frequency corresponding to the desired reaction pathway was detected. For further verification the transition state was connected to the precursor and product by intrinsic reaction pathway calculations.

Kinetic Monte Carlo calculations (KMC) (*Equation Set S1*): The model was developed based on the stochastic simulation algorithm by Gillespie.[11,12] Continuum-based reaction rates were converted to number-based probabilities using the following equations:

$$kMC_{\mathrm{II}} = \frac{k_{\mathrm{II}}}{(\mathrm{N}V)^{1/4}} \tag{1.1}$$

$$kMC_{\mathrm{4MS4MS}} = \frac{k_{\mathrm{4MS4MS}}}{(\mathrm{N}V)^{1/2}} \tag{1.2}$$

$$kMC_{\mathrm{I4MS}} = \frac{k_{\mathrm{I4MS}}}{(\mathrm{N}V)^{1/4}} \tag{1.3}$$

$$kMC_{\mathrm{4MSI}} = \frac{k_{\mathrm{4MSI}}}{(\mathrm{N}V)^{1/2}} \tag{1.4}$$

Concentrations have been converted by multiplying with Avogadros' number N and simulation volume V. The typical simulation volume was in range of 8E-16 L to 8E-19 L. For each simulation 500000 chains were used. All simulations were performed up to 99 % conversion. Each reaction probability was calculated based on the fraction of the total reaction rate:

$$P_v = \frac{R_V}{\sum_M^{v=1} R_V} \tag{1.5}$$

The corresponding reaction was chosen using a uniform distributed random number $r_1 = [0..1]$ based on the reaction probabilities:

$$\sum_{v=1}^{\mu-1} P_v < r_1 < \sum_{v}^{\mu} P_v \tag{1.6}$$

The time interval corresponding to the chosen reaction step was calculated using another uniformly distributed random number $r_2 = [0..1]$:

$$\tau = \frac{1}{\sum_M^{v=1} R_v} \ln\left(\frac{1}{r_2}\right) \tag{1.7}$$

After a reaction was stochastically selected, one randomly corresponding chain was chosen and used to proceed the reaction step. The monomer composition of all chains

was tracked. The number and weight average sequence length was calculated using the following equations:

$$\langle N \rangle_{\mathrm{n}} = \frac{\sum_i i N_i}{\sum_i N_i} \tag{1.8}$$

$$\langle N \rangle_{\mathrm{w}} = \frac{\sum_i i^2 N_i}{\sum_i i N_i} \tag{1.9}$$

N_i represents the number of segments with the size i.

For performance improvement the main stochastic model was implemented in C code, compiled using MinGW GCC compiler 5.1.0, while evaluation of the computed data was performed using custom written MATLAB scripts.

2.1.6.2 Real-time NMR kinetics results and evaluation

Real-time (*in-situ*) ^{1}H-NMR kinetics studies of the copolymerization of isoprene and styrene (I/S)

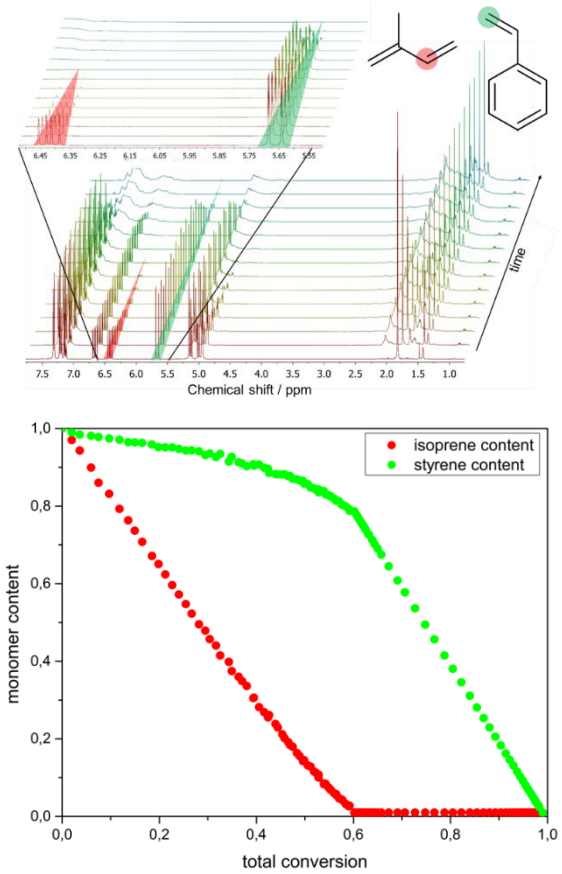

Figure S1: Left: real-time ^{1}H-NMR measurements of the copolymerization of isoprene and styrene (selected spectra), right: monomer concentration of isoprene (red) and styrene (green) vs. total conversion.

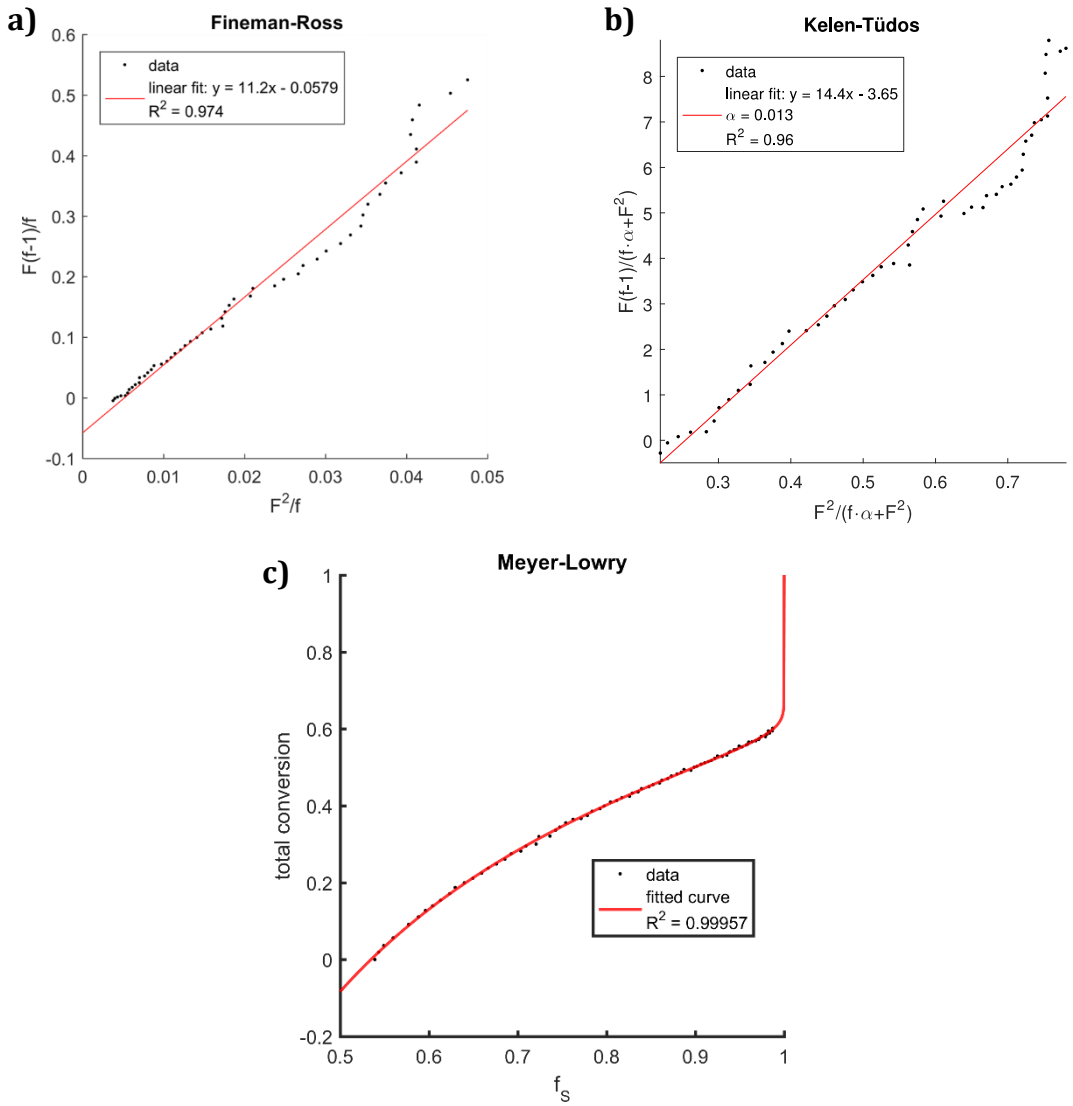

Figure S2: a,b,c: Determination of reactivity ratios by a) Fineman-Ross, b) Kelen-Tüdös and c) Meyer-Lowry formalism for the copolymerization of isoprene and styrene in cyclohexane.

Table S1: Summarized reactivity ratios for styrene/isoprene system in cyclohexane from all used methods and literature.

Method	$r_{isoprene}$	$r_{styrene}$
Fineman Ross	11.21	0.058
Kelen Tüdös	10.71	0.049
Meyer-Lowry	11.07	0.040
Average Value	11.0	0.049
Literature Value[13]	14.4	0.045
Literature Value[14]	12.8	0.051

Real-time NMR-kinetics studies of the copolymerization of isoprene and 4-methylstyrene (I/4MS)

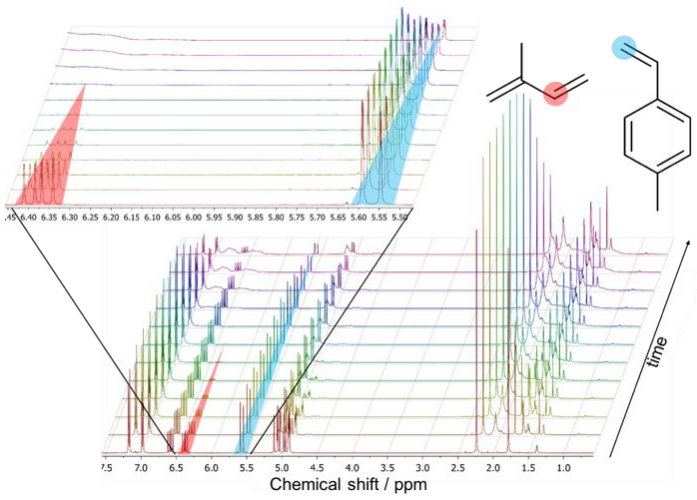

Figure S3: Real-time ^{1}H-NMR measurement of the copolymerization of isoprene and 4-methylstyrene.

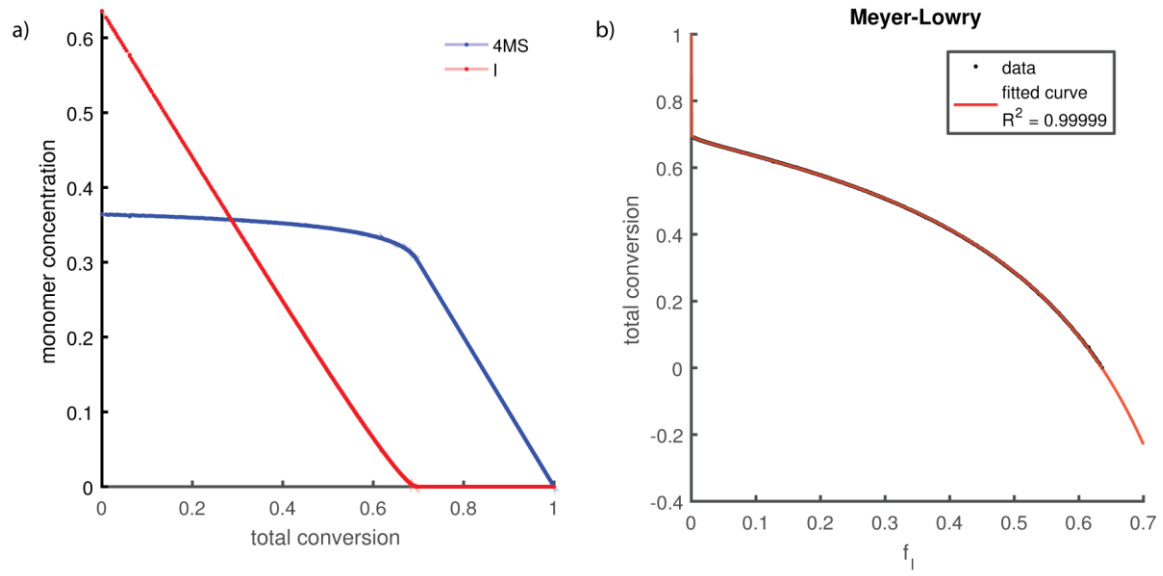

Figure S4: a) Normalized monomer concentration (total = 1) versus total conversion of 4MS (blue) and isoprene (red). b) Total conversion versus instantaneous monomer incorporation, f, of isoprene, and Meyer-Lowry fitted curve.

Real-time ^{1}H-NMR kinetics studies of 4MS homopolymerization

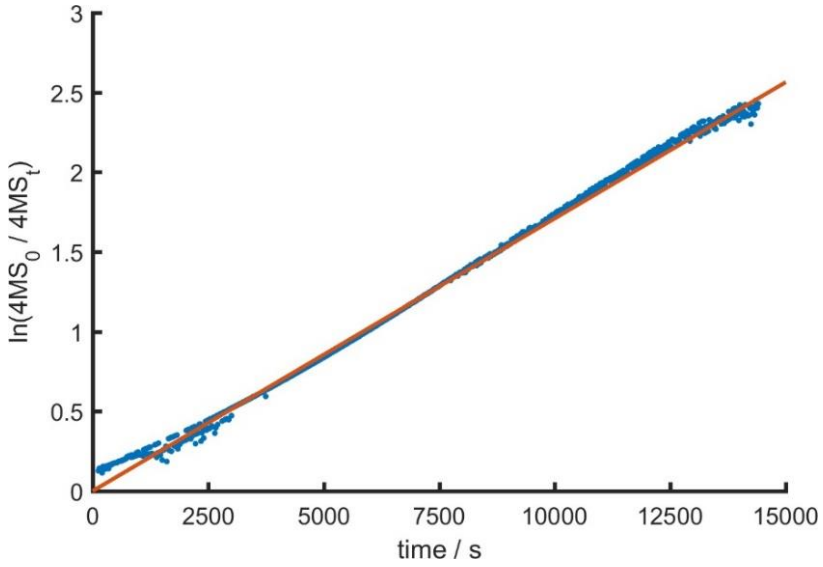

Figure S5: First-order time-conversion plot of the homopolymerization of 4MS determined from NMR measurements. The slope of the linear regression is the apparent rate constant, k_{app} = 1.71x10^{-4} s^{-1}.

2.1.6.3 DFT studies and simulated monomer distributions for tapered copolymers

DFT Studies of 4MS and styrene homopolymerization

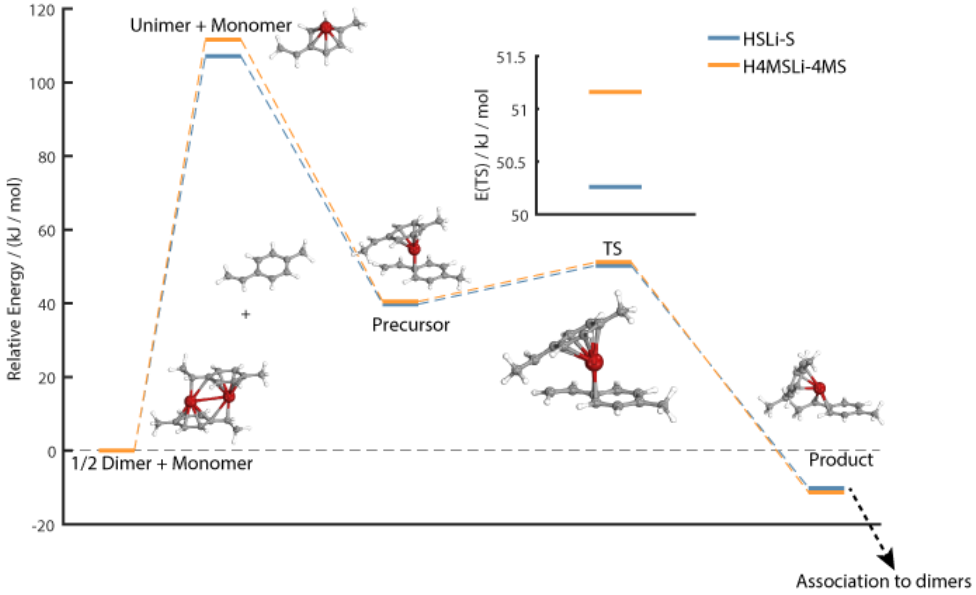

Figure S6: Energy diagrams of homopolymerization of 4MS (orange) and S (blue), respectively. 3D representation shows the corresponding structures for 4MS.

Table S2: top: calculated energies (B3LYP-D3-gCP/def2-TZVP//B3LYP-D3-gCP/def2-TZVP) of styrene and 4MS homopolymerization normalized to the energy level of the sum ½ dimer and one monomer (bottom).

Eletronic energy / Hartree		
	Styrene	**4MS**
H-Li	-8.0727743	-8.0727743
Monomer	-309.5797979	-348.8853499
Dimer	-635.4888281	-714.0959984
Unimer	-317.7036257	-357.0054778
Precursor	-627.3090579	-705.9179168
Transition state	-627.3050683	-705.9138637
Product	-627.3280816	-705.9376713

Normalized eletronic energy / kJ / mol		
	Styrene	**4MS**
1/2 Dimer + Monomer	0	0
Unimer + Monomer	107.089747	111.639804
Precursor	39.7871027	40.5174511
Transition state	50.2616137	51.1589702
Product	-10.1596742	-11.3480936

Equation Set S2: Copolymerization kinetics equations for 4MS/I.

$$(\mathrm{P4MSLi})_2 \underset{\leftarrow}{\rightarrow} 2\ \mathrm{P4MSLi} \tag{2.1}$$

$$\mathrm{P4MSLi} + 4\mathrm{MS} \rightarrow (\mathrm{P4MS})4\mathrm{MSLi} \tag{2.2}$$

$$\mathrm{P4MSLi} + \mathrm{I} \rightarrow (\mathrm{P4MS})\mathrm{ILi} \tag{2.3}$$

$$(\mathrm{PI})_4 \underset{\leftarrow}{\rightarrow} 4\ \mathrm{PILi} \tag{2.4}$$

$$\mathrm{PI} + 4\mathrm{MS} \rightarrow (\mathrm{PI})4\mathrm{MSLi} \tag{2.5}$$

$$\mathrm{PI} + \mathrm{I} \rightarrow (\mathrm{PI})\mathrm{ILi} \tag{2.6}$$

$$\frac{\mathrm{d}[\mathrm{I}]}{\mathrm{d}t} = k_{\mathrm{II}}[\mathrm{I}][\mathrm{PILi}]^{1/4} - k_{4\mathrm{MSI}}[\mathrm{I}][\mathrm{P4MSLi}]^{1/2} \tag{2.7}$$

$$\frac{\mathrm{d}[4MS]}{\mathrm{d}t} = k_{4\mathrm{MS4MS}}[4MS][P4MSLi]^{1/2} - k_{\mathrm{I4MS}}[4\mathrm{MS}][\mathrm{PILi}]^{1/4} \tag{2.8}$$

$$\frac{\mathrm{d}[\mathrm{P4MSLi}]}{\mathrm{d}t} = k_{4\mathrm{MSI}}[\mathrm{I}][\mathrm{P4MSLi}]^{1/2} + k_{\mathrm{I4MS}}[4\mathrm{MS}][\mathrm{PILi}]^{1/4} \tag{2.9}$$

$$\frac{\mathrm{d}[\mathrm{PILi}]}{\mathrm{d}t} = -\frac{\mathrm{d}[\mathrm{P4MSLi}]}{\mathrm{d}t} \tag{2.10}$$

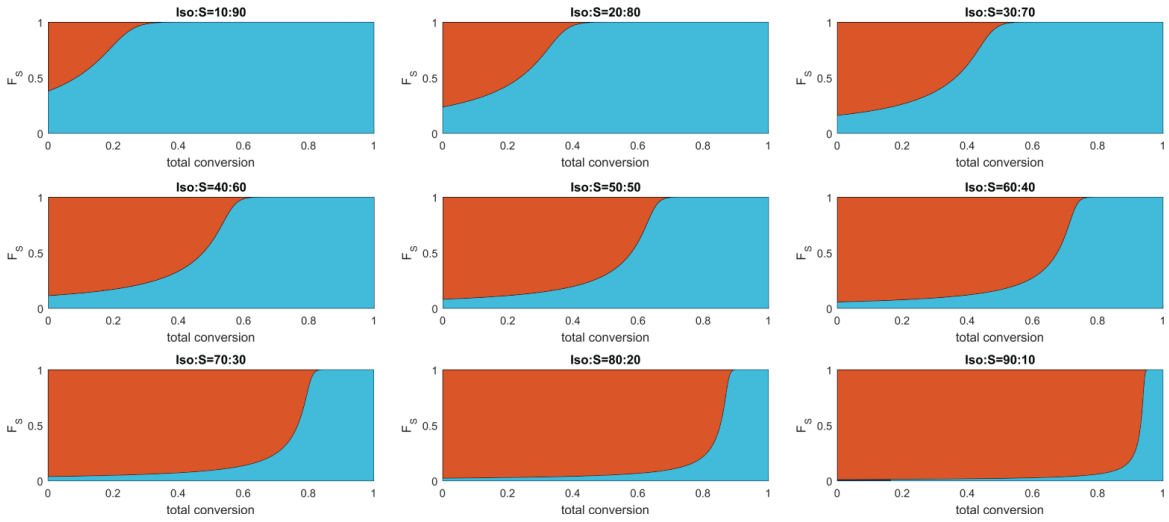

Figure S7: isoprene/styrene system: simulated plots of incorporated fraction of styrene (FS, light blue) and isoprene (red) versus total conversion for different initial monomer feed ratios. The reactivity ratios were directly derived from 1H real-time NMR measurements.

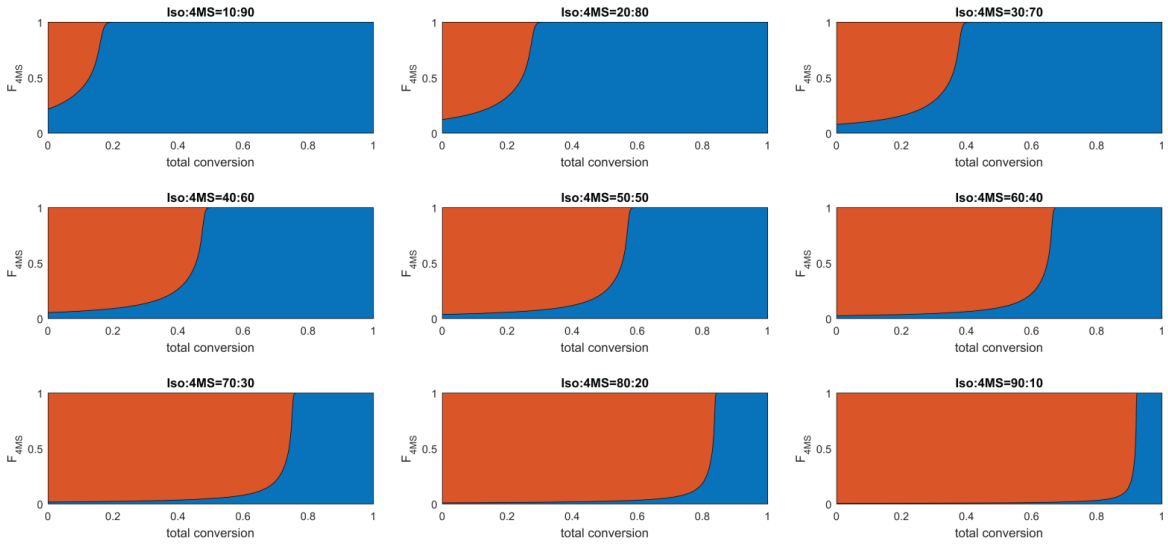

Figure S8, isoprene/4-methylstyrene system: Simulated plots of the incorporated fraction of 4MS (F_{4MS}, blue) and isoprene (blue) versus total conversion for different initial monomer feed ratios I/4MS. The data employed for the simulation are directly derived from ^{1}H real-time NMR kinetics measurements.

2.1.6.4 Characterization of the copolymers prepared by statistical copolymerization

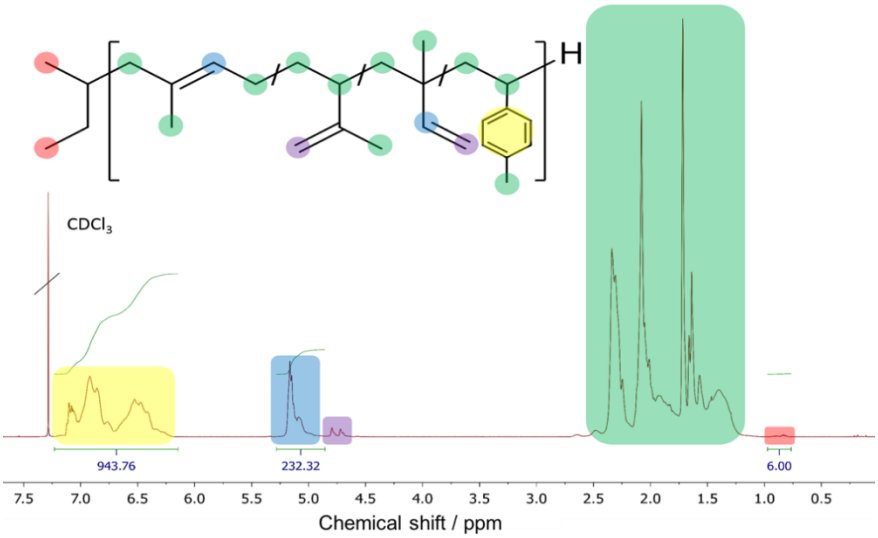

Figure S9: ^{1}H-NMR spectrum (400 MHz) of a statistical copolymer of I/4MS in $CDCl_3$ (entry 3 in Table S3).

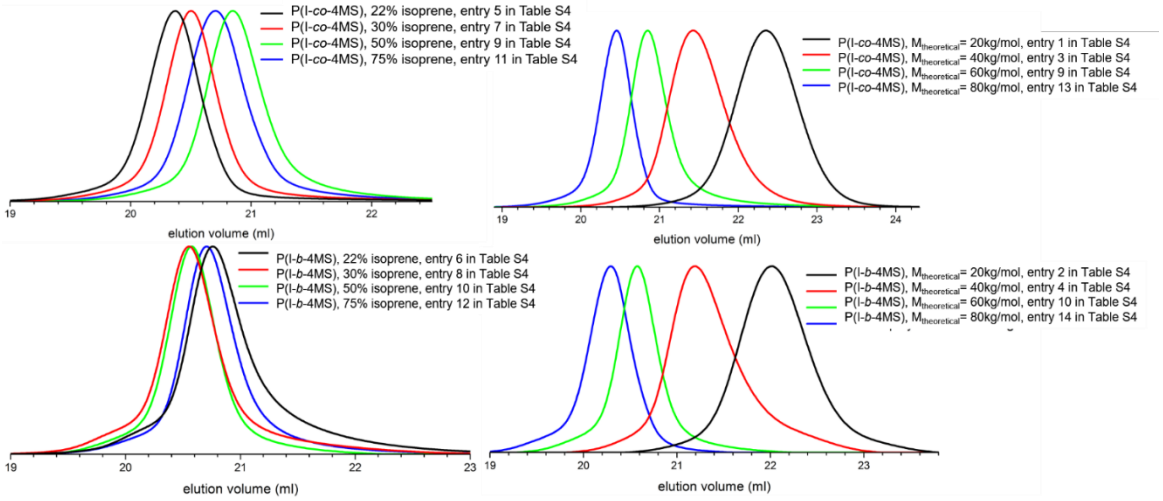

Figure S10: SEC traces of gradient and block copolymers of I/4MS prepared under argon atmosphere in a glove box. Dispersity range of the polymers: 1.08 – 1.16.

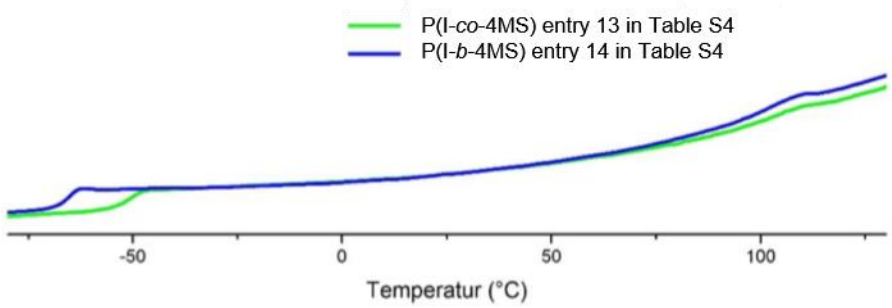

Figure S11: DSC thermogram of entry 13 (green) and 14 (blue) (Table S3). Heating rate: 10 K/min.

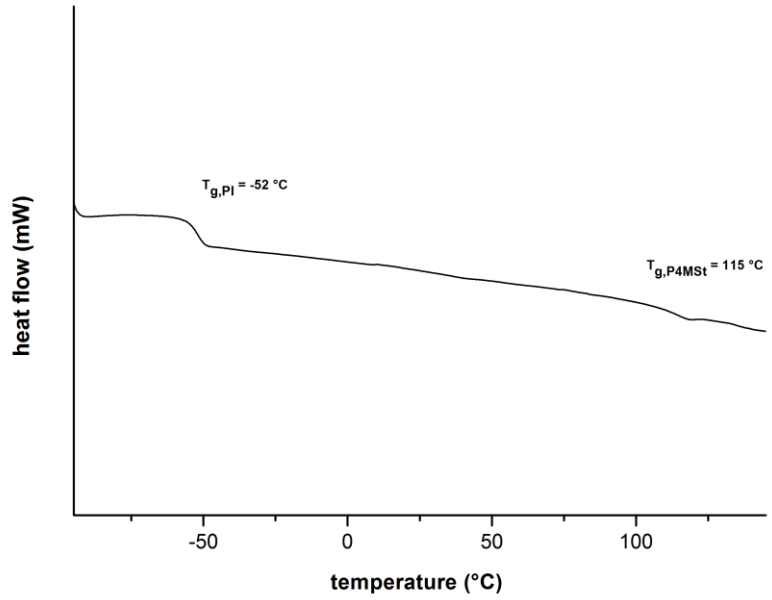

Figure S12. DSC thermogram of sample entry 16 (Table S3). Heating rate: 10 K/min.

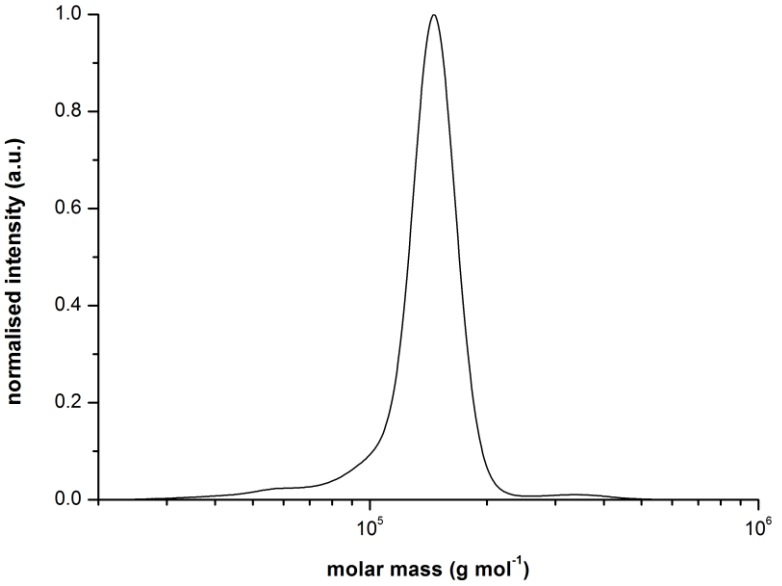

Figure S13. Typical molar mass distributions obtained by SEC measurements vs. PS standards in THF obtained for sample entry 16 (Table S3).

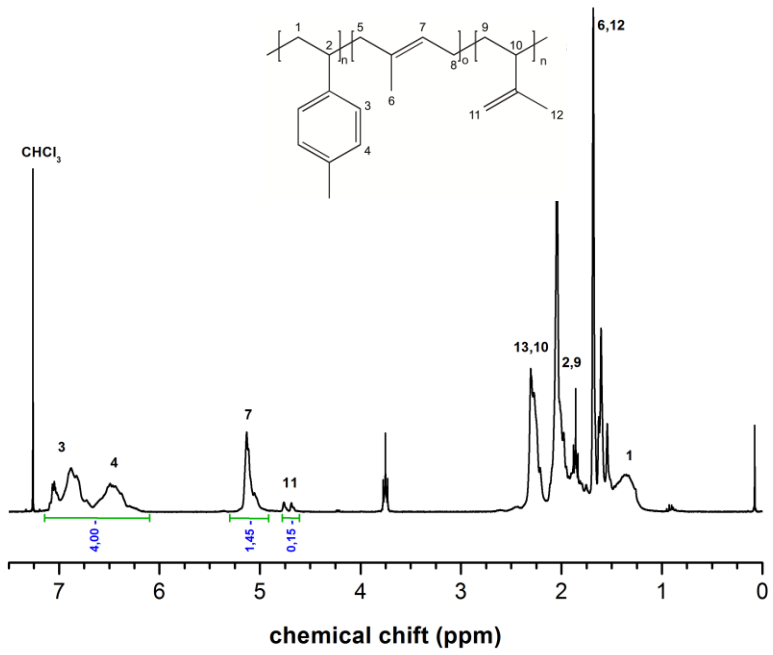

Figure S14. ^{1}H NMR spectrum of entry 16 (Table S3) in $CDCl_3$.

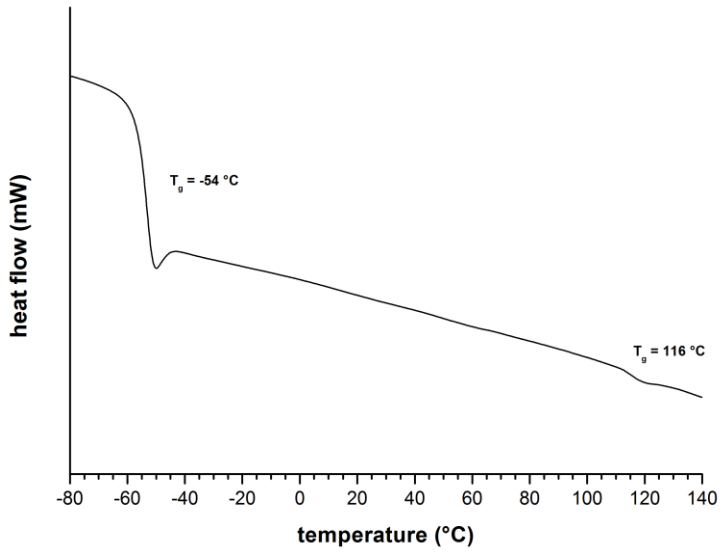

Figure S15. DSC thermogram of entry 17 (Table S3) (heating rate 10 K/min).

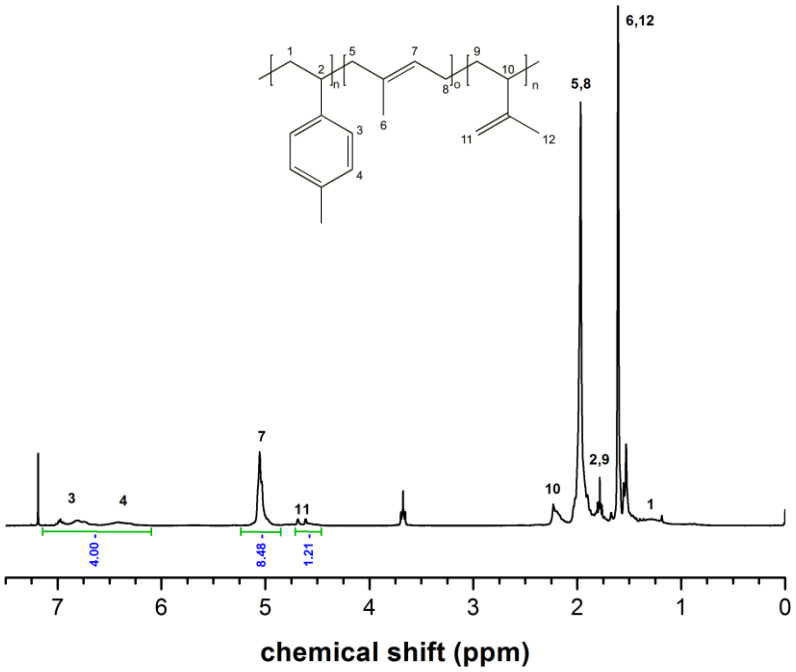

Figure S16. ^{1}H NMR spectrum of entry 17 (Table S3) in $CDCl_3$.

Table S3: Summarized results of copolymer characterization by NMR, SEC and DSC.

Entry	Polymer composition[a]	Isoprene content [%]	Target M_n [kg/mol]	M_n (SEC)[b] [kg/mol]	$Đ$	v_I[c] [%]	T_g[d] (I/*4MS*) [°C]
1	P(I-*co*-4MS)	50	20	38.6	1.08	40	-45/45
2	PI-*b*-P4MS	50	20	46.5	1.08	41	-63/70
3	P(I-*co*-4MS)	50	40	38.6	1.09	39	-50/86
4	PI-*b*-P4MS	50	40	46.5	1.09	41	-65/89
5	P(I-*co*-4MS)	22	60	77.3	1.10	18	-/87
6	PI-*b*-P4MS	22	60	57.6	1.11	17	-/87
7	P(I-*co*-4MS)	30	60	76.3	1.12	24	-46/93
8	PI-*b*-P4MS	30	60	71.1	1.14	23	-70/97
9	P(I-*co*-4MS)	50	60	55.8	1.12	40	-51/102
10	PI-*b*-P4MS	50	60	76.6	1.10	39	-65/98
11	P(I-*co*-4MS)	75	60	65.4	1.11	60	-56/-
12	PI-*b*-P4MS	75	60	62.4	1.12	61	-57/-
13	P(I-*co*-4MS)	50	80	77.4	1.08	41	-52/100
14	PI-*b*-P4MS	50	80	101.9	1.08	40	-65/105
15	P(I-*co*-4MS)	50	400	360	1.07	40	-55/99
16	P(I-*co*-4MS)	60	130	133	1.09	50	-52/115
17	P(I-*co*-4MS)	90	1300	1250	1.32	86	-54/116
18	P(I-*co*-4MS)	50	2.5	4.4	1.20	29	26
19	PI-*b*-P4MS	50	2.5	3.8	1.12	30	-/-
20	P4MS-*b*-PI	50	2.5	2.4	1.06	40	20
21	P(I-*co*-4MS)	50	5	4.7	1.16	30	-15/21
22	PI-*b*-P4MS	50	5	5.4	1.09	36	-41/11
23	P4MS-*b*-PI	50	5	3.7	1.06	40	-47/6
24	P(I-*co*-4MS)	50	10	7.4	1.13	38	-31/16
25	PI-*b*-P4MS	50	10	8.6	1.09	39	-43/21
26	P4MS-*b*-PI	50	10	7.4	1.07	39	-43/23

[a] Polymer composition and preparation route with targeted isoprene and 4MS content: "*b*" sequential addition of both monomers, "*co*" translates to direct (i.e., statistical) copolymerization; [b] Size exclusion chromatography (SEC) in THF at 25 °C. [c] calculated volume fractions based on densities from reference 15 [d] via differential scanning calorimetry (DSC). Samples 16 and 17 (entry 16 and 17 in Table S3) show higher glass transition temperatures for the 4MS block due to their higher molecular weight and the use of a different experimental setup than the other samples.

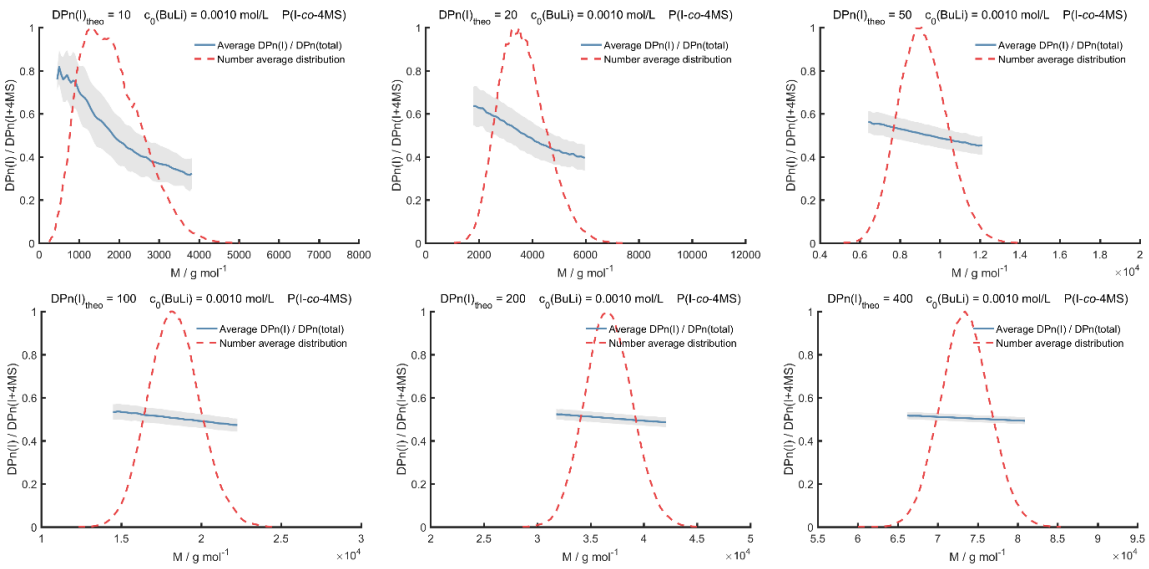

Figure S17: Average ratio of the degree polymerization of isoprene (DP_n(I)) and the total DP_n (blue) of P(I-*co*-4MS) copolymers versus total molecular weight at an initial initiator concentration of 10^{-3} mol/L. The shaded area shows the standard deviation of the average DP_n(I) / DP_n(total) ratio. The red curve shows the normalized number average distribution of the simulated copolymers.

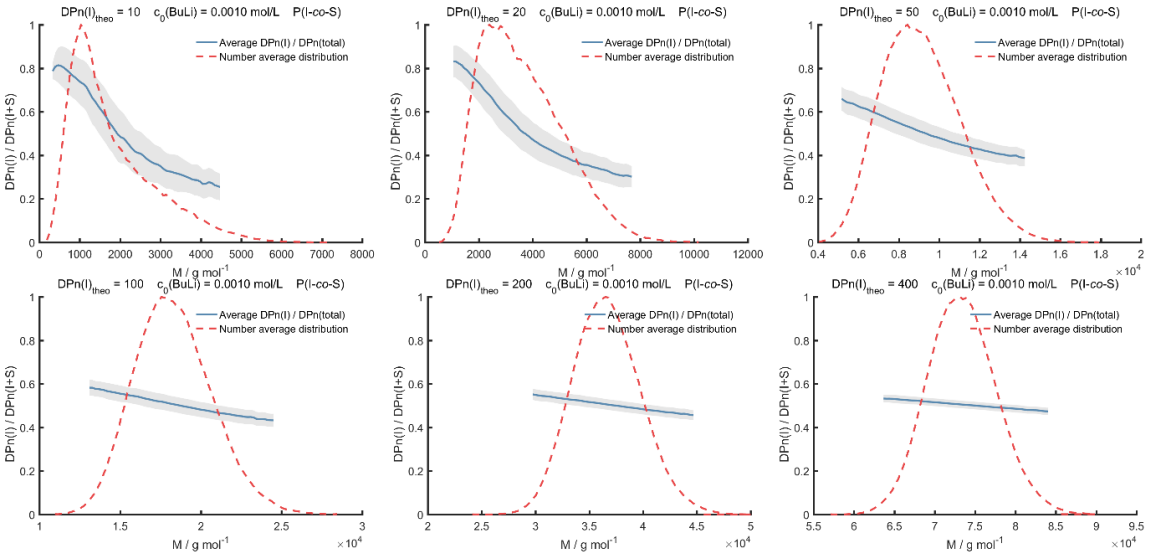

Figure S18: Average ratio of the degree polymerization of isoprene (DP_n(I)) and the total DP_n (blue) of P(I-*co*-S) copolymers versus total molecular weight at an initial initiator concentration of 10^{-3} mol/L. The shaded area shows the standard deviation of the average DP_n(I) / DP_n(total) ratio. The red curve shows the normalized number average distribution of the simulated copolymers.

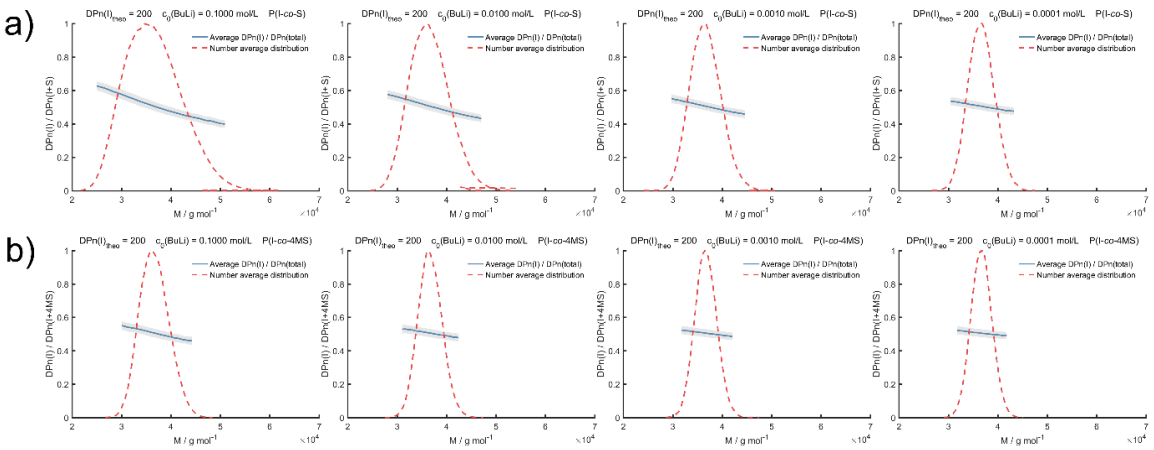

Figure S19: Average ratio of the degree polymerization of isoprene (DP_n(I)) and the total DP_n (blue) of (a) P(I-*co*-S) and (b) P(I-*co*-4MS) copolymers versus total molecular weight at different initial initiator concentrations. The shaded area shows the standard deviation of the average DP_n(I) / DP_n(total) ratio. The red curve shows the normalized number average distribution of the simulated copolymers.

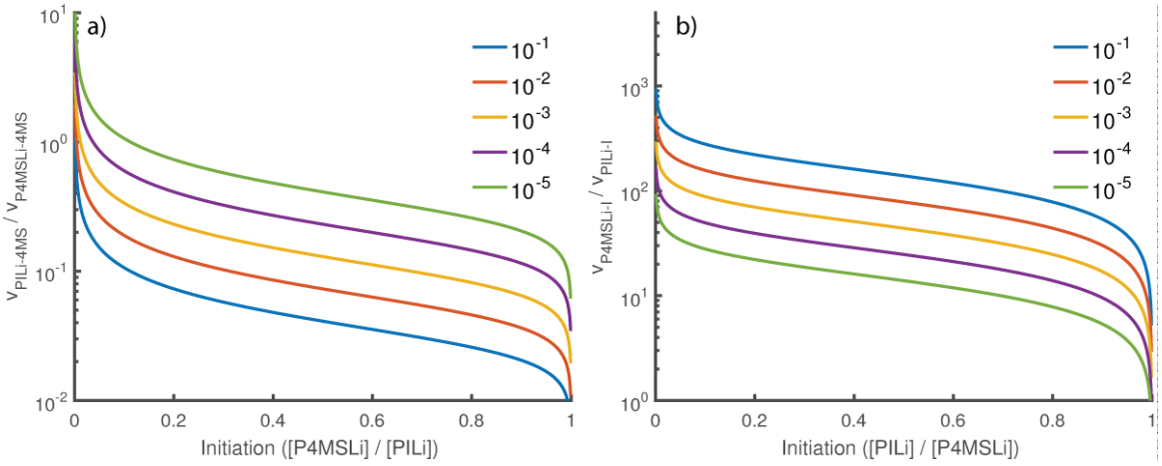

Figure S20: Ratio of initiation rate to propagation rate versus initiation amount at various initiator concentrations. At an initiation amount of 1 all chains have been successful initiated. a) Initiation of a 4MS block by a PILi macroinitiator. b) Initiation of an isoprene block by a P4MSLi macroinitiator.

Equation Set S3: Mathematical derivation of initiation rate versus propagation rate dependence from initiator concentration in case of dimeric polystyryllithium and tetrameric polyisoprenyllithium chain ends starting from a PILi macroinitiator.

$$R_{\mathrm{I4MS}} = k_{\mathrm{I4MS}}[\mathrm{4MS}][\mathrm{PILi}]^{1/4} \tag{3.1}$$

$$R_{\mathrm{4MS4MS}} = k_{\mathrm{4MS4MS}}[\mathrm{4MS}][\mathrm{P4MSLi}]^{1/2} \tag{3.2}$$

$$[\mathrm{PILi}] + [\mathrm{P4MSLi}] = [\mathrm{PILi}]_0 \tag{3.3}$$

$$\frac{R_{\mathrm{I4MS}}}{R_{\mathrm{4MS4MS}}} = \frac{k_{\mathrm{I4MS}}}{k_{\mathrm{4MS4MS}}}\frac{[\mathrm{PILi}]^{1/4}}{[\mathrm{P4MSLi}]^{1/2}} = \frac{k_{\mathrm{I4MS}}}{k_{\mathrm{4MS4MS}}}\frac{([\mathrm{PILi}]_0 - [\mathrm{P4MSLi}])^{1/4}}{[\mathrm{P4MSLi}]^{1/2}} = \alpha_{\mathrm{Ini}} \tag{3.4}$$

$$\beta = \frac{[\mathrm{PILi}]_1}{[\mathrm{PILi}]_2} \qquad \gamma = \frac{[\mathrm{PILi}]_n}{[\mathrm{P4MSLi}]_n} \tag{3.5}$$

$$\begin{aligned}\frac{\alpha_{\mathrm{Ini},1}}{\alpha_{\mathrm{Ini},2}} &= \frac{([\mathrm{PILi}]_1 - [\mathrm{P4MSLi}]_1)^{1/4}}{([\mathrm{PILi}]_2 - [\mathrm{P4MSLi}]_2)^{1/4}}\frac{[\mathrm{P4MSLi}]_2{}^{1/2}}{[\mathrm{P4MSLi}]_1{}^{1/2}} \\ &= \frac{([\mathrm{PILi}]_1 - \gamma[\mathrm{PILi}]_1)^{1/4}}{([\mathrm{PILi}]_2 - \gamma[\mathrm{PILi}]_2)^{1/4}}\frac{(\gamma\,[\mathrm{PILi}]_2)^{1/2}}{(\gamma[\mathrm{PILi}]_1)^{1/2}}\end{aligned} \tag{3.6}$$

$$\frac{\alpha_{\mathrm{Ini},1}}{\alpha_{\mathrm{Ini},2}} = \left(\frac{[\mathrm{PILi}]_1(1-\gamma)}{[\mathrm{PiLi}]_2(1-\gamma)}\right)^{1/4}\left(\frac{[\mathrm{PILi}]_2}{[\mathrm{PILi}]_1}\right)^{1/2} = \beta^{1/4}\beta^{-1/2} = \beta^{-1/4} \tag{3.7}$$

2.1.6.5 TEM measurements (transmission electron microscopy)

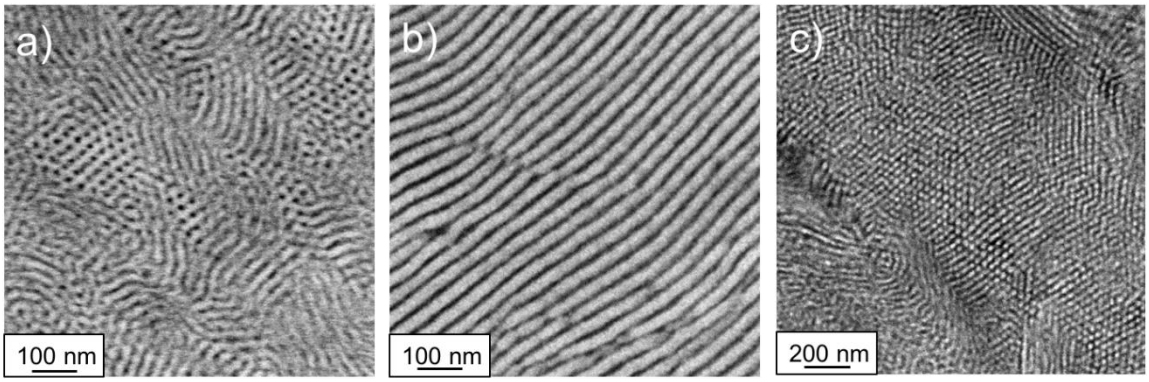

Figure S21: TEM images of gradient copolymers of isoprene and 4-methylstyrene after staining with osmium tetroxide, a) P(I-co-4MS) (entry 7 in Table S3), isoprene cylinders in poly(4-methylstyrene) matrix; b) P(I-co-4MS) (entry 9 in Table S3), lamella; c) P(I-co-4MS) (entry 11 in Table S3), 4-methylstyrene cylinders in polyisoprene matrix.

2.1.6.6 References

(1) Fineman, M.; Ross, S. D. Linear method for determining monomer reactivity ratios in copolymerisation. *J. Polym. Sci.* **1950**, *5*, 259–262.

(2) Kelen, T.; Tüdős, F. A new improved linear graphical method for determing copolymerisation reactivity ratios. *React Kinet. Catal. Lett.* **1974**, *1*, 487–492.

(3) Meyer, V. E.; Lowry, G. G. Integral and differential binary copolymerisation equations. *J. Polym. Sci. A Gen. Pap*. **1965**, *3*, 2843–2851.

(4) van den Brink, M.; van Herk, A. M.; German, A. L. Nonlinear regression by visualization of the sum of residual space applied to the integrated copolymerisation equation with errors in all variables. I. Introduction of the model, simulations and design of experiments. *J. Polym. Sci. A Polym. Chem.* **1999**, *37*, 3793–3803.

(5) Neese, F. The ORCA program system. *WIREs Comput Mol Sci* **2012**, *2*, 73–78.

(6) Grimme, S.; Antony, J.; Ehrlich, S.; Krieg, H. A consistent and accurate ab initio parametrization of density functional dispersion correction (DFT-D) for the 94 elements H-Pu. *J. Chem. Phys.* **2010**, *132*, 154104.

(7) Grimme, S.; Ehrlich, S.; Goerigk, L. Effect of the damping function in dispersion corrected density functional theory. *J. Comput. Chem.* **2011**, *32*, 1456–1465.

(8) Schäfer, A.; Horn, H.; Ahlrichs, R. Fully optimized contracted Gaussian basis sets for atoms Li to Kr. *J. Chem. Phys.* **1992**, *97*, 2571–2577.

(9) Weigend, F.; Ahlrichs, R. Balanced basis sets of split valence, triple zeta valence and quadruple zeta valence quality for H to Rn: Design and assessment of accuracy. *Phys. Chem. Chem. Phys.* **2005**, *7*, 3297–3305.

(10) Neese, F.; Wennmohs, F.; Hansen, A.; Becker, U. Efficient, approximate and parallel Hartree–Fock and hybrid DFT calculations. A 'chain-of-spheres' algorithm for the Hartree–Fock exchange. *Chem. Phys.* **2009**, *356*, 98–109.

(11) Gillespie, D. T. A general method for numerically simulating the stochastic time evolution of coupled chemical reactions. *J. Comput. Phys.* **1976**, *22*, 403–434.

(12) Gillespie, D. T. Exact stochastic simulation of coupled chemical reactions. *J. Phys. Chem.* **1977**, *81*, 2340–2361.

(13) Worsfold, D. J. Anionic copolymerisation of styrene and isoprene in cyclohexane. *J. Polym. Sci. A-1 Polym. Chem.* **1967**, *5*, 2783–2789.

(14) Quinebèche, S.; Navarro, C.; Gnanou, Y.; Fontanille, M. In situ mid-IR and UV–visible spectroscopies applied to the determination of kinetic parameters in the anionic copolymerisation of styrene and isoprene. *Polymer* **2009**, *50*, 1351–1357.

(15) Wu, L.; Lodge, T. P.; Bates, F. S. Bridge to Loop Transition in a Shear Aligned Lamellae Forming Heptablock Copolymer. *Macromolecules* **2004**, *37*, 8184–8187.

Chapter 3: Linear alternating $(AB)_n$ multiblock copolymers

3.1 Anionic Copolymerization Enables the Scalable Synthesis of Alternating $(AB)_n$ Multiblock Copolymers with High Molecular Weight in *n* Steps

Eduard Grune,[a,b] Michael Appold,[c] Axel H. E. Müller,[a] Markus Gallei,[c] Holger Frey*,[a]

[a] Institute of Organic Chemistry, Johannes Gutenberg University, Duesbergweg 10-14, 55128 Mainz (Germany)

[b] Graduate School Materials Science in Mainz, Staudinger Weg 9, 55128, Mainz (Germany)

[C] Macromolecular Chemistry Department, TU Darmstadt, Alarich-Weiss Str. 4, 64287 Darmstadt (Germany)

Published in *ACS Macro Letter* **2018,** 7, 807-810.

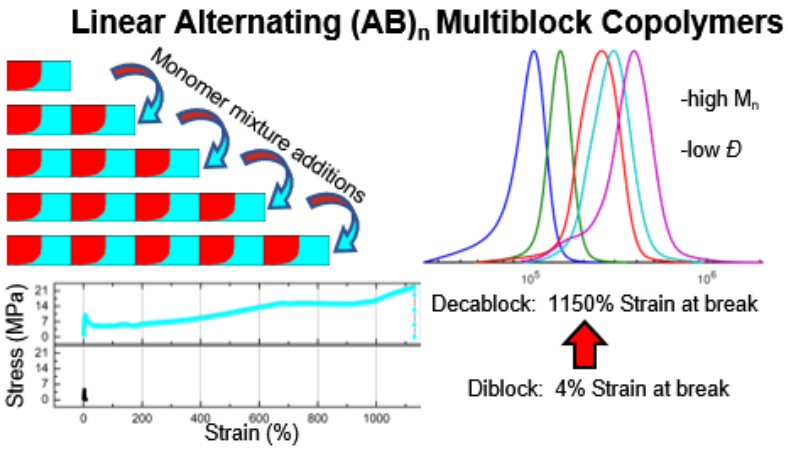

3.1.1 Abstract

Based on the highly disparate reactivities of isoprene (I, r_I = 25.4) and 4-methylstyrene (4MS, r_{4MS} = 0.007) in the anionic copolymerization in nonpolar media, a general strategy for the rapid and scalable synthesis of tapered multiblock copolymers with an extremely steep gradient has been developed. A repetitive addition strategy of a mixture of isoprene and 4MS leads to a tapered diblock in each case, giving access to linear alternating multiblock copolymers of the $(AB)_n$ type with up to 10 blocks. All multiblock copolymers showed narrow molecular weight distributions (dispersity $Đ$ = 1.04 – 1.12). High molecular weights in the range of 80 to 400 kg mol^{-1} were achieved. Due to the incompatibility of PI and P4MS segments, the multiblock copolymers exhibit nanophase separation, manifested by separate glass transitions for both constituents. Stress-strain measurements revealed extraordinary toughness and elongations up to 1150% strain at break, even at a 50/50 molar ratio I/4MS (i.e., 37 weight% isoprene). Our synthesis permits access to a wide range of tapered multiblock copolymer architectures with rigid (P4MS, high glass transition, T_g) and flexible (low T_g) chains, in n steps, while keeping overall dispersity low.

3.1.2 Introduction

The multiblock principle plays a key role in natural scleroproteins showing extraordinary mechanical properties, such as silk fibroin and collagen. They consist of alternating flexible and rigid, crystalline chain segments in repetitive sequences.[1-3] The increasing interest in synthetic architectures consisting of several different blocks has led to elegant works, demonstrating the enormous potential of innovative polymer synthesis in this area.[4-7] AB diblock copolymers consisting of two immiscible polymer chains have been intensely studied for applications in many fields of current nanotechnology, such as block copolymer lithography, membranes and nanoreactors, but generally suffer from low mechanical strength.[8-10] To overcome this limitation, multiblock copolymers can be used, which combine excellent mechanical properties due to bridging of segregated nanodomains with the desirable phase segregation known for diblock copolymers. A universe of achievable structures and hitherto elusive properties was predicted in an excellent feature article by Bates et al. as well

as in a comprehensive review recently.[4,11,12] Multiblock approaches that rely on controlled radical polymerization strategies leading to more than 20 short blocks were introduced by Perrier et al. and Haddleton et al.[13-16] However, the block lengths reported to date are usually not able to effect peculiar order, morphological effects or specific mechanical properties. Also catalytic precision polymerization has shown enormous progress in recent years, permitting the synthesis of polyolefin and polyester multiblock structures.[17-19] These approaches demonstrate the broad and vivid interest in synthetic strategies for well-defined multiblock copolymers.

For the preparation of block copolymers with high molecular weights, complex structures and low dispersity living anionic polymerization is an established and versatile approach. Long ago, Corbin and Prud'Homme suggested that monomer pairs with strongly diverging reactivities could be employed to prepare block copolymers with several blocks, albeit the dispersities reported for the respective polymers were rather high.[20,21] A similar approach was established two decades later, leading to the development of commercially relevant materials Styroflex® and Styrolux®.[22,23] The synthesis of these structures usually includes several additions of styrene and butadiene as well as mixtures of these monomers and a final linkage step via coupling agents. Several research groups, mainly Spontak et. al., Watanabe et. al. and Matsushita et al. impressively demonstrated the potential of carbanionic polymerization for the preparation of multiblock structures.[24-27]

To the best of our knowledge, tapered multiblock copolymers with narrow molecular weight distribution have not been reported to date. A scalable synthetic strategy for $(AB)_n$ multiblock copolymers with low dispersity has to rely on a highly controlled, living chain growth mechanism.

The respective strategy should fulfil the following requirements: (i) each synthesis of a new block must be carried out with as low loss of active chain ends as possible. It is easy to conceive that a loss of only 2% of living chain ends upon each addition step after 9 monomer additions would lead to merely 83% perfect $(AB)_5$ decablock copolymer. Hence, (ii) a suitable strategy should be based on a minimum of monomer addition steps to suppress termination. Most importantly, (iii) a relevant synthetic approach should permit the formation of blocks with molar masses sufficient for phase separation. As a general estimate, based on the respective χ-parameter of a block copolymer system, the molar mass required is in the range of 3 8 kg mol^{-1}.

Finally, (iv) in order to provide larger amounts of the materials in a scalable approach, demanding break-seal techniques should be circumvented.

3.1.3 Results and Discussion

In a recent work we reported the one-pot tapered block copolymer synthesis via direct copolymerization of isoprene and 4MS, monitored by *in-situ* NMR kinetics studies.[28] NMR mapping of the diblock subunit shows an extremely steep gradient for the isoprene/4-MS system (Scheme 1a). In this work we report a rapid and scalable strategy to alternating tapered $(AB)_n$ multiblock copolymers exhibiting an alternation of steep gradient and sharp block boundary by repeated addition of the I/4MS monomer mixture (Scheme 1b).

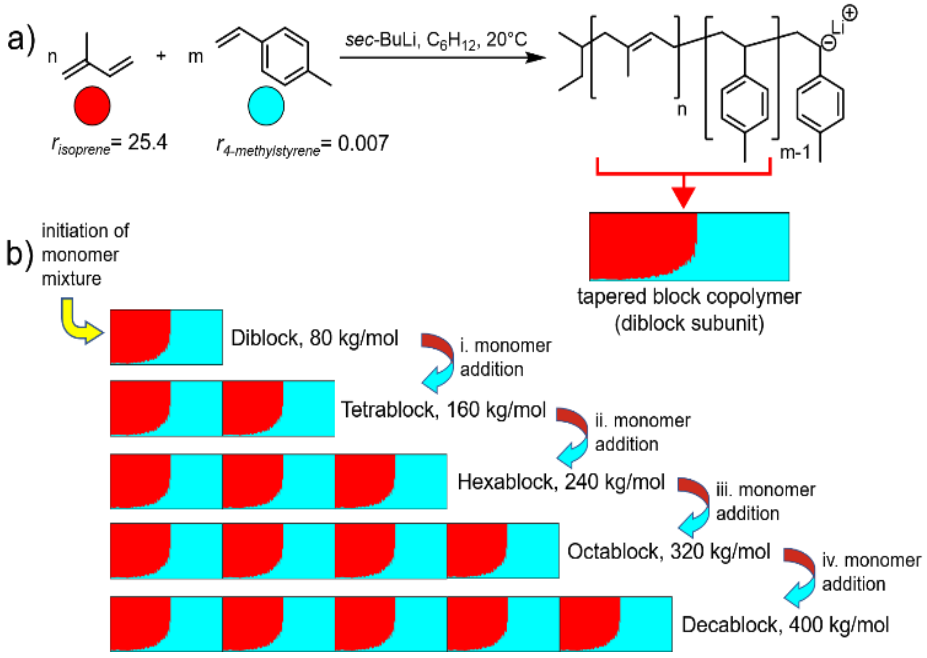

Scheme 1: (a) One-pot synthesis of tapered block copolymers from isoprene/4MS and resulting microstructure; (b) repetitive addition of I/4MS mixture for multiblock copolymers (MBC).

All polymerizations were carried out in all-glass reactors with teflon stopcocks at 20°C in cyclohexane (for details see Supporting Information), and no further polymer fractionation was applied beyond mere precipitation after the synthesis. In order to prepare a linear tetrablock copolymer, a I/4MS mixture of the desired monomer ratio was initiated by *sec*-butyllithium. The characteristic color change of colorless polyisoprenyllithium to the dark orange poly-4-methylstyryllithium marks the

succesful crossover from one living chain end to another. Once full monomer conversion was attained, the same amount of the I/4MS monomer mixture was added again. The strongly favoured incorporation of isoprene was visible by instant decoloration of the polymer solution, due to the rapid crossover to isoprenyl carbanions. Capitalizing on the combination of statistical copolymerization and sequential monomer mixture addition, the polymer chains possess a tapered $(AB)_n$ multiblock structure, AB representing a tapered diblock subunit with a steep gradient and n giving the total amount of AB diblock subunits in the chain. 2n is thus the total number of blocks in the tapered multiblock chains formed. The typical scale of every polymerization was 25 g, however this was scaled up to 100 g in several cases. All obtained polymers showed narrow molecular weight distributions and a slight tailing towards lower molecular weights, induced by a small percentage of termination during monomer addition (Figure 1).

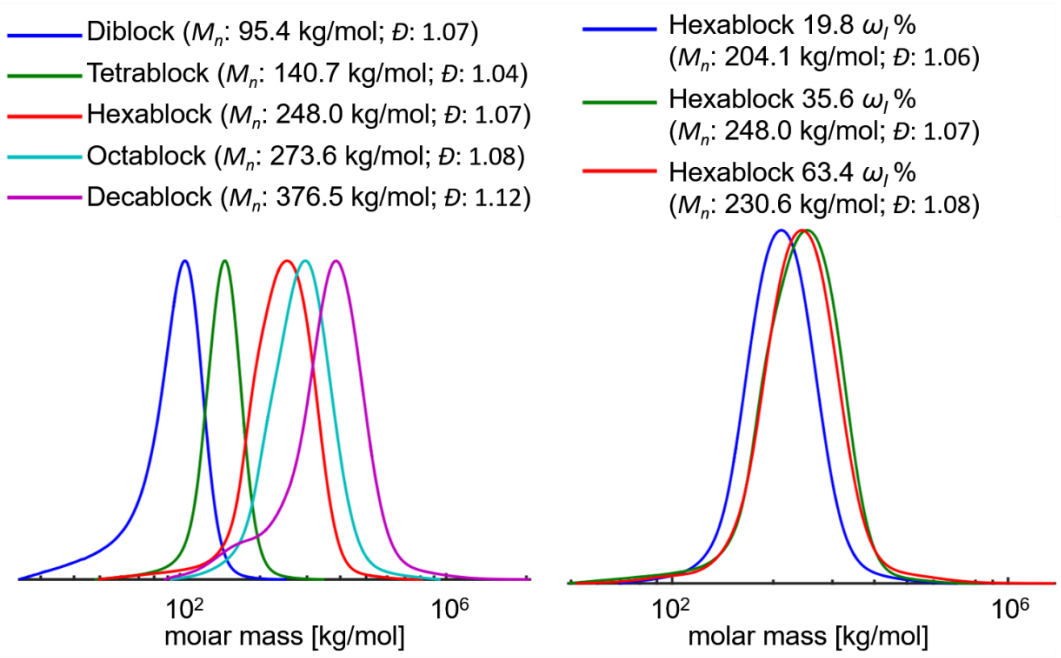

Figure 1: SEC diagrams (THF, PS calibration); left: di-, tetra-, hexa-, octa- and decablock copolymers; (right) hexablock copolymers with varying isoprene content.

The difference between targeted and measured molecular weight (Supp. Inf.) is due the calibration with polystyrene standards, which does not give absolute molecular weights. However, since the molecular weight of the AB diblock structure (diblock, Figure 1) correlates with expectation based on monomer /initiator ratio, SEC calibrated with PS standards gives a reasonable estimate. Due to the incompatibility

of PI and P4MS and the high molecular weights of each polymer segment, all multiblock copolymers show two glass transition temperatures, T_g (Table 1). All glass transitions of the PI and P4MS segments deviate from those of the respective homopolymers (-69 °C and 106 °C). This deviation is mainly attributed to the compatibilization effect of the short gradient section, which is formed during the statistical copolymerization and the alternating $(AB)_n$ structure.[28,27] Compared to the diblock, the deviation of the T_gs from the glass transition of the homopolymers increases very slightly with increasing n (Table 1, Entry 2-5). This leads to the conclusion, that the T_gs of a linear $(AB)_n$ copolymer are mainly affected by the molecular weight and structure of the diblock subunits and the effect of the alternating structure is only of minor importance.

Table 1: Results of DSC measurements

Sample	Number of blocks	Isoprene content[a] (mol%/weight%)	$M_{n,\,theoretical}$ (kg mol^{-1})	$T_{g,\,I}$ (°C)	$T_{g,\,4MS}$ (°C)
1	2	50 / 36.6	80	-51	93
2	4	50 / 36.6	160	-48	78
3	6	49 / 35.6	240	-48	76
4	8	48 / 34.7	320	-48	75
5	10	49 /35.6	400	-46	75
6	6	30 /19.8	240	-35	69
7	6	75 / 63.4	240	-55	82

[a] Determined by NMR in $CDCl_3$

To examine the correlation between block number and mechanical characteristics, particularly with respect to the toughness of the materials, stress-strain experiments were performed on thin films of each polymer (Figure 2). At a constant isoprene content of 50 mol% (37 weight%) all multiblock copolymers showed a tremendous increase of strain at break as compared to a diblock copolymer, which is a consequence of bridging of the lamellar domains by the multiblock chains, in analogy to the results of Watanabe, Spontak and Bates.[24-27,29] This effect is particularly pronounced on going from the tapered diblock to the tetrablock sample, evidencing

the onset of domain bridging. Further diblock addition shows a smaller effect on the mechanical properties. No direct correlation of block number and strain at break was observed. However, the toughness of the materials greatly increased with the number of blocks (Figure 2a). Based on the results of Fleury and Bates, the increased toughness can mainly be attributed to the increasing molecular weight, although an effect of the increasing number of blocks and consequently bridging of more than two nanodomains is possible.[30] This explanation is also supported by a comparison of two tapered diblock copolymers with varying molecular weights (Figure S7).

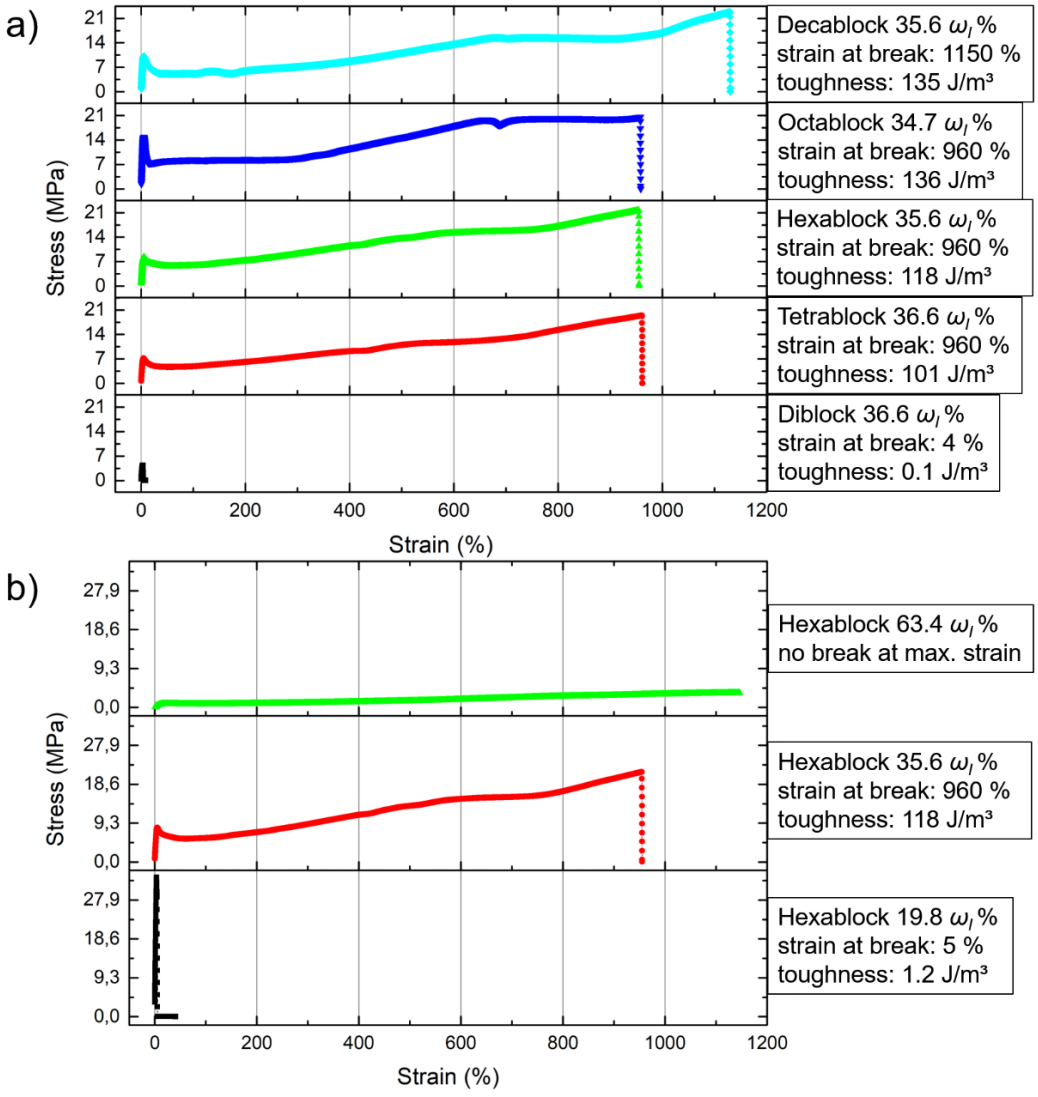

Figure 2: Stress-strain curves of (a) linear multiblock copolymers (isoprene content given in weight%), varying number of blocks and molecular weights from 80 to 400 kg mol^{-1}; (b) hexablock copolymers with varying isoprene content from 19.8 to 63.4 weight%.

In a second series of measurements three hexablock copolymers with similar molecular weights, but varying isoprene content from 30 to 75 mol% (that is from 19.8 to 63.4 weight%; Table 1, samples 3,6,7) were examined. As expected, high isoprene content of 75 mol% results in a rubber with very low modulus and toughness, but extremely high strain at break, exceeding the maximum extension of the setup. The hysteresis was approximately 12% (Supp. Inf.). On the other hand, a low isoprene content of 19.8 weight% yielded a high modulus material with low strain at break.

3.1.4 Conclusions

In conclusion, we report a scalable strategy giving rapid access to linear alternating, tapered $(AB)_n$ multiblock copolymers, capitalizing on the statistical anionic copolymerization of the common monomers isoprene and 4-methylstyrene. The strategy relies on the highly disparate reactivity ratios of isoprene (I, r_I = 25.4) and 4-methylstyrene (4MS, r_{4MS} = 0.007) in the anionic copolymerization in nonpolar media. Low dispersities and high molecular weights up to 400 kg mol^{-1} were achieved. This approach is of a general nature and can be transferred to any living copolymerization with similarly disparate reactivity ratios. Obviously, crossover in both directions is a key requirement. The tapered decablock structure presented here does certainly not yet represent the limiting block number of this approach. The obtained linear alternating multiblock copolymers combine essential features of established AB diblock copolymers, particularly nanophase segregation with exceptional mechanical properties without further chemical crosslinking. Toughness and maximum strain increase nonlinearly with increasing number of blocks, and the increase of toughness is more pronounced than the increase of strain at break. Phase-segregated lamellar morphologies for two of the samples, diblock and tetrablock, are given in the Supp. Inf. document. Further detailed morphological studies, including small-angle X-ray scattering (SAXS) are under way.

The repeated addition of monomer mixtures to generate tapered multiblock copolymers represents a general strategy for the copolymerization of dienes and a variety of styrene derivatives, which might eventually permit to subdivide synthetic polymer chains in flexible and rigid segments in a highly controlled manner ad

libitum. Tapered multiblocks are a promising class of materials for many of the applications established or discussed for di- and triblock copolymers at present, particularly when nanosegregation in combination with mechanical properties is important.

3.1.5 Acknowledgement

M.G. and M.A. acknowledge the German Research Foundation (DFG GA 2169/1-1) for partial financial support of this work. The authors also thank the RMU Mainz-Darmstadt for funding.

3.1.6 References

(1) Yarger, J. L.; Cherry, B. R.; van der Vaart, A. Uncovering the structure–function relationship in spider silk. *Nat. Rev. Mater.* **2018**, *3*, 1–11.

(2) Heim, M.; Keerl, D.; Scheibel, T. Spider silk: From soluble protein to extraordinary fiber. *Angew. Chem. Int. Ed.* **2009**, *48*, 3584–3596.

(3) Keten, S.; Xu, Z.; Ihle, B.; Buehler, M. J. Nanoconfinement controls stiffness, strength and mechanical toughness of beta-sheet crystals in silk. *Nat. Mater.* **2010**, *9*, 359–367.

(4) Bates, F. S.; Hillmyer, M. A.; Lodge, T. P.; Bates, C. M.; Delaney, K. T.; Fredrickson, G. H. Multiblock Polymers: Panacea or Pandora. *Science* **2012**, *336*, 434–440.

(5) Radlauer, M. R.; Fukuta, S.; Matta, M. E.; Hillmyer, M. A. Controlled synthesis of ABCA' tetrablock terpolymers. *Polymer* **2017**, *124*, 60–67.

(6) Ntaras, C.; Polymeropoulos, G.; Zapsas, G.; Ntetsikas, K.; Liontos, G.; Karanastasis, A.; Moschovas, D.; Rangou, S.; Stewart-Sloan, C.; Hadjichristidis, N. *et al.* Synthesis, characterization and self-assembly of well-defined linear heptablock quaterpolymers. *J. Polym. Sci. Part B: Polym. Phys.* **2016**, *54*, 1443–1449.

(7) Takada, K.; Ito, T.; Kitano, K.; Tsuchida, S.; Takagi, Y.; Chen, Y.; Satoh, T.; Kakuchi, T. Synthesis of Homopolymers, Diblock Copolymers, and Multiblock Polymers by Organocatalyzed Group Transfer Polymerization of Various Acrylate Monomers. *Macromolecules* **2015**, *48*, 511–519.

(8) Schacher, F. H.; Rupar, P. A.; Manners, I. Functional Block Copolymers: Nanostructured Materials with Emerging Applications. *Angew. Chem. Int. Ed.* **2012**, *51*, 7898–7921.

(9) Bates, C. M.; Maher, M. J.; Janes, D. W.; Ellison, C. J.; Willson, C. G. Block Copolymer Lithography. *Macromolecules* **2013**, *47*, 2–12.

(10) Park, C.; Yoon, J.; Thomas, E. L. Enabling nanotechnology with self assembled block copolymer patterns. *Polymer* **2003**, *44*, 6725–6760.

(11) Gaymans, R. J. Segmented copolymers with monodisperse crystallizable hard segments: Novel semi-crystalline materials. *Prog. Polym. Sci.* **2011**, *36*, 713–748.

(12) Kim, H.-C.; Park, S.-M.; Hinsberg, W. D. Block Copolymer Based Nanostructures: Materials, Processes, and Applications to Electronics. *Chem. Rev.* **2010**, *110*, 146–177.

(13) Simula, A.; Nikolaou, V.; Anastasaki, A.; Alsubaie, F.; Nurumbetov, G.; Wilson, P.; Kempe, K.; Haddleton, D. M. Synthesis of well-defined α,ω-telechelic multiblock copolymers in aqueous medium: In situ generation of α,ω-diols. *Polym. Chem.* **2015**, *6*, 2226–2233.

(14) Zhang, J.; Deubler, R.; Hartlieb, M.; Martin, L.; Tanaka, J.; Patyukova, E.; Topham, P. D.; Schacher, F. H.; Perrier, S. Evolution of Microphase Separation with Variations of Segments of Sequence-Controlled Multiblock Copolymers. *Macromolecules* **2017**, *50*, 7380–7387.

(15) Gody, G.; Maschmeyer, T.; Zetterlund, P. B.; Perrier, S. Rapid and quantitative one-pot synthesis of sequence-controlled polymers by radical polymerization. *Nat. Commun.* **2013**, *4*, 2505.

(16) Engelis, N. G.; Anastasaki, A.; Whitfield, R.; Jones, G. R.; Liarou, E.; Nikolaou, V.; Nurumbetov, G.; Haddleton, D. M. Sequence-Controlled Methacrylic Multiblock Copolymers: Expanding the Scope of Sulfur-Free RAFT. *Macromolecules* **2018**, *51*, 336–342.

(17) Chen, C. Designing catalysts for olefin polymerization and copolymerisation: Beyond electronic and steric tuning. *Nat. Rev. Chem.* **2018**, *2*, 6–14.

(18) Zhu, Y.; Radlauer, M. R.; Schneiderman, D. K.; Shaffer, M. S. P.; Hillmyer, M. A.; Williams, C. K. Multiblock Polyesters Demonstrating High Elasticity and Shape Memory Effects. *Macromolecules* **2018**, *51*, 2466–2475.

(19) Romain, C.; Zhu, Y.; Dingwall, P.; Paul, S.; Rzepa, H. S.; Buchard, A.; Williams, C. K. Chemoselective Polymerizations from Mixtures of Epoxide, Lactone, Anhydride, and Carbon Dioxide. *J. Am. Chem. Soc.* **2016**, *138*, 4120–4131.

(20) Corbin, N.; Prud'Homme, J. Multiblock copolymers of styrene and isoprene. II. Microstructure and dilute solution properties. *J. Polym. Sci. Polym. Phys. Ed.* **1977**, *15*, 1937–1951.

(21) Corbin, N.; Prud'Homme, J. Multiblock copolymers of styrene and isoprene. I. Synthesis and characterization. *J. Polym. Sci. Polym. Chem. Ed.* **1976**, *14*, 1645–1659.

(22) Daniel Wagner; Konrad Knoll. Styrol-Butadien-Blockcopolymere: Designerprodukte aus dem Baukasten. *Kunststoffe* **2010**, *9*, 186–189.

(23) Knoll, K.; Nießner, N. Styrolux and styroflex from transparent high impact polystyrene to new thermoplastic elastomers. *Macromolecular Symposia* **1998**, *132*, 231–243.

(24) Matsumiya, Y.; Watanabe, H.; Takano, A.; Takahashi, Y. Uniaxial Extensional Behavior of $(SIS)_p$-Type Multiblock Copolymer Systems: Structural Origin of High Extensibility. *Macromolecules* **2013**, *46*, 2681–2695.

(25) Watanabe, H.; Matsumiya, Y.; Sawada, T.; Iwamoto, T. Rheological and Dielectric Behavior of Dipole-Inverted (SIS) p -Type Multiblock Copolymers: Estimates of Bridge/Loop Fractions for Respective I Blocks and Effect of Loops on High Extensibility of Bridges. *Macromolecules* **2007**, *40*, 6885–6897.

(26) Matsushita, Y.; Mogi, Y.; Mukai, H.; Watanabe, J.; Noda, I. Preparation and morphology of multiblock copolymers of the (AB)n type. *Polymer* **1994**, *35*, 246–249.

(27) Spontak, R. J.; Smith, S. D. Perfectly-alternating linear (AB)n multiblock copolymers: Effect of molecular design on morphology and properties. *J. Polym. Sci. Part B: Polym. Phys.* **2001**, *39*, 947–955.

(28) Grune, E.; Johann, T.; Appold, M.; Wahlen, C.; Blankenburg, J.; Leibig, D.; Müller, A. H. E.; Gallei, M.; Frey, H. One-Step Block Copolymer Synthesis versus Sequential Monomer Addition: A Fundamental Study Reveals That One Methyl Group Makes a Difference. *Macromolecules* **2018**, *51*, 3527–3537.

(29) Lee, I.; Bates, F. S. Synthesis, Structure, and Properties of Alternating and Random Poly(styrene- b -butadiene) Multiblock Copolymers. *Macromolecules* **2013**, *46*, 4529–4539.

(30) Fleury, G.; Bates, F. S. Structure and Properties of Hexa- and Undecablock Terpolymers with Hierarchical Molecular Architectures. *Macromolecules* **2009**, *42*, 3598–3610.

3.1.7 Supporting Information

3.1.7.1 Materials

All chemicals and solvents were purchased from Acros Organics Co. and Sigma-Aldrich Co. Isopropyl alcohol, chloroform and *sec*-butyllithium were used as received without further purification. Cyclohexane was purified via distillation over sodium and degassed by three freeze-thaw cycles prior to use. Isoprene and 4-methylstyrene were purified by distillation over CaH_2 and degassed by three cycles of freeze-thaw prior to use.

3.1.7.2 General polymerization procedure for the synthesis of multiblock copolymers

A mixture of isoprene and 4-methylstyrene was dried over CaH_2, degassed by three cycles of freeze-thaw and distilled into a graduated ampule. 100 ml dried and degassed Cyclohexane (78.5 g, 932 mmol) was distilled into an all glass reactor equipped with a magnetic stir bar. The reactor was flushed with argon, 5.2 g of the monomer mixture (4MS: 3.3 g, 27.9 mmol, 262 mol/L; I: 1.9 g, 27.9 mmol, 262 mol/L) were added through the ampule and initiated by adding 0.05 ml (0.065 mmol, 1.3 M

solution in cyclohexane) of *sec*-butyllithium via syringe. After 24 h the next load of 5.2 g of the monomer solution were added. The addition of the monomer mixture was repeated, until the desired number of blocks was achieved. The polymerization was terminated by adding 1 ml of degassed isopropyl alcohol via syringe. To precipitate the polymer, the mixture was poured into a 8-fold excess of isopropyl alcohol.

3.1.7.3 Characterization

Instrumentation: NMR spectra were recorded on a Bruker Avance II 400 spectrometer working 400 MHz (^{1}H NMR). NMR chemical shifts are referenced to tetramethylsilane. Standard SEC was performed with THF as the mobile phase (flow rate 1 mL min-1) on a SDV column set from PSS (SDV 103, SDV 105, SDV 106) at 30°C. Calibration was carried out using PS standards (from Polymer Standard Service, Mainz). For determining the thermal properties of the polymers differential scanning calorimeter (DSC) was performed with a Mettler Toledo DSC-1 in a temperature range from -90°C to 150°C with a heating rate of 10 K min-1.

Tensile Testing: All films were obtained from a 5 wt% solution in chloroform by slow evaporation of the solvent. The test specimens were punched out using a bone shaped stamp. All measurements were repeated with 3 different samples of the respective multiblock copolymer sample.

TEM Measurements: TEM experiments were carried out on a Zeiss EM 10 electron microscope operating at 60 kV. All shown images were recorded with a slow-scan CCD camera obtained from TRS (Tröndle) in bright field mode. Camera control was computer-aided using the ImageSP software from TRS.

3.1.7.4 ^{1}H-NMR spectra

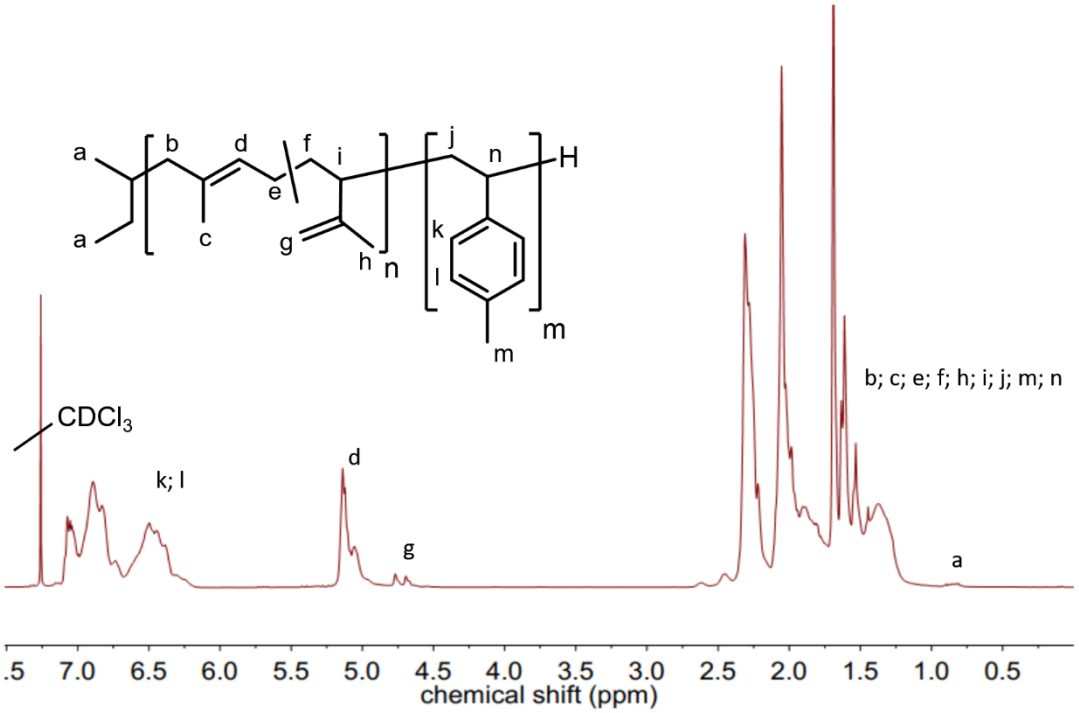

Figure S1: ^{1}H-NMR spectrum (400 MHz) of a tapered multiblock copolymer in $CDCl_3$ (decablock, sample 5 in Table S1).

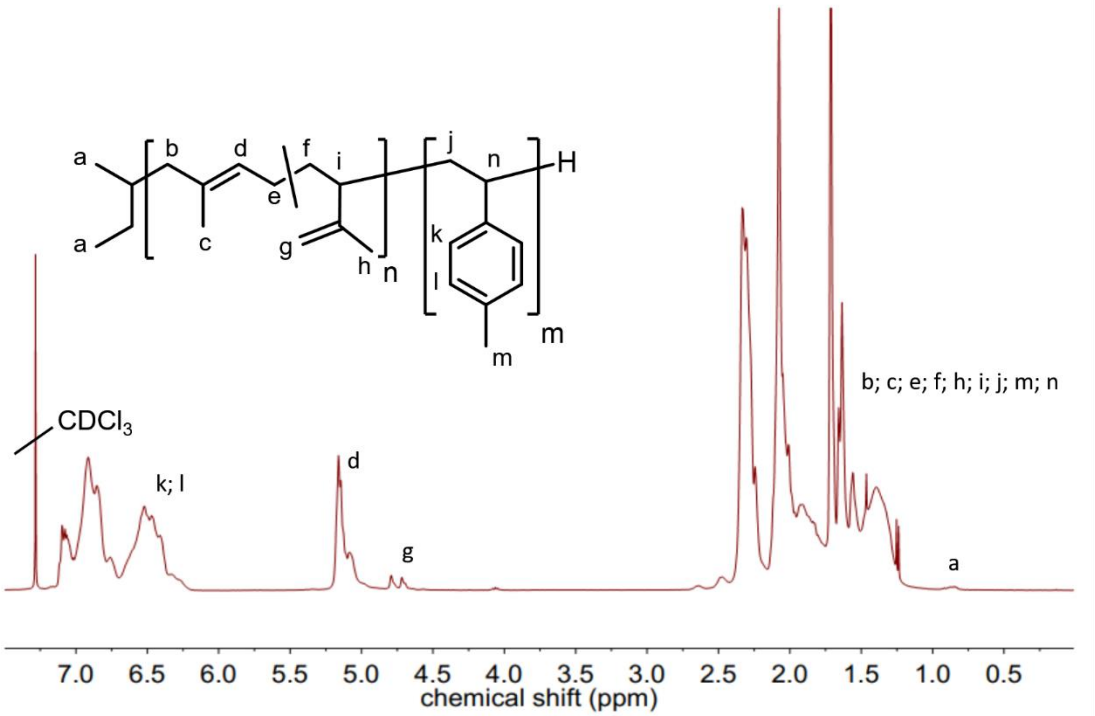

Figure S2: ^{1}H-NMR spectrum (400 MHz) of hexablock copolymer in $CDCl_3$ (sample 3 in Table S1).

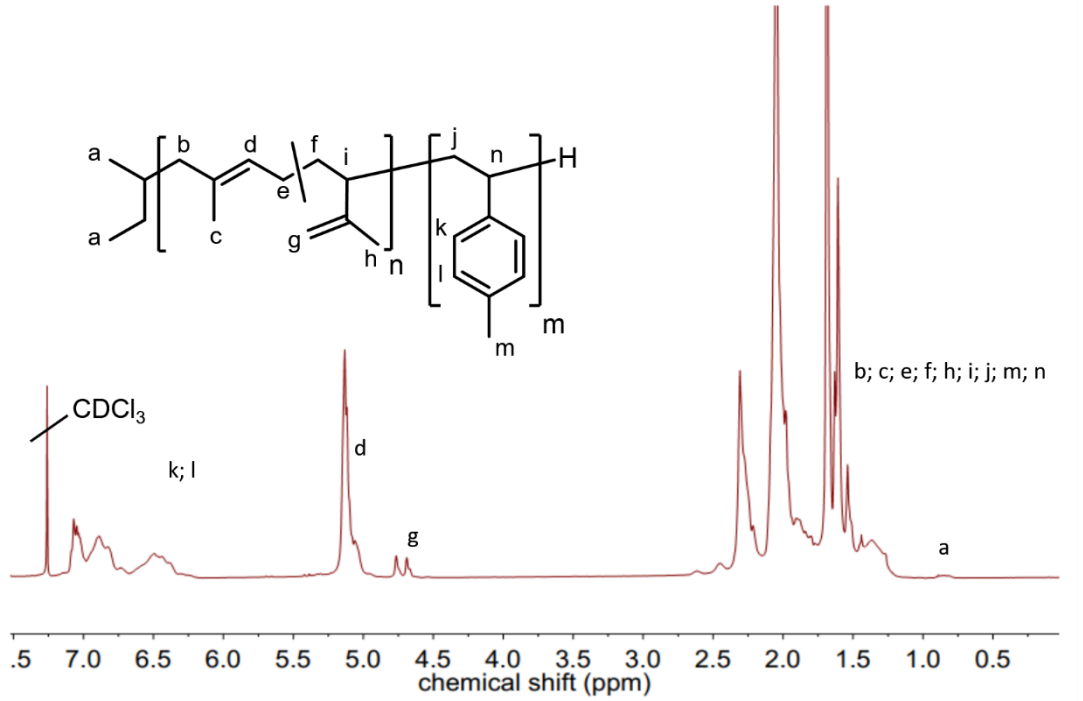

Figure S3: ^{1}H-NMR spectrum (400 MHz) of hexablock copolymer in $CDCl_3$ (sample 6 in Table S1).

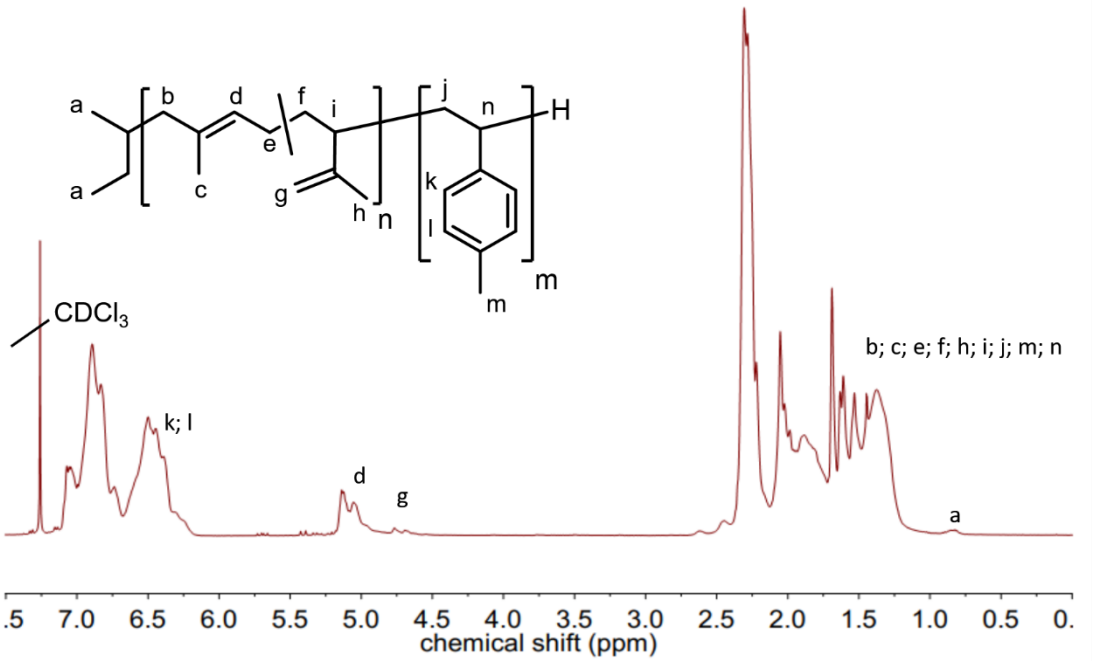

Figure S4: ^{1}H-NMR spectrum (400 MHz) of hexablock copolymer in $CDCl_3$ (sample 7 in Table S1).

3.1.7.5 Summary of Characterization Results for Multiblock Copolymers

Table S1: Summary of characterization results of tapered multiblock copolymers by NMR, SEC, DSC and tensile testing; each tapered diblock structure was set to 80 kg/mol by the monomer/initiator ratio.

Sample	Number of blocks	Isoprene content[a] (mol%)	*targeted* M_n, (kg/mol)	M_n[b] (kg/mol)	$Đ$[b]	$T_{g,1}$[c] (°C)	$T_{g,4MS}$[c] (°C)	Strain at Break[d] (%)
1	2	50	80	95.4	1.07	-51	93	4
2	4	50	160	140.7	1.04	-48	78	960
3	6	49	240	248.0	1.07	-48	76	960
4	8	48	320	273.6	1.08	-48	75	960
5	10	49	400	376.5	1.12	-46	75	1150
6	6	30	240	204.1	1.06	-35	69	5
7	6	75	240	230.6	1.08	-55	82	/

[a] Determined by NMR in $CDCl_3$; [b] SEC in THF at 25 °C; [c] via DSC; [d] determined by tensile testing.

3.1.7.6 Multiblock copolymer DSC diagram

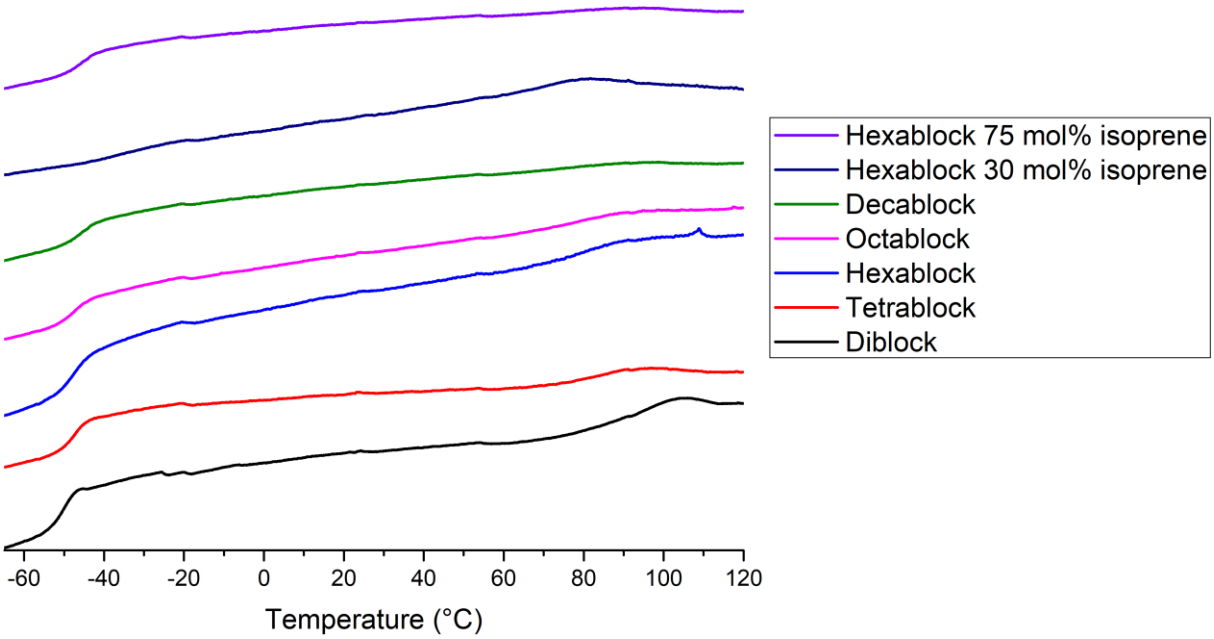

Figure S5: DSC thermograms of all multiblock samples. Heating rate 10 K/min; first heating of film obtained after slow solvent evaporation.

3.1.7.7 Tensile Testing

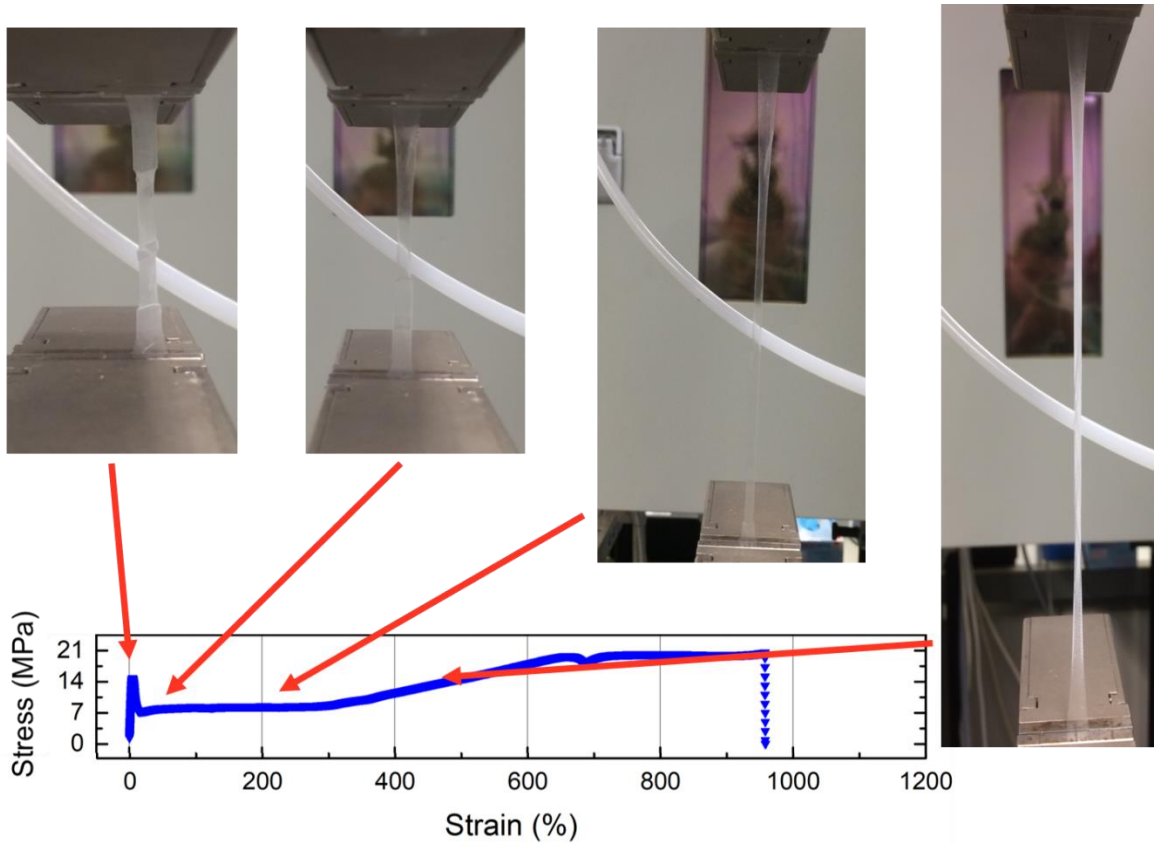

Figure S6: Tensile testing of octablock film sample (entry 4, Table S1), visualizing the different stages of elongation during tensile testing.

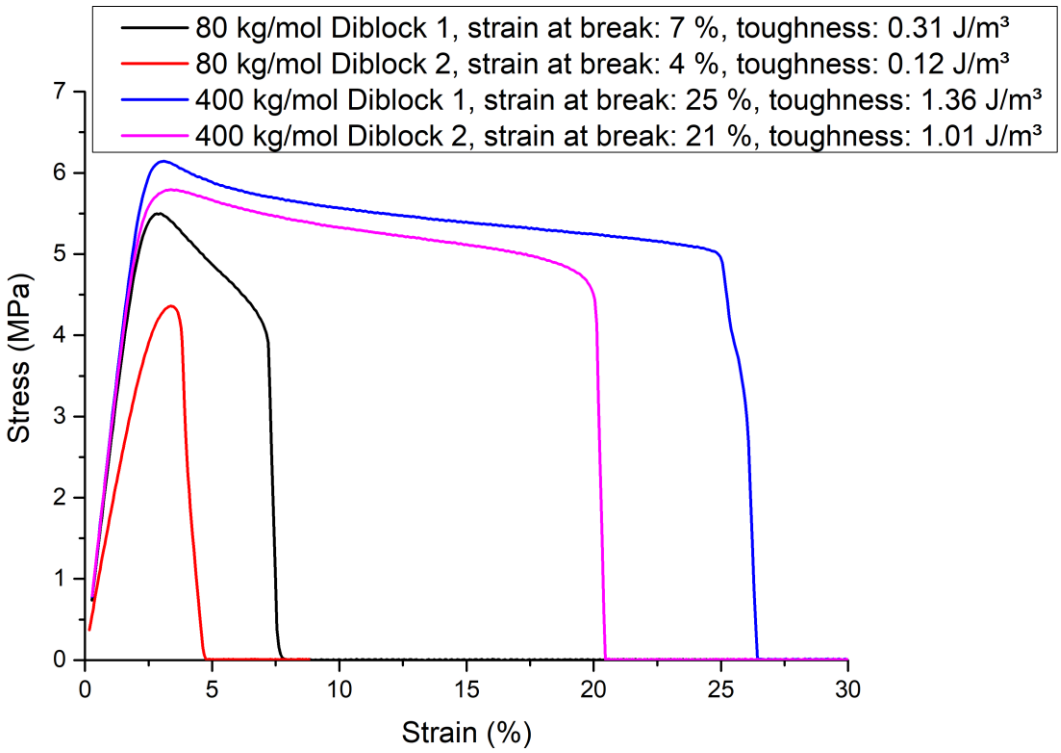

Figure S7: Stress-strain curve of diblock copolymers with different molecular weights (80 kg/mol and 400 kg/mol).

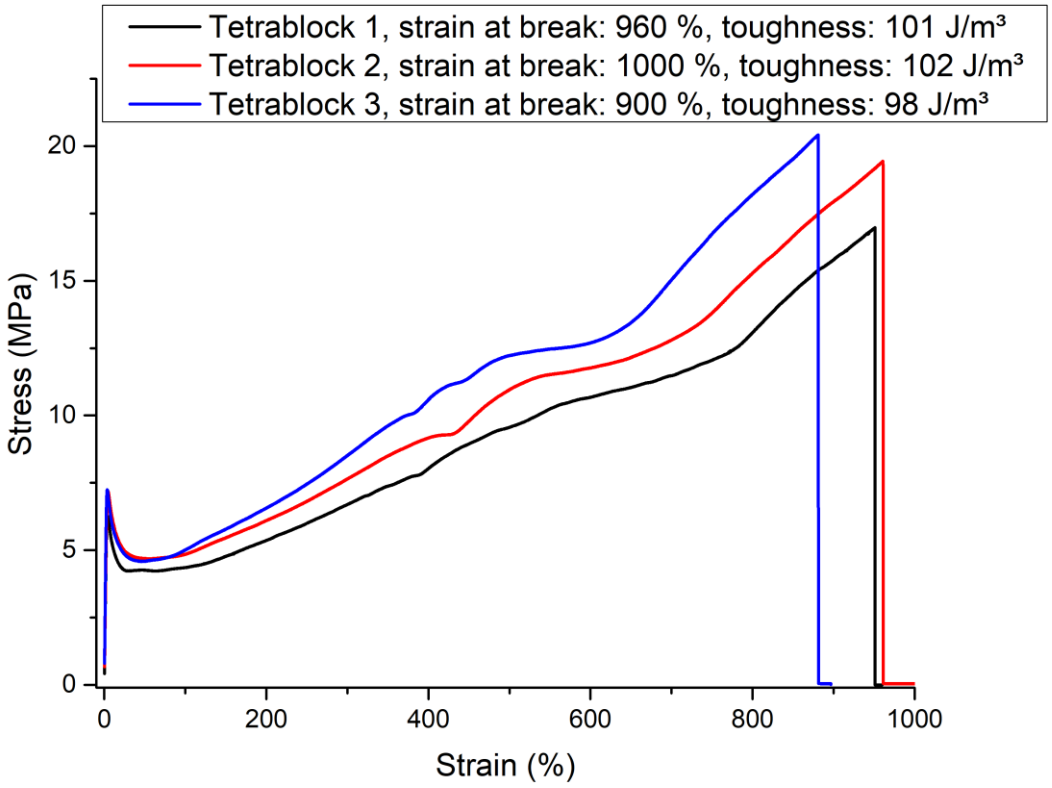

Figure S8: Stress-strain curve of a tetrablock copolymer.

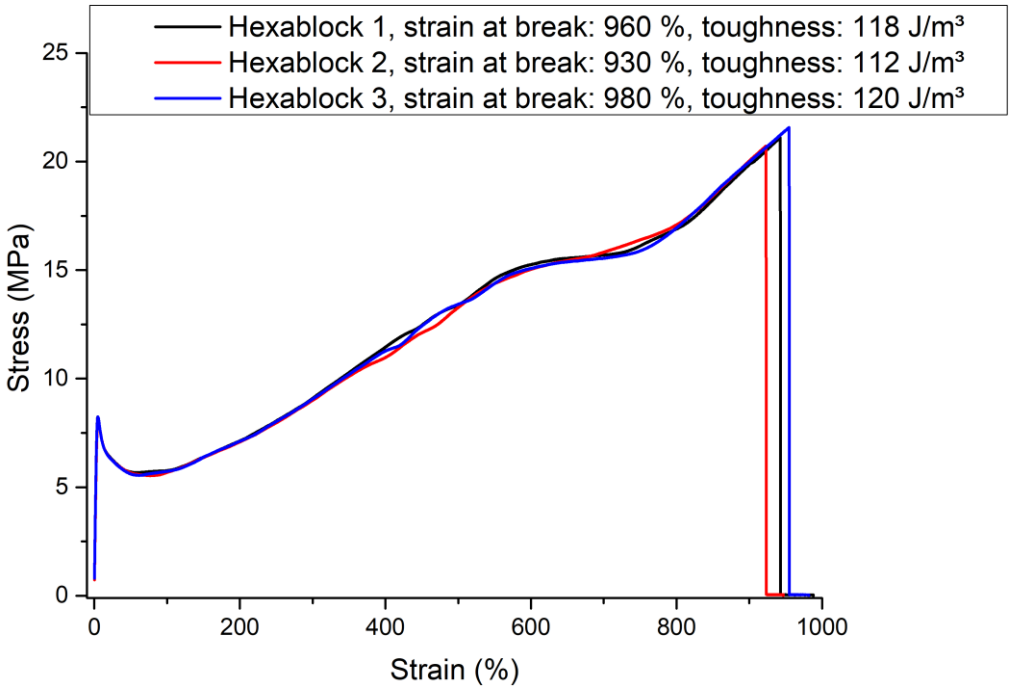

Figure S9: Stress-strain curve of a hexablock copolymer.

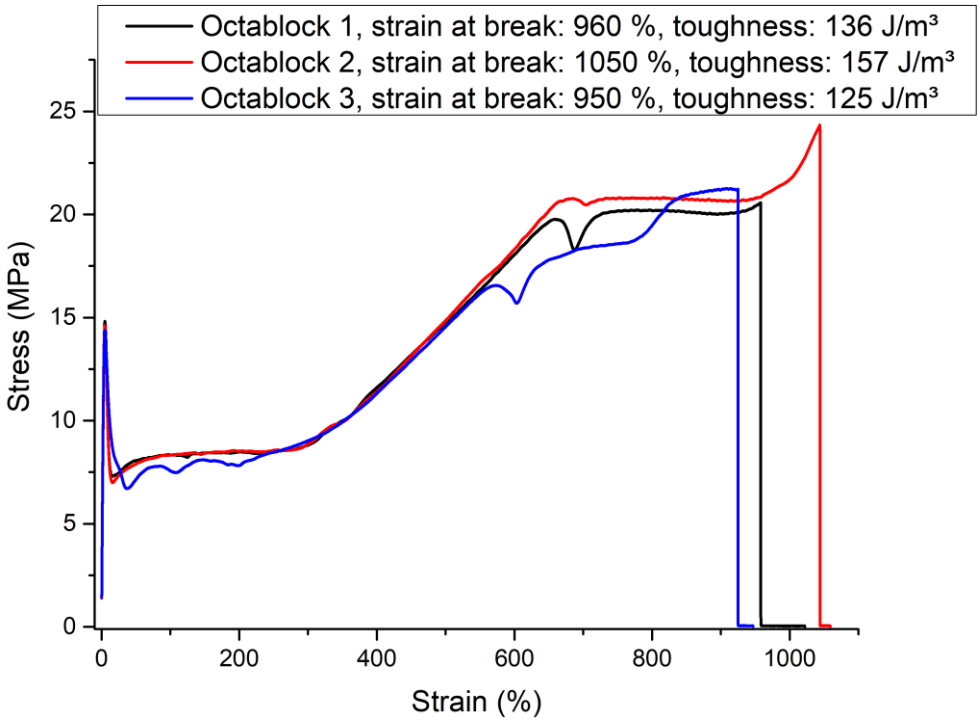

Figure S10: Stress-strain curve of an octablock copolymer.

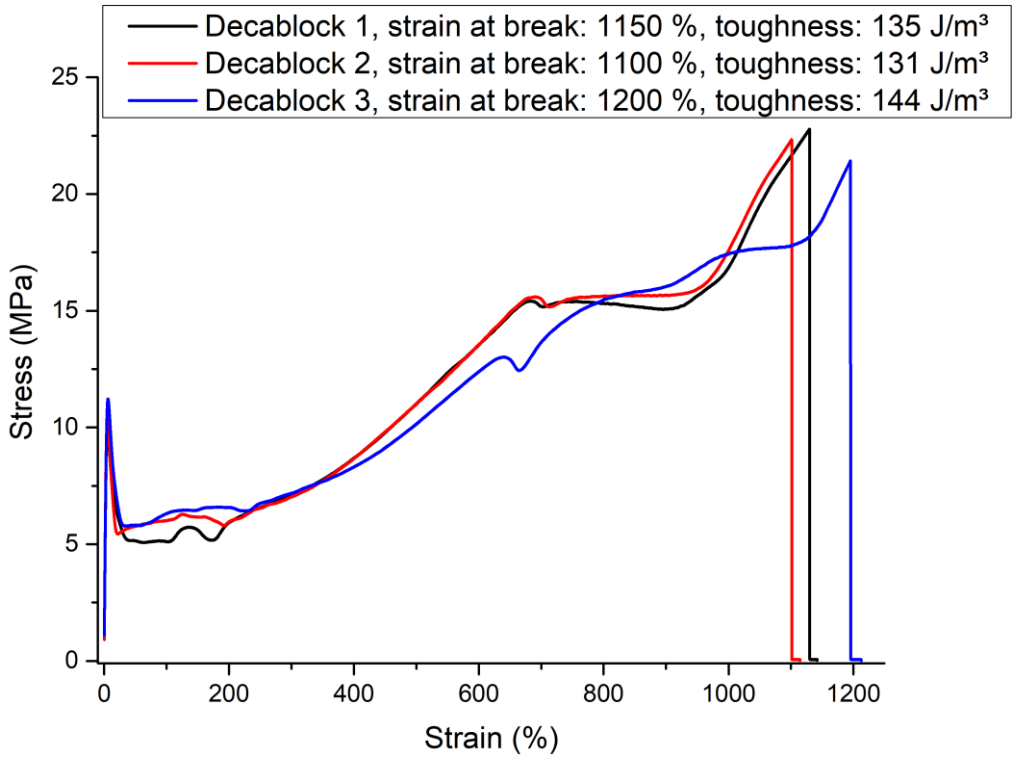

Figure S11: Stress-strain curve of a decablock copolymer.

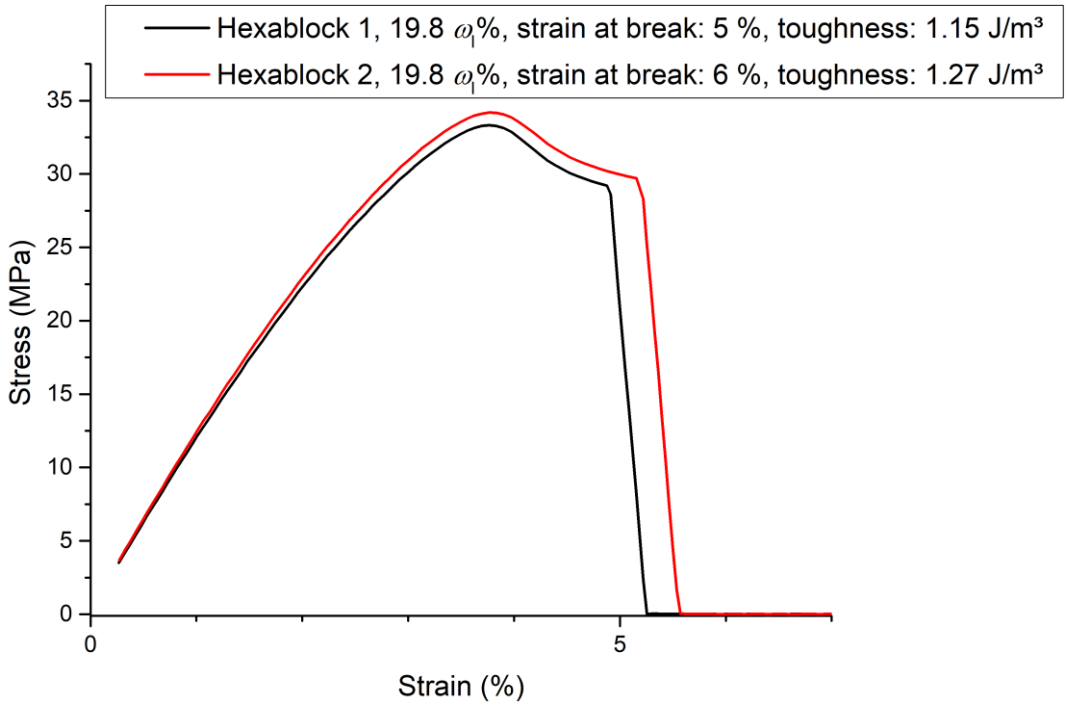

Figure S12: Stress-strain curve of a hexablock copolymer with an isoprene content of 30 mol% (19.8 ω_I%).

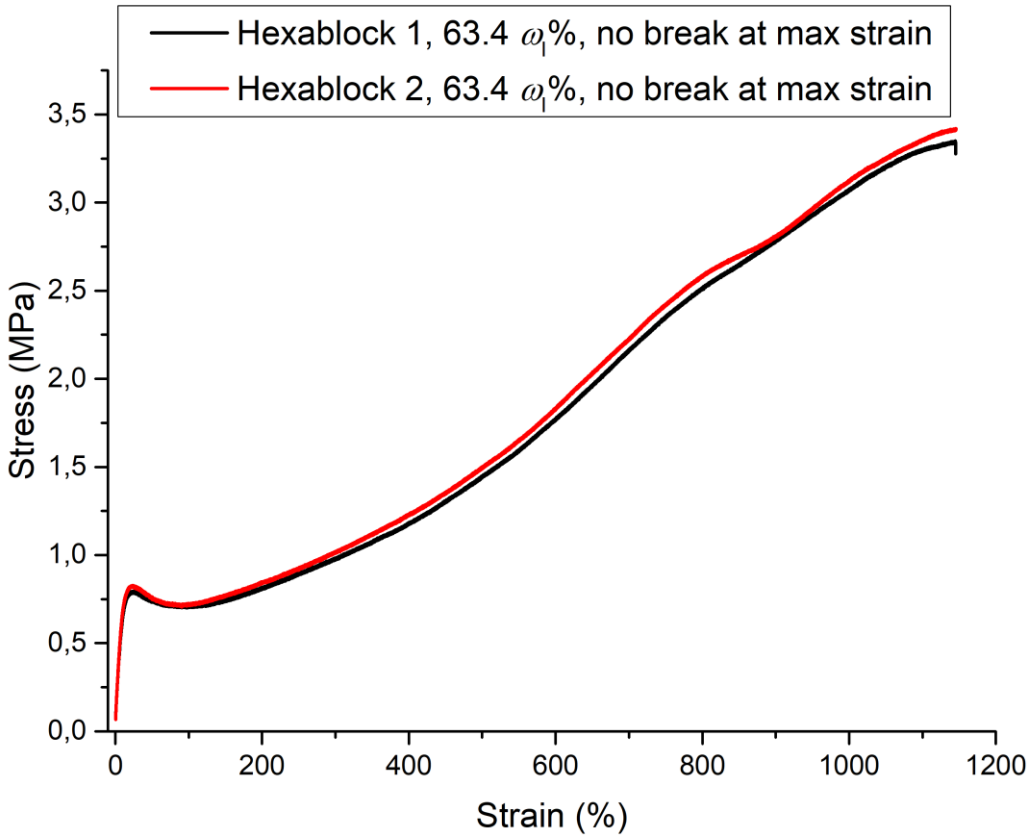

Figure S13: Stress-strain curve of a hexablock copolymer with an isoprene content of 75 mol% (63.4 ω_I%).

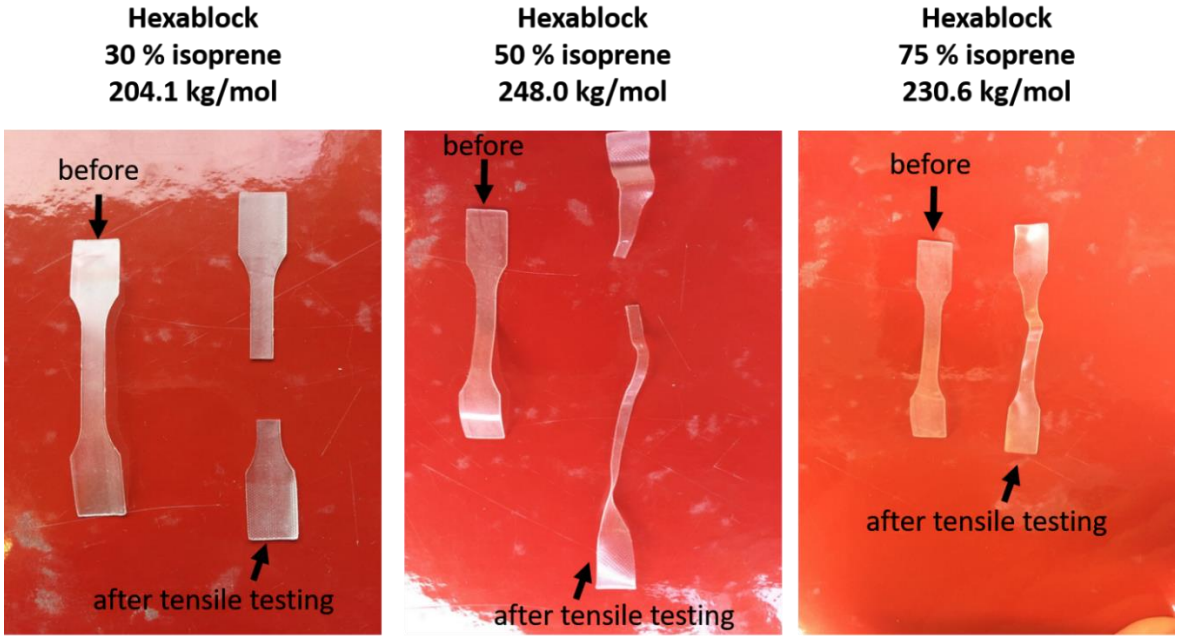

Figure S14: Typical specimens of tapered hexablock multiblock copolymers before and after tensile testing, isoprene content in mol%; left: sample 6; middle: sample 3; right: sample 7 in Table S1; sample 7 shows 10-15% hysteresis.

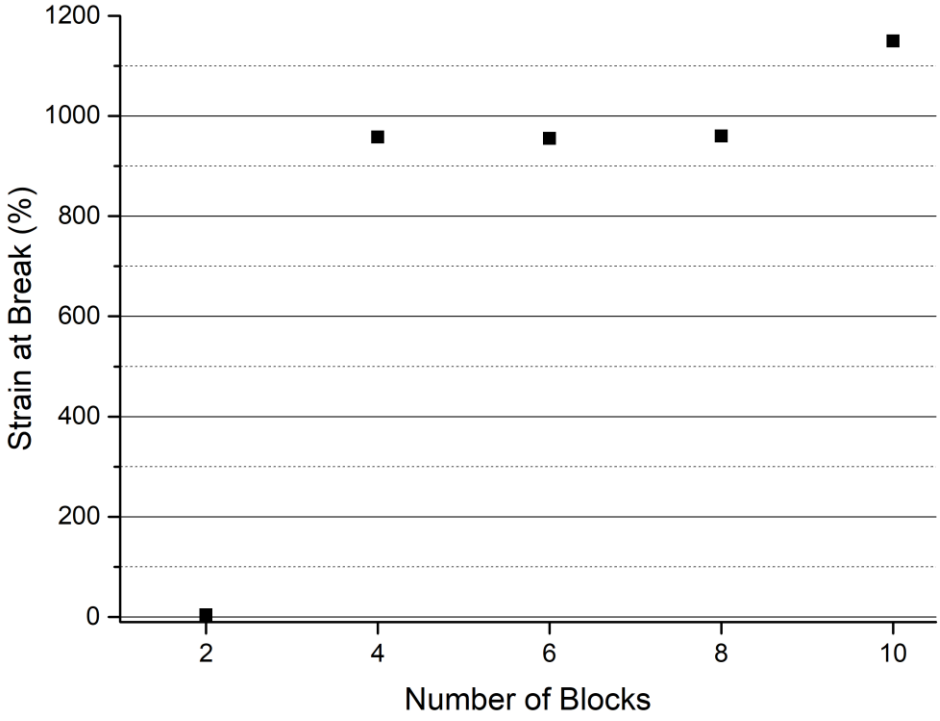

Figure S15: Strain at break vs. number of blocks (samples 1-5, Table 1).

3.1.7.8 Transmission electron microscopy

Samples were stained with OsO_4; PI-phase dark, P4MS-phase bright color, lamellar morphologies for tapered diblock and tetrablock copolymer.

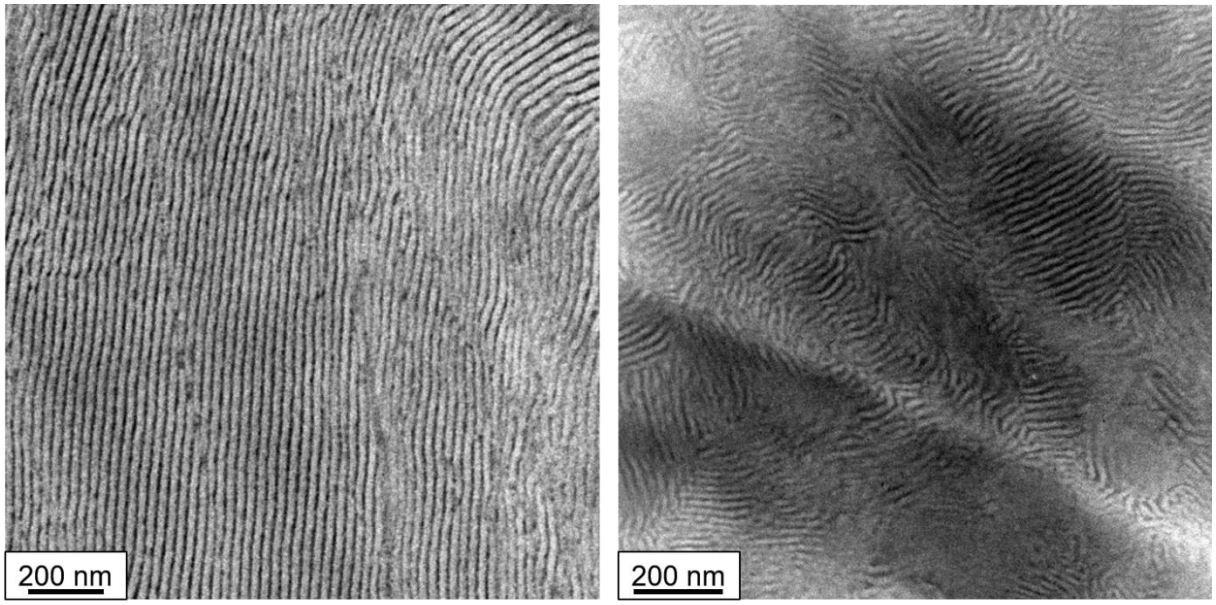

Figure S16: TEM images of entry 1 (tapered diblock, left) and entry 2 (tapered tetrablock, right) in Table S1. Both samples show lamellar morphologies; 37 weight% isoprene, 63 weight% 4-methylstyrene.

3.2 Tapered multiblock copolymers based on isoprene and 4-methylstyrene: Does a steep gradient make a difference?

Eduard Grune,[a,b] Christian Wahlen,[a] Michaele Appold,[c] Axel H. E. Müller,[a] Markus Gallei,[c], Holger Frey[a], George Floudas*,[d]

[a] Institute of Organic Chemistry, Johannes Gutenberg University, Duesbergweg 10-14, 55128 Mainz, Germany

[b] Graduate School Materials Science in Mainz, Staudinger Weg 9, 55128 Mainz, Germany

[c] Macromolecular Chemistry Department, TU Darmstadt, Alarich-Weiss Str. 4, 64287 Darmstadt, Germany

[d] Department of Physics, University of Ioannina, P.O. Box 1186, 45110 Ioannina, Greece

to be submitted to Macromolecules

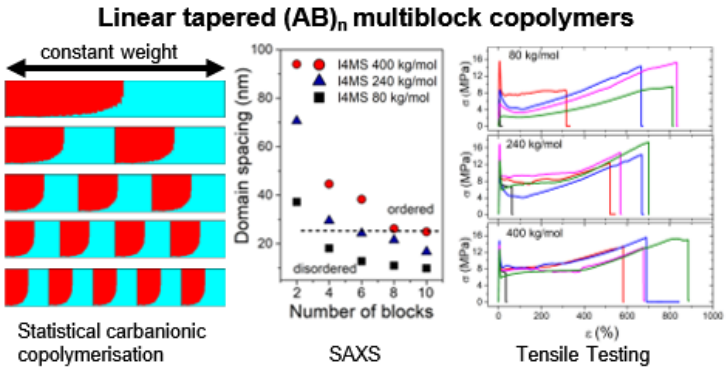

3.2.1 Abstract

The statistical carbanionic copolymerization of isoprene (I) and 4-methylstyrene (4MS) yields block like tapered copolymers due to the markedly different reactivity ratios of I/4MS (r_I = 25.4; r_{4MS} = 0.007). The combination of simultaneous copolymerization and sequential additions of I/4MS mixtures permits rapid access to linear tapered $(AB)_n$ multiblock copolymers in n steps. Three series of tapered $(AB)_n$ multiblock copolymers with constant molecular weights of 80 kg/mol, 240 kg/mol and 400 kg/mol and varying block numbers ranging from 2 (n=1) to 10 (n=5) were prepared to examine their thermal, morphological and mechanical properties. All multiblock copolymers were characterised by SEC, showing narrow dispersities ($Đ$ = 1.05 – 1.26) and the desired molecular weights. Due to the incompatibility of the PI and P4MS segments, two distinct T_gs could be observed via DSC measurements for all samples. For the fist time, the χ-parameter of I/4MS ($\chi_{FH,\ I/4MS}$=36.0/T-0.041), could be determined, revealing a much weaker immiscibility of I/4MS than for I/S monomer ($\chi_{FH,\ I/S}$=71.4/T-0.0857). However, in-depth SAXS studies showed that I/4MS based tapered $(AB)_n$ multiblock copolymers form ordered structures for tetra- and hexablock copolymers, while larger block numbers show only weak segregation or disordered regimes. Tensile tests revealed a dramatic enhancement of the strain at break; from about 10% in the tapered diblock copolymers to as high as 800% in several tapered multiblock copolymers with a concomitant increase in toughness. Furthermore, it could be concluded that the non-linear and linear viscoelastic response can be fine-tuned by the judicious selection of molecular weights and number of blocks.

3.2.2 Introduction

Block copolymers represent a commercially highly relevant polymer type and can be found in many applications like footwear, adhesives or asphalt modifiers.[1,2] Especially triblock copolymers consisting of hard and glassy outer blocks and a rubbery middle block represent the predominant structure for applications requiring high toughness and resilience.[3] The combination of immiscible hard and soft segments leads to strong microphase segregation, which is crucial for good mechanical properties.[4,5] In recent years linear alternating $(AB)_n$ multiblock copolymers, consisting of immiscible hard

and soft segments, have been studied in several works, demonstrating their superior properties when compared to ABA triblock copolymers.[6-9] The first concept for such a structure dates back to 1959, when Korotkov et al. used living anionic copolymerization and sequential monomer addition, to present the first linear alternating multiblock copolymers.[10] More than two decades later, Corbin and Prud'Homme continued and extended this idea. Taking advantage of the vigorously different reactivities of styrene and isoprene, Corbin and Prud'Homme added isoprene several times to a living polystyryllithium solution to prepare linear alternating tapered copolymers.[11,12] However, both approaches did not afford highly defined multiblock copolymers with narrow molecular weight distributions.

Since then various synthetic approaches based on controlled radical polymerization and catalytic precision polymerization have been developed, enabling the introduction of functional groups and the incorporation of more than three different monomers.[13-19] Nevertheless, the majority of highly defined multiblock copolymers with low dispersities and phase separated high molecular weight blocks is still prepared by living anionic polymerization. Despite the challenging synthesis, several groups like Spontak et al., Matsushita et al., Watanabe et al. and Bates et al. impressively demonstrated the capability of carbanionic polymerization for the preparation of high molecular weight multiblock copolymers with low dispersity and morphologically relevant block sizes capable of phase segregation.[20-23] Furthermore, the abovementioned groups carried out in depth mechanical and morphological studies, leading to fundamental concepts for the correlation between polymer architecture and mechanical response.[24-28]

Like in diblock and triblock copolymers the phase separation behaviour of multiblock copolymers mainly depends on the incorporated monomers, the composition and the structure of the polymer chain.[20,21] The main difference between di- and multiblock copolymers is their conformation in bulk morphologies. While a diblock is restricted to merely one conformation, where each block is located in its specific domain, a multiblock can form loops and bridges to build up microdomain interconnectivity.[20,25] It is obvious that increasing the number of blocks of $(AB)_n$ multiblocks will increase the concentration of loops and bridges and therefore enhance resilience and toughness.[25] In addition to this general observation, *n* can be seen as a further parameter to tune morphological, mechanical and thermochemical properties like

strain at break, toughness, domain sizes, order disorder transition temperature (T_{ODT}) and glass transition temperature (T_g).

While the morphology of multiblock copolymers mainly depends on composition, size and structure of the AB subunits, their domain sizes will decrease with increasing *n.*[20,21] Furthermore, a convergence of the glass transition temperatures was observed at an increasing number of blocks.[14,20] In both cases the looping and bridging of the midblocks leads to intermolecular constraints and lower free volumes, resulting in lower segment mobility and therefore a higher fraction of a mixed interphase.[14,20,21] At the same time the increased bridging and looping conformations and the inhibited phase demixing results in an increase of toughness, maximum strain and the T_{ODT}.[22,25,28,29] In consequence, the number of blocks effects almost all properties of multiblock copolymer at the same. Hence, it is inevitable to understand the correlation between polymer architecture and polymer properties to be able to predict the mechanical response of multiblock polymer.

In a previous work, we presented a novel synthetic approach for linear alternating multiblock copolymers, based on a monomer system with highly diverging reactivities. The statistical copolymerization of isoprene (I) and 4-methylstyrene (4MS) in nonpolar solvents results in block like tapered copolymers. Combining this one-step block copolymer approach with sequential monomer addition leads to a rapid and scalable approach for the preparation of linear tapered alternating multiblock copolymers. Strain stress experiments of the first series of tapered multiblock copolymers with constant block sizes or constant molecular weights and varying block numbers showed an enormous increase of maximum strain and toughness with increasing number of blocks.[30,31]

This work focuses on the correlation between polymer architecture and thermal, morphological and mechanical properties of tapered $(AB)_n$ multiblock copolymers of 4-methylstyrene and isoprene with constant molecular weights and varying numbers of blocks. In a recent study, our research group examined linear tapered multiblock copolymers based on isoprene and styrene (S), revealing highly ordered multiblock structures and a good mechanical response.[31] Compared to I/S copolymers, the I/4MS monomer system provides a more block like structure with a much shorter and steeper gradient spacer between the I and 4MS segments.[33] The tapered section provides a compatibilizing effect for the diene and styrenic sections of the polymer

and enhances mixing of both phases. Therefore, it can be assumed that this effect is less pronounced for I/4MS based multiblocks, causing stronger phase segregation and better order at larger block numbers than in the case of I/S multiblock copolymers.

In order to verify this assumption and to examine the correlation between polymer architecture and mechanical and morphological properties, three series of $(AB)_n$ multiblock copolymers with varying block number but constant molecular weights have been prepared and extensively examined by DSC, SAXS and DMA as well as stress-strain characterization.

3.2.3 Experimental Section

Materials: All chemicals and solvents were purchased from Acros Organics Co. and Sigma-Aldrich Co. Isopropyl alcohol and methanol were used as received without further purification. Cyclohexane was purified via distillation over sodium and degassed by three freeze-thaw cycles prior to use. Myrcene, isoprene, styrene and 4-methylstyrene were purified by distillation over CaH_2 and degassed by three cycles of freeze-thaw prior to use.

Preparation of multiblock copolymers: The I/4MS monomer mixture was dried over CaH_2 and trioctylaluminum. Cyclohexane was dried by a living polystyrene solution. All monomers and solvents were degassed by three freeze-thaw cycles prior to use. The monomer mixture was distilled into a graduated ampule equipped with a teflon stop cock. Cyclohexane was distilled directly into the all glass reactor under reduced pressure. For the preparation of a tapered multiblock copolymer, a specific amount of the monomer mixture was added to the cyclohexane and initiated by *sec*-butyllithium via syringe. All polymerizations were carried out at 30°C and argon atmosphere. Depending on the block sizes, the next load of monomers was added after 12; 24 or 36 hours. The colour change from the almost colourless polyisoprenyllithium to the dark orange poly-4-methylstyryllithium marked the successful crossover from the polyisoprene to the poly-4-methylstyrene section. The polymerization was terminated by adding degassed isopropyl alcohol and the polymer solution was precipitated into an eight-fold excess of isopropyl alcohol. All

samples were dried under reduced pressure und stored at -18 °C. Yields were generally quantitative (~95%).

NMR Spectroscopy: NMR spectra were recorded on a Bruker Avance II 400 spectrometer with 400 MHz (^{1}H-NMR) or 101 MHz (^{13}C-NMR) and are referenced internally to residual proton signals of the deuterated solvent.

Standard Size Exclusion Chromatography (SEC): SEC measurement was performed with THF as the mobile phase (flow rate 1 mL min-1) on an SDV column set from PSS (SDV 103, SDV 105, SDV 106) at 30 °C. Polymer concentrations with a maximum of 1 mg/mL turned out to be suitable to prevent concentration effects. Calibration was carried out using Polystyrene standards (from Polymer Standard Service, Mainz).

Differential Scanning Calorimetry (DSC): The thermal properties of the tapered multiblock copolymers were studied with a Q2000 (TA Instruments) differential scanning calorimeter (DSC). The instrument was calibrated for best performance on the specific temperature range and heating/cooling rate. The calibration sequence included a baseline calibration for the determination of the time constants and capacitances of the sample and reference sensor using a sapphire standard, an enthalpy and temperature calibration for the correction of thermal resistance using indium as standard (ΔH=28.71 J/g, T_m=428.8 K), and a heat capacity calibration with sapphire standard. Two cooling and heating cycles were performed at a rate of 10 K/min in a temperature range between 173 K and 433 K and the glass temperatures corresponding to PI and P4MS were extracted from the second cycle.

Small-angle X-Ray Scattering (SAXS): measurements were made using CuKα radiation (RigakuMicroMax 007 x-ray generator, Osmic Confocal Max-Flux curved multilayer optics). 2D diffraction patterns were recorded on an Mar345 image plate detector at a sample-detector distance of 2060 mm. Intensity distributions as a function of the modulus of the total scattering vector, $q = (4\pi/\lambda)\sin(2\theta/2)$, where 2θ is the scattering angle, were obtained by radial averaging of the 2D datasets. Samples

in the form of thick films (~1 mm) were prepared by slow solvent casting (chloroform). Temperature-dependent measurements of 1 hour long were made by heating the films from 298 K to 473 K in 5 K steps aiming at obtaining the structure factor and further identifying the corresponding order-to-disorder transition temperatures.

Dynamic mechanical analysis: A TA Instruments, AR-G2, with a magnetic bearing that allows for nanotorque control was used for recording the viscoelastic properties of the polymer electrolytes. Measurements were made with the environmental test chamber (ETC) as a function of temperature. Samples were prepared on the lower rheometer plate (8 mm and 25 mm), the upper plate was brought into contact, and the gap thickness was adjusted. The linear and nonlinear viscoelastic regions were determined by the strain amplitude dependence of the complex shear modulus |G*| at ω = 10 rad/s. Evidently, tapered multiblock copolymers orient easily by the application of strain. A low strain amplitude (typically below 1.5 %) was used to avoid non-linearities in the multiblock copolymers. Subsequent measurements involved (i) isothermal frequency scans within the range $10^{-1}<\omega<10^{2}$ rad/s at several temperatures and (ii) isochronal temperature ramps with ω = 1 rad/s between 298 K and 473 K.

Tensile Tests: Tensile tests were performed using a materials testing machine Z005 (Zwick/Roell, Germany). Tensile tests were carried out by exposing the stamped polymer dogbones to a uniaxial tension. Bone shape samples with thicknesses around 0.2 mm were drawn with rate of 10 mm/min at room temperatures. A Pre-Load of 0.1 N was applied with a Pre-Load speed of 5mm/min. Dependencies of stress vs. draw ratio were recorded. Elastic modulus, elongation at break and stress at break were determined as averages of 2–5 independent drawing experiments performed at the same conditions. All films were obtained by slow evaporation from a chloroform solution followed a full removal of the solvent under reduced pressure. Samples were used for tensile tests without thermal annealing.

TEM Measurements: For characterization of the tapered block copolymer morphology in the bulk state, the as films prepared samples were microtomed from

surface to surface at -80 °C into thin slices of 50-70 nm thickness. The collected ultrathin sections were subsequently stained with osmium tetroxide (OsO_4) for selective staining of the PI domains, followed by investigation by TEM measurements. Transmission electron microscopy (TEM) experiments were carried out using a Zeiss EM 10 electron microscope (Oberkochen, Germany) operating at 60 kV with a slow-scan CCD camera obtained from TRS (Tröndle, Morrenweis, Germany) in bright field mode. Camera was computer-aided using the ImageSP software from TRS.

3.2.4 Results and Discussion

3.2.4.1 Preparation of multiblock copolymers

In a previous short account we described a synthetic approach for $(AB)_n$ multiblock copolymers, based on the highly disparate reactivity ratios of isoprene (I) and 4-methylstyrene (4MS) (r_I = 25.4; r_{4MS} = 0.007).[32] Due to the highly favoured incorporation of I, the statistical copolymerization of I/4MS yields tapered block copolymer in one step.[33] The living chain end permits further addition of I/4MS monomer mixtures, providing rapid access to linear tapered $(AB)_n$ multiblock copolymers (Figure 1 a). This general synthetic approach was used in our recent study to generate tapered multiblock copolymers based on isoprene and styrene.[31] The resulting $(AB)_n$ multiblocks showed ordered structures for up to ten blocks (n=5) and extraordinary toughness. To examine whether multiblock properties like state of order and mechanical response are affected by length and shape of the tapered interface, three series of $(AB)_n$ multiblock copolymers with varying block number, but constant molecular weights of 80 kg/mol; 240 kg/mol and 400 kg/mol were prepared based on isoprene and 4-methylstyrene (Figure 1 b).

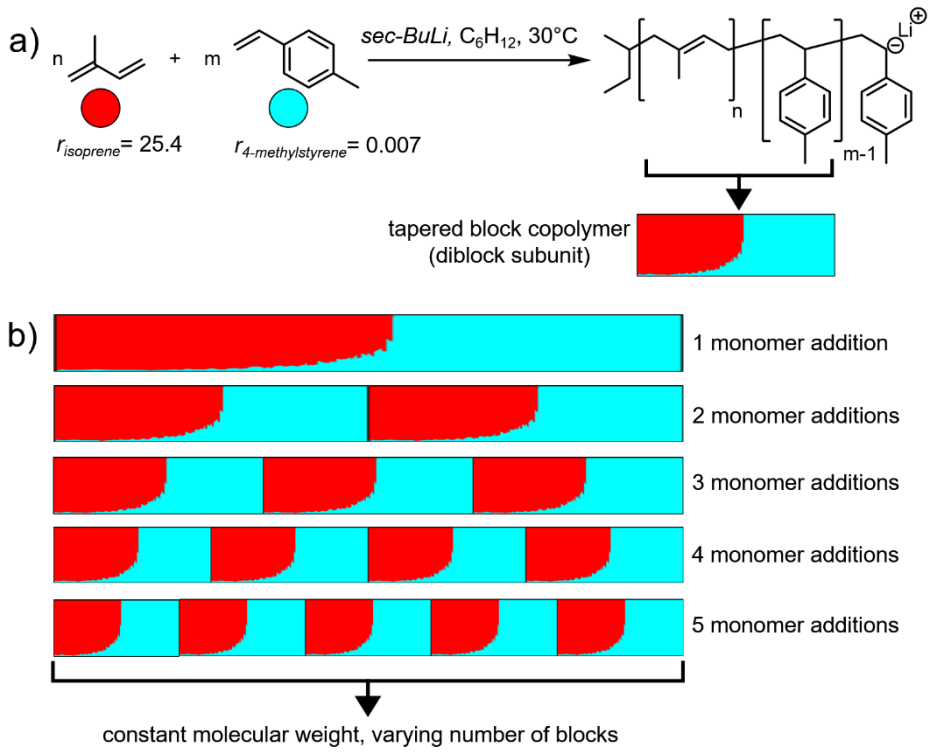

Figure 23: a) one-step tapered block copolymer formation; b) composition profile of multiblock copolymers with constant molecular weights and varied block numbers.

For a better comparison of the samples, we aimed for a constant isoprene content of 50 mol% for all copolymers. The discrepancies between the targeted molecular weights and the molecular weights determined by SEC are, mainly caused by the calibration with polystyrene standards. However, the SEC results provide a sufficient estimation of the actual molecular weights (Table 1). The dispersities of the multiblock samples showed a broadening of the molecular weight distributions and the appearance of small shoulders at low molecular weights for increasing molecular weights and an increasing number of monomer additions (Supp. Inf. Figure S2). Both effects can be explained by a small percentage of termination during every monomer addition step. However, considering the high molecular weights and the high number of blocks, the dispersities are still very narrow and demonstrate the potential and applicability of this synthetic approach for well-defined linear multiblock copolymers.

Table 1. Molecular characteristics of the tapered multiblock copolymers P(I-*co*-4MS) and of the sequential P(I-*b*-4MS) (i.e. "normal") and P(4MS-*b*-I) (i.e. "inverse") diblock copolymers.

Entry	Sample	number of blocks	M_n^{theo} (kg/mo)l	M_n^a (kg/mol)	$Đ^a$	Isoprene content^{theo} (mol%)
1	80K2B	2	80	94.7	1.06	50
2	80K4B	4		82.4	1.12	50
3	80K6B	6		81.1	1.10	50
4	80K8B	8		78.7	1.15	50
5	80K10B	10		77.5	1.18	50
6	240K2B	2	240	237.8	1.11	50
7	240K4B	4		227.2	1.11	50
8	240K6B	6		308.1	1.26	50
9	240K8B	8		253.1	1.24	50
10	240K10B	10		232.2	1.17	50
11	400K2B	2	400	481.2	1.09	50
12	400K4B	4		313.4	1.05	50
13	400K6B	6		356.3	1.11	50
14	400K8B	8		431,7	1.22	50
15	400K10B	10		423,9	1.23	50

[a] Determined by SEC at 25°C in THF

3.2.4.2 Thermodynamics

It is known that DSC alone cannot account for thermodynamic miscibility/immiscibility in multicomponent polymer systems as even miscible blends/copolymers exhibit dual glass temperatures. Nevertheless, based on the broadening of the heat capacity curves at the respective T_g's conclusions can be drawn on the purity of phases at the probed length scale. In accordance with this expectation, DSC curves of multiblock copolymers revealed two glass temperatures, independent of the phase state of the copolymers (ordered or disordered). This is depicted in Figure 2, where the first derivative of the heat flow obtained during the second heating runs are shown. The lower and higher peaks in this representation

correspond to the PI and P4MS glass temperatures, respectively. Although the lower T_g – albeit broad – is always evident, the high T_g is less pronounced especially in the tapered multiblock (tetra-, hexa-, octa- and deca-block) copolymers. In the tapered copolymers with the lower molecular weight (M_w~80 kg/mol) the two peaks approach each other especially in the octablock and decablock cases meaning that segmental mobilities are in proximity. In addition to the high and low glass temperatures, another very broad peak around 303 K is evident for the 240 kg/mol and 400 kg/mol copolymers. This feature can be interpreted as an "interphase T_g" of those segments that are intimately mixed within the I/4MS interface.

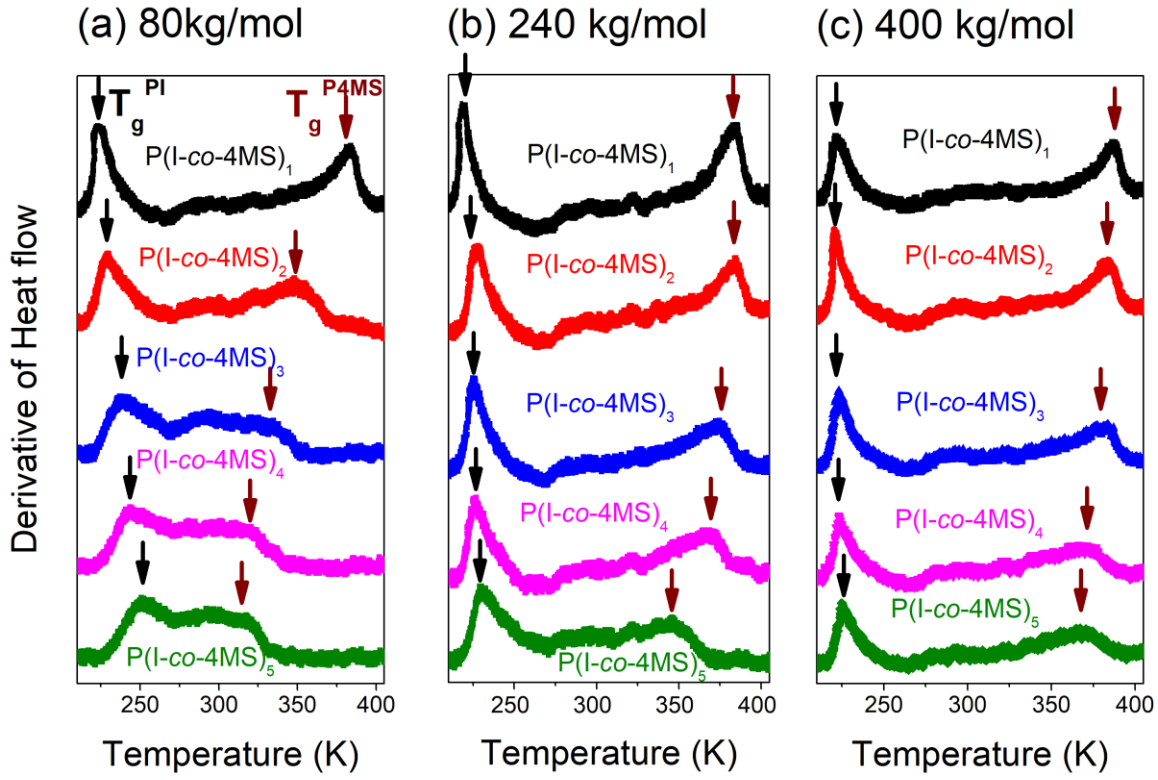

Figure 24: Derivative of heat flow obtained during the second heating runs of the I/4MS tapered multiblock copolymers with overall molecular weights of 80 kg/mol (a), 240 kg/mol (b) and 400 kg/mol (c) with a rate of 10 K/min. Vertical arrows in black and orange colors indicate the PI and P4MS glass temperatures, respectively.

The results from the DSC investigation with respect to the PI and P4MS glass temperatures are summarized in Figure 3. The Figure shows dual glass temperatures in all copolymers with a temperature separation that decreases with the number of blocks and with decreasing total molecular weight. In addition, the PI T_g is higher than

for a homopolymer PI (T_g=-65 °C) as a result of the incorporation of 4-methylstyrene segments within the PI chain. Nevertheless, these results are in good agreement with previous studies on non-tepered linear multiblock copolymers, which also show a convergency of T_gs for increasing block numbers.[14,20]

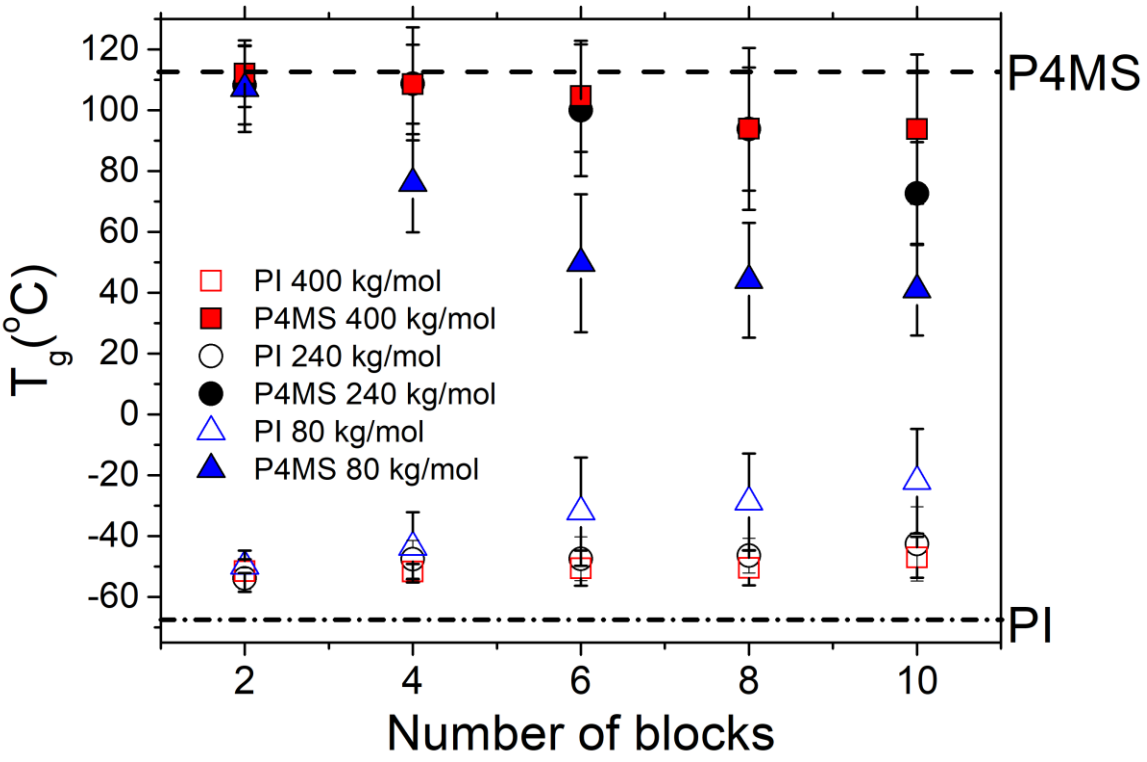

Figure 25: Glass temperatures in the tapered multiblock copolymers corresponding to P4MS (filled symbols) and PI (open symbols). Vertical bars indicate the temperature range of the respective glass temperatures (taken as the full width at half maximum). Dashed and dash-dotted lines give the glass temperature of P4MS and PI homopolymers, respectively.

3.2.4.3 Self-assembly

The phase state of the multiblock copolymers is controlled by (i) the interaction parameter between isoprene and 4-methylstyrene, (ii) the composition profile of 4MS, (iii) the total molecular weight, and (iv) the number of blocks. The highly disparate reactivity ratios of I and 4MS (r_I=25.4, r_{4MS}=0.007) lead to a short tapered midblock and to a very block like composition profile. To this end, the I/4MS system shows a better controlled monomer distribution composition and a shorter tapered structure in comparison to the known I/S copolymer (r_I=11.0, r_{4MS}=0.053). However,

weather the more block like structure of I/4MS will be the dominant factor controlling the phase state of the multiblock copolymers of P(I-co-4MS) and P(I-co-S) requires additional knowledge of the interaction parameter in the respective sequential copolymers P(I-*b*-4MS) and P(I-*b*-S).

Sequential and symmetric diblock copolymers, according to the mean-field theory (MFT), undergo a second order phase transition from the disordered to the lamellar phase by lowering temperature at the critical point (χN=10.495, f=1/2). The MFT structure factor in the disordered phase is predicted,

$$\frac{N}{S(q)} = F(x,f) - 2\chi N \qquad (1)$$

where $F(x,f)$ is a combination of Debye factions and $x=q^2R_g^2$, q, is the modulus of the scattering vector. However, the MFT predictions for the structure factor apply only at temperatures much above the order-to-disorder transition temperature (T_{ODT}). On approaching the T_{ODT} from higher temperatures, fluctuation corrections become important. This becomes evident as within MFT, $1/S(q)$, is proportional to $1/T$ in the disordered phase (in the simplest approximation χ is inversely proportional to T). However, at $T>T_{ODT}$ there exists a pronounced curvature which cannot be accounted by the MFT. Furthermore, the peak intensity at the transition remains finite and $S(q^*)$ is discontinuous at the transition. Subsequently, Fredrickson and Helfand[34] demonstrated that with the introduction of fluctuation corrections, the critical point is suppressed and is replaced by a weakly first order transition (f=0.6) at

$$(\chi N)_{ODT} = 11.2 + \frac{46.1}{\bar{N}^{1/3}} \qquad (2)$$

Fluctuation corrections apply to both the disordered and ordered phases in the vicinity of the transition. In the disordered phase the structure factor is

$$\frac{N}{S(q)} = F(x,f) - 2\chi N + \frac{c^3 d\lambda}{\bar{N}^{1/2}} \frac{\sqrt{S(q^*)}}{\sqrt{N}} \qquad (3)$$

In eq. 3, $d=3x^*/2\pi$ and c, λ are composition dependent coefficients, where $\overline{N}=N\alpha^6/u^2$, and α, u are the statistical segment length and volume, respectively (in the present case of f=0.6; c=1.126, λ=132, and d=1.835). Thus, approaching the T_{ODT} from high temperatures the predicted intensities are lower than the ones expected from Leibler's theory[35] and give rise to a non-linear dependence of $1/S(q)$ on $1/T$ which is in qualitative agreement with the non-linear dependence obtained experimentally (see below).

Herein we determine the interaction parameter, $\chi_{I\text{-}4MS}$, based on the T_{ODT} values of three P(I-*b*-4MS) copolymers prepared by sequential addition (Supp. Inf. Table S1 Entries 16, 18 and 20). For this purpose, we employ rheology that is a sensitive probe of the order-to-disorder transition temperature. Figure 4 gives the storage moduli in three diblock copolymers under isochronal conditions (ω=1 rad/s). The fluctuation induced first order transition is evident by the drop in the shear storage modulus G'(T) at the T_{ODT}. By forcing the MFT and FH predictions (Eqs. (1) and (2)) to the T_{ODT} we obtain (Figure 4) $\chi_{MFT}=23.2/T-0.024$ and $\chi_{FH}=36.0/T-0.041$, respectively, for the interaction parameters in the mean-field and fluctuation approach. These dependencies are weaker than in the poly(isoprene-*b*-styrene) copolymers ($\chi_{FH}=71.4/T-0.0857$) revealing that a methyl group in the former system is responsible for the change in polarizability and the alleviated immiscibility relative to P(I-*b*-S). In addition, block copolymers prepared by the reverse sequential addition of monomer, *i.e.*, reverse block copolymers (P(4MS-*b*-I)) (Supp. Inf. Table S1 Entries 17, 19 and 21), display small changes at the order-to-disorder transition temperatures relative to the respective normal copolymers (Supp. Inf. Figure S3).

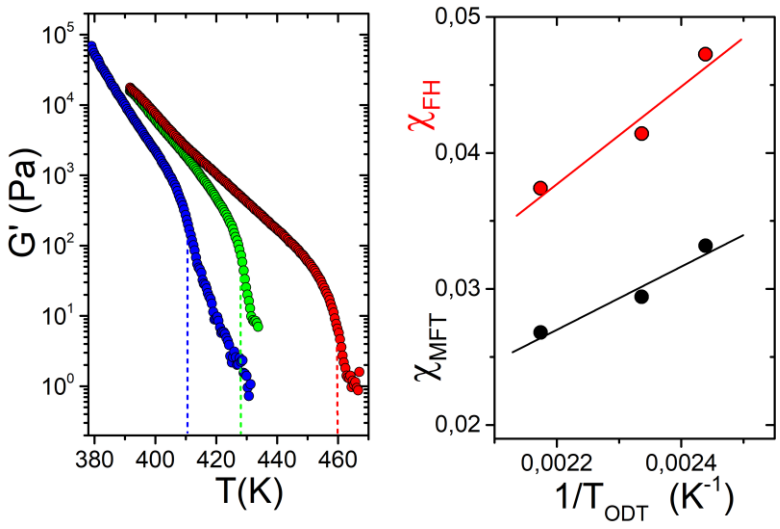

Figure 26: (Left) Temperature dependence of the storage modulus, G', obtained at a frequency of ω=1 rad/s with a low strain amplitude on heating the sequential diblock copolymers 30KP(I-*b*-4MS) (Supp. Inf. Table S1 Entry 16) (blue), 35KP(I-*b*-4MS) (Supp. Inf. Table S1 Entry 18) (green) and 40KP(I-*b*-4MS) (Supp. Inf. Table S1 Entry 20) (red). Vertical lines indicate the T_{ODT}'s. (Right) Temperature dependence of the interaction parameter within the MFT (black symbols) and the FH (red symbols) approach.

3.2.4.4 TEM

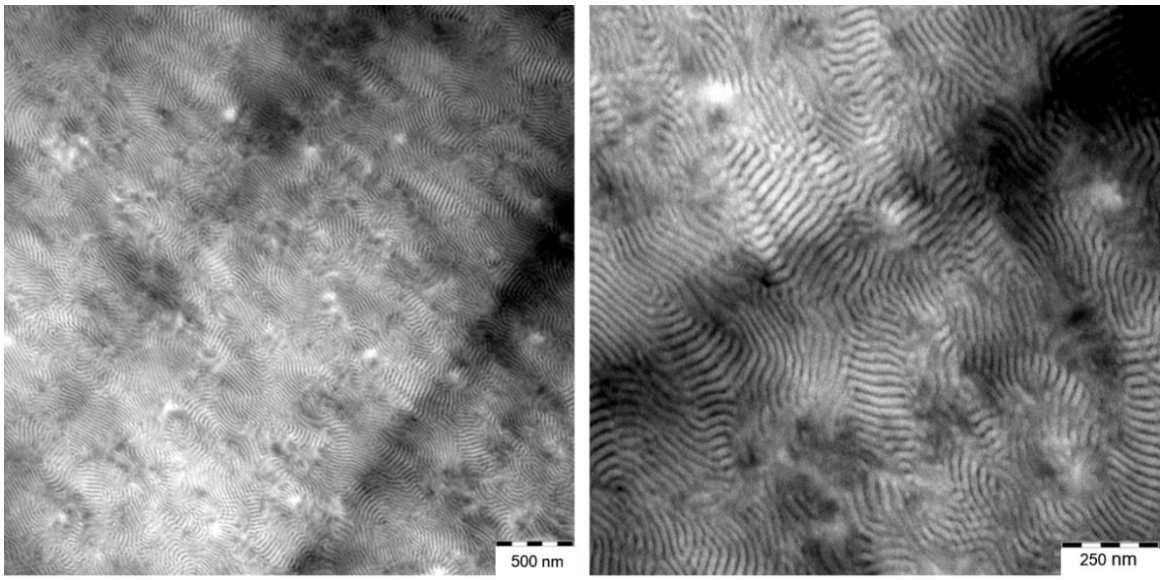

Figure 27: TEM images of 400K4B (Table 1 Entry 12).

The results from the TEM study on the real-space nanodomain morphology can be compared with the morphology obtained by SAXS (Figure 5). The SAXS results for the tapered multiblock copolymers with approximate molecular weights of 80 kg/mol, 240 kg/mol and 400 kg/mol are shown in Figure 6 at ambient temperature. The curve for the tapered diblock copolymer with M_w~80 kg/mol show Bragg reflections with positions 1:2 relative to the first peak corresponding to a lamellar morphology. The curves for the tapered tetrablock, hexablock, octablock and decablock copolymers reveal a single and broad peak corresponding to scattering from the disordered state (correlation hole scattering). The SAXS results for the tapered multiblock copolymers with molecular weight of 240 kg/mol, reveal ordered phases with the expected nanodomain morphology (lamellar). This is evident by the Bragg reflections with positions 1:2:3:4:5 relative to the first peak in the tapered diblock copolymer. However, the curves of the octablock and decablock copolymers reflect only weakly ordered structures. Similarly, for the copolymers with molecular weight of 400 kg/mol, ordered phases are obtained (in the tapered diblock copolymer case with long-range order) with the exception of the decablock copolymer (disordered state). The final assignment of the exact phase state in the tapered multiblock copolymers (ordered vs disordered) as well as the location of the order-to-disorder transition temperature, T_{ODT}, requires temperature-dependent SAXS measurements and/or rheology (see below).[36,37]

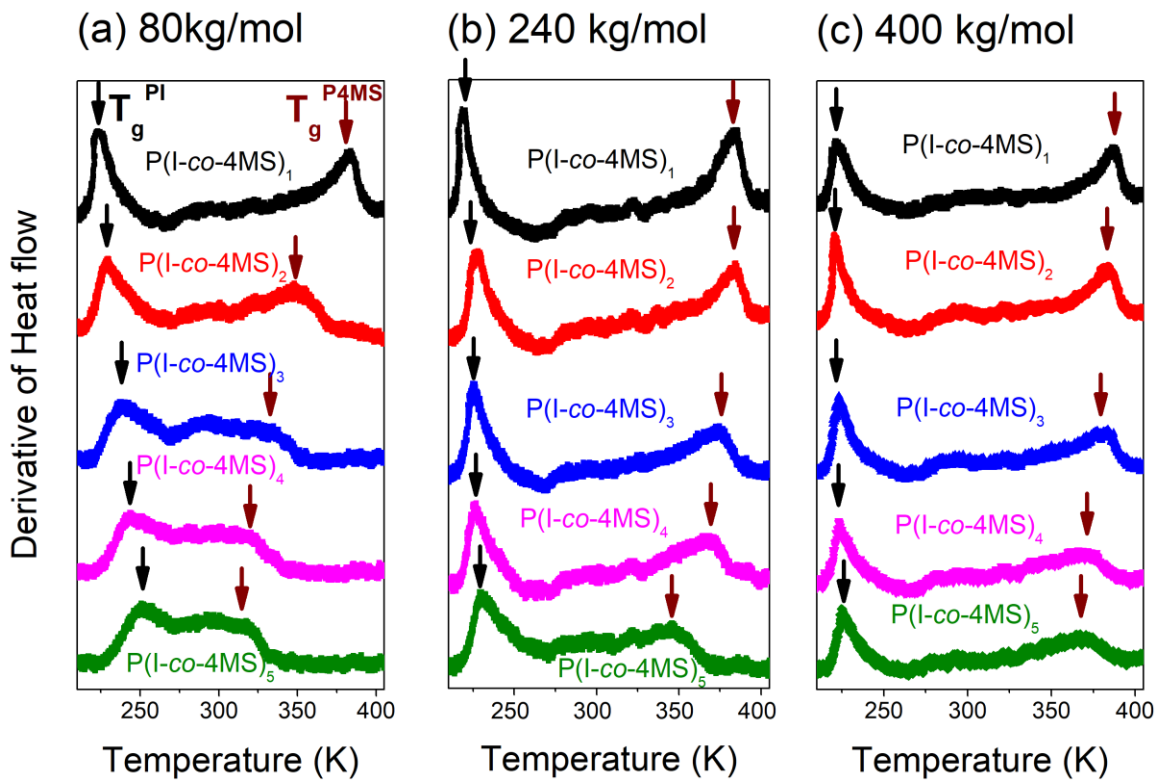

Figure 28: SAXS patterns for the tapered multiblock copolymers with approximate molecular weights of 80 kg/mol (left), 240 kg/mol (centre) and 400 kg/mol (right) obtained at ambient temperature. Arrows give the positions of the Bragg reflections corresponding to a lamellar morphology. The same colour code is used for the different samples.

The domain spacing, d, obtained from SAXS (as $d=2\pi/q^*$, q^* is the modulus of the scattering vector corresponding to the first maximum) for the tapered multiblock copolymers can be compared to the corresponding spacing in P(I-*b*-4MS) copolymers made by sequential addition (Figure 7). The figure depicts the domain spacing obtained at ambient temperature as a function of the number of blocks for the different molecular weights and as a function of the total molecular weight, the latter in a double logarithmic representation. For the sequential diblock copolymers the domain spacing varies as $\log(d/\mathrm{nm}) = -1.61+0.65\ \log(M_n/(\mathrm{g/mol}))$ suggesting extended chains. Under conditions applicable to the strong segregation limit (SSL), the molecular weight dependence of the nanodomain spacing scales as $d\sim N^{\delta}$, with $\delta\sim 2/3$, as opposed to $\delta=½$ for the unperturbed (Gaussian) chains. Helfand and Wasserman[34] predicted a nanodomain spacing scaling as: $d\sim\alpha N^{9/14}\chi^{1/7}$ whereas

Semenov argued[38] that the copolymers are strongly segregated with $d \sim \alpha N^{2/3}\chi^{1/6}$. Interestingly, the molecular weight dependence in the tapered multiblock copolymers is weaker, with $\delta \sim 0.55 \pm 0.02$ suggesting that chains are stretched - albeit to a lesser degree - with non-ideal (Gaussian) configurations.

Additional information on the chain configuration in the tapered multiblock copolymers can result by comparing their domain spacings with the corresponding diblock copolymers made sequentially. Strikingly, Figure 7b reveals that the tapered diblock copolymers have approximately the same domain spacing as the corresponding P(I-*b*-4MS) copolymers made sequentially. The difference in domain spacing is even smaller considering that SEC overestimates the molecular weight of the copolymers. Evidently, the vastly different reactivity ratios of I and 4MS in cyclohexane lead to a tapered diblock with the same (narrow) interface as a block copolymer made by sequential addition. This feature permits an estimation of the width of the interface. In the limit of very long diblock copolymers (SSL), the interfacial width can be estimated according to Helfand[34] and co-workers as

$$\Delta_\infty = \frac{2\alpha}{\sqrt{6\chi}} \tag{4}$$

where a is the statistical segment length (we further assumed $a_{PI} \approx a_{4PMS}$). For a diblock copolymer of finite molecular weight the interfacial width increases and now depends on block incompatibility as

$$\Delta \approx \Delta_\infty \left[1 + \frac{1.34}{(\chi N)^{1/3}}\right] \tag{5}$$

Based on the above equations, a typical interfacial thickness for a phase-separated P(I-*b*-4MS) diblock copolymer with N=1000, $a \approx$ 0.635 nm, and χ_{FH} =0.076 at 303 K, is $\Delta \sim$2.5 nm, meaning that ~7% of segments are at the interface. A similarly small interfacial width is expected for the tapered diblock copolymer as well.

Multiblock copolymers prepared by the repeated addition of mixtures of 4-methylstyrene and isoprene, however, show very different domain spacings and henceforth much broader effective interfacial widths. In the tetrablock copolymer the domain spacing is reduced by 52%, relative to the diblock whereas in the octablock the reduction amounts to 74%. The reinforcement of the interface with bridged configurations by increasing the number of

blocks at a fixed overall molecular weight is expected to affect the mechanical properties of the multiblock copolymers (see below).

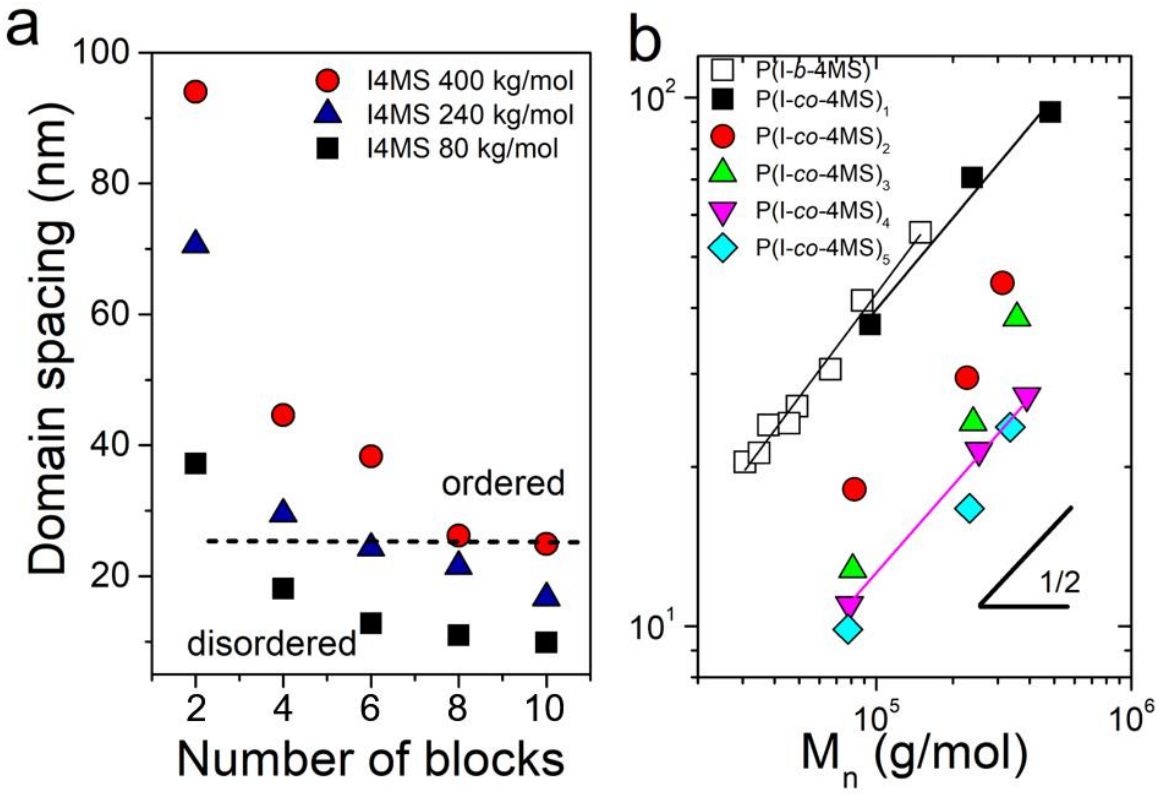

Figure 29: (a) Domain spacing obtained from SAXS plotted as a function of the number of blocks for the tapered multiblock copolymers with approximate molecular weights of 80 kg/mol (squares), 240 kg/mol (triangles) and 400 kg/mol (circles). The dashed line separates the ordered from the disordered states. (b) Domain spacing plotted as a function of molecular weight in a log-log representation for the tapered multiblock copolymers (filled symbols) and for sequential PI-*b*-P4MS copolymers (open squares). Lines are fits to the experimental data for the multiblock copolymers and have slopes of 0.57 and 0.55 for the diblock and octablock, respectively. A line with a slope of ½ is also shown for comparison.

More information on the phase state can be obtained by following the structure factor, $S(q)$, of the tapered multiblock copolymers as a function of temperature. As an example, the static structure factor for the tapered tetrablock copolymer with a total molecular weight of 85.7 kg/mol is shown in Figure 8 as a function of temperature. A broad liquid-like peak is observed suggesting that all curves are located at $T>T_{ODT}$, *i.e.,*

in the disordered phase. In accord with this expectation, there is no discontinuous change of the peak intensity as evidenced in the $1/S(q^*)$ vs $1/T$ representation. Furthermore, the $1/S(q^*)$ vs $1/T$ has a non-linear dependence as expected from the theory that includes fluctuation corrections (Eq. 3). The latter representation shows, additionally, the role of the P4MS glass temperature in the $S(q)$. Crossing the T_g^{P4MS} influences the peak intensity through the change in macroscopic density and the concomitant change in the electron density for P4MS.

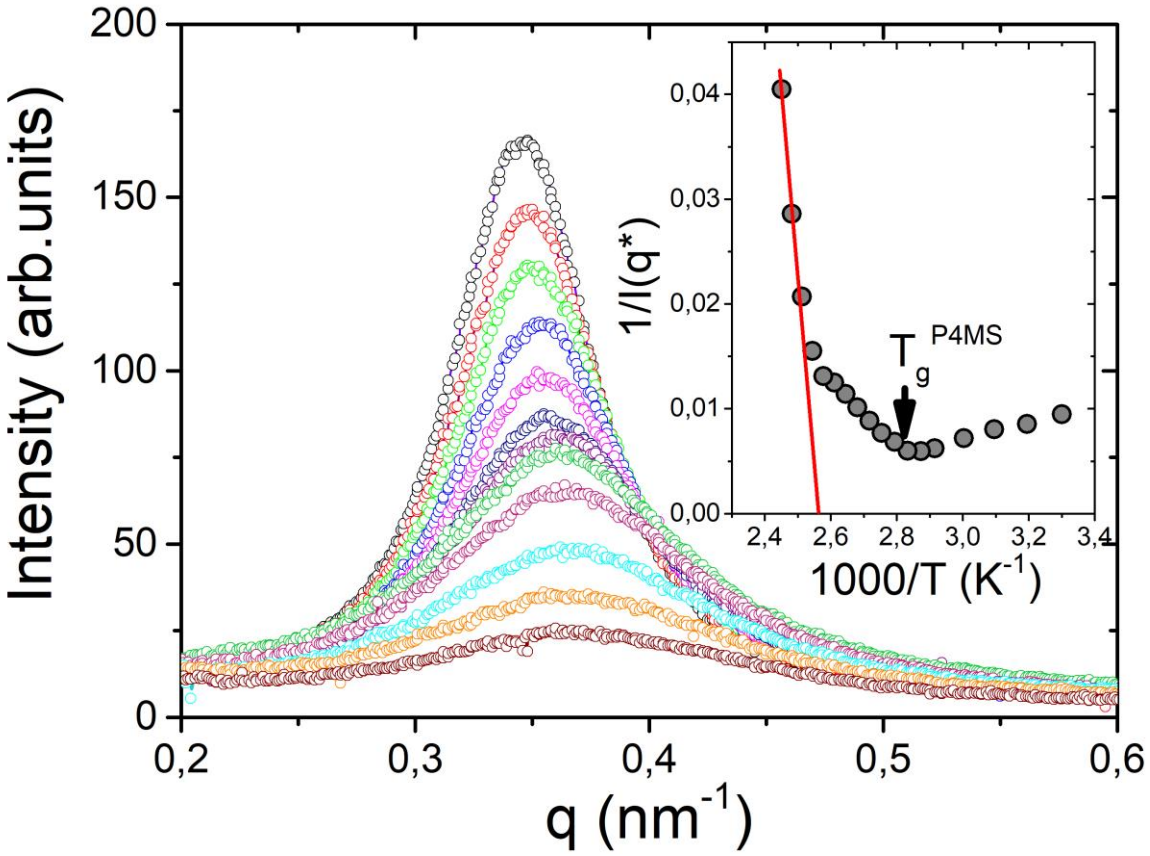

Figure 30: SAXS curves of the tapered tetrablock copolymer (80K4B, Table 1 Entry 2)plotted at different temperatures; T=353 K (black); 358 K (red); 363 K (green); 368 K (blue); 373 K (magenta); 378 K (dark blue), 383 K (purple), 388 K (light green), 393 K (violet), 398 K (cyan), 403 K (orange) and 408 K (wine). The inverse peak intensity is plotted versus inverse temperature in the inset. The solid line indicates the MFT predictions. The vertical arrow indicates the T_g of the P4MS phase.

3.2.4.5 Rheology and Mechanical properties

Rheology has been employed as a sensitive probe of the order-to-disorder transition and of the different ordered nanophases. This sensitivity originates from the large

viscoelastic contrast of the disordered and the different ordered phases. Isochronal measurements of the storage modulus performed at low frequencies with low strain amplitudes by slowly heating the specimen provide a way of locating the T_{ODT} (Figure 4). Figure 9a shows the result of the isochronal measurements of the storage (G') and loss (G") moduli at ω=1rad/s obtained on heating for the series of the tapered multiblock copolymers with molecular weight of ~80 kg/mol. The figure depicts one tapered copolymer that remains in the ordered phase over the whole temperature range (the diblock), and four multiblock copolymers (tetra-, hexa-, octa- and deca-block) that are in their disordered state. Overall, there is an excellent agreement with the SAXS results (Figure 6) with respect to the phase state of the copolymers. In addition to the phase state the figure depicts the very different viscoelastic responses of the copolymers that are largely controlled by the glass temperature of the hard phase (P4MS) being a strong function of the number of blocks (Figures 2 and 3) and the overall molecular weight.

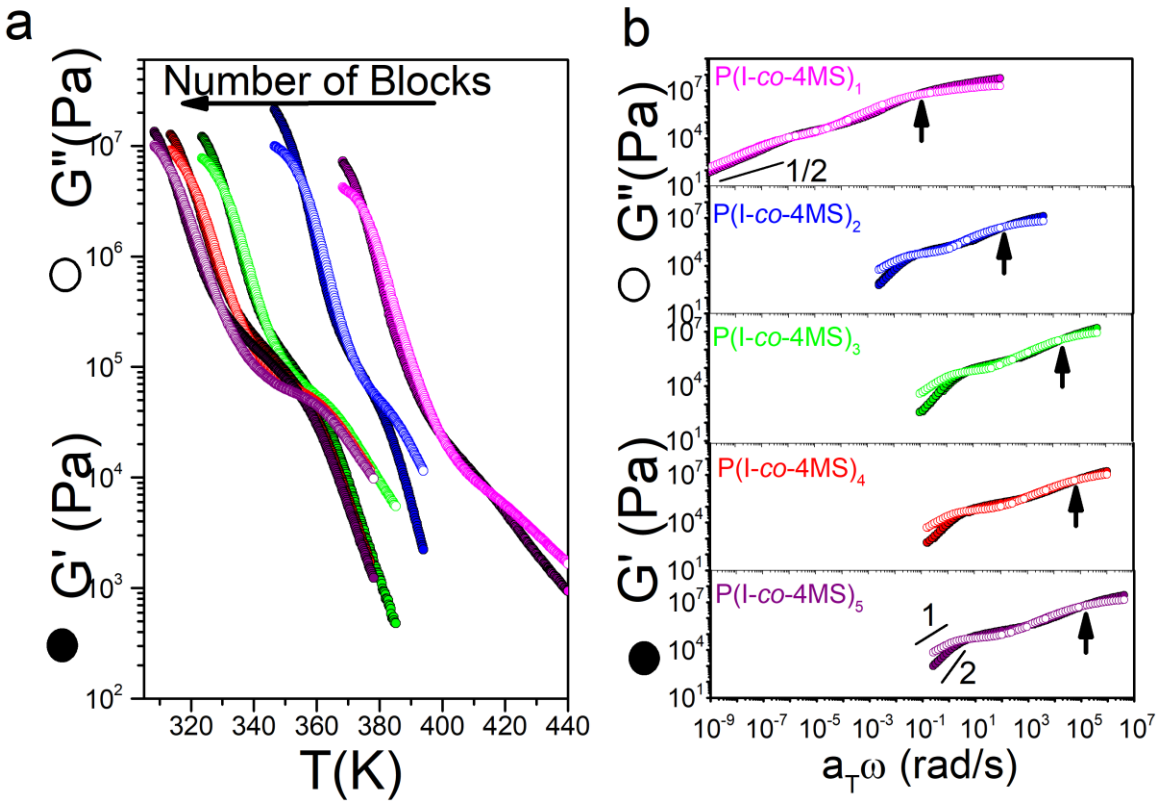

Figure 31: (a) Storage (filled symbols) and loss (open symbols) shear moduli during heating with a rate of 1 K/min at a frequency of 1 rad/s for the different tapered multiblock copolymers with a total molecular weight of 80 kg/mol

(Table 1 Entries 1-5). The strain amplitude was below 4% for the diblock and below 2% for the rest of the multiblock copolymers. (b) Master-curves of the storage (filled symbols) and loss (open symbols) shear moduli at a reference temperature of 367 K. Lines with slopes of 1 and 2 are shown for the P(I-*co*-4MS)$_5$ and a line with a slope of ½ for the P(I-*co*-4MS)$_1$. Vertical arrows indicate the P4MS glass temperatures.

More informative of the viscoelastic response of block copolymers is the use of isothermal measurements as a function of frequency. As an example, master-curves of the storage and loss moduli for the same tapered multiblock copolymers are shown in Figure 9b at a reference temperature of 367 K. The viscoelastic response of disordered block copolymers is usually similar to that observed for homopolymer melts. At high and intermediate frequencies two relaxation processes affect the viscoelastic response: the segmental and chain relaxation, respectively. At $T>T_{ODT}$, the time-temperature superposition (*tT*s) works well and the moduli exhibit typical terminal behaviour ($G'\sim\omega^2$ and $G''\sim\omega$). When examined over a broad temperature range, however, *tT*s is violated due to the order-to-disorder transition that drives the system from the disordered state to a nanophase separated state. At $T<T_{ODT}$ and at low frequencies, the moduli exhibit weak frequency dependencies of the order of $\omega^{1/2}$ (for symmetric block copolymers) to $\omega^{1/4}$. This results from the appearance of an ultra-slow relaxation process related to morphological rearrangements. As an example, the "master curve" for the P(I-*co*-4MS)$_1$ exhibits the segmental relaxation of P4MS, the chain relaxation and at lower frequencies the structural relaxation. The breakdown of *tT*s is observed at low frequencies where the Newtonian behaviour of the disordered state is replaced by a rubbery state related to the un-relaxed morphology.

The linear viscoelastic properties of nanophase separated block copolymers have been the subject of theoretical studies. In the study by Rubinstein and Obukhov both microscopic and mesoscopic mechanisms have been invoked which were attributed, respectively, to the dispersion in the number of entanglements of a chain with the opposite brush (high frequency response) and to the collective diffusion of copolymer chains along the interface. The latter mechanism is controlled by defects in lamellar orientation and contributes to the low-frequency side. For the disordered lamellar

mesophase they predicted: $G'(\omega) \sim G''(\omega) \sim \omega^{1/2}$. On the other hand, Kawasaki and Onuki proposed that overdamped second-sound modes in an orientationally disordered lamellar phase could result in a complex shear modulus proportional to $(i\omega)^{1/2}$. The experimental low-frequency data for P(I-*co*-4MS)$_1$ also show a parallel dependence of the moduli with $G'(\omega) \sim G''(\omega) \sim \omega^{1/2}$ as suggested from theory for a lamellar morphology.

Apart from the linear viscoelastic properties examined above with shear rheometry, of particular interest for applications are the tensile properties of the tapered multiblock copolymers. Some representative stress-strain curves for the different series of molecular weights all at ambient temperature are depicted in Figure 10.

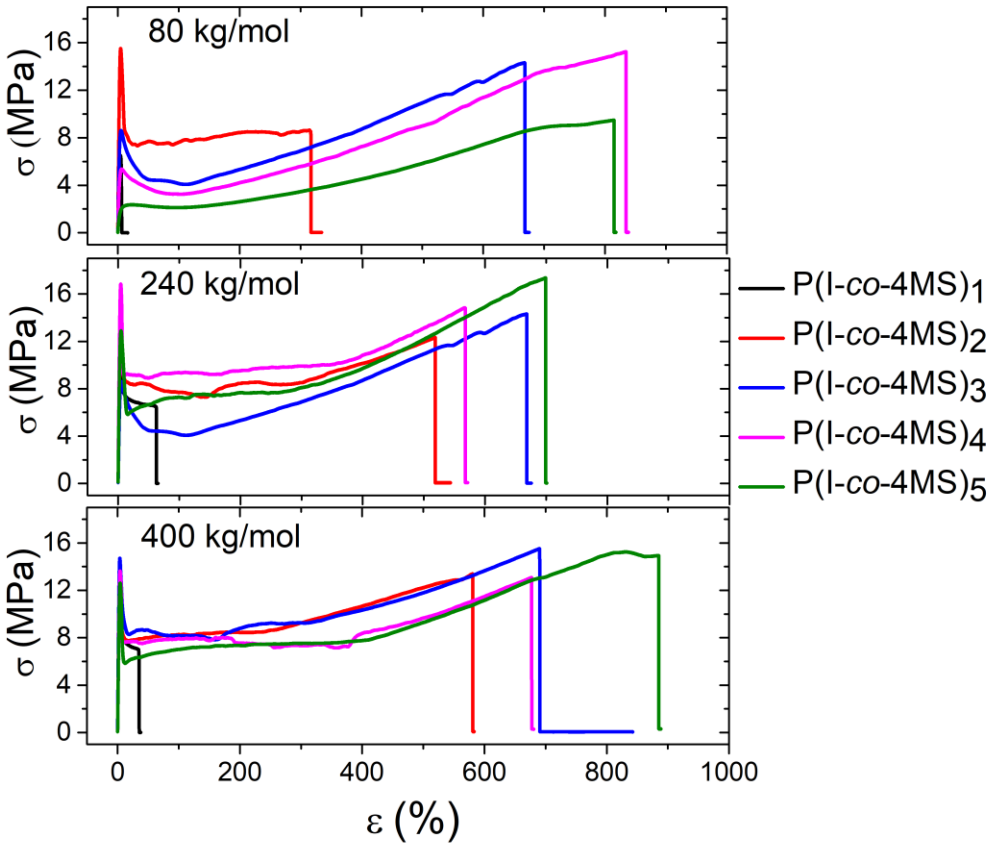

Figure 32: Representative stress-strain curves for the tapered multiblock copolymers with approximate molecular weights of 80 kg/mol (top), 240 kg/mol (center) and 400 kg/mol (bottom) obtained at ambient temperature. The same color code is used for the different samples.

In general, all P(I-*co*-4MS)$_1$ copolymers are brittle with an elongation at break below 10%, for the 80 kg/mol, and below 40% for the 400 kg/mol series. This is in pronounced contrast to the situation of the tetrablock copolymers with respective elongation at break of 300% and about 600% for the 80 kg/mol and 400 kg/mol copolymer series. Depending on the overall molecular weight, the number of blocks, the state of nanophase separation (ordered, weakly ordered vs disordered states) of the copolymers and the proximity to the P4MS glass temperature a high elongation at break as high as 800 % could be obtained. The tensile properties unambiguously show a transition from brittle to ductile behaviour in going from the P(I-*co*-4MS)$_1$ to the tapered multiblock copolymers. These results can also be discussed in terms of the increased toughness shown in Figure 11. As expected, P(I-*co*-4MS)$_1$ exhibits little toughness independent of the molecular weight. In the tapered multiblock copolymers there is a 35-fold (in the 400 kg/mol) to 200-fold (in the 80 kg/mol) increase in toughness. In addition to the number of blocks and total molecular weight, the state of order and proximity to the P4MS glass temperature also plays a role. The highest increase in toughness is obtained for nanophase separated copolymers where, in addition, P4MS is well into the glassy state. These findings suggest an enhanced interfacial strength as a result of bridged configurations of chains in the tapered multiblock copolymers.

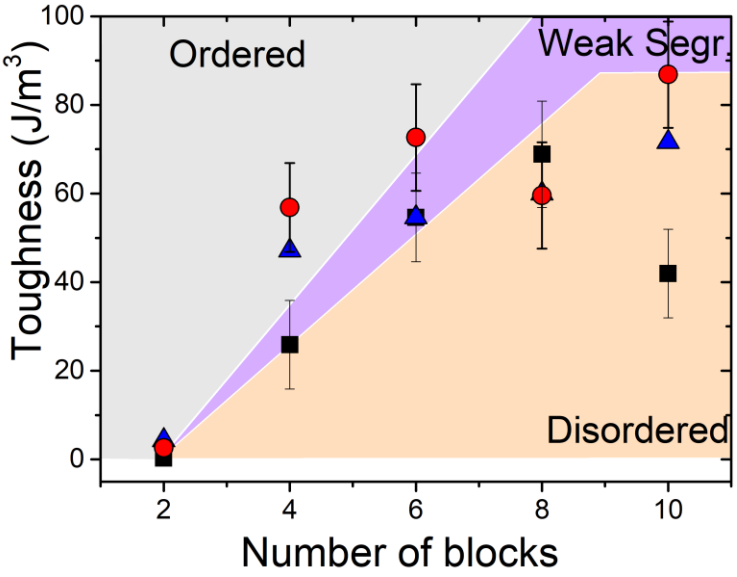

Figure 33: Toughness of the tapered multiblock copolymers with approximate molecular weights of 80 kg/mol (black squares), 240 kg/mol (blue triangles) and 400 kg/mol (red circles) obtained from the stress-strain curves at ambient temperature. Areas in grey, magenta and orange indicate, respectively, ordered, weakly ordered and disordered regimes.

3.2.5 Conclusions

In this study the repeated statistical carbanionic copolymerization and sequential monomer addition was used to prepare three series of linear tapered alternating $(AB)_n$ multiblock copolymers based on isoprene and 4-methylstyrene. The respective series had constant molecular weights of 80 kg/mol, 240 kg/mol and 400 kg/mol and varying number of blocks, ranging from two (n=1) to 10 (n=5). All samples showed two glass transition temperatures corresponding to P4MS-rich and PI-rich domains and a convergency of both T_gs for an increasing number of blocks. Furthermore, the DSC measurements provided evidence for a third mixed I/4MS interphase with a separate T_g at 30 °C.

Based on the order-to-disorder transition temperatures of P(I-*b*-4MS) diblock copolymers prepared by sequential monomer addition, the Flory-Huggins interaction parameter of I/4MS could be determined for the first time. Forcing the T_{ODT} to the Mean Field Theory (MFT) and Flory-Huggins (FH) predictions resulted to $\chi_{MFT}=23.2/T-0.024$ and $\chi_{FH}=36.0/T-0.041$, revealing a much weaker repulsion of the I and 4MS segments than for structurally related I/S monomer systems

(χ_{FH}=71.4/T-0.0857). These findings suggest that the phase segregation of the tapered multiblock copolymers is controlled by the interaction parameter, the composition profile (polymer architecture) as well as by the number of blocks and total molecular weight.

In depth examination by SAXS revealed that the domain spacing in the tapered P(I-*co*-4MS) is almost identical to corresponding diblock copolymers prepared by sequential addition, which can be attributed to the strongly block like structure of statistical I/4MS copolymers. Tapered multiblock copolymers also showed ordered regimes for tetra- and hexablock copolymers, while larger block numbers showed only weakly ordered and disordered phases. The correlation between the state of order and molecular weight and number of blocks was also observed for the domain spacing, showing a significant decrease of domain spacing for increasing block numbers. Compared to I/S, the I/4MS monomer system shows a shorter and steeper gradient but smaller χ-parameter, resulting in a higher miscibility of the PI and P4MS blocks, than corresponding multiblocks based on I/S. Temperature-dependent SAXS results showed a fluctuation-induced first order transition from the ordered to the disordered state for tapered I/4MS multiblock copolymers and a stretching of chains and non-ideal configurations.

The non-linear response obtained in the tensile tests revealed a dramatic enhancement of the strain at break; from about 10% in the diblock copolymers to as high as 800% in several tapered multiblock copolymers with a concomitant increase in toughness. The improved mechanical properties reflect the enhanced interfacial strength as a result of bridged configurations of the blocks. The results of the non-linear and linear viscoelastic response suggest that the mechanical behaviour of these materials is mainly controlled by the overall molecular weight and number of blocks, permitting to selectively adjust the mechanical properties by tuning these parameters.

All these findings are in good agreement with previous studies on non-tapered linear multiblock copolymers, confirming the strong block character of tapered multiblock copolymers based on I/4MS. Furthermore, the highly ordered nanostructures for up to six blocks, extraordinary toughness and strain at break and an easy accessibility of linear tapered I/4MS copolymers, demonstrate their potential for a variety of applications that require tough and resilient materials.

3.2.6 Author Information

E.G. and C.W. prepared all polymers, performed the strain-stress experiments and contributed equally in this work. M.A. carried out the TEM measurements. A.H.E., M.G., H.F. and G.F. supervised the project. G.F. performed and evaluated the DSC, SAXS and DMA measurements.

3.2.6 References

(1) Bates, C. M.; Bates, F. S. 50th Anniversary Perspective: Block Polymers Pure Potential. *Macromolecules* **2017**, *50*, 3–22.

(2) Schacher, F. H.; Rupar, P. A.; Manners, I. Functional Block Copolymers: Nanostructured Materials with Emerging Applications. *Angew. Chem. Int. Ed. Engl.* **2012**, *51*, 7898–7921.

(3) Knoll, K.; Nießner, N. Styrolux and styroflex from transparent high impact polystyrene to new thermoplastic elastomers. *Macromol. Symp.* **1998**, *132*, 231–243.

(4) Miyamoto, T.; Kodama, K.; Shibayama, K. Structure and properties of a styrene–butadiene–styrene block copolymer. *J. Polym. Sci. A-2 Polym. Phys.* **1970**, *8*, 2095–2103.

(5) Fredrickson, G. H.; Bates, F. S. Dynamics of Block Copolymers: Theory and Experiment. *Annu. Rev. Mater. Sci.* **1996**, *26*, 501–550.

(6) Ntaras, C.; Polymeropoulos, G.; Zapsas, G.; Ntetsikas, K.; Liontos, G.; Karanastasis, A.; Moschovas, D.; Rangou, S.; Stewart-Sloan, C.; Hadjichristidis, N. *et al.* Synthesis, characterization and self-assembly of well-defined linear heptablock quaterpolymers. *J. Polym. Sci. Part B: Polym. Phys.* **2016**, *54*, 1443–1449.

(7) Lee, I.; Bates, F. S. Synthesis, Structure, and Properties of Alternating and Random Poly(styrene- b -butadiene) Multiblock Copolymers. *Macromolecules* **2013**, *46*, 4529–4539.

(8) Matsumiya, Y.; Watanabe, H.; Takano, A.; Takahashi, Y. Uniaxial Extensional Behavior of (SIS)p-Type Multiblock Copolymer Systems: Structural Origin of High Extensibility. *Macromolecules* **2013**, *46*, 2681–2695.

(9) Fleury, G.; Bates, F. S. Structure and Properties of Hexa- and Undecablock Terpolymers with Hierarchical Molecular Architectures. *Macromolecules* **2009**, *42*, 3598–3610.

(10) Korotkov, A. A.; Chesnokova, N. N.; Trukhmanova, L. B. Polymerization of isoprene with a butyl lithium catalyst. *Polym. Sci. USSR* **1960**, *1*, 10–20.

(11) Corbin, N.; Prud'Homme, J. Multiblock copolymers of styrene and isoprene. I. Synthesis and characterization. *J. Polym. Sci. Polym. Chem. Ed.* **1976**, *14*, 1645–1659.

(12) Corbin, N.; Prud'Homme, J. Multiblock copolymers of styrene and isoprene. II. Microstructure and dilute solution properties. *J. Polym. Sci. Polym. Phys. Ed.* **1977**, *15*, 1937–1951.

(13) Simula, A.; Nikolaou, V.; Anastasaki, A.; Alsubaie, F.; Nurumbetov, G.; Wilson, P.; Kempe, K.; Haddleton, D. M. Synthesis of well-defined α,ω-telechelic multiblock copolymers in aqueous medium: In situ generation of α,ω-diols. *Polym. Chem.* **2015**, *6*, 2226–2233.

(14) Zhang, J.; Deubler, R.; Hartlieb, M.; Martin, L.; Tanaka, J.; Patyukova, E.; Topham, P. D.; Schacher, F. H.; Perrier, S. Evolution of Microphase Separation with Variations of Segments of Sequence-Controlled Multiblock Copolymers. *Macromolecules* **2017**, *50*, 7380–7387.

(15) Gody, G.; Maschmeyer, T.; Zetterlund, P. B.; Perrier, S. Rapid and quantitative one-pot synthesis of sequence-controlled polymers by radical polymerization. *Nat. Commun.* **2013**, *4*, 2505.

(16) Engelis, N. G.; Anastasaki, A.; Whitfield, R.; Jones, G. R.; Liarou, E.; Nikolaou, V.; Nurumbetov, G.; Haddleton, D. M. Sequence-Controlled Methacrylic Multiblock Copolymers: Expanding the Scope of Sulfur-Free RAFT. *Macromolecules* **2018**, *51*, 336–342.

(17) Chen, C. Designing catalysts for olefin polymerization and copolymerization: Beyond electronic and steric tuning. *Nat. Rev. Chem.* **2018**, *2*, 6–14.

(18) Zhu, Y.; Radlauer, M. R.; Schneiderman, D. K.; Shaffer, M. S. P.; Hillmyer, M. A.; Williams, C. K. Multiblock Polyesters Demonstrating High Elasticity and Shape Memory Effects. *Macromolecules* **2018**, *51*, 2466–2475.

(19) Romain, C.; Zhu, Y.; Dingwall, P.; Paul, S.; Rzepa, H. S.; Buchard, A.; Williams, C. K. Chemoselective Polymerizations from Mixtures of Epoxide, Lactone, Anhydride, and Carbon Dioxide. *J. Am. Chem. Soc.* **2016**, *138*, 4120–4131.

(20) Smith, S. D.; Spontak, R. J.; Satkowski, M. M.; Ashraf, A.; Heape, A. K.; Lin, J. S. Microphase-separated poly(styrene-b-isoprene)n multiblock copolymers with constant block lengths. *Polymer* **1994**, *35*, 4527–4536.

(21) Matsushita, Y.; Mogi, Y.; Mukai, H.; Watanabe, J.; Noda, I. Preparation and morphology of multiblock copolymers of the (AB)n type. *Polymer* **1994**, *35*, 246–249.

(22) Wu, L.; Cochran, E. W.; Lodge, T. P.; Bates, F. S. Consequences of Block Number on the Order−Disorder Transition and Viscoelastic Properties of Linear (AB) n Multiblock Copolymers. *Macromolecules* **2004**, *37*, 3360–3368.

(23) Watanabe, H.; Matsumiya, Y.; Sawada, T.; Iwamoto, T. Rheological and Dielectric Behavior of Dipole-Inverted (SIS) p -Type Multiblock Copolymers: Estimates of Bridge/Loop Fractions for Respective I Blocks and Effect of Loops on High Extensibility of Bridges. *Macromolecules* **2007**, *40*, 6885–6897.

(24) Nagata, Y.; Masuda, J.; Noro, A.; Cho, D.; Takano, A.; Matsushita, Y. Preparation and Characterization of a Styrene−Isoprene Undecablock Copolymer and Its Hierarchical Microdomain Structure in Bulk. *Macromolecules* **2005**, *38*, 10220–10225.

(25) Spontak, R. J.; Fung, J. C.; Braunfeld, M. B.; Sedat, J. W.; Agard, D. A.; Ashraf, A.; Smith, S. D. Architecture-Induced Phase Immiscibility in a Diblock/Multiblock Copolymer Blend. *Macromolecules* **1996**, *29*, 2850–2856.

(26) Spontak, R. J.; Smith, S. D. Perfectly-alternating linear (AB)n multiblock copolymers: Effect of molecular design on morphology and properties. *J. Polym. Sci. Part B: Polym. Phys.* **2001**, *39*, 947–955.

(27) Hermel, T. J.; Hahn, S. F.; Chaffin, K. A.; Gerberich, W. W.; Bates, F. S. Role of Molecular Architecture in Mechanical Failure of Glassy/Semicrystalline Block Copolymers: CEC vs CECEC Lamellae. *Macromolecules* **2003**, *36*, 2190–2193.

(28) Koo, C. M.; Hillmyer, M. A.; Bates, F. S. Structure and Properties of Semicrystalline−Rubbery Multiblock Copolymers. *Macromolecules* **2006**, *39*, 667–677.

(29) Wu, L.; Lodge, T. P.; Bates, F. S. Effect of block number on multiblock copolymer lamellae alignment under oscillatory shear. *J. Rheol.* **2005**, *49*, 1231–1252.

(30) Appold, M.; Grune, E.; Frey, H.; Gallei, M. One-Step Anionic Copolymerization Enables Formation of Linear Ultrahigh-Molecular-Weight Block Copolymer Films Featuring Vivid Structural Colors in the Bulk State. *ACS Appl. Mater. Interfaces* **2018**, *10*, 18202–18212.

(31) Steube, M.; Johann, T.; Galanos Eftyxis; Appold, M.; Rüttinger, C.; Metzger, M.; Gallei, M.; Müller, A. H.E.; Floudas, G.; Frey, H. Isoprene/Styrene Tapered Multiblock Copolymers with up to 10 Blocks: Synthesis, Phase Behavior, Order and Mechanical Properties. *Macromolecules* **2018**, in revision.

(32) Grune, E.; Appold, M.; Müller, A. H. E.; Gallei, M.; Frey, H. Anionic Copolymerization Enables the Scalable Synthesis of Alternating (AB) n Multiblock Copolymers with High Molecular Weight in n /2 Steps. *ACS Macro Lett.* **2018**, 807–810.

(33) Grune, E.; Johann, T.; Appold, M.; Wahlen, C.; Blankenburg, J.; Leibig, D.; Müller, A. H. E.; Gallei, M.; Frey, H. One-Step Block Copolymer Synthesis versus Sequential Monomer Addition: A Fundamental Study Reveals That One Methyl Group Makes a Difference. *Macromolecules* **2018**, *51*, 3527–3537.

(34) Fredrickson, G. H.; Helfand, E. Fluctuation effects in the theory of microphase separation in block copolymers. *The Journal of Chemical Physics* **1987**, *87*, 697–705.

(36) Matsen, M. W.; Bates, F. S. Unifying Weak- and Strong-Segregation Block Copolymer Theories. *Macromolecules* **1996**, *29*, 1091–1098.

(37) Hadjichristidis, N.; Floudas, G.; Pispas, S. *Block copolymers: Synthetic strategies, physical properties, and applications*; Wiley-Interscience: Hoboken, N.J, 2003.

(38) Semonov A. N. Contribution to the theory of microphase layering in block-copolymer melts. *Sov. Phys. JETP* **1985**, 733–742.

3.2.7 Supporting Information

3.2.7.1 ^{1}H NMR Analysis

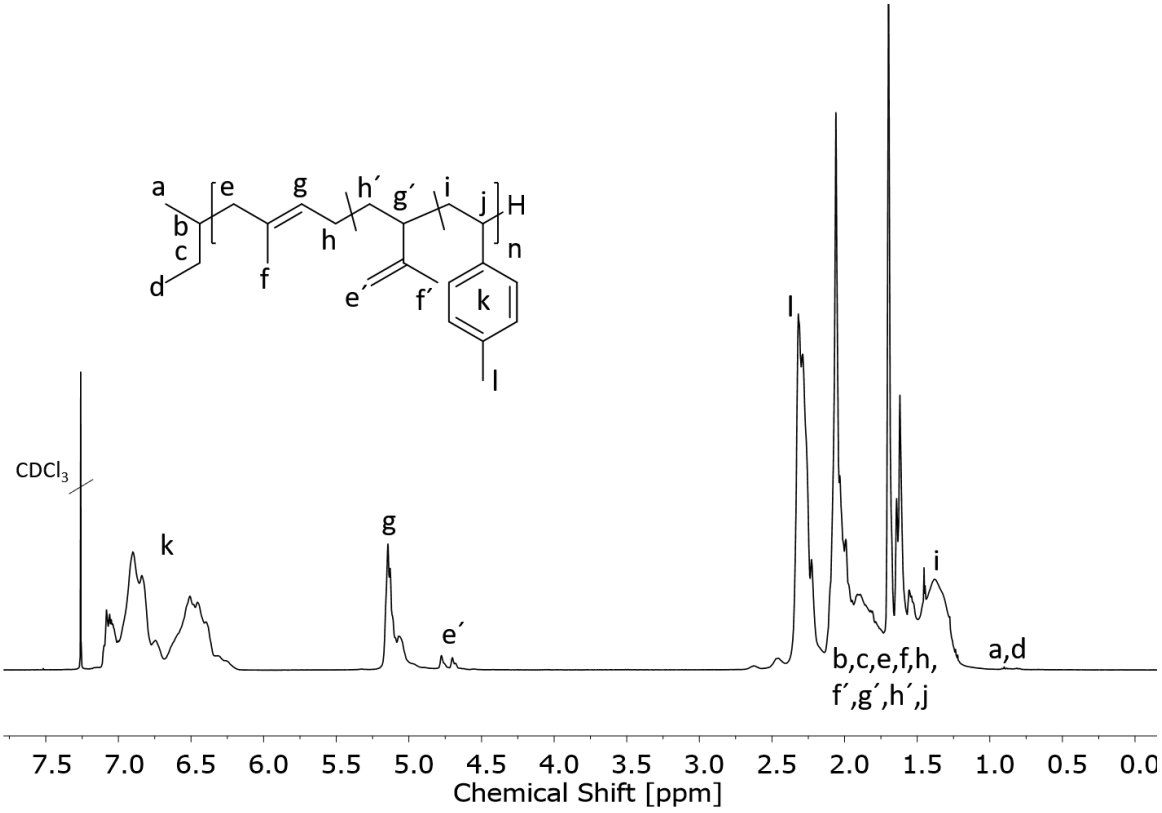

Figure S1: ^{1}H-NMR spectrum (400 MHz) of 400K10B in $CDCl_3$ (Table S1 Entry 15).

3.2.7.2 Size Exclusion Chromatography (SEC)

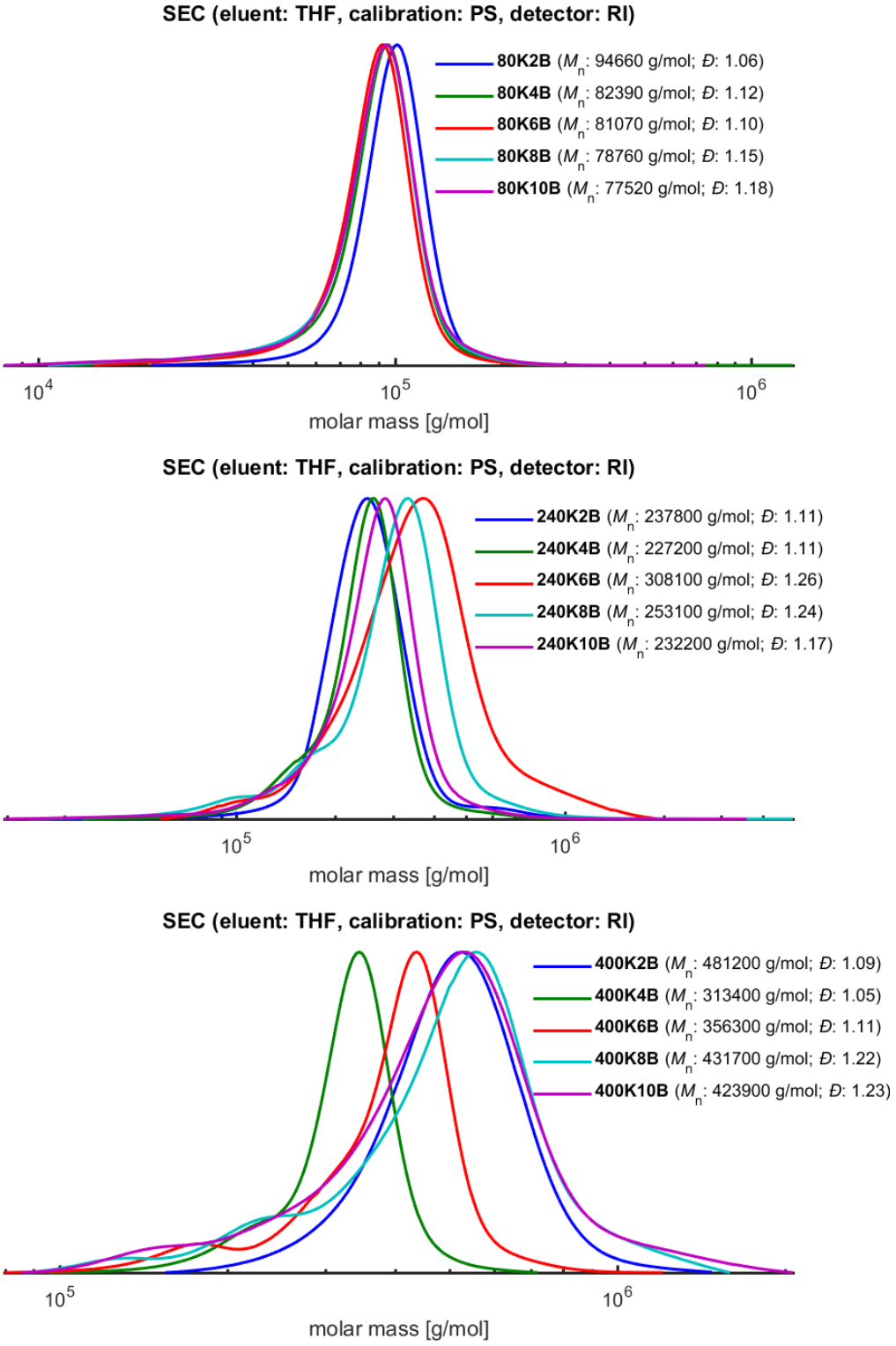

Figure S2: SEC elugrams of I/4MS multiblock copolymers (Table S1 Entries 1-15).

3.2.7.3 Dynamic Mechanical Analysis (DMA)

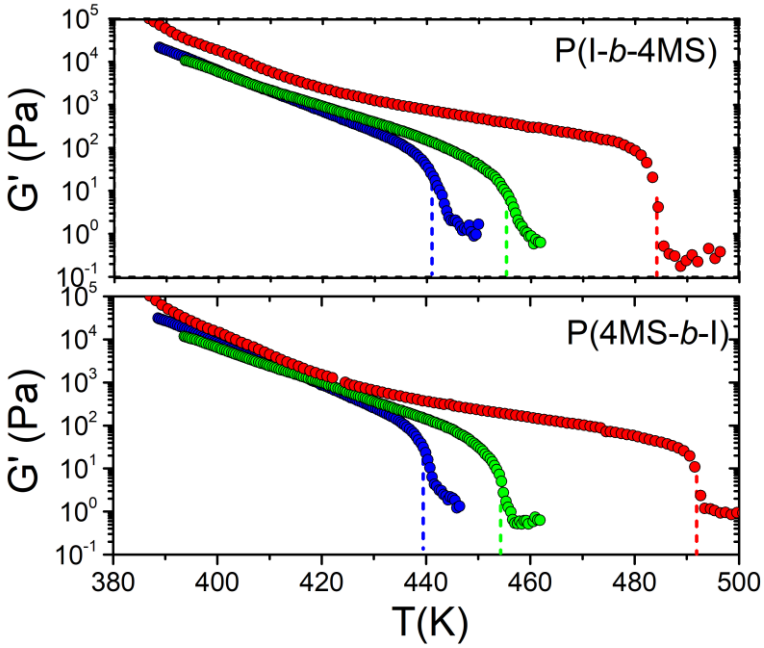

Figure S3: Temperature dependence of the storage modulus, G', obtained at a frequency of ω=1 rad/s with a low strain amplitude on heating the sequential diblock copolymers 30KP(I-*b*-4MS) (Table S1 Entry 16) (blue), 35KP(I-*b*-4MS) (Table S1 Entry 18) (green) and 40KP(I-*b*-4MS) (Table S1 Entry 20) (red) (top) and the inverse diblock copolymers 30KP(4MS-*b*-I) (Table S1 Entry 17) (blue), 35KP(4MS-*b*-I) (Table S1 Entry 19) (green) and 40KP(4MS-*b*-I) (Table S1 Entry 21) (red) (bottom). Vertical dashed lines indicate the respective T_{ODT}s.

3.2.7.4 Tensile Testing

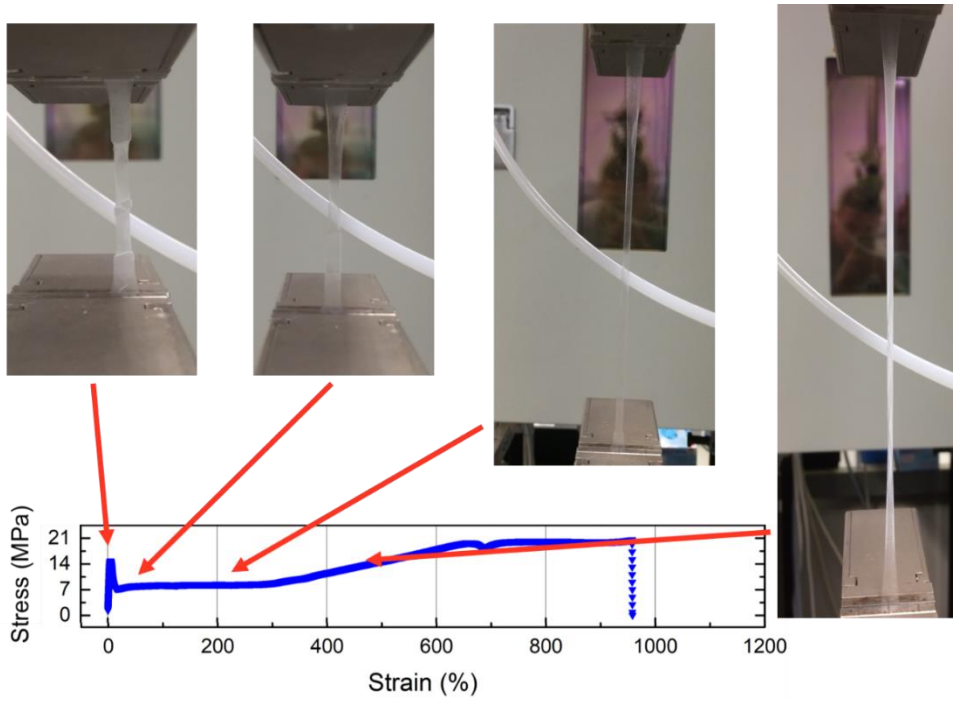

Figure S4: Tensile testing of a multiblock sample.

3.2.7.5 Summarized Results

Table S1. Molecular characteristics of the tapered multiblock copolymers P(I-*co*-4MS) and of the sequential P(I-*b*-4MS) (i.e. "normal") and P(4MS-*b*-I) (i.e. "inverse") diblock copolymers.

Entry	Sample	number of blocks	M_n^{theo} (kg/mo)l	M_n^{a} (kg/mol)	$Đ^{a}$	Isoprene content^{theo} (mol%)
1	80K2B	2	80	94.7	1.06	50
2	80K4B	4		82.4	1.12	50
3	80K6B	6		81.1	1.10	50
4	80K8B	8		78.7	1.15	50
5	80K10B	10		77.5	1.18	50
6	240K2B	2	240	237.8	1.11	50
7	240K4B	4		227.2	1.11	50
8	240K6B	6		308.1	1.26	50
9	240K8B	8		253.1	1.24	50
10	240K10B	10		232.2	1.17	50
11	400K2B	2	400	481.2	1.09	50
12	400K4B	4		313.4	1.05	50
13	400K6B	6		356.3	1.11	50
14	400K8B	8		431,7	1.22	50
15	400K10B	10		423,9	1.23	50
16	30KP(I-*b*-	2	30	38.3	1.15	50
17	30KP(4MS-*b*-	2		37.7	1.17	50
18	35KP(I-*b*-	2	35	41.8	1.15	50
19	35KP(4MS-*b*-	2		40.3	1.16	50
20	40KP(I-*b*-	2	40	45.6	1.17	50
21	40KP(4MS-*b*-	2		46.4	1.18	50

[a] Determined by SEC at 25°C in THF

Chapter 4: Bio-based polymers

4.1 Towards bio-based tapered block copolymers: the behaviour of myrcene in the statistical anionic copolymerization

Eduard Grune,[a,b] Jennifer Bareuther,[c] Jan Blankenburg,[a,b] Michael Appold,[c] Lloyd Shaw,[d] Axel H. E. Müller,[a] George Floudas,[d] Lian R. Hutchings,*[,e] Markus Gallei*[,c] and Holger Frey*[,a]

[a] Institute of Organic Chemistry, Johannes Gutenberg University, Duesbergweg 10-14, 55128 Mainz, Germany

[b] Graduate School Materials Science in Mainz, Staudinger Weg 9, 55128 Mainz, Germany

[c] Macromolecular Chemistry Department, TU Darmstadt, Alarich-Weiss Str. 4, 64287 Darmstadt, Germany

[d] Department of Physics, University of Ioannina, P.O. Box 1186, 45110 Ioannina, Greece

[e] Durham Centre for Soft Matter, Department of Chemistry, Durham University, DH1 3LE Durham, United Kingdom

to be submitted

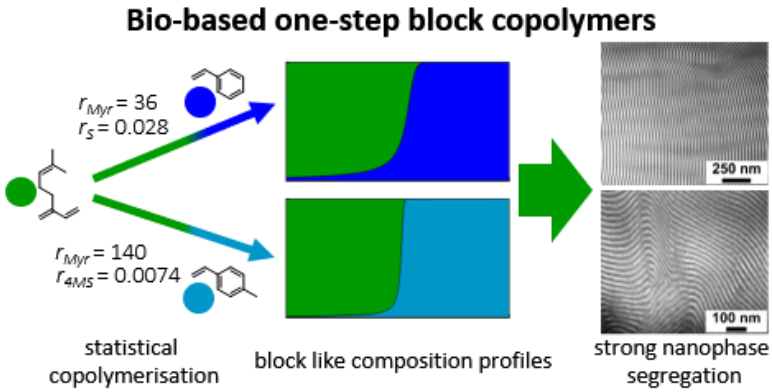

4.1.1 Abstract

To explore the potential of myrcene (Myr) as a bio-based monoterpene comonomer for styrenic monomers and to further explore its general applicability for the carbanionic copolymerization, several copolymerizations of myrcene and common monomers like isoprene (I), styrene (S) and 4-methylstyrene (4MS) were carried out in cyclohexane and monitored by *in situ* ^{1}H NMR spectroscopy. Real-time NMR kinetics studies permitted to determine the reactivity ratios and the copolymer composition profile for each monomer combination. While the copolymerization of Myr/I yielded a gradient copolymer and reactivity ratios of moderate disparity (r_{Myr} = 4.4; r_{I} = 0.23), the copolymerization of Myr/S and Myr/4MS afforded strongly block-like, tapered copolymers due to highly diverging reactivity ratios (r_{Myr} = 36; r_{S} = 0.028 and r_{Myr} = 140; r_{4MS} = 0.0074). Furthermore, a terpolymerization of Myr/I/4MS was studied by real-time NMR kinetics, revealing an alteration of the composition profile of 4MS towards a more block like structure. Based on the kinetic studies, a series of Myr/I/4MS terpolymers and Myr/S copolymers was prepared by statistical living anionic copolymerization. All copolymers showed narrow molecular weight distributions (SEC) and two glass transition temperatures ($T_{g,1}$ = -51 -62 °C; $T_{g,2}$ = 93 – 107 °C), indicating phase segregation. TEM and SAXS measurements revealed highly ordered lamellar morphologies for all copolymers with long range correlation and confirmed the block like structure of Myr/S and Myr/4MS copolymers prepared by statistical carbanionic copolymerization.

4.1.2 Introduction

ABA triblock copolymers based on inexpensive petroleum based monomers like isoprene (I), butadiene (B) and styrene (S) are highly established and can be found in various applications ranging from footwear to asphalt modifiers.[1] The respective, well-defined block copolymers are predominantly prepared by living anionic copolymerization using sequential monomer addition. Like no other polymerization technique, carbanionic polymerization provides a high level of molecular weight control and low dispersity, which are key features for the preparation of versatile materials with tailor-made properties based on vinyl monomers.[2,3]

However, dwindling petrochemical resources and an increasing environmental awareness have motivated the interest for bio-based polymer materials from renewable sources. Among the variety of bio-based monomers, especially myrcene (Myr) garnered considerable interest due to its convenient availability and structural similarity to isoprene and butadiene. Myrcene belongs to the class of monoterpenes and can be found in many plants like conifers, wild thyme and hops.[4,5] Commercially, myrcene is generated on large scale by pyrolysis of β-pinene, and recent developments in metabolic engineering also enable the microbial synthesis of myrcene.[5,6] Like its petroleum-derived diene counterparts, myrcene can be polymerised by various polymerization techniques like emulsion polymerization, controlled and free radical polymerization and living anionic polymerization.[7-10] The carbanionic copolymerization of myrcene has only been studied in a few works that lack in depth kinetic studies.[9,11-13] To explore the potential of myrcene as a comonomer for styrenic monomers and to establish its applicability for carbanionic copolymerization it is indispensable to investigate myrcenes copolymerization kinetics in depth.

Previous studies by Quirk et al. and Bolton et al. have shown that myrcene can be copolymerised with styrene. Polymyrcene provides similar properties as polyisoprene, such as a low T_g (- 65 °C) and high content of 1,4 units when polymerised in nonpolar solvents (Figure 1).[9,11,12]

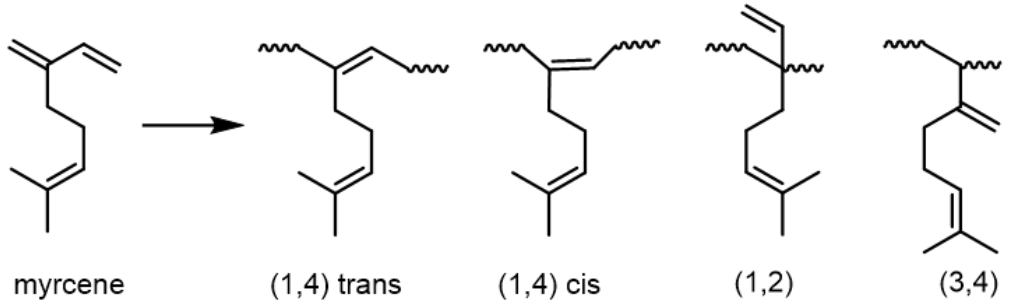

Figure 1: Structure of myrcene (left) and possible microstructures of polymyrcene.

Besides sequential monomer addition, the statistical anionic copolymerization is a very important synthetic strategy to prepare tough materials and to tune materials properties.[14-17] Especially the statistical living anionic copolymerization of styrene/isoprene and styrene/butadiene are highly relevant for commercial applications and have been extensively studied.[17-20] The great importance of these monomer combinations arises from the special kinetics of styrenic and diene

monomers. In nonpolar solvents dienes show much higher reactivity than styrenic monomers, resulting in a highly preferred homopolymerization of the diene monomer and a considerably faster cross-over reaction from a styrenic living chain end to the diene carbanion than the reversed cross-over reaction.[21,22] Consequently, the incorporation of the diene monomer is highly favoured, yielding tapered copolymers with almost pure diene and styrenic blocks in the polymer chains and a mixed midblock.[23,24] Altering shape and length of this tapered section has an impact on the mechanical response, i.e., the composition profile is an important "setting screw" for the mechanical properties.[25-28] Understanding the kinetics of a monomer system permits to predict and to alter the composition profile and therefore to tailor the mechanical characteristics. Recent studies by Yang et al. and by our group revealed a high sensitivity of the living anionic copolymerization kinetics towards even small changes of the electron density of the double bond induced by alkyl groups at styrene.[17,29] Hence, it can be assumed that the inductive effect of the large alkyl substituent of myrcene will have a significant effect on its copolymerization behaviour, when compared to isoprene and butadiene.

To the best of our knowledge, no kinetic studies on the statistical copolymerization of myrcene have been carried out to date. In this study, we present in-depth kinetics studies of different copolymerizations of myrcene in nonpolar solvents as well as a detailed characterization of myrcene copolymers. For this purpose, the copolymerizations Myr/I; Myr/S; Myr/4MS and the terpolymerization Myr/I/4MS were monitored by *in-situ* ^{1}H NMR kinetics in cyclohexane, permitting to calculate the reactivity ratios and composition profiles of each monomer combination. The results revealed block like composition profiles for Myr/S; Myr/4MS and Myr/I/4MS copolymers, indicating the formation of tapered block copolymers in one step. To confirm this assumption several Myr/S; Myr/4MS and Myr/I/4MS copolymers were prepared by simultaneous copolymerization and characterised by SEC, DSC, SAXS and TEM. All copolymers showed narrow dispersities and well defined morphologies, confirming the blocky character of these copolymers.

4.1.3 Experimental Section

4.1.3.1 Materials

All chemicals and solvents were purchased from Acros Organics Co. and Sigma-Aldrich Co. Isopropyl alcohol and methanol were used as received without further purification. Cyclohexane was purified via distillation over sodium and degassed by three freeze-thaw cycles prior to use. Myrcene, isoprene, styrene and 4-methylstyrene were purified by distillation over CaH_2 and degassed by three cycles of freeze-thaw prior to use.

4.1.3.2 Instrumentation

NMR spectra were recorded on a Bruker Avance II 400 spectrometer working 400 MHz (^{1}H NMR). NMR chemical shifts are referenced relative to tetramethylsilane. Standard SEC was performed with THF as the mobile phase (flow rate 1 mL min^{-1}) on a SDV column set from PSS (SDV 10^3, SDV 10^5, SDV 10^6) at 30 °C. Calibration was carried out using PS standards (from Polymer Standard Service, Mainz). For determination of the thermal properties of the polymers differential scanning calorimetry (DSC) was performed with a Mettler Toledo DSC-1 in a temperature range from -100 °C to 150 °C with a heating rate of 10 K min^{-1}.

4.1.3.3 TEM Measurements

TEM experiments were carried out on a Zeiss EM 10 electron microscope operating at 60 kV. All shown images were recorded with a slow-scan CCD camera obtained from TRS (Tröndle) in bright field mode. Camera control was computer-aided using the ImageSP software from TRS.

4.1.3.4 SAXS Measurements

Small angle X-ray scattering (SAXS) was performed using a laboratory set-up (Molecular Metrology, Northampton, MA, USA). We used the Kα-line of a copper X-ray tube with a wavelength of λ = 1.54Å monochromated and focused by a X-ray mirror and collimated by a pinhole collimation system. Data were recorded on a 2-D multiwire detector. Since all samples scattered isotropically, data was radially

averaged resulting in intensity vs. magnitude of the scattering vector $q=(4\pi/\lambda)\sin\theta$, with 2θ denoting the scattering angle. With the given sample-detector distance of 1.5 metres, the accessible range of scattering vectors was 0.008 Å-1 ≤ q ≤ 0.25 Å-1. q-scaling was calibrated by measuring silver behenate. The sample holder was sealed by aluminum foil.

4.1.3.5 ^{1}H-NMR kinetics studies

Monomer/solvent mixtures (20 wt% in cyclohexane-d_{12}) were prepared in a glove box. All compounds were purified via distillation over CaH_2 prior to use. The mixtures were filled in conventional NMR tubes and sealed with rubber septa. A ^{1}H NMR spectrum of the mixture was measured prior to the initiation step. After the initiation with one drop of *sec*-butyllithium (1.3 M in cyclohexane/hexane 92/8) the ^{1}H NMR experiments were started without locking and shimming of the polymerization mixture. All spectra were measured with 1 scan per minute at 400 MHz and a time interval of 20 seconds between the spectra. The reaction temperature was kept constant at 23 °C. Typically, 150-250 ^{1}H NMR spectra were recorded and evaluated.

4.1.3.6 Determination of reactivity ratios and microstructure

To determine the reactivity ratios, the proton signals 5.54-5.64 ppm (4MS), 5.6-5.7 ppm (S), 6.29-6.37 ppm (Myr) and 6.34-6-44 (I) were used. Data from the copolymerization experiments was fitted to both the ideal, non-ideal model ($r_1 \cdot r_2$=1) and the terminal model (Mayo-Lewis).[31] The ideal model was fitted by an equation recently reported (Supp. Inf. Table S1 Entry 3).[30] The Mayo-Lewis model in its integrated form, i.e., the Meyer-Lowry equation was used to fit the terminal model.[31,32] The experimental data can be sufficiently described by the non-terminal model. The reactivity ratios determined by this method were therefore used to simulate the gradient structure of the co- and terpolymerization. The procedures are explained in detail in the Supporting Information.

4.1.3.7 General polymerization procedure for myrcene copolymerizations

All copolymerizations were carried out in cyclohexane in an argon atmosphere and at room temperature in a glove-box in 30 ml glass flasks equipped with septa. The degassed monomer/ solvent (20 wt%) was initiated with *sec*-butyllithium (1.3 M in cyclohexane/hexane 92/8) via syringe. The solution was stirred over night to ensure full monomer conversion. The polymerization was terminated by adding 0.5 ml of degassed isopropyl alcohol by a syringe. The polymers were precipitated in a large excess of isopropanol, dried at reduced pressure and stored at -18 °C.

4.1.4 Results and Discussion

4.1.4.1 Microstructure analysis of myrcene copolymers

Like polyisoprene and polybutadiene, polymyrcene shows a high content of 1,4 units (95%) and a low percentage of 3,4 units (5%), when polymerised in non-polar solvents (Figure 2). The formation of 1,2 units was not observed, which can be explained by the steric hindrance of this double bond. The double bond of the alkyl side chain remains inactive throughout the carbanionic polymerization of myrcene, providing a high density of dangling double bonds, which can be used for a variety of postmodification reactions without affecting the 1,4 backbone microstructure.[13,33]

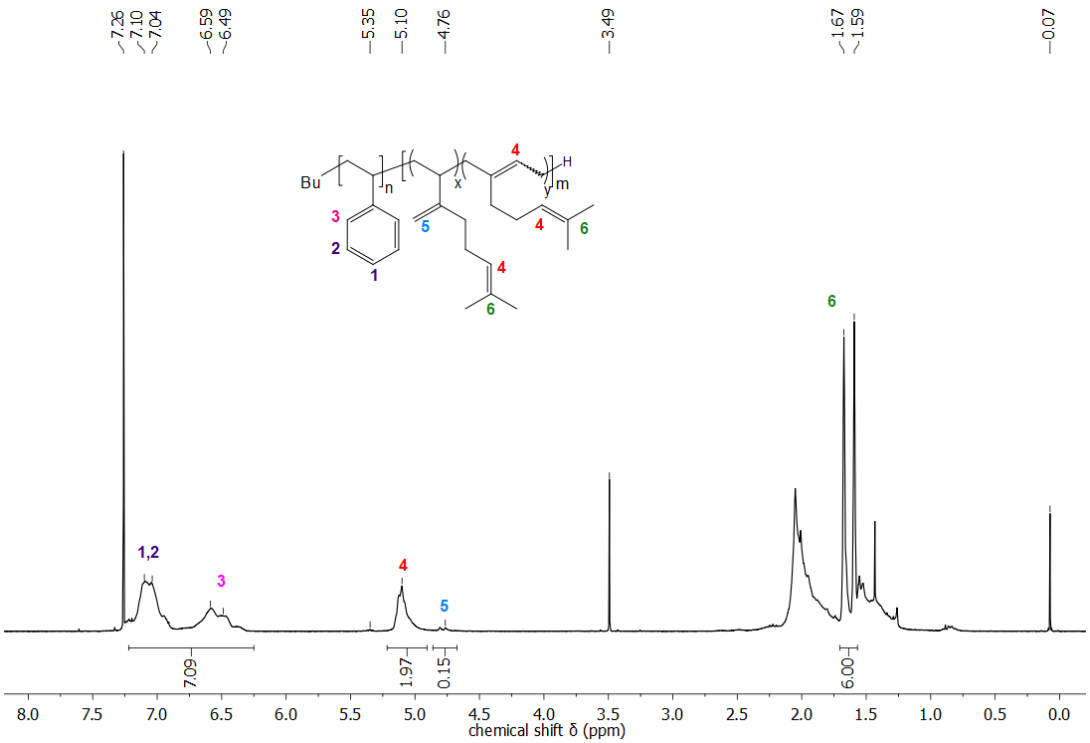

Figure 2: ^{1}H NMR spectrum of copolymer $Myr_{0.42}$-$S_{0.58}$ (Table 1 Entry 7) in $CDCl_3$ at 23 °C.

4.1.4.2 *In-situ* ^{1}H NMR kinetic studies of myrcene copolymerizations

To investigate the copolymerization kinetics of myrcene, copolymerization experiments with isoprene, styrene and 4-methylstyrene, respectively were carried out and monitored by real-time ^{1}H NMR spectroscopy (Figure 3:). The corresponding kinetic curves and evaluations are given in Figures S8-S10 and S1-S3 (Supp. Inf.), respectively.

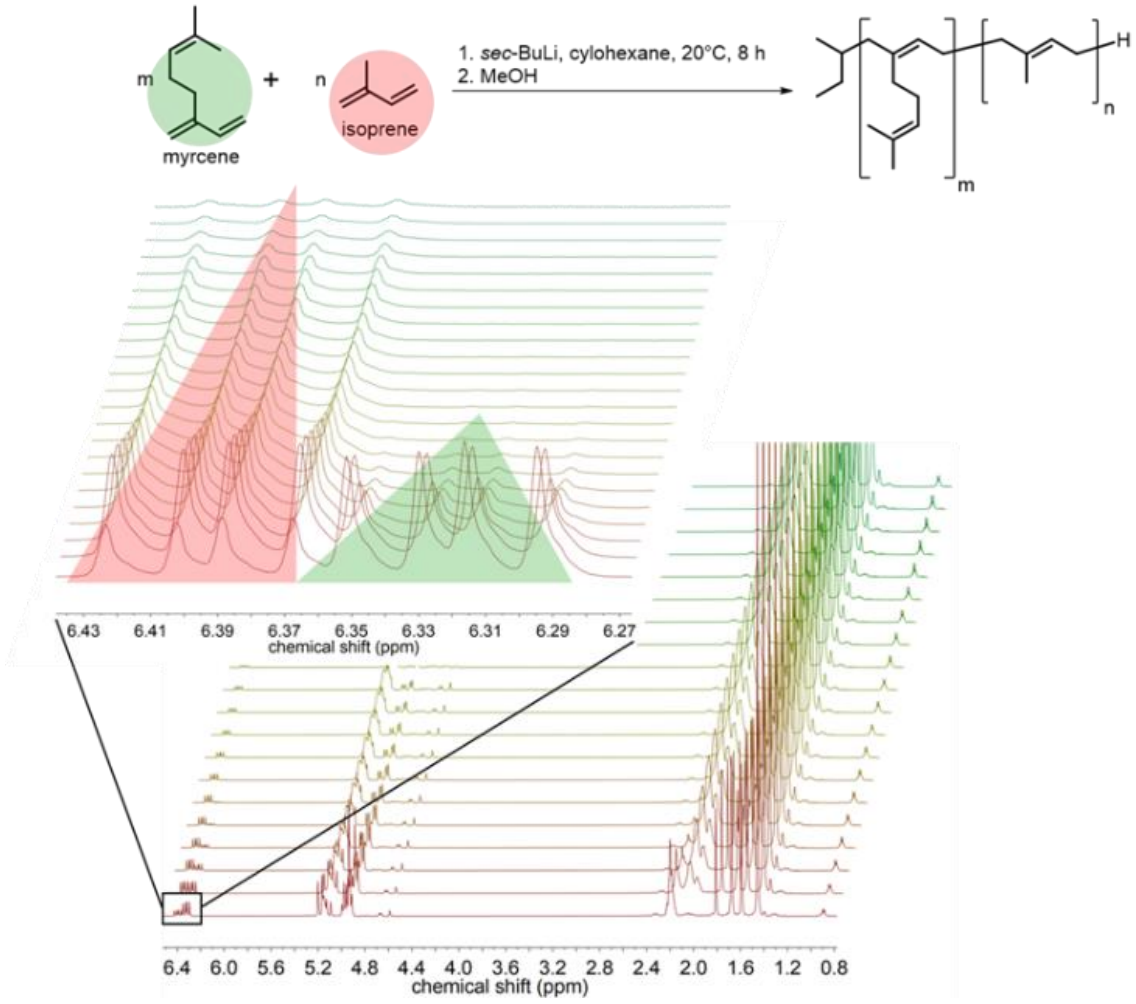

Figure 3: Reaction conditions of the *in-situ* NMR kinetics experiment (top) and monitoring of decreasing monomer signals by real-time ^{1}H NMR spectroscopy.

Following the decrease of the specific monomer signals permits the calculation of the reactivity ratios of each monomer combination. The experimental data could be adequately described with the ideal, non-terminal copolymerization model first described by Wall.[34] The explanatory power (R^2) did not increase significantly for the more elaborated Mayo-Lewis terminal model. To avoid overfitting, the ideal model was used to determine the reactivity ratios (a more detailed explanation of the

methods can be found in the Supporting Information). This model can also be directly applied to describe the terpolymerization. In a second step, the reactivity ratios were used to simulate the composition profiles of each monomer combination (Figure 4) (a more detailed discussion of the determination of the reactivity ratios and the simulation of the composition profiles can be found in the Supporting Information).

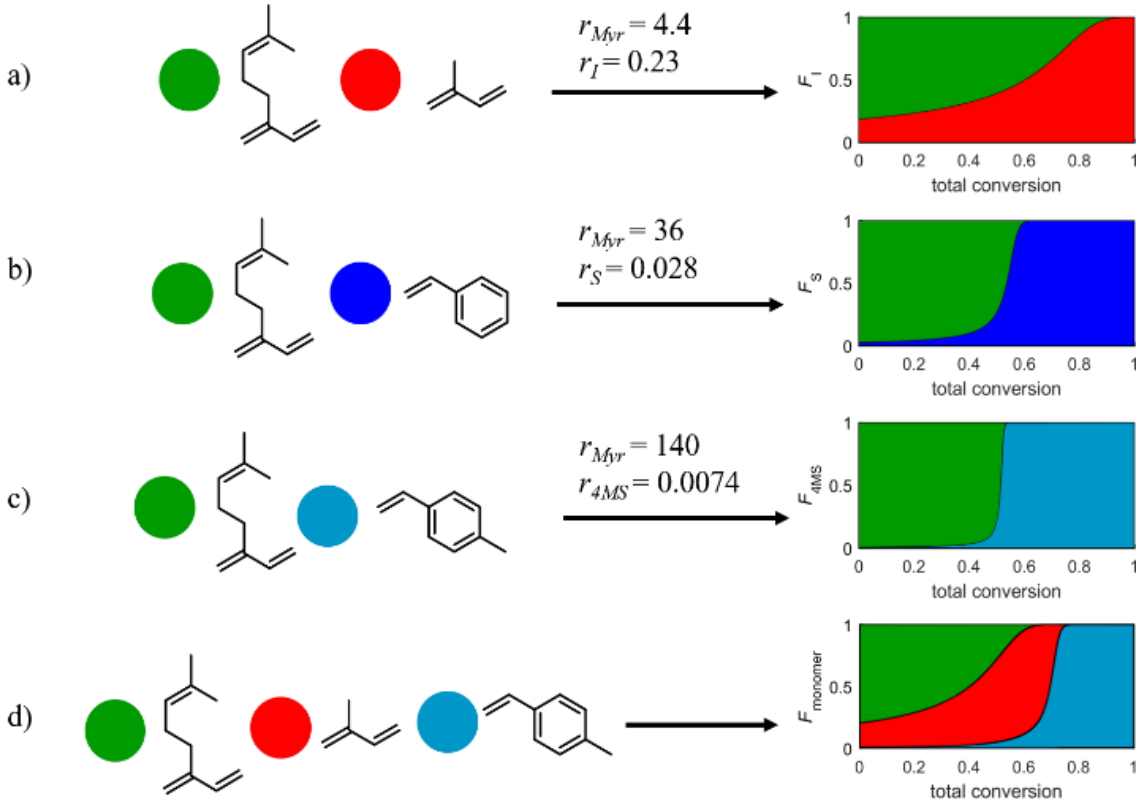

Figure 4: Simulated composition profiles of myrcene co- and terpolymers.

For a better comparison of the composition profiles, all simulations are given at equimolar monomer ratios. In the statistical copolymerization of myrcene and isoprene, myrcene was consumed faster than isoprene due to its higher reactivity ($r_{Myr} = 4.4$; $r_I = 0.23$). The resulting gradient copolymer showed a gradient composition profile with a gradual increase of the isoprene content at higher conversion (Figure 4 a). A similar ratio of reactivities was observed for the copolymerization of isoprene and butadiene in nonpolar solvents ($r_I = 3.6$; $r_B = 0.5$).[35] In both monomer combinations, the electron donating effect of the alkyl substituent of isoprene and myrcene is responsible for the increased monomer reactivities. The reactivity can be correlated to the strength of the electron donating effect, with a correlation between electron density of the double bond and the reactivity of the diene monomer.

Turning to the copolymerization of myrcene with styrene and 4-methylstyrene, the formation of block-like composition profiles with almost pure diene and styrenic blocks and a very short and steep gradient spacer was observed (Figure 4 b and c). The block-like structure is very pronounced for Myr/4MS copolymers and can be attributed to the vigorously different reactivities (r_{Myr} = 140; r_{4MS} = 0.0074). This tremendous disparity of the reactivity ratios can again be explained by the electron donating effect of the alkyl substituents. The alteration of the electron density at the double bond of a monomer has a contrary effect on the monomer reactivity and the reactivity of the carbanionic living chain end of the respective monomer. During the anionic polymerization, the monomer addition step is a nucleophilic attack of the carbanion chain end at the monomers´ double bond. Enhancing the electron density at the double bond lowers its electrophilicity and therefore its reactivity towards a nucleophilic attack.[36,37] On the other hand, an increased electron density enhances the nucleophilicity of the living chain end, resulting in a higher reactivity.[29] In the case of myrcene and 4-methylstyrene the increase of the living chain end reactivities is more distinct than the decrease of the monomer reactivity. This results in a highly favoured homopolymerization of myrcene and very fast cross-over reaction from poly-4-methylstyryllithium to polymyrcenyllithium. The opposite cross-over reaction as well as the homopolymerization of 4MS are less favoured and much slower. This results in high ratios of cross-over and homopolymerization rates, permitting the formation of a very block like, tapered copolymers in one step.

In the case of myrcene and styrene, this effect is less pronounced, due to the lower electron density of styrene´s vinyl group as compared to 4-methylstyrene. This results in a higher monomer reactivity than 4MS and therefore a more favoured incorporation of styrene. The resulting composition profile is very similar to the composition profile of I/4MS,[18] since both monomer system possess similar reactivity ratios (r_{Myr} = 36; r_S = 0.028 and r_I = 25.4; r_{4MS} = 0.07).[17] Compared to copolymers from Myr/4MS, Myr/S copolymers exhibit a longer tapered section and a higher content of styrene units in the diene section, yielding a less blocklike structure than Myr/4MS. It can be assumed that the longer taper will affect the physicochemical properties and the phase segregation behaviour due to its compatibilising effect.[17]

In a recent study, Hutchings et al. demonstrated the alteration of the composition profile of B/S by the addition of 1,1-diphenylethylene (DPE).[38] The statistical

terpolymerization of B/S/DPE yielded more block-like structures than statistical B/S copolymers, which can be attributed to a significant change of the B/S copolymerization kinetics induced by DPE. In order to investigate whether a similar effect can be achieved for I/4MS copolymers, a terpolymerization of Myr/I/4MS was carried out and monitored by *in-situ* NMR spectroscopy (Figure 4 d and Figure S4-S7, Supp. Inf.).

A direct comparison of the composition profiles of statistical copolymers of I/4MS and Myr/I/4MS reveals only minor differences (Figure 5). However, the addition of myrcene to the copolymerization of I/4MS lowers the content of 4MS impurities in the diene section, resulting in a higher "structural purity" of the diene block, providing a more block like structure.

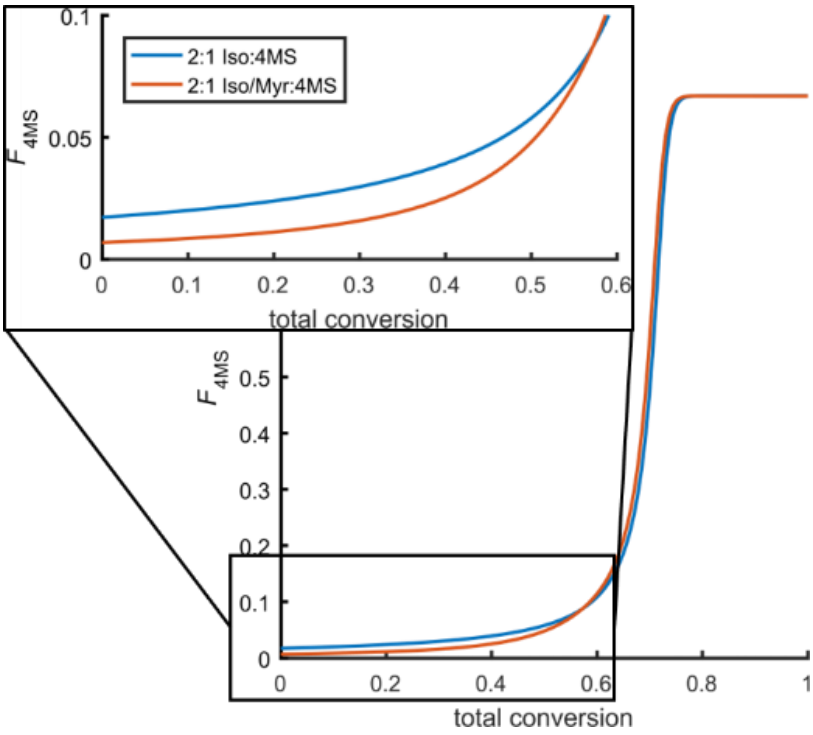

Figure 5: Simulated composition profile of 4-methylstyrene in a statistical copolymerization of I/4MS (blue) and a statistical terpolymer of Myr/I/4MS (red). For a better comparison of the composition profiles the region at a total conversion from 0 to 60 % was magnified.

4.1.4.3 Thermal behaviour of co- and terpolymers

To investigate the influence of the composition profile on the thermochemical properties, a series of myrcene copolymers was prepared by statistical carbanionic copolymerization. All polymers showed high molecular weights and narrow molecular weight distributions (Table 1, Figure S11 -S12). Our previous studies on block-like tapered copolymers revealed a strong correlation between the shape and length of the tapered section and the glass transition temperatures of the individual segments.[17,39] Due to the compatibilising effect of the gradient, a long tapered section results in the convergence of both glass transitions. A short taper, on the other hand, does not affect the T_gs significantly, rendering the tapered copolymers virtually indistinguishable from a perfect diblock copolymer. This correlation was also observed for this series of myrcene copolymers. The kinetic studies revealed a less block like structure for Myr/S copolymers than for Myr/4MS copolymers. Consequently, the $T_{g,\,Myr}$ of $Myr_{0.42}$-$S_{0.58}$ is significantly higher than $T_{g,\,Myr}$ of $Myr_{0.5}$-$4MS_{0.5}$, due to the lower purity of the myrcene segment of $Myr_{0.42}$-$S_{0.58}$ (Table 1, Entry 6 and 7). The longer taper of $Myr_{0.42}$-$S_{0.58}$ also has an impact on $T_{g,S}$, showing a significant decrease compared to the glass transition of PS homopolymer ($T_{g,\,S}$ = 100°C).

Table 1: Results of DSC characterization of myrcene copolymers.

Entry	Sample composition [a] (mol%)	M_n [b] (kg/mol)	$Đ$ [b]	$T_{g,1}$ [c] (°C)	$T_{g,2}$ [c] (°C)
1	$I_{0.5}$-$4MS_{0.5}$	64.1	1.07	-51	103
2	$Myr_{0.1}$-$I_{0.4}$-$4MS_{0.5}$	67.0	1.08	-53	106
3	$Myr_{0.2}$-$I_{0.3}$-$4MS_{0.5}$	65.9	1.08	-57	107
4	$Myr_{0.3}$-$I_{0.2}$-$4MS_{0.5}$	71.5	1.09	-59	101
5	$Myr_{0.4}$-$I_{0.1}$-$4MS_{0.5}$	64.0	1.12	-61	102
6	$Myr_{0.5}$-$4MS_{0.5}$	63.8	1.14	-62	107
7	$Myr_{0.42}$-$S_{0.58}$	49.4	1.04	-54	93
8	$Myr_{0.26}$-$S_{0.74}$	161.5	1.04	-52	107

[a] The indices give the mole fractions as determined by ^{1}H NMR spectroscopy in $CDCl_3$; [b] determined by SEC in THF at 30°C; [c] determined by DSC, heating rate 10 K/min

Furthermore, the kinetic studies indicated an alteration of the composition profile of I/4MS towards a more block like structure, which is induced by the addition of myrcene. To verify this observation, a series of terpolymers with a targeted molecular weight of 60 kg/mol and a constant 4MS content but varying contents of I and Myr was prepared and examined by SEC and DSC. In all cases a slightly higher molecular weight was observed, which can be mainly attributed to the calibration with polystyrene standards. In addition, a slight increase of the dispersity with increasing content of myrcene was observed for samples 2 to 6 (Table 1).

A tentative explanation is based on the very slow cross over reaction from polymyrcenyllithium to 4MS, which translates to inhomogeneous initiation, resulting in a higher dispersity of the 4MS segments. All terpolymers showed two T_gs, clearly indicating the presents of a mixed Myr/I and a pure 4MS segment, which is in good agreement with the results of the *in-situ* NMR kinetic measurements. The alteration of the myrcene content of the terpolymers showed only minor changes of $T_{g,\,4MS}$ but a significant decrease of the T_g of the mixed Myr/I section for an increasing myrcene content, when compared to a corresponding I/4MS copolymers (Table 1, Entries 1-5). These results can be explained by the enhancement of the block character induced by the addition of myrcene, verifying the observations of the real-time NMR kinetic studies.

4.1.4.4 Phase segregation behaviour

The existence of two discrete glass transition temperatures of all copolymers, derived by statistical anionic copolymerization in nonpolar solvents is a first evidence for phase segregation. To verify these findings the morphologies of four statistical block copolymer samples were investigated by TEM and SAXS measurements. For this purpose, bulk characterization was accomplished after solvent evaporation of the block copolymers in chloroform or tetrahydrofuran followed by thermal annealing at 130 °C in a nitrogen atmosphere for 24 hours. The polymer films were cut into thin slices of 50-70 nm by ultramicrotomy and the collected thin slices were stained with osmium tetroxide, OsO_4, for selective staining of the PI- and PMyr-containing domains. In Figure 6, a corresponding TEM image of sample $Myr_{0.42}$-$S_{0.58}$ (Table 1 Entry 7) after staining is given revealing a lamellar morphology with lamellar periods, that is, the distance of two lamellae, of about 30.7 nm.

To gain more insights into the microphase separated structure, SAXS measurements of the sample $Myr_{0.42}$-$S_{0.58}$ was carried out. The corresponding SAXS pattern is shown in Figure 6 b revealing several pronounced diffraction peaks. Based on the results from our TEM investigations they can be assigned as first to third order peaks of the lamellar structure. Fitting a sum of Gaussian functions with fixed relative positions leads to a lamellar thickness of d = 34.0 nm, in good agreement with TEM measurements. The resulting fit is shown as a full red curve in Figure 6b.

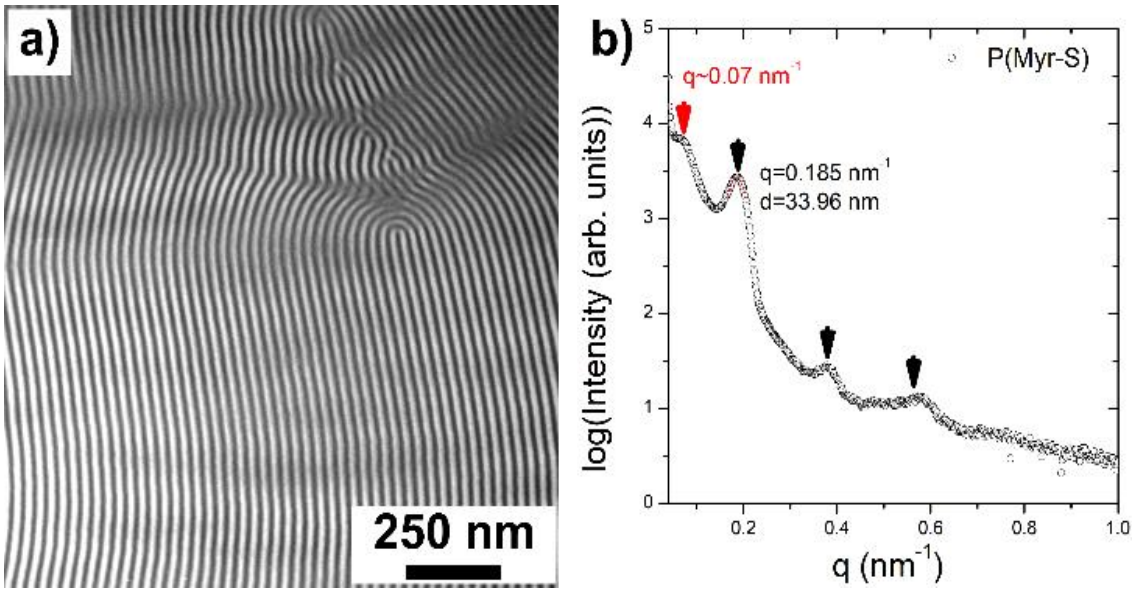

Figure 6: a) TEM image from the bulk morphology characterization for the polymer $Myr_{0.42}$-$S_{0.58}$. Thin section microtomed at -80 °C with 50 nm thickness, the sample was annealed at 130 °C for 24 hours. PMyr domain were stained with OsO_4. b) SAXS pattern for the sample $Myr_{0.42}$-$S_{0.58}$. Arrows give the position of the Bragg reflections corresponding to a lamellar morphology.

In Figure 7, a TEM image of sample $I_{0.5}$-$4MS_{0.5}$ (Table 1 Entry 1) after staining with OsO_4 is given, revealing a lamellar morphology with a lamellar period of 24.4 nm. Additionally, the SAXS pattern is also shown **in Figure 7 b,** displaying the first to third order peak of the lamellar structure with a lamellar thickness of *d* = 27.8 nm, in accordance with the TEM measurements.

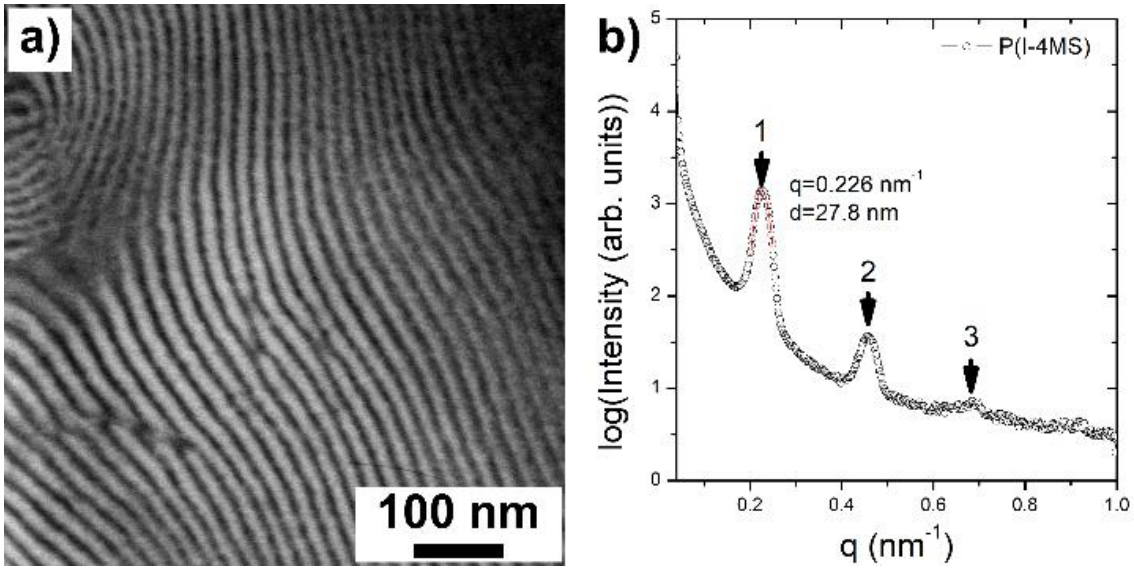

Figure 7: a) TEM image from the bulk morphology characterization for the polymer $I_{0.5}$-$4MS_{0.5}$. Thin section microtomed at -80 °C with 50 nm thickness, the sample was annealed at 130 °C for 24 hours. PMyr domain were stained with OsO_4. b) SAXS pattern for the sample $I_{0.5}$-$4MS_{0.5}$. Arrows give the positions of the Bragg reflections corresponding to a lamellar morphology.

In Figure 8, a TEM image of sample $Myr_{0.2}$-$I_{0.3}$-$4MS_{0.5}$ (Table 1 Entry 3) after staining with OSO_4 is given, revealing a lamellar morphology with a lamellar period of 30.1 nm. Additionally, the SAXS pattern is also shown in Figure 8 displaying the first to third order peak of the lamellar structure with a lamellar thickness of *d* = 32.3 nm. Again, these results are in good agreement with TEM measurements.

Furthermore, the morphology of sample $Myr_{0.5}$-$4MS_{0.5}$ (Table 1 Entry 6) was investigated. Exemplarily, a TEM image after staining with OsO_4 is shown in Figure 9 revealing a lamellar morphology with a lamellar period of 28.7 nm. Additionally, the SAXS pattern is also shown in Figure 9 b displaying the first to third order peak oh the lamellar structure with a lamellar thickness of *d* = 29.4 nm, in accordance with TEM measurements.

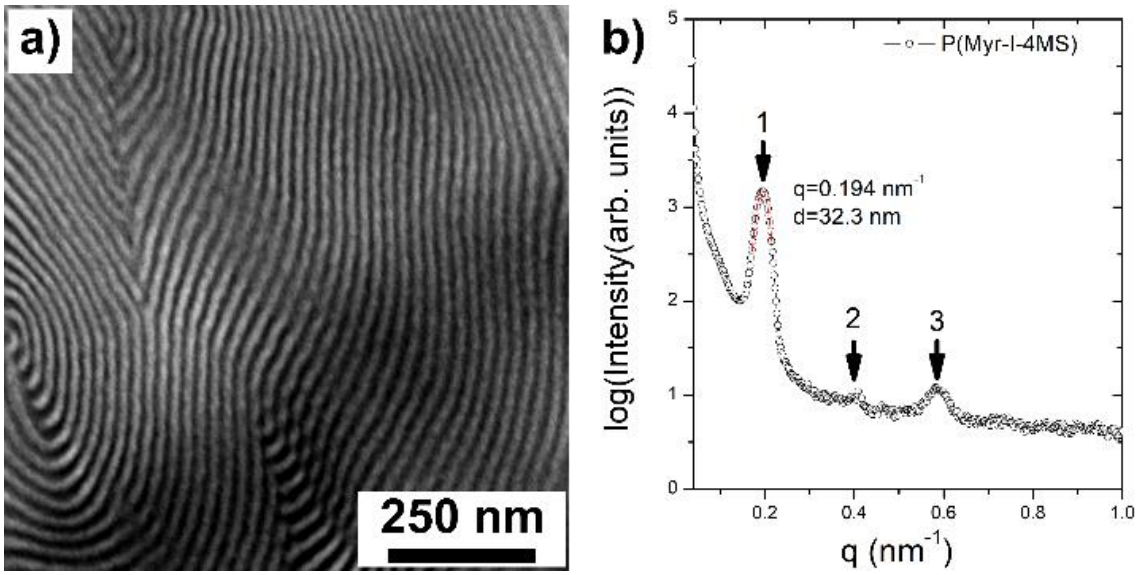

Figure 8: a) TEM image from the bulk morphology characterization for the polymer $Myr_{0.2}$-$I_{0.3}$-$4MS_{0.5}$. Thin section microtomed at -80 °C with 50 nm thickness, the sample was annealed at 130 °C for 24 hours. PMyr domain were stained with OsO_4. b) SAXS pattern for the sample $Myr_{0.2}$-$I_{0.3}$-$4MS_{0.5}$. Arrows give the posotions of the Bragg reflections corresponding to a lamellar morphology.

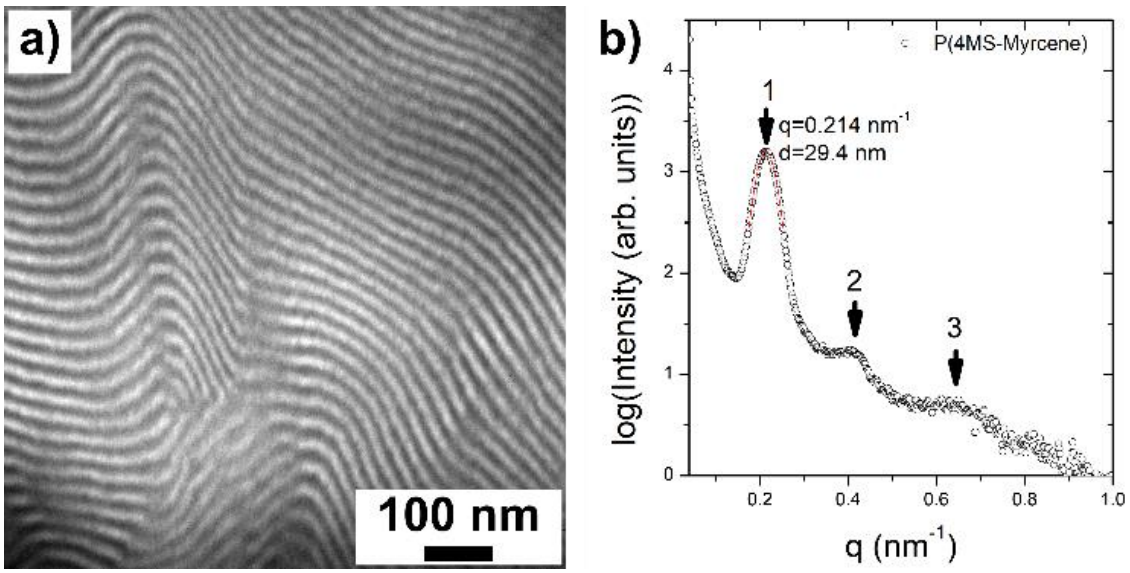

Figure 9: a) TEM image from the bulk morphology characterization for the polymer $Myr_{0.5}$-$4MS_{0.5}$. Thin section microtomed at -80 °C with 50 nm thickness, the sample was annealed at 130 °C for 24 hours. PMyr domain were stained with OsO_4. b) SAXS pattern for the sample $Myr_{0.5}$-$4MS_{0.5}$. Arrows give the position of the Bragg reflections corresponding to a lamellar morphology**.**

Table 2: Lamellar periods obtained by TEM and SAXS measurements.

Entry	Sample composition (mol%)	d_{TEM} (nm)	d_{SAXS} (nm)
1	$I_{0.5}$-$4MS_{0.5}$	24.4	27.8
2	$Myr_{0.2}$-$I_{0.3}$-$4MS_{0.5}$	30.1	32.3
3	$Myr_{0.5}$-$4MS_{0.5}$	28.7	29.4
4	$Myr_{0.42}$-$S_{0.58}$	30.7	34.0

All four tapered block copolymers generated by statistical anionic copolymerization in nonpolar solvents show excellent phase segregated domains. As expected from the composition, the block copolymers revealed all lamellar morphologies and the domain sizes obtained by TEM and SAXS measurements are summarised in Table 2. Furthermore, this general synthetic approach is also suitable for the preparation of bio-based high molecular weight copolymers in one step (**Table 1 Entry 8**). Corresponding to its composition, $Myr_{0.26}$-$S_{0.74}$ shows a well defined asymmetric lamellar morphology and large domain sizes (Supp Inf. **Figure S20** and **S25**).

4.1.4 Conclusions

In this work the statistical anionic copolymerization of the terpene-monomer myrcene with isoprene, styrene and 4-methylstyrene, respectively has been extensively studied by real-time ^{1}H NMR spectroscopy. Following the monomer consumption led to a detailed understanding of the composition profiles of the resulting copolymers and permitted the calculation of reactivity ratios for each monomer combination. For all monomer combinations, myrcene was consumed significantly faster than the respective comonomers, yielding tapered composition profiles. This effect was especially pronounced in the copolymerizations of Myr/S and Myr/4MS. Both combinations showed highly diverging reactivities, resulting in block-like structures with almost pure polydiene and styrenic blocks and only very short and steep gradients. Furthermore, kinetic studies of the terpolymerization of Myr/I/4MS revealed an alteration of the composition profile of 4MS towards a more block like structure, when compared to a corresponding I/4MS copolymer. To verify the block character of these copolymers, several Myr/4MS and Myr/S copolymers and a series of Myr/I/4MS terpolymers with varying Myr/I content were prepared by

direct, i.e., statistical carbanionic copolymerization. All samples showed two distinct glass transitions, confirming the (tapered) block character of these copolymers. This conclusion is also supported by TEM and SAXS measurements, showing that all samples undergo microphase separation and form lamellar morphologies with high long range order. All these findings clearly demonstrate the high potential of myrcene for the carbanionic one-step synthesis of block-like copolymers, which is also important when targeting bio-based thermoplastic elastomers.

4.1.5 Acknowledgments

The authors acknowledge the German Research Foundation (DFG GA 2169/1-1) and the "Verband der chemischen Industrie e.V." (VCI) for partial financial support of this work. The authors thank Prof. Bernd Stühn and Ann-Kathrin Grefe (TU Darmstadt, Institute of Condensed Matter Physics) for kind discussions and additional SAXS measurements.

4.1.6 References

(1) Bates, C. M.; Bates, F. S. 50th Anniversary Perspective: Block Polymers Pure Potential. *Macromolecules* **2017**, *50*, 3–22.

(2) Schacher, F. H.; Rupar, P. A.; Manners, I. Functional Block Copolymers: Nanostructured Materials with Emerging Applications. *Angew. Chem. Int. Ed. Engl.* **2012**, *51*, 7898–7921.

(3) Hadjichristidis, N.; Floudas, G.; Pispas, S. *Block copolymers: Synthetic strategies, physical properties, and applications*; Wiley-Interscience: Hoboken, N.J, 2003.

(4) Sarkar, P.; Bhowmick, A. K. Synthesis, characterization and properties of a bio-based elastomer: Polymyrcene. *RSC Adv.* **2014**, *4*, 61343–61354.

(5) Behr, A.; Johnen, L. Myrcene as a Natural Base Chemical in Sustainable Chemistry: A Critical Review. *ChemSusChem* **2009**, *2*, 1072–1095.

(6) Kim, E.-M.; Eom, J.-H.; Um, Y.; Kim, Y.; Woo, H. M. Microbial Synthesis of Myrcene by Metabolically Engineered Escherichia coli. *J. Agric. Food. Chem.* **2015**, *63*, 4606–4612.

(7) Sarkar, P.; Bhowmick, A. K. Terpene Based Sustainable Elastomer for Low Rolling Resistance and Improved Wet Grip Application: Synthesis, Characterization and Properties of Poly(styrene- co -myrcene). *ACS Sustainable Chem. Eng.* **2016**, *4*, 5462–5474.

(8) Métafiot, A.; Kanawati, Y.; Gérard, J.-F.; Defoort, B.; Marić, M. Synthesis of β-Myrcene-Based Polymers and Styrene Block and Statistical Copolymers by SG1 Nitroxide-Mediated Controlled Radical Polymerization. *Macromolecules* **2017**, *50*, 3101–3120.

(9) Satoh, K. Controlled/living polymerization of renewable vinyl monomers into bio-based polymers. *Polym. J.* **2015**, *47*, 527–536.

(10) Ávila-Ortega, A.; Aguilar-Vega, M.; Loría Bastarrachea, M. I.; Carrera-Figueiras, C.; Campos-Covarrubias, M. Anionic synthesis of amine ω-terminated β-myrcene polymers. *J. Polym. Res.* **2015**, *22*, 8.

(11) Bolton, J. M.; Hillmyer, M. A.; Hoye, T. R. Sustainable Thermoplastic Elastomers from Terpene-Derived Monomers. *ACS Macro Lett.* **2014**, *3*, 717–720.

(12) Quirk, R. P. US Patent 4374957 A, 1983.

(13) Matic, A.; Schlaad, H. Thiol-ene photofunctionalization of 1,4-polymyrcene. *Polym. Int.* **2018**, *67*, 500–505.

(14) Knoll, K.; Nießner, N. Styrolux and styroflex from transparent high impact polystyrene to new thermoplastic elastomers. *Macromol. Symp.* **1998**, *132*, 231–243.

(15) Morris, M. A.; Gartner, T. E.; Epps III, T. H. Tuning Block Polymer Structure, Properties, and Processability for the Design of Efficient Nanostructured Materials Systems. *Macromol. Chem. Phys.* **2017,** *218*, 1600513.

(16) Roy, R.; Park, J. K.; Young, W.-S.; Mastroianni, S. E.; Tureau, M. S.; Epps, T. H. Double-Gyroid Network Morphology in Tapered Diblock Copolymers. *Macromolecules* **2011**, *44*, 3910–3915.

(17) Grune, E.; Johann, T.; Appold, M.; Wahlen, C.; Blankenburg, J.; Leibig, D.; Müller, A. H. E.; Gallei, M.; Frey, H. One-Step Block Copolymer Synthesis versus Sequential Monomer Addition: A Fundamental Study Reveals That One Methyl Group Makes a Difference. *Macromolecules* **2018**, *51*, 3527–3537.

(18) Hsieh, H. L. Kinetics of polymerization of butadiene, isoprene, and styrene with alkyllithiums. Part II. Rate of initiation. *J. Polym. Sci., Part A: Polym. Chem.* **1965**, *3*, 163–172.

(19) Bywater, S.; Worsfold, D. J. The Effect of Dielectric Constant on the Rate of Anionic Polymerization. *J. Phys. Chem.* **1966**, *70*, 162–166.

(20) Fetters, L. J.; Balsara, N. P.; Huang, J. S.; Jeon, H. S.; Almdal, K.; Lin, M. Y. 53 Aggregation in Living Polymer Solutions by Light and Neutron Scattering A Study of Model Ionomers // Aggregation in Living Polymer Solutions by Light and Neutron Scattering: A Study of Model Ionomers. *Macromolecules* **1995**, *28*, 4996–5005.

(21) Worsfold, D. J. Anionic copolymerization of styrene and isoprene in cyclohexane. *J. Polym. Sci., Part A: Polym. Chem.* **1967**, *5*, 2783–2789.

(22) Hsieh, H. L.; Glaze, W. H. Kinetics of Alkyllithium Initiated Polymerizations. *Rubber Chem. Technol.* **1970**, *43*, 22–73.

(23) Tsukahara, Y.; Nakamura, N.; Hashimoto, T.; Kawai, H.; Nagaya, T.; Sugimura, Y.; Tsuge, S. Structure and Properties of Tapered Block Polymers of Styrene and Isoprene. *Polym. J.* **1980**, *12*, 455–466.

(24) Hashimoto, T.; Tsukahara, Y.; Tachi, K.; Kawai, H. Structure and properties of tapered block polymers. 4. "Domain-boundary mixing" and "mixing-in-domain" effects on microdomain morphology and linear dynamic mechanical response. *Macromolecules* **1983**, *16*, 648–657.

(25) Hodrokoukes, P.; Floudas, G.; Pispas, S.; Hadjichristidis, N. Microphase Separation in Normal and Inverse Tapered Block Copolymers of Polystyrene and Polyisoprene. 1. Phase State. *Macromolecules* **2001**, *34*, 650–657.

(26) Hodrokoukes, P.; Pispas, S.; Hadjichristidis, N. Controlling Micellar Properties of Styrene/Isoprene Copolymers by Altering the Monomer Arrangement along the Chain. *Macromolecules* **2002**, *35*, 834–840.

(27) Mastroianni, S. E.; Epps III, T. H. Interfacial manipulations: Controlling nanoscale assembly in bulk, thin film, and solution block copolymer systems. *Langmuir* **2013**, *29*, 3864–3878.

(28) Luo, M.; Brown, J. R.; Remy, R. A.; Scott, D. M.; Epps III, T. H. Determination of Interfacial Mixing in Tapered Block Polymer Thin Films: Experimental and Theoretical Investigations. *Macromolecules* **2016**, *49*, 5513-5222.

(29) Yang, L.; Ma, H.; Han, L.; Liu, P.; Shen, H.; Li, C.; Li, Y. Sequence Features of Sequence-Controlled Polymers Synthesized by 1,1-Diphenylethylene Derivatives with Similar Reactivity during Living Anionic Polymerization. *Macromolecules* **2018**, *51*, 5891–5903.

(30) Blankenburg, J.; Kersten, E.; Maciol, K.; Wagner, M.; Zarbakhsh, S.; Frey, H. Characterizing and Controlling the microstructure of poly(propylene oxide-co-ethylene oxide) copolymers under different catalytic conditions. *to be submitted*.

(31) Mayo, F. R.; Lewis, F. M. Copolymerization. I. A Basis for Comparing the Behavior of Monomers in Copolymerization; The Copolymerization of Styrene and Methyl Methacrylate. *J. Am. Chem. Soc.* **1944**, *66*, 1594–1601.

(32) Meyer, V. E.; Lowry, G. G. Integral and differential binary copolymerization equations. *J. Polym. Sci., Part A: Polym. Chem.* **1965**, *3*, 2843–2851.

(33) Zhou, C.; Wei, Z.; Jin, C.; Wang, Y.; Yu, Y.; Leng, X.; Li, Y. Fully biobased thermoplastic elastomers: Synthesis of highly branched linear comb poly(β-myrcene)- graft -poly(l -lactide) copolymers with tunable mechanical properties. *Polymer* **2018**, *138*, 57–64.

(34) Wall, F. T. The Structure of Vinyl Copolymers. *J. Am. Chem. Soc.* **1941**, *63*, 1862–1866.

(35) Hsieh, H.; Quirk, R. P. *Anionic polymerization: Principles and practical applications*, CRC Press, 1996.

(36) Dhami, K. S.; Stothers, J. B. 13C NMR Studies: Part III. Carbon-13 NMR Spectra of Substituted Acetophenones. *Can. J. Chem.* **1965**, *43*, 479–497.

(37) Ishizone, T.; Hirao, A.; Nakahama, S. Anionic polymerization of monomers containing functional groups. 6. Anionic block copolymerization of styrene derivatives para-substituted with electron-withdrawing groups. *Macromolecules* **1993**, *26*, 6964–6975.

(38) Hutchings, L. R.; Brooks, P. P.; Shaw, P.; Ross-Gardner, P. Fire and Forget!: One-Shot Synthesis and Characterization of Block-Like Statistical Terpolymers via Living Anionic Polymerization. *J. Polym. Sci. A Polym. Chem.* **2018**, *5*, 1-13.

(39) Appold, M.; Grune, E.; Frey, H.; Gallei, M. One-Step Anionic Copolymerization Enables Formation of Linear Ultrahigh-Molecular-Weight Block Copolymer Films Featuring Vivid Structural Colors in the Bulk State. *ACS Appl. Mater. Interfaces* **2018**, *10*, 18202–18212.

4.1.5 Supporting Information

4.1.5.1 Comparison of kinetic models

1941 Wall introduced the first model to describe copolymerizations.[1] The Mayo-Lewis model was developed a few years later and made it possible to describe non-ideal behaviour. This extension was necessary to describe alternating copolymerization behaviour as observed in the radical copolymerization of styrene and methyl methacrylate.2 Both models are identical for the exceptional case of $r_1 \cdot r_2 = 1$. For high conversion the integrated form of the Mayo-Lewis model is necessary to accurately describe the copolymerization.[2] The integration can be performed by the Skeist relation.[3] In this way the Meyer-Lowry equation was derived (Table S1 Entry 3).[4] Recently our group derived an analogous equation for the ideal Wall Model (Table S1 Entry 3).[5] In the following the two models in differential and integral form are summarized:

Table S3: Summary and comparison of the kinetic models of Wall and Mayo-Lewis.

Entry	Non-terminal (ideal) model (Wall)[1]	Terminal model (Mayo Lewis)[2]
	Differential form	
1	$\frac{dM_1}{dM_2} = r\frac{M_1}{M_2}$	$\frac{dM_1}{dM_2} = \frac{M_1}{M_2}\frac{r_1 M_1 + M_2}{r_2 M_2 + M_1}$
	Differential form in molar fraction form with:	$f = \frac{M_1}{M_1 + M_2}$ and $F = \frac{dM_1}{dM_1 + dM_2}$
2	$F = \frac{rf}{rf - f + 1}$	$F = \frac{r_1 \cdot f^2 + f(1-f)}{r_1 \cdot f^2 + 2f(1-f) + r_2(1-f)^2}$
	Integrated of differential fractional form with Skeist[3] relation: $\frac{df_x}{dX} = \frac{f_x - F_x}{1 - X}$	
3	$X = 1 - \left(\frac{f}{f_0}\right)^{\frac{1}{r-1}} \cdot \left(\frac{1-f}{1-f_0}\right)^{\frac{r}{1-r}}$ Integrated ideal equation[5]	$X = 1 - \left(\frac{f}{f_0}\right)^{\frac{r_2}{1-r_2}} \cdot \left(\frac{1-f}{1-f_0}\right)^{\frac{r_1}{1-r_1}} \cdot \left(\frac{f - \frac{1-r_2}{2-r_1-r_2}}{f_0 - \frac{1-r_2}{2-r_1-r_2}}\right)^{\frac{1-r_1 r_2}{(1-r_1)(1-r_2)}}$ Meyer-Lowry equation[4]

The integrated form of both models was used to fit the experimental data of the copolymerization experiments. As recently described by our group, overfitting in the analysis of reactivity ratios is a problem which was not taken into account so far. Overfitting is a statistical phenomenon that occurs, when data is fitted to a model which is more complex than it needs to be. This is the case when a model with more parameters than necessary is used to explain the variation in the data. The use of a model with irrelevant parameters makes worse descriptions of the behaviour as the parameters are fitted to random variation (noise).[6] For this reason, the simplest model which can successfully describe the data should always be used. In the case of reactivity ratios the simple Wall-Model needs just one reactivity parameter ($r_2=1/r_1$) for the description of copolymerization data while the Mayo-Lewis model relies on two independent reactivity ratios. In the case of an ideal copolymerization r_2 is completely described as r_1^{-1}, making the independent determination of both parameters redundant. Lynd and co-workers showed that many ionic copolymerizations can be described with the ideal model, however the equation did not allow the direct comparison of the ideal model with the terminal Mayo Lewis model.7 The "ideal integrated" equation can be directly compared to the fit of the more elaborated terminal model (Meyer-Lowry equation) (Figure S1, S2 and S3).

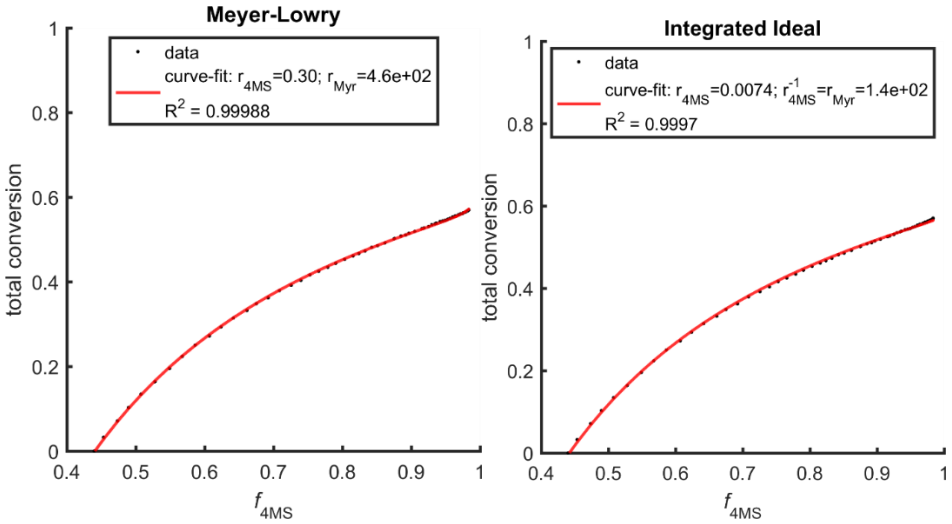

Figure S5: Comparison of the Meyer-Lowry evaluation and the integrated Ideal model for the copolymerization of myrcene (Myr) and 4-methylstyrene (4MS).

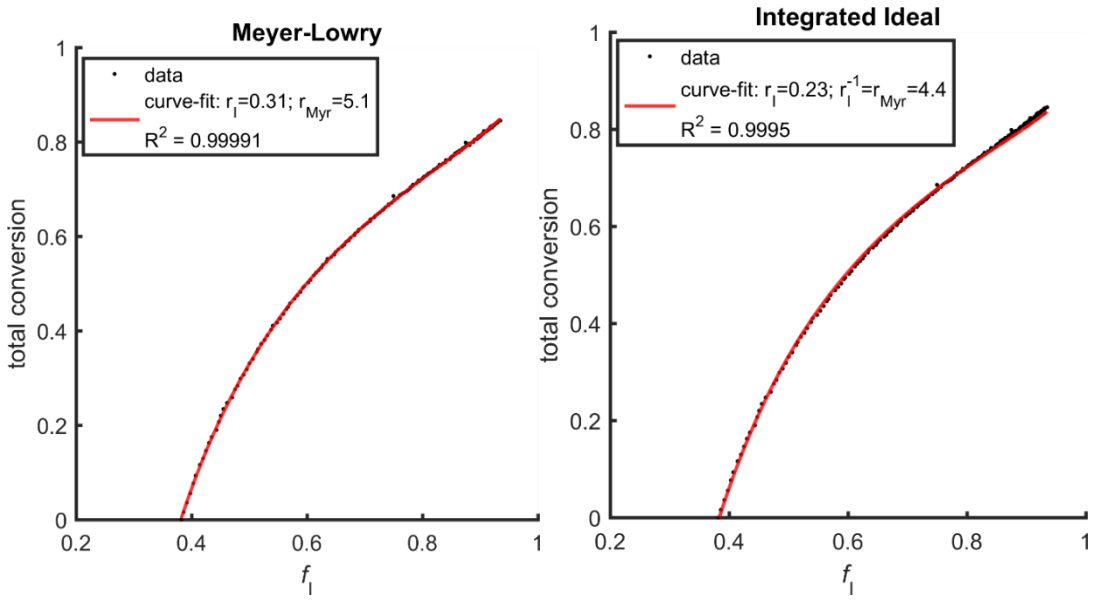

Figure S6: Comparison of the Meyer-Lowry evaluation and the integrated Ideal model for the copolymerization of myrcene (Myr) and isoprene (I).

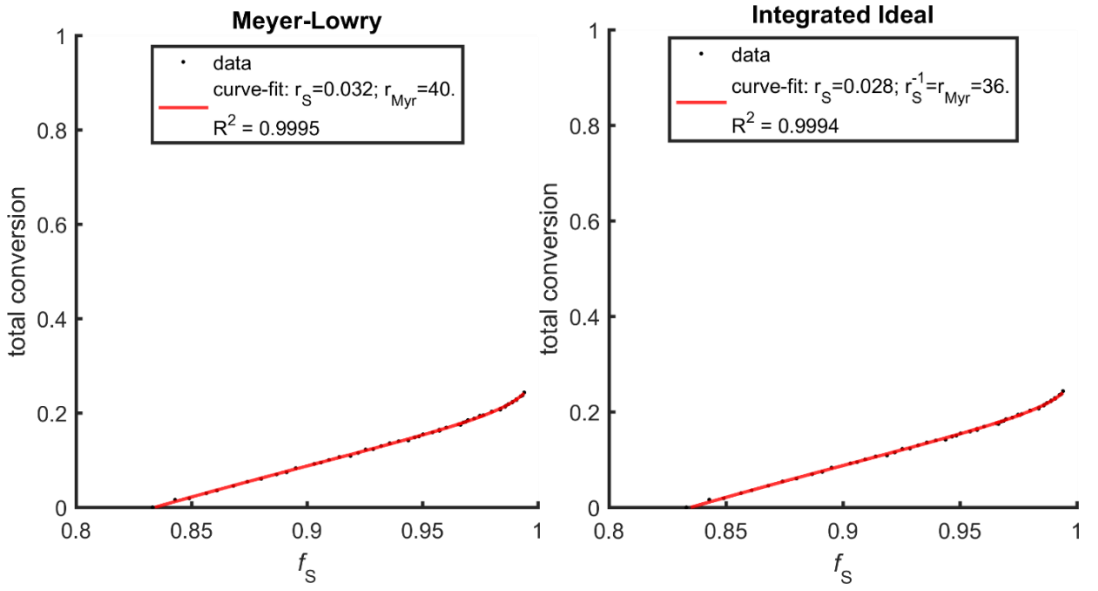

Figure S7: Comparison of the Meyer-Lowry evaluation and the integrated Ideal model for the copolymerization of myrcene (Myr) and styrene (S).

The results of the fits of both models to the data of the three copolymerization experiments are shown in Figure S5, S2 and S3. As is evident the Integrated ideal fit can very well describe the experimental data and the more elaborate Meyer-Lowry fit negligibly increases the quality of the fit. This is strong supported for ideal copolymerization behaviour.

4.1.5.2 Description of the terpolymerization of Myr/I/4MS

For the accurate description of a terpolymerization by the non-ideal Mayo-Lewis model seven independent reactivity parameters are required.[8] However, in the ideal case only the decrease of the three monomers (myrcene, isoprene and 4-methylstyrene) is taken into account (active chain end has no influence) a terpolymerization can be easily described as two simultaneous copolymerizations. From two reactivity ratios in the ideal case all other can be derived as shown in (1 and 2). The ideal behaviour can be confirmed by the pairwise fitting of the ideal model to the data of the terpolymerization experiment. The results of these fits are shown in Figures S4, S5 and S6 and confirm this conjecture.

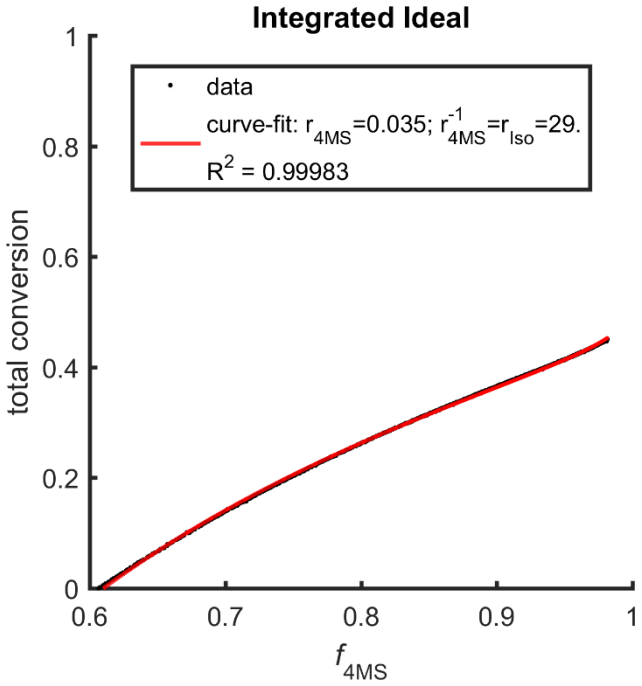

Figure S8: Pairwise Ideal Integrated Model of 4MS and I regarding terpolymerization of Myr/I/4MS.

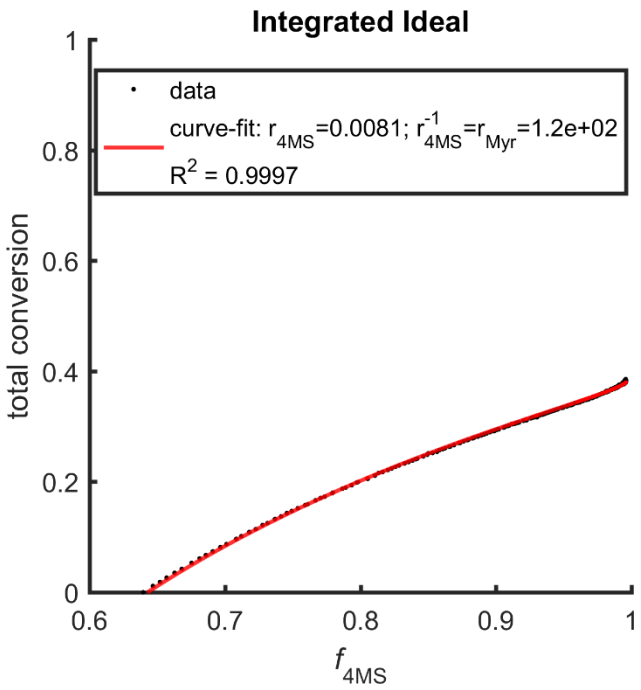

Figure S9: Pairwise Ideal Integrated Model of Myr and 4MS regarding terpolymerization of Myr/I/4MS.

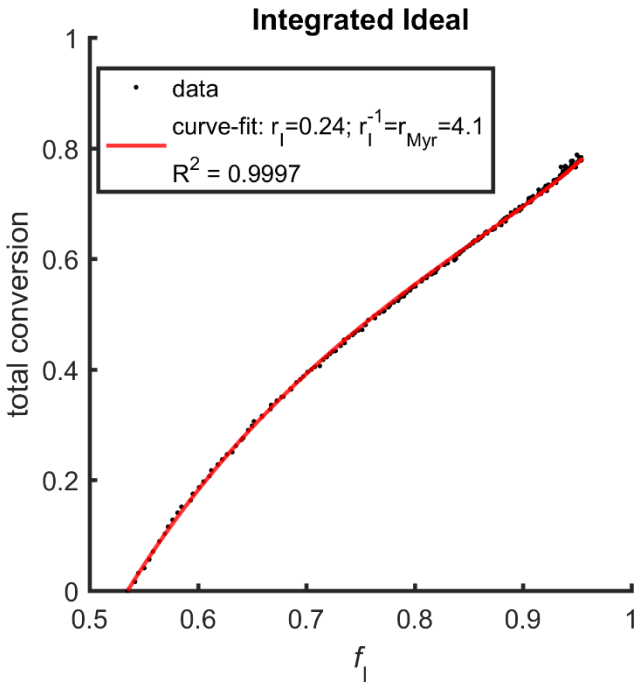

Figure S10: Pairwise Ideal Integrated Model of Myr and I regarding terpolymerization of Myr/I/4MS.

This shows that the terpolymerization can be well-described with ideal behaviour. Another property of an ideal copolymerization is the fact that reactivity ratios are multiplicative:

$$r_{A/B} = \frac{k_A}{k_B};\ r_{A/C} = \frac{k_A}{k_C}; r_{A/A} = r_{A/B}^{-1} \tag{1}$$

$$r_{A/B} = r_{B/A} \cdot r_{A/C} = \frac{k_B}{k_A} \cdot \frac{k_A}{k_C} = \frac{k_B}{k_C} = r_{C/C} \tag{2}$$

To model the terpolymer microstructure, we choose the following approach: using the Wall model, the concentration of every monomer can be expressed as a function of the concentration of monomer A.

$$\frac{d[A]}{d[B]} = r_{A/B}\frac{[A]}{[B]} \Rightarrow \frac{[A]}{[A_0]} = \left(\frac{[B]}{[B_0]}\right)^{r_{A/B}} \tag{3}$$

$$[B] = [B_0]\left(\frac{[A]}{[A_0]}\right)^{r_{B/A}} \tag{4}$$

$$[C] = [C]\left(\frac{[A]}{[A_0]}\right)^{r_{A/C}} \tag{5}$$

Monomer A is set as the reference monomer. It is favourable to choose the least reactive monomer, because its concentration is non-zero throughout the whole polymerization and approaches 0 only at full monomer conversion. An array for Monomer A is created with values in the interval $[0,[A_0]]$. The values for the arrays for B and C can be calculated from the equations (4, 5) above.

From the data for all monomers the array for the total conversion can be calculated:

$$X = 1 - \frac{[A] + [B] + [C]}{[A_0] + [B_0] + [C_0]} \tag{6}$$

In analogy the instantaneous incorporation of monomer A was calculated from the following relation:

$$\frac{d[A]}{d[A]} = 1;\ \frac{d[B]}{d[A]} = r_{B/A}\frac{[B]}{[A]};\ \frac{d[C]}{d[A]} = r_{C/A}\frac{[C]}{[A]} \tag{7}$$

$$\frac{d[B]}{d[A]} + \frac{d[C]}{d[A]} + \frac{d[A]}{d[A]} = r_{B/A}\frac{[B]}{[A]} + r_{C/A}\frac{[C]}{[A]} + 1 \tag{8}$$

$$\frac{d[A]+d[B]+d[C]}{d[A]} = \frac{r_{B/A}[B]+r_{C/A}[C]+[A]}{[A]} \quad (9)$$

$$F_A = \frac{d[A]}{d[A]+d[B]+d[C]} = \frac{[A]}{[A]+r_{B/A}[B]+r_{C/A}[C]} \quad (10)$$

Analogously follows for the instantaneous incorporation for B and C:

$$F_B = \frac{d[B]}{d[A]+d[B]+d[C]} = \frac{r_{B/A}[B]}{[A]+r_{B/A}[B]+r_{C/A}[C]} \quad (11)$$

$$F_B = \frac{d[C]}{d[A]+d[B]+d[C]} = \frac{r_{C/A}[C]}{[A]+r_{B/A}[B]+r_{C/A}[C]} \quad (12)$$

F_A, F_B and F_C are calculated for all values in the arrays. Note that F_A+F_B+F_C always yield 1 at every point. For better visualization it is favourable to plot F_A and F_A+F_B as a function of X (F_C corresponds to the distance of F_A+F_B to value 1). This representation is shown in Figure S11.

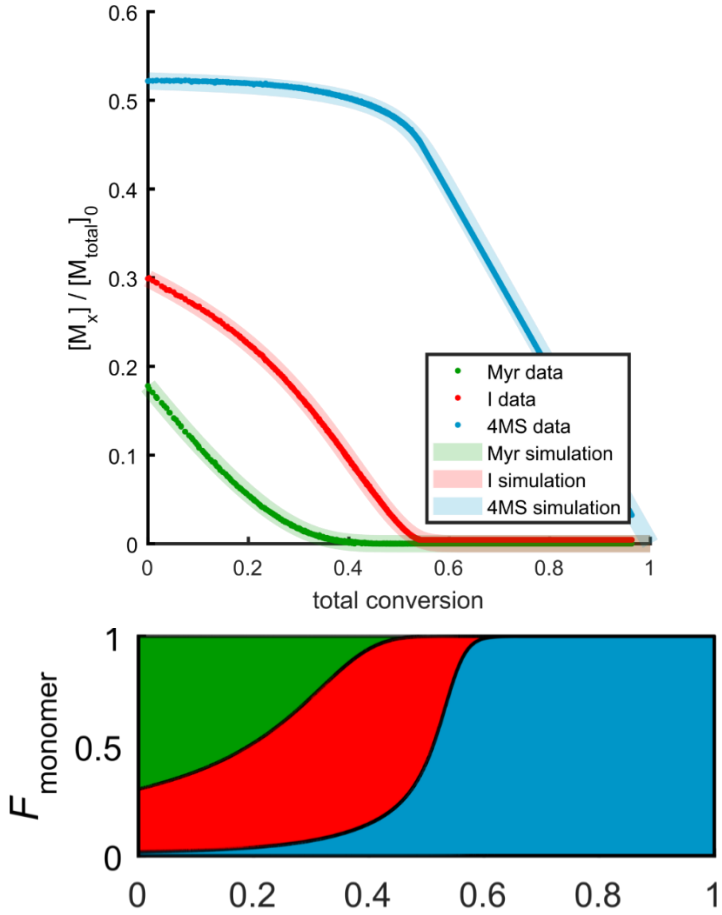

Figure S11: Copolymerization experiment and simulation with ideal copolymerization model for the terpolymerization of Myr/I/4MS.

As is evident, the simulation in Figure S11 describes the terpolymerization well. Note that for the simulation only the values for A_0, B_0 and C_0 as two reactivity ratios are required. An analogous simulation with $A_0 = B_0 = C_0$ was performed to create Figure 4 and Figure 5 in the main manuscript.

4.1.5.3 *In-situ* ^{1}H NMR Kinetics

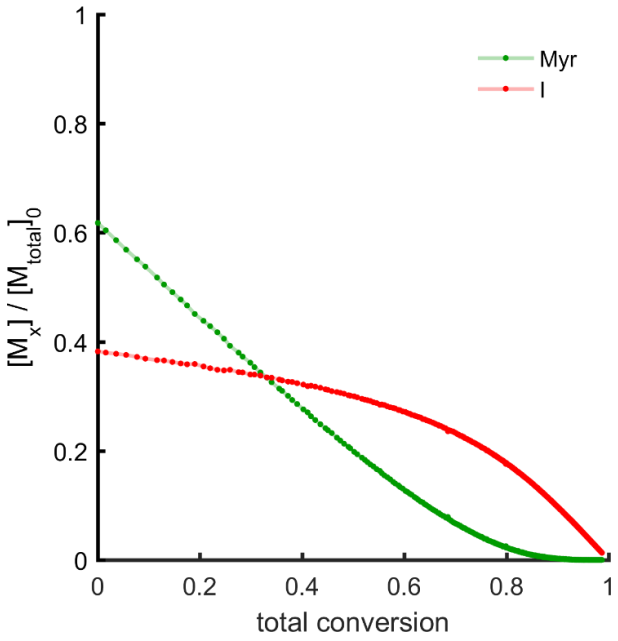

Figure S12: Monomer conversion for the copolymerization of Myr/I, determined from *in-situ* ^{1}H NMR spectroscopy.

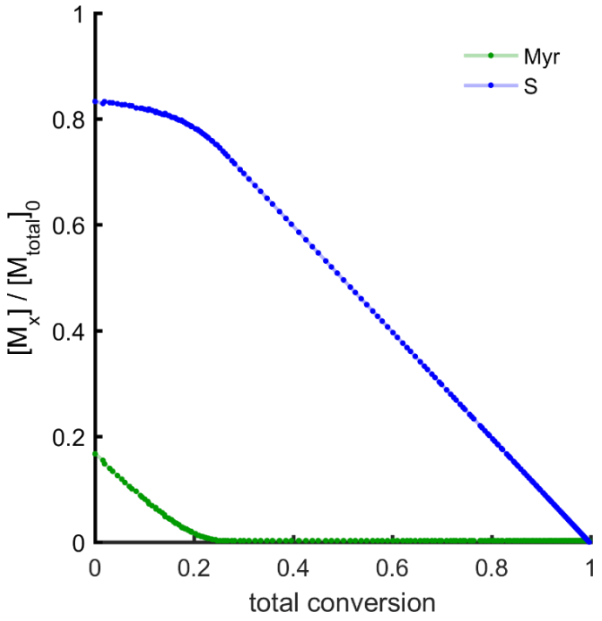

Figure S13: Monomer conversion of the copolymerization of Myr/S, determined from *in-situ* ^{1}H NMR spectroscopy.

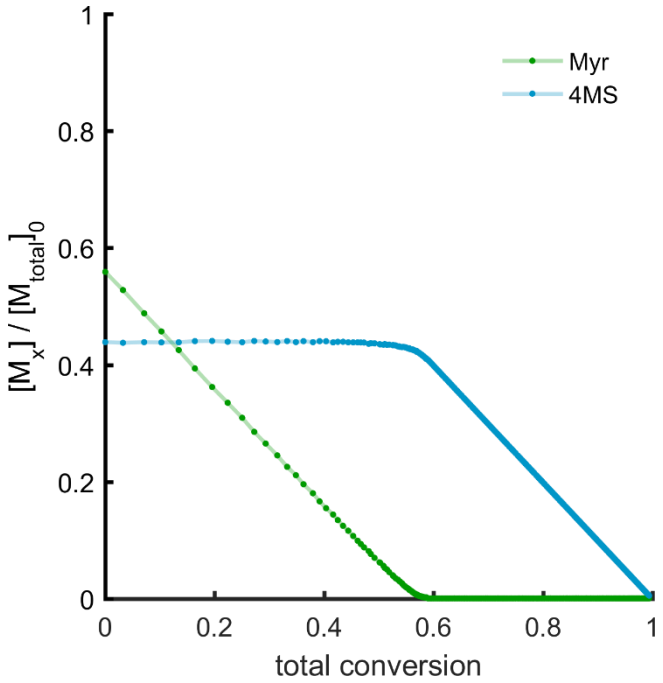

Figure S 14: Monomer conversion of the copolymerization of Myr/4MS, determined from *in-situ* ^{1}H NMR spectroscopy.

4.1.5.4 Size Exclusion Chromatography (SEC)

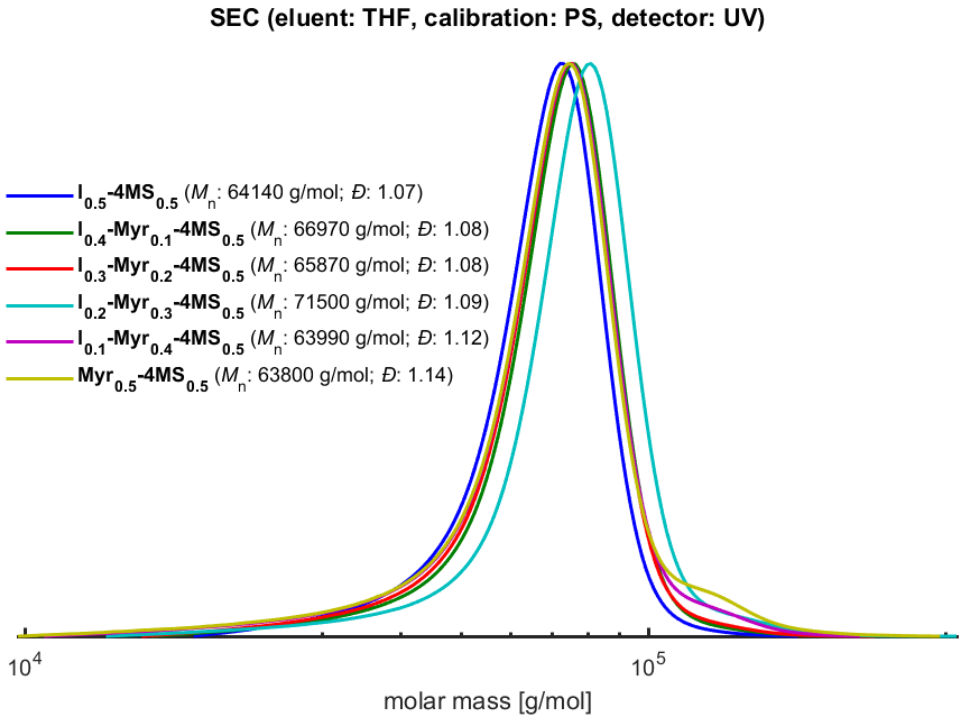

Figure S15: SEC elugrams of 4MS copolymers (Table S2 Entry 1 - 6).

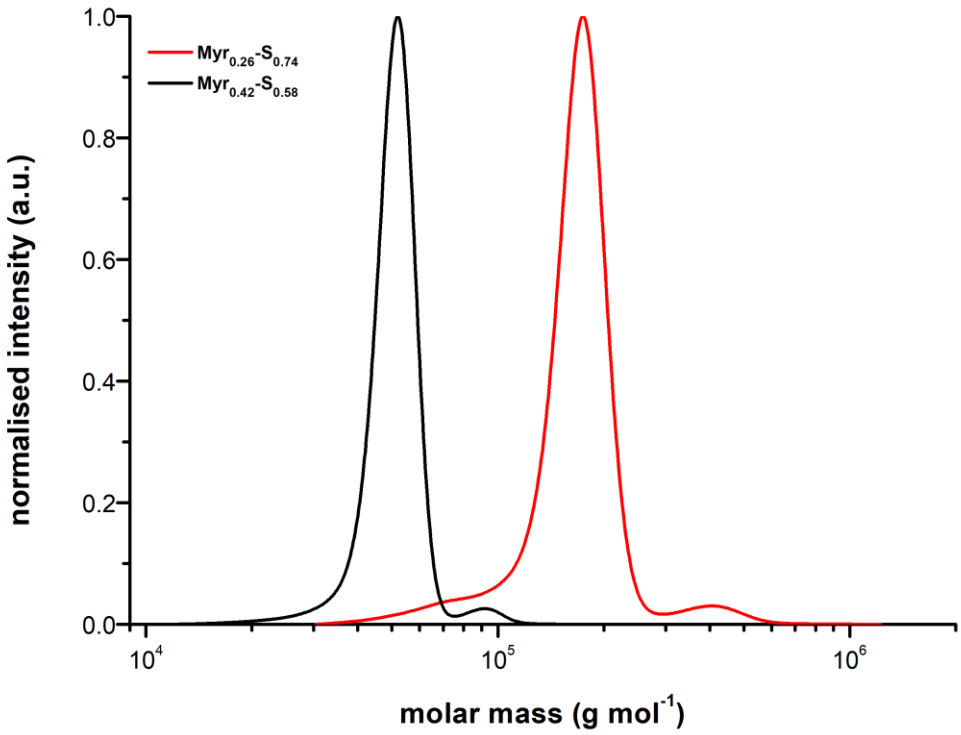

Figure S16: SEC elugrams of styrene (S) copolymers (Table S2 Entries 7 and 8).

4.1.5.5 Dynamic Scanning Calorimetry (DSC)

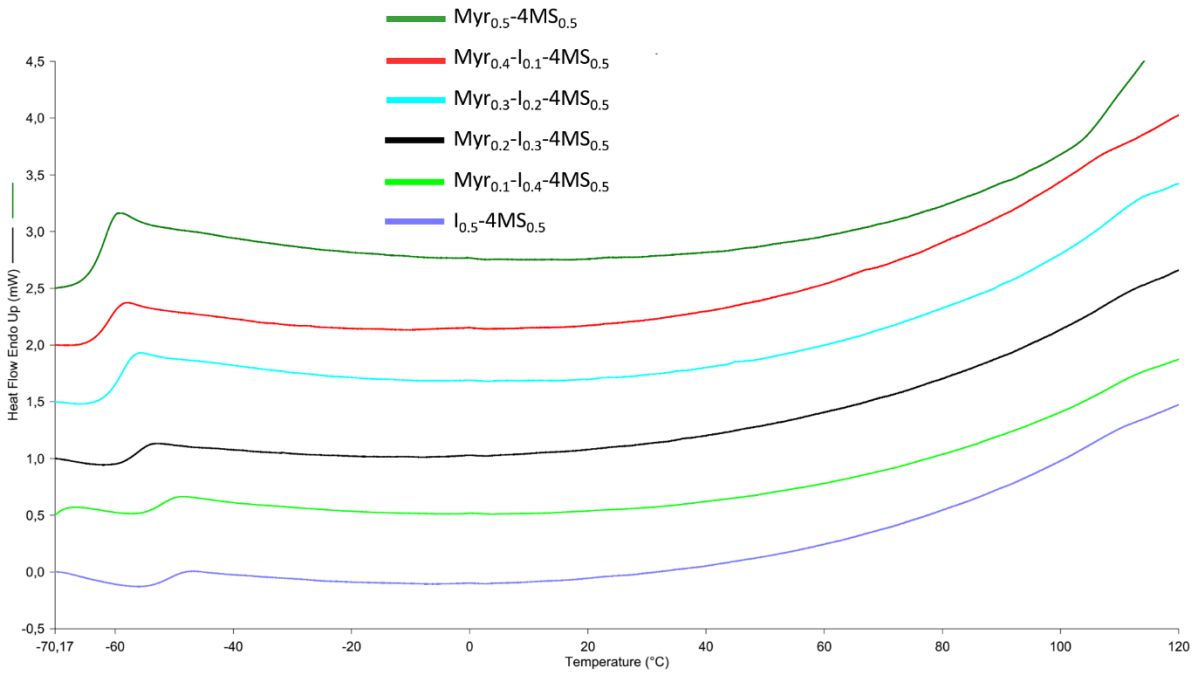

Figure S17: DSC thermograms of 4MS copolymers (Table S2 Entry 1 - 6), heating rate 10 K/min.

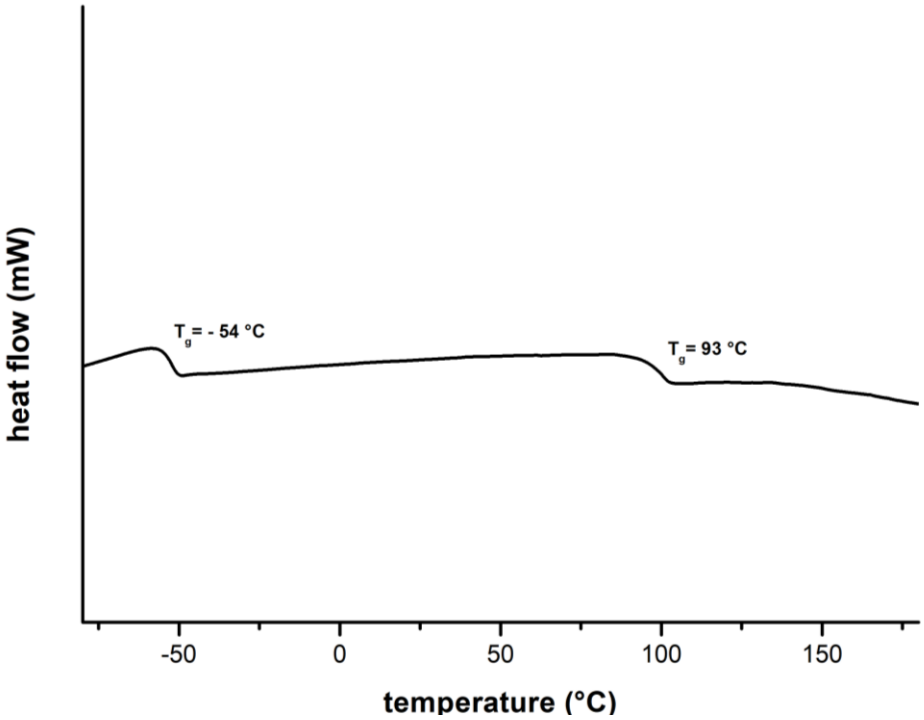

Figure S18: DSC thermogram of $Myr_{0.42}$-$S_{0.58}$ (Table S2 Entry 7), heating rate 10 K/min.

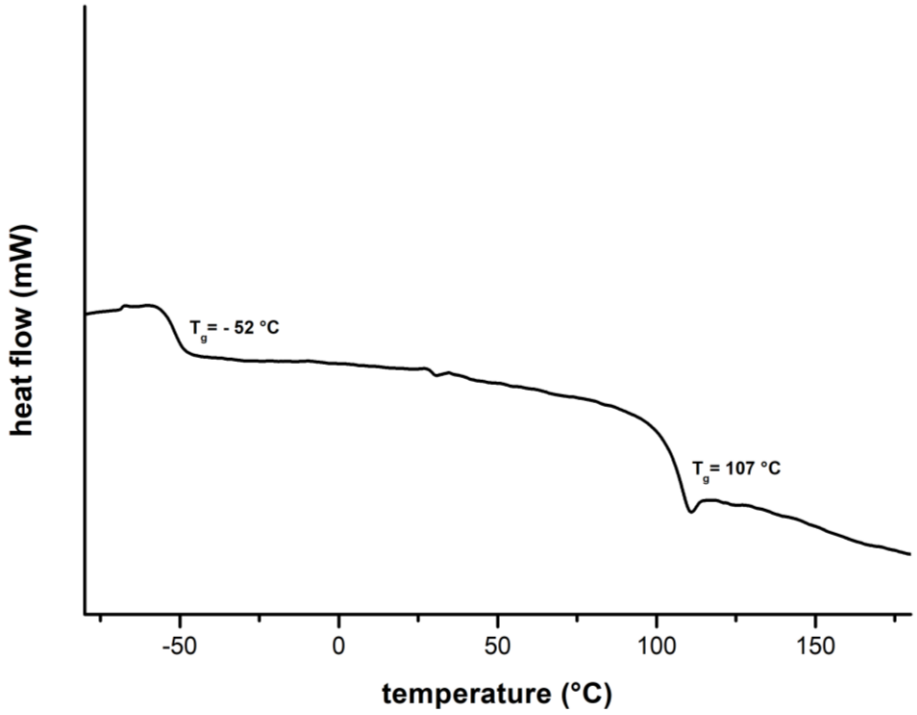

Figure S19: DSC thermogram of $Myr_{0.26}$-$S_{0.74}$ (Table S2 Entry 8), heating rate 10 K/min.

4.1.5.6 Transmission Electron Microscopy (TEM)

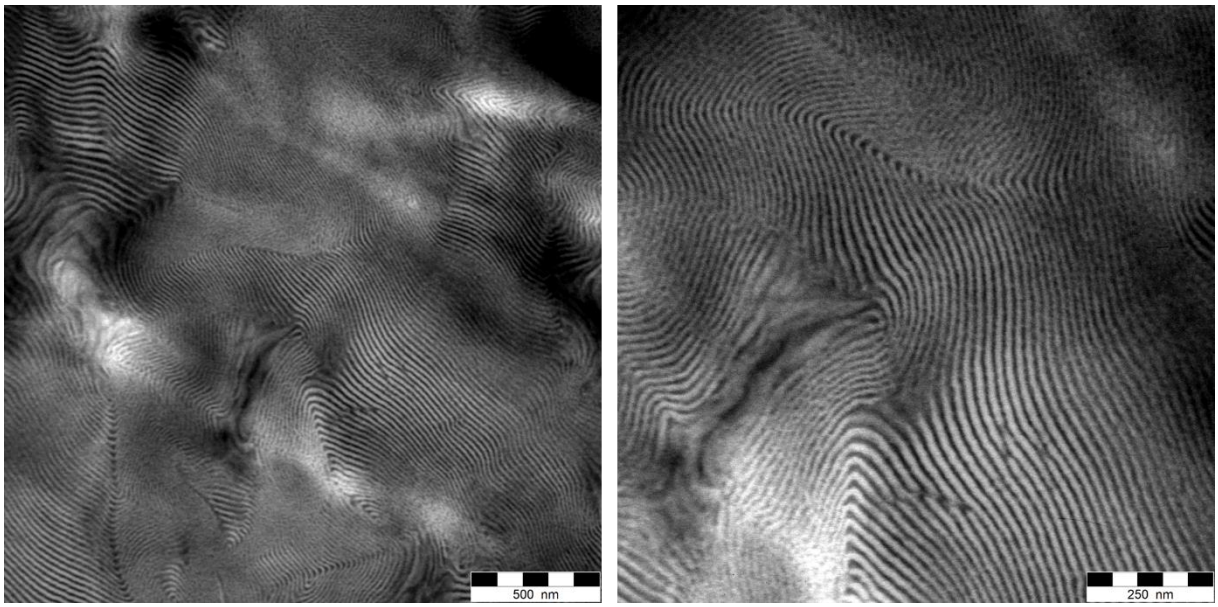

Figure S20: TEM image of $I_{0.5}$-$4MS_{0.5}$ (Table S2 Entry 1).

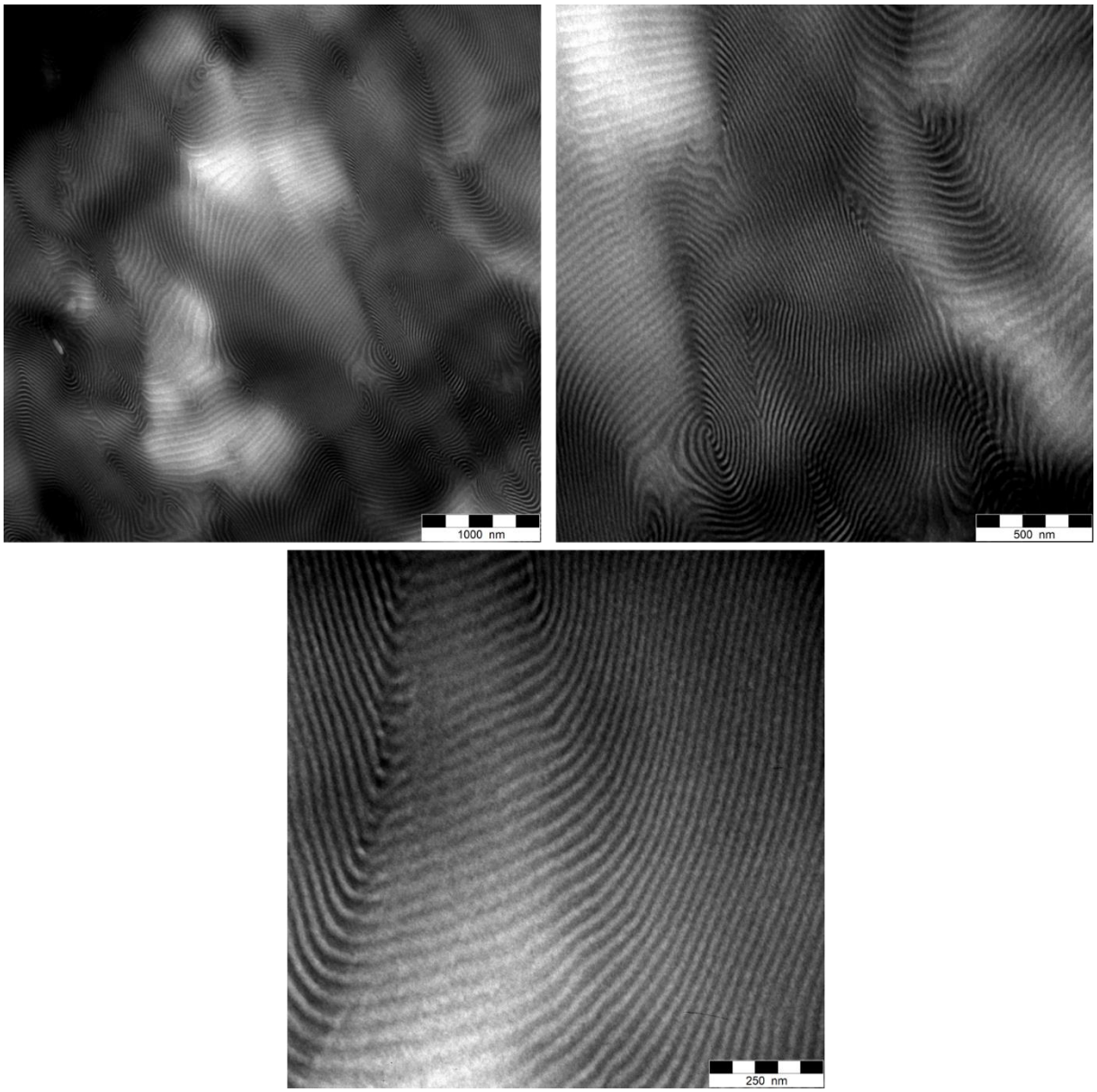

Figure S21: TEM image of $Myr_{0.3}$-$I_{0.2}$-$4MS_{0.5}$ (Table S2 Entry 4).

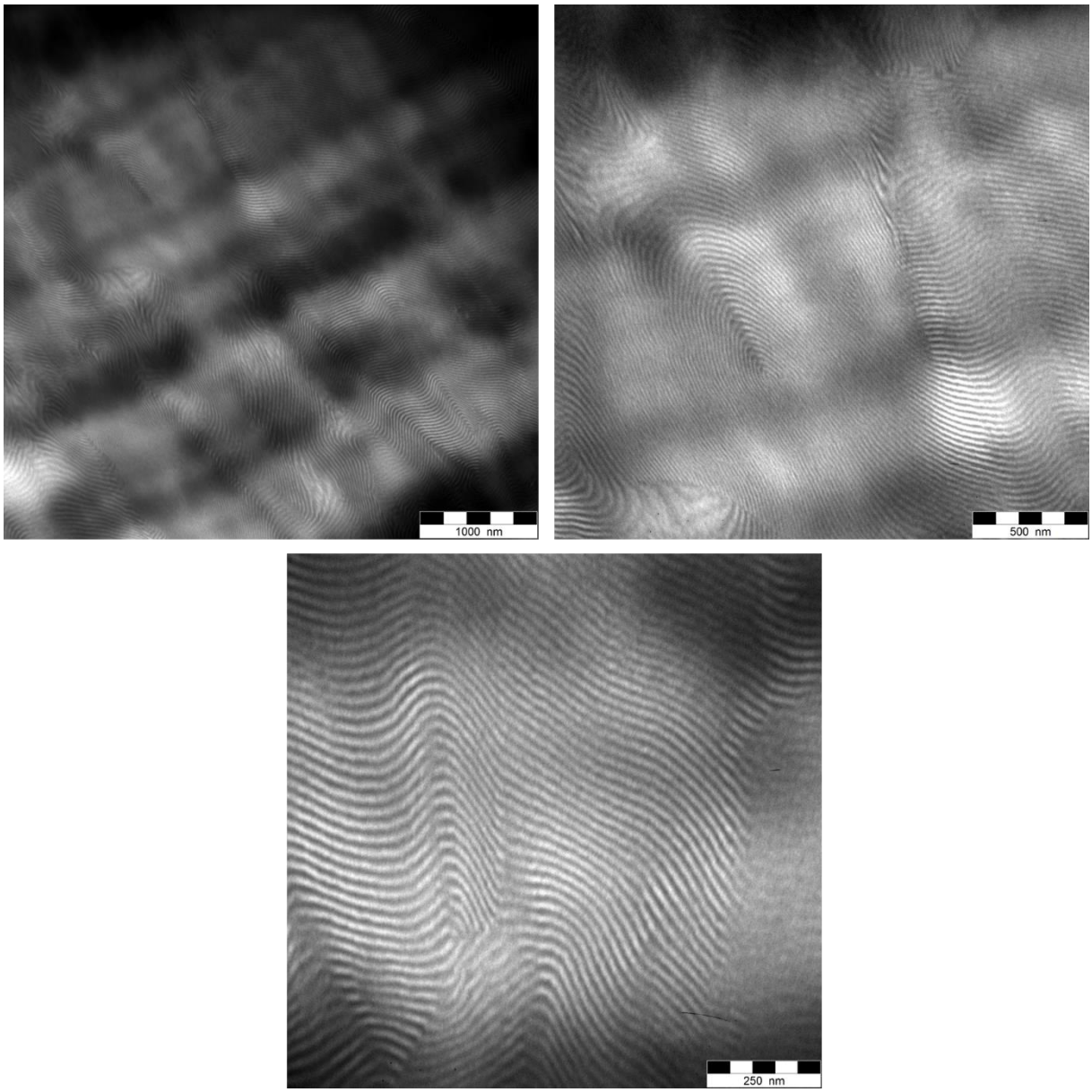

Figure S22: TEM image of $Myr_{0.5}$-$4MS_{0.5}$ (Table S2 Entry 6).

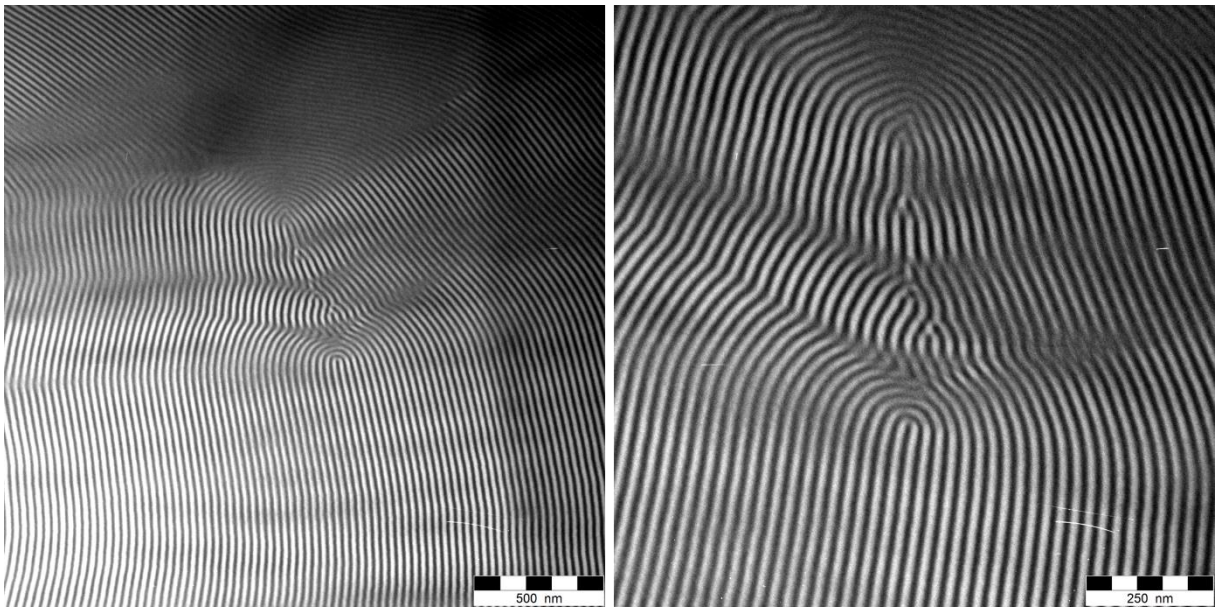

Figure S23: TEM image of $Myr_{0.42}$-$S_{0.58}$ (Table S2 Entry 7).

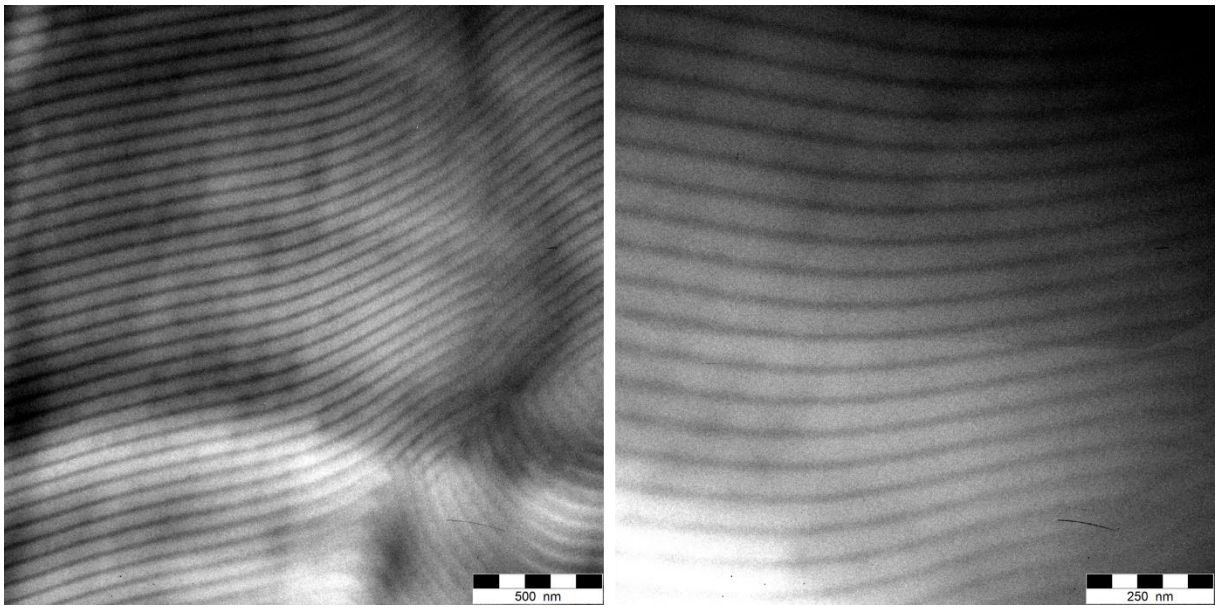

Figure S24: TEM image of $Myr_{0.26}$-$S_{0.74}$ (Table S2 Entry 8).

4.1.5.7 Small Angle X-Ray Scattering (SAXS)

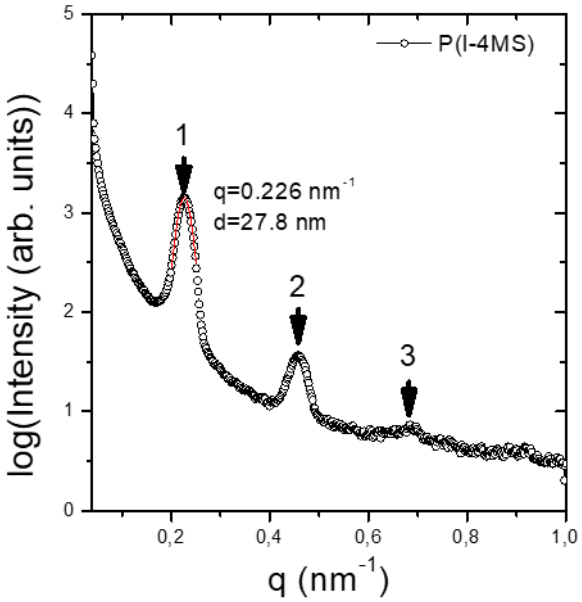

Figure S25: SAXS measurements of $I_{0.5}$-$4MS_{0.5}$ (Table S2 Entry 1).

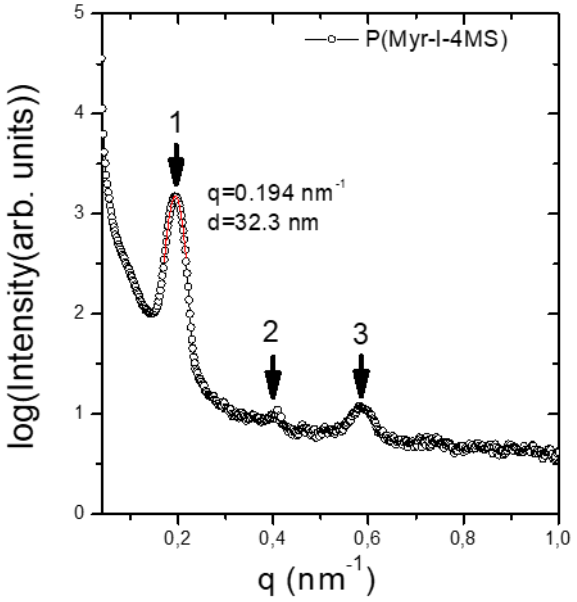

Figure S26: SAXS measurement of $Myr_{0.3}$-$I_{0.2}$-$4MS_{0.5}$ (Table S2 Entry 4).

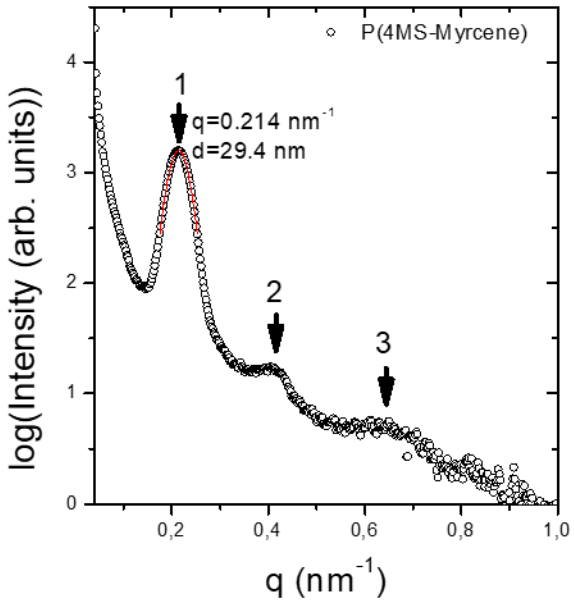

Figure S27: SAXS measurement of $Myr_{0.5}$-$4MS_{0.5}$ (Table S2 Entry 6).

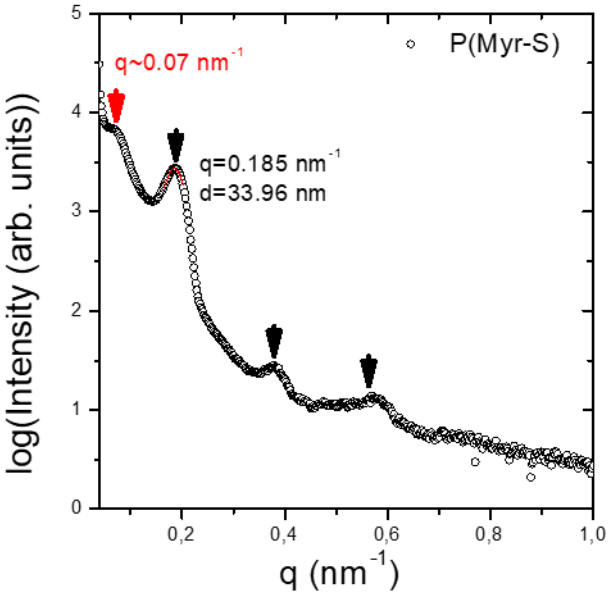

Figure S28: SAXS measurement of $Myr_{0.42}$-$S_{0.58}$ (Table S2 Entry 7).

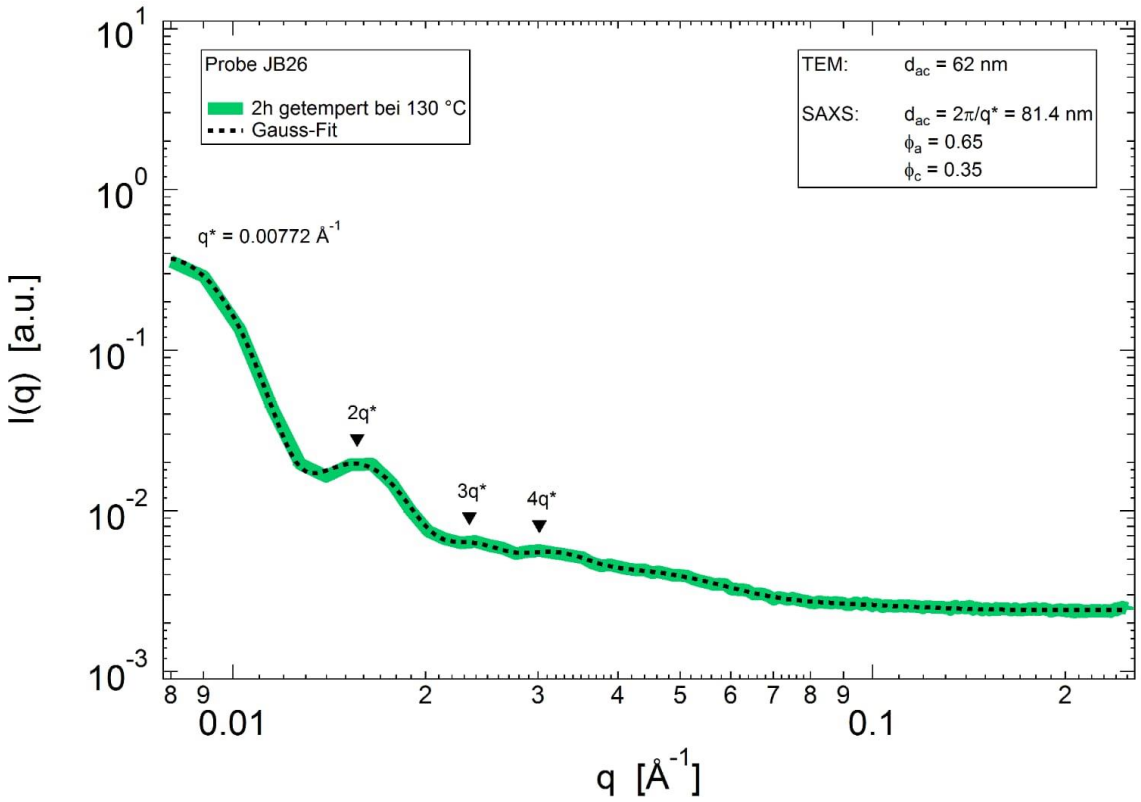

Figure S29: SAXS Measurement of $Myr_{0.26}$-$S_{0.74}$ (Table S2 Entry 9).

4.1.5.8 Summarized Results

Table S2 Summary of results of all characterization methods.

Entry	Sample composition [a] (mol%)	M_n [b] (kg/mol)	$Đ$ [b]	$T_{g,1}$ [c] (°C)	$T_{g,2}$ [c] (°C)	d_{TEM} (nm)	d_{SAXS} (nm)
1	$I_{0.5}$-$4MS_{0.5}$	64.1	1.07	-51	103	24.4	27.8
2	$Myr_{0.1}$-$I_{0.4}$-$4MS_{0.5}$	67.0	1.08	-53	106		
3	$Myr_{0.2}$-$I_{0.3}$-$4MS_{0.5}$	65.9	1.08	-57	107		
4	$Myr_{0.3}$-$I_{0.2}$-$4MS_{0.5}$	71.5	1.09	-59	101	30.1	32.3
5	$Myr_{0.4}$-$I_{0.1}$-$4MS_{0.5}$	64.0	1.12	-61	102		
6	$Myr_{0.5}$-$4MS_{0.5}$	63.8	1.14	-62	107	28.7	29.4
7	$Myr_{0.42}$-$S_{0.58}$	49.4	1.04	-54	93	30.7	34.0
8	$Myr_{0.26}$-$S_{0.74}$	161.5	1.04	-52	107		

[a] Determined by ^{1}H NMR spectroscopy in $CDCl_3$; [b] determined by SEC in THF at 30°C; [c] determined by DSC, heating rate 10 K/min.

4.1.5.9 References

(1) Wall, F. T. The Structure of Vinyl Copolymers. *J. Am. Chem. Soc.* **1941**, *63*, 1862–1866.

(2) Mayo, F. R.; Lewis, F. M. Copolymerisation. I. A Basis for Comparing the Behavior of Monomers in Copolymerisation; The Copolymerisation of Styrene and Methyl Methacrylate. *J. Am. Chem. Soc.* **1944**, *66*, 1594–1601.

(3) Skeist, I. Copolymerisation: The Composition Distribution Curve. *J. Am. Chem. Soc.* **1946**, *68*, 1781–1784.

(4) Meyer, V. E.; Lowry, G. G. Integral and differential binary copolymerisation equations. *J. Polym. Sci. A Gen. Pap.* **1965**, *3*, 2843–2851.

(5) Blankenburg, J.; Kersten, E.; Maciol, K.; Wagner, M.; Zarbakhsh, S.; Frey, H. Characterizing and Controlling the microstructure of poly(propylene oxide-co-ethylene oxide) copolymers under different catalytic conditions. *to be submitted*.

(6) Hawkins, D. M. The problem of overfitting. *Journal of chemical information and computer sciences* **2004**, *44*, 1–12.

(7) Beckingham, B. S.; Sanoja, G. E.; Lynd, N. A. Simple and Accurate Determination of Reactivity Ratios Using a Nonterminal Model of Chain Copolymerisation. *Macromolecules* **2015**, *48*, 6922–6930.

(8) Alfrey, T.; Goldfinger, G. Copolymerisation of Systems Containing Three Components. *J. Chem. Phys.* **1946**, *14*, 115–116.

Appendix

A1 Controlling the Polymer Microstructure in Anionic Polymerization by Compartmentalization

Elisabeth Rieger,[†] Jan Blankenburg,[‡§] Eduard Grune,[‡§] Manfred Wagner,[†] Katharina Landfester*[,†] and Frederik R. Wurm*[,†]

[†]Max Planck Institute for Polymer Research, Ackermannweg 10, 55128 Mainz, Germany

[‡]Institute of Organic Chemistry, Johannes Gutenberg-University Mainz, Duesbergweg 10-14, 55128 Mainz, Germany

[§]Graduate School Materials Science in Mainz, Staudingerweg 9, 55128 Mainz, Germany

Published in *Angewandte Chemie International Edition* **2018,** 57, 2483-2487

GDCh Communications Angewandte International Edition Chemie

Gradient Copolymers Hot Paper

International Edition: DOI: 10.1002/anie.201710417
German Edition: DOI: 10.1002/ange.201710417

Controlling the Polymer Microstructure in Anionic Polymerization by Compartmentalization

Elisabeth Rieger, Jan Blankenburg, Eduard Grune, Manfred Wagner, Katharina Landfester, and Frederik R. Wurm**

Abstract: *An ideal random anionic copolymerization is forced to produce gradient structures by physical separation of two monomers in emulsion compartments. One monomer (M) is preferably soluble in the droplets, while the other one (D) prefers the continuous phase of a DMSO-in-cyclohexane emulsion. The living anionic copolymerization of two activated aziridines is thus confined to the DMSO compartments as polymerization occurs selectively in the droplets. Dilution of the continuous phase adjusts the local concentration of monomer D in the droplets and thus the gradient of the resulting copolymer. The copolymerizations in emulsion are monitored by real-time ^{1}H NMR kinetics, proving a change of the reactivity ratios of the two monomers upon dilution of the continuous phase from ideal random to adjustable gradients by simple dilution.*

Compartmentalization is the spatial separation of reagents within organisms, which allows nature to prepare complex molecules. Proteins with their perfect amino acid sequence leading to complex 3D structures are only one example that was developed by evolution and relies on the compartmentalization of reagents.[1,2]

Controlling the sequence in synthetic peptides (or other polymers) is typically achieved by the sequential addition of reagents—either by manual injection or complex setups with automated addition (e.g. peptide synthesizer).[3] In contrast, nature separates several reagents by cell membranes or in different organelles within cells. The easiest mimic of such compartmentalization in the synthesis lab is the formation of an emulsion with reagents separated in the dispersed and the continuous phase.

Through this strategy we could force the competing anionic copolymerization of two monomers to produce, instead of the random copolymer, gradient copolymers with adjustable gradient structure, depending on the ratio of the dispersed to continuous phase; we did not resort to opening of the reactor or adding the monomers sequentially.

Such gradient copolymers, exhibiting a gradual, continuous change in the chemical composition, provide access to unique materials with interesting properties.[4] A recent review summarizes conventional methods for the preparation of gradient polymers (e.g. microfluidics, copolymerization, controlled monomer addition, etc.).[5]

Emulsion polymerizations are already well established and widely used in industry for the large-scale production of numerous products for daily life. The controlled environment in suspensions or (mini- and micro-) emulsions offer many advantages, in particular for radical polymerizations, which are not producible in solution.[6–10]

Despite the development of living and controlled polymerization techniques in the last decades,[11] the use of competitive copolymerization to control monomer sequences was not well established; however, many complex macromolecular architectures are currently available by sequential or iterative protocols.[12] Simultaneous copolymerization of two comonomers was used recently to prepare block copolymers[13] and sequence-controlled polymers[14] in radical emulsion polymerization, as emulsion templating reduces the number of radical side reactions.[6,15–18] Other strategies that rely on spatial separation to control polymer sequence are based on freezing out of one phase[19] or overlaying two immiscible solvents.[20]

We present a straightforward approach to force a comonomer pair, which undergoes random anionic copolymerization in solution, to form gradient structures only through physical separation. The different solubilities of the monomers in each of the phases are exploited by reaction in a (mini)emulsion with nanometer-sized droplets as the compartments.

We have chosen the living anionic ring-opening polymerization (AROP) of sulfonyl aziridines to achieve selective copolymerization in emulsified compartments (Figure 1).[21] The monomer reactivity of sulfonyl aziridines depends strongly on the nature of the sulfonyl group: more electron-withdrawing groups increase the polymerization rate, in the order nosyl > brosyl > tosyl > mesyl.[22–24] In contrast, *n*-alkyl substituents on the aziridine ring only slightly influence the kinetics of the ROP. Thus we can manipulate the monomers at this position and fine-tune, for example, their solubility profile, without altering the comonomer reactivity. This makes the aziridines an ideal model system for competing polymerization in emulsion.

With this toolbox, the random copolymerization of 2-methyl-*N*-tosylaziridine (**1**, M, TsMAz) and 2-decyl-*N*-tosyl-

[*] E. Rieger, Dr. M. Wagner, Prof. Dr. K. Landfester, Dr. F. R. Wurm
Max Planck Institute for Polymer Research
55128 Mainz (Germany)
E-mail: landfester@mpip-mainz.mpg.de
wurm@mpip-mainz.mpg.de
J. Blankenburg, E. Grune
Institute for Organic Chemistry
Johannes Gutenberg-University Mainz
55128 Mainz (Germany)
and
Graduate School Materials Science in Mainz
55128 Mainz (Germany)
Supporting information and the ORCID identification number(s) for the author(s) of this article can be found under:
https://doi.org/10.1002/anie.201710417.

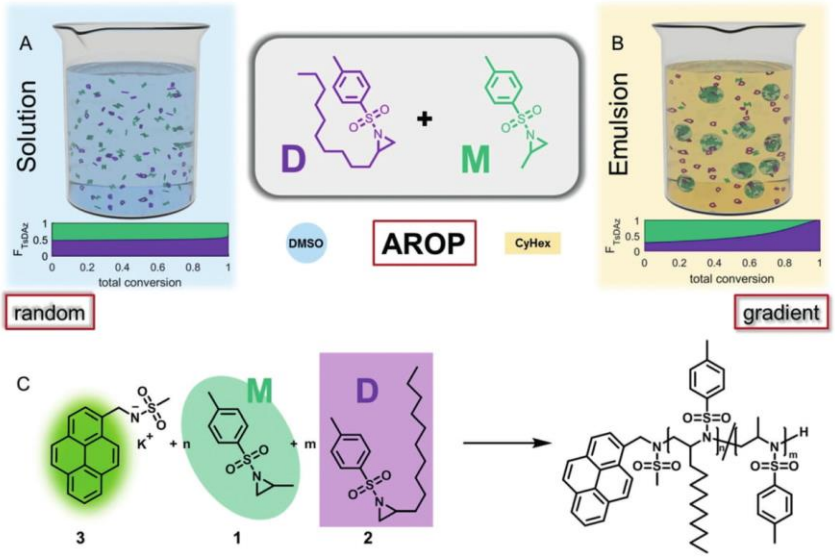

Figure 1. Azaanionic polymerization (1:50:50) in solution (A) leading to a random copolymer or in a 1:4 DMSO/CyHex emulsion (B) leading to a gradient microstructure. C) Reaction scheme for the copolymerization of **1** and **2**.

aziridine (**2**, D, TsDAz) in homogeneous solution is the obvious result (Figure 1 A). However, if these two monomers are spatially separated in an emulsion due to their selective solubility, the preferred random copolymerization is forced to produce gradient up to almost block-like structures. Monomer **1** is preferably soluble in the dispersed phased, in our case DMSO, while monomer **2** dissolves (due to the long alkyl tail) preferably in the continuous cyclohexane phase (Figure 1 B). The copolymers are soluble in DMSO and insoluble in cyclohexane. In addition, we have proven that no propagation occurs in the continuous phase (cyclohexane) for the azaanionic polymerization of aziridines: thus the propagation is located selectively within the DMSO droplets.[25] The location of the polymerization was further visualized by the use of a pyrene derivative as the initiator of the polymerization (Figure 2 B shows a fluorescent microscopy image, proving fluorescence only inside of the dispersed phase.) This implies that the copolymer composition depends only on the local monomer concentration within the DMSO droplets, which re-equilibrates as the monomer is consumed. The anionic polymerization proceeds in the emulsion either with or without the addition of a surfactant, making the polymers interesting for further applications, where surfactant might be beneficial or not necessary. This monomer sequence control confers potential for molecular targeting, recognition, and biocatalysis.

To determine the reactivity ratios in homogeneous solution, the simultaneous copolymerization of the two monomers was investigated by real-time ^{1}H NMR spectroscopy. Due to their similar reactivity, the shift in the composition of the monomer mixture is small and multiple ^{1}H NMR kinetic measurements with different monomer ratios were combined. The data were evaluated by the methods of Fineman–Ross[26] and Kelen–Tüdos[11,27] and proved that the two monomers have almost equal reactivity: $r_1(\mathbf{1}) = 1.08$, $r_2(\mathbf{2}) = 0.98$, $r_1 r_2 = 1.05$ (Kelen–Tüdos) (cf. Supporting Information, pp. S13–S19), revealing an almost ideal copolymerization in DMSO (ideal is defined with $r_1 = 1$ and $r_2 = 1$ or $r_1 r_2 = 1$). The microstructure of the 1:1 polymer was predicted by numerical integration of the Mayo–Lewis equation,[28] showing a slightly favored incorporation of TsMAz (**1**, M, green) at the beginning of the copolymer and a slightly favored incorporation of TsDAz (**2**, D, purple) at the end of the polymer (Figure 1 A).[29]

As the two monomers exhibit distinctively different solubilities, we physically separated them in a DMSO-in-cyclohexane (mini)emulsion. Monomer **1** prefers DMSO, while **2** with its long alkyl tail has a higher solubility in cyclohexane. Physical separation of the monomers was achieved either by surfactant-free emulsification with continuous, vigorous stirring or by the addition of surfactant and ultrasound mixing to form a stable miniemulsion (Figures S1 and S4). The copolymerization behavior was studied by real-time ^{1}H NMR spectroscopy of the miniemulsions, as phase separation in the non-stirred NMR tube is efficiently prevented by the surfactant. From these spectra (Figure 2 A) both monomer consumptions and propagation rates (k_p) were calculated.[25] The miniemulsions were stable for at least

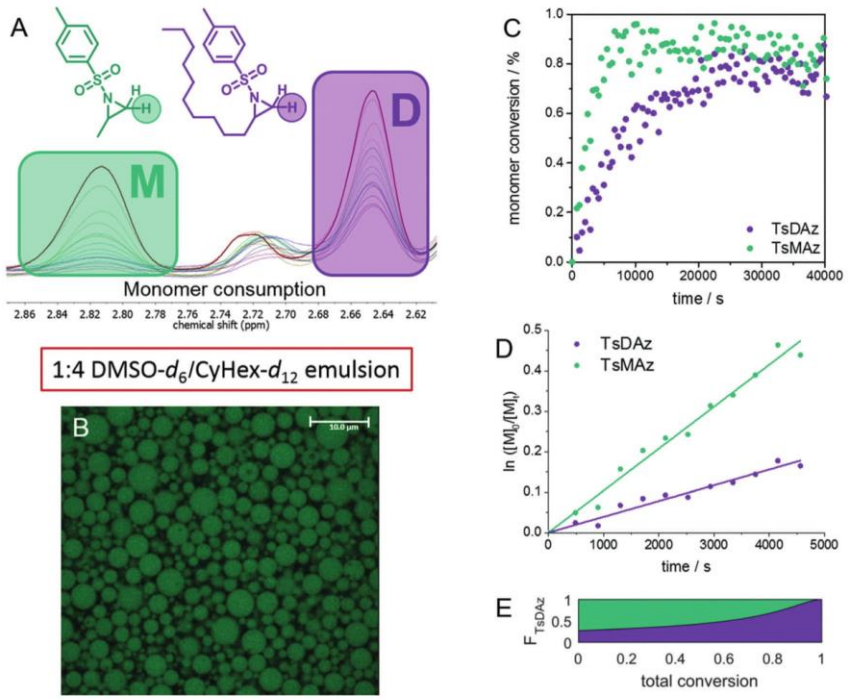

Figure 2. Azaanionic copolymerization of TsMAz (**1**, M) and TsDAz (**2**, D) in emulsion at 50 °C: A) Real-time ^{1}H NMR kinetics of copolymerization in emulsion. B) cLSM image of the emulsion showing the fluorescent initiator inside of the droplets. C) Monomer conversion vs. time. D) Kinetic plots of $\ln([M]_0/[M]_t)$ vs. time. E) Incorporation probability of TsDAz (F_{TsDAz}) vs. total conversion.

several days under these conditions, with droplet diameters between 200 and 800 nm. ^{1}H NMR and size-exclusion chromatography (SEC) data demonstrated that the azaanionic polymerization remained living in the (mini)emulsion process and provided polymers with monomodal and rather narrow molecular weight distributions. ($Đ < 1.2$, a slightly higher dispersity than that in a normal glass reactor might be rationalized, as the contents of the NMR tube are not stirred during the polymerization, but shaken by hand after every fourth spectra.) The living character of the AROP was proven by chain-extension experiments and the linear slope of the plots $\ln([M]_0/[M]_t)$ vs. time (cf. Figure 2, Figure 3, and S3). Polymerizations reached almost complete monomer conversion (ca. 90 %). More importantly, HPLC measurements indicate that the surfactant was not involved in the polymerization (Figure S5). Interfacial tension (γ) between water and toluene was measured in the presence of the different copolymers by the spinning-drop method: The random P(**1**-*co*-**2**), prepared from solution, reduces γ only slightly from 32 mN m^{-1} to 29.1 mN m^{-1}, while the amphiphilic block copolymer prepared by sequential monomer addition, P**1**-*b*-P**2**, reduces γ to 22 mN m^{-1}. The gradient P(**1**-*gr*-**2**) prepared from the 1:10 mixture reduces γ to 27 mN m^{-1}, an intermediate value, proving the effect of gradient formation during the confined copolymerization in emulsion.

Separation of the monomers by an emulsion clearly forces them to produce gradient copolymers (Figure 2), as the local concentration in the DMSO droplets of both monomers is controlled by their solubility profiles. Since the kinetics of an anionic polymerization strongly depend on the solvent polarity, it is important that the copolymerization is restricted to one solvent (here, the DMSO compartments). Thus, we assume that the reactivity ratios do not change during the polymerization in emulsion and that only the dilution of the continuous phase affects the monomer feed of **2** into the DMSO compartments. This changes the comonomer incorporation, which results in apparent reactivity ratios (r_{app}) that are only dependent on the solvent ratios and are necessary for the comparison of the two-phase systems with homogeneous polymerization. As $r_1(\mathbf{1})\,r_2(\mathbf{2}) \approx 1$ in solution, the copolymerization can be assumed as ideal, which simplifies the Mayo–Lewis equation and enables the determination of the apparent reactivity ratios directly from the propagation ratios, as $r_1 = k_p(\mathbf{1})/k_p(\mathbf{2})$ and vice versa $r_2 = k_p(\mathbf{2})/k_p(\mathbf{1})$.[30–32]

By variation of the dilution of the continuous phase, the local monomer concentration of **2**, that is, the partitioning of

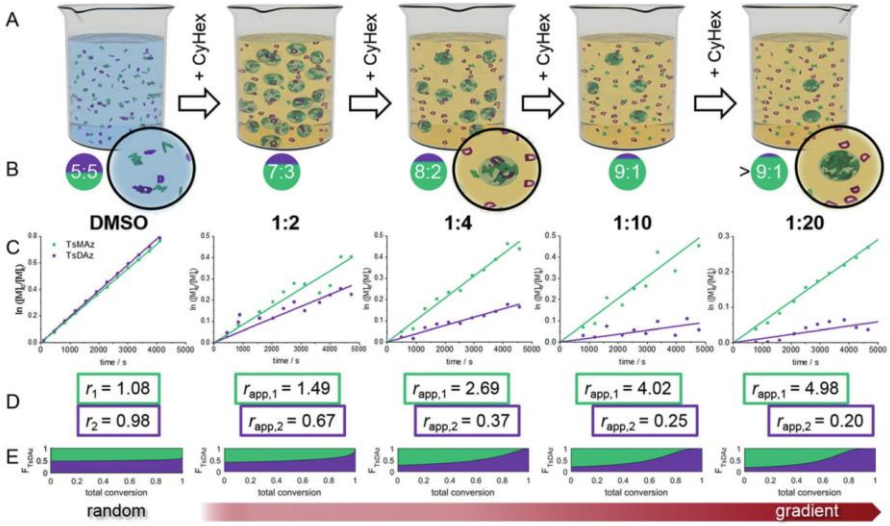

Figure 3. Controlling the monomer separation by dilution of the emulsion: A) Adjustment of the DMSO (blue)/cyclohexane (yellow) ratio. B) Monomer ratio within the DMSO droplets, determined by HPLC and enlarged image: with increasing cyclohexane dilution, M is enriched within the DMSO droplets. C) Kinetic plots of $\ln([M]_0/[M]_t)$ vs. time of TsMAz (**1**, M), TsDAz (**2**, D) in different emulsions. D) Reactivity ratios of the different solvent mixtures. F) Incorporation probability of TsDAz (F_{TsDAz}) vs. total conversion proves increased gradients upon dilution.

the two monomers between the phases, can be further adjusted, which will directly influence the gradient in the product (cf. Figure 3B). From HPLC measurements, the partition coefficients ($\log P$ values, ($\log P_{CyHex/DMSO} = \log([M]_{CyHex}/[M]_{DMSO})$) of the monomer pair in DMSO and cyclohexane were calculated, proving the preference of TsMAz for DMSO. Monomer partitioning can be also tuned by other solvent pairs: DMF was used as the dispersed phase, resulting in a slightly lower monomer separation (cf. Supporting Information, pp. S25–S27). Different ratios of the dispersed to the continuous phase (1:2, 1:4, 1:10, 1:20) were explored, with increasing amount of cyclohexane. For the 1:2 DMSO/CyHex solvent ratio, the initial monomer ratio in the DMSO droplets is ca. 7:3 (TsMAz/TsDAz) and the ratio increases to 8:2 (for DMSO/CyHex = 1:4) to 9:1 (1:10) up to more than >9:1 (for 1:20). The differential Mayo–Lewis equation was solved numerically to reveal the microstructure of a copolymerization ratio pair and a given initial monomer ratio (Figures 3E).[29,32] With increasing dilution, the apparent reactivity ratios (Figure 3D) changed from an ideal random copolymerization into more pronounced gradient copolymers.

In conclusion, by compartmentalization and spatial separation of two monomers in an emulsion, we were able to force a random copolymerization to produce gradient copolymers with adjustable gradient strength. This is the first example of forcing copolymerization behavior by spatial separation of the reaction mixture in an emulsion for an anionic copolymerization, resulting in gradient copolymers with surface-active properties. Real-time ^{1}H NMR spectroscopy was used to monitor the reactions and calculate the final copolymer microstructure. As the propagation of the living anions occurs selectively within the DMSO compartments, dilution of the continuous phase made it possible to adjust the gradient strength of the copolymers. Apparent reactivity ratios (r_{app}) were calculated, which depend only on the local concentration in the compartments. For the first time, this allowed us to control the comonomer sequence distribution along a polymer chain by simple dilution of the emulsion with the continuous solvent.

The emulsion platform for the anionic polymerization might be used for several applications, as it is free of heavy metals and can be performed with or without surfactants. We believe that this strategy can be extended to other monomers and will give access to libraries of copolymers with adjustable gradient strength in a closed one-pot reaction, just by changing the ratio of dispersed to continuous phase in a (mini)emulsion.

Acknowledgements

We thank the Deutsche Forschungsgemeinschaft (DFG WU750/7-1) and the BMBF/MPG network MaxSynBio for funding. We thank Stefan Spang for the NMR measurements, Anke Kaltbeitzel for cLSM measurements, and Beate Müller for HPLC measurements.

Conflict of interest

The authors declare no conflict of interest.

Keywords: anionic polymerization · aziridines · compartmentalization · copolymeruzation · emulsions

How to cite: *Angew. Chem. Int. Ed.* **2018**, *57*, 2483–2487
Angew. Chem. **2018**, *130*, 2509–2513

[1] M. Eigen, R. Winkler, *Steps towards Life: A Perspective on Evolution*, Oxford University Press, Incorporated, **1992**.
[2] J. M. Berg, J. L. Tymoczko, L. Stryer, *Biochemistry*, 8th ed., W. H. Freeman, New York, **2015**.
[3] R. B. Merrifield, *J. Am. Chem. Soc.* **1963**, *85*, 2149–2154.
[4] F. Jasinski, V. L. Teo, R. P. Kuchel, M. Mballa Mballa, S. C. Thickett, R. H. G. Brinkhuis, W. Weaver, P. B. Zetterlund, *Polym. Chem.* **2017**, *8*, 495–499.
[5] K. U. Claussen, T. Scheibel, H. W. Schmidt, R. Giesa, *Macromol. Mater. Eng.* **2012**, *297*, 938–957.
[6] P. B. Zetterlund, S. C. Thickett, S. Perrier, E. Bourgeat-Lami, M. Lansalot, *Chem. Rev.* **2015**, *115*, 9745–9800.
[7] N. P. Truong, M. R. Whittaker, A. Anastasaki, D. M. Haddleton, J. F. Quinn, T. P. Davis, *Polym. Chem.* **2016**, *7*, 430–440.
[8] R. G. Gilbert, *Emulsion Polymerization: A Mechanistic Approach*, Academic Press, New York, **1995**.
[9] S. C. Thickett, R. G. Gilbert, *Polymer* **2007**, *48*, 6965–6991.
[10] K. Piradashvili, E. M. Alexandrino, F. R. Wurm, K. Landfester, *Chem. Rev.* **2016**, *116*, 2141–2169.
[11] G. Odian, *Principles of Polymerization*, Wiley, Hoboken, **2004**.
[12] M. Ouchi, N. Badi, J.-F. Lutz, M. Sawamoto, *Nat. Chem.* **2011**, *3*, 917–924.
[13] C. Lu, M. W. Urban, *ACS Macro Lett.* **2015**, *4*, 1317–1320.
[14] N. G. Engelis, A. Anastasaki, G. Nurumbetov, N. P. Truong, V. Nikolaou, A. Shegiwal, M. R. Whittaker, T. P. Davis, D. M. Haddleton, *Nat. Chem.* **2017**, *9*, 171–178.
[15] P. B. Zetterlund, Y. Kagawa, M. Okubo, *Chem. Rev.* **2008**, *108*, 3747–3794.
[16] P. B. Zetterlund, G. Gody, S. Perrier, *Macromol. Theory Simul.* **2014**, *23*, 331–339.
[17] A. Tardy, K. A. Bhullar, D. Q. Lim, S. C. Thickett, P. B. Zetterlund, *J. Polym. Sci. Part A* **2017**, *55*, 1590–1600.
[18] P. B. Zetterlund, *Polym. Chem.* **2011**, *2*, 534–549.
[19] R. N. Carmean, C. A. Figg, T. E. Becker, B. S. Sumerlin, *Angew. Chem. Int. Ed.* **2016**, *55*, 8624–8629; *Angew. Chem.* **2016**, *128*, 8766–8771.
[20] M. Yamada, T. Nishikawa, A. Kanazawa, S. Kanaoka, S. Aoshima, *J. Polym. Sci. Part A* **2016**, *54*, 2656–2661.
[21] E. Rieger, A. Manhart, F. R. Wurm, *ACS Macro Lett.* **2016**, *5*, 195–198.
[22] E. Rieger, A. Alkan, A. Manhart, M. Wagner, F. R. Wurm, *Macromol. Rapid Commun.* **2016**, *37*, 833–839.
[23] T. Homann-Müller, E. Rieger, A. Alkan, F. R. Wurm, *Polym. Chem.* **2016**, *7*, 5501–5506.
[24] L. Reisman, C. P. Mbarushimana, S. J. Cassidy, P. A. Rupar, *ACS Macro Lett.* **2016**, *5*, 1137–1140.
[25] E. Rieger, T. Gleede, K. Weber, A. Manhart, M. Wagner, F. R. Wurm, *Polym. Chem.* **2017**, *8*, 2824–2832.
[26] M. Fineman, S. D. Ross, *J. Polym. Sci.* **1950**, *5*, 259–265.
[27] T. Kelen, F. Tüdos, *J. Macromol. Sci. Chem.* **1975**, *9*, 1–27.
[28] F. R. Mayo, F. M. Lewis, *J. Am. Chem. Soc.* **1944**, *66*, 1594–1601.
[29] I. Skeist, *J. Am. Chem. Soc.* **1946**, *68*, 1781–1784.
[30] F. T. Wall, *J. Am. Chem. Soc.* **1941**, *63*, 1862–1866.
[31] V. V. Jaacks, *Makromol. Chem.* **1967**, *105*, 289–291.
[32] J. Blankenburg, M. Wagner, H. Frey, *Macromolecules* **2017**, *50*, 8885–8893.

Manuscript received: October 9, 2017
Accepted manuscript online: December 13, 2017
Version of record online: January 18, 2018

A2 One-Step Anionic Polymerization for the Formation of Linear Ultra-High Molecular Weight Block Copolymer Films Featuring Vivid Structural Colors in the Bulk State

Michael Appold[1], Eduard Grune[2,3], Holger Frey[2], Markus Gallei[1,*]

[1]Ernst-Berl-Institute for Chemical Engineering and Macromolecular Chemistry, Technische Universität Darmstadt, Alarich-Weiss-Straße 4, 64287 Darmstadt, Germany

[2]Institute of Organic Chemistry, Johannes Gutenberg-University, Duesbergweg 10-14, 55128 Mainz, Germany

[3]Graduate School of Excellence Materials Science in Mainz (MAINZ), Staudingerweg 9, 55128 Mainz, Germany

Published in *ACS Applied Materials & Interfaces* **2018,** 10, 18202-18212

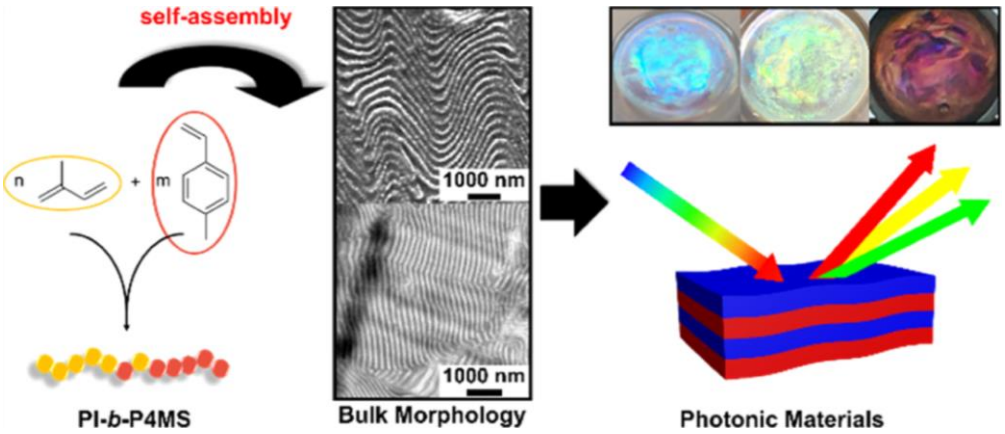

ACS APPLIED MATERIALS & INTERFACES

Research Article

Cite This: ACS Appl. Mater. Interfaces 2018, 10, 18202−18212

www.acsami.org

One-Step Anionic Copolymerization Enables Formation of Linear Ultrahigh-Molecular-Weight Block Copolymer Films Featuring Vivid Structural Colors in the Bulk State

Michael Appold,[†] Eduard Grune,[‡,§] Holger Frey,[‡] and Markus Gallei*[,†]

[†]Ernst-Berl-Institute for Chemical Engineering and Macromolecular Chemistry, Technische Universität Darmstadt, Alarich-Weiss-Straße 4, 64287 Darmstadt, Germany

[‡]Institute of Organic Chemistry, Johannes Gutenberg-University Mainz, Duesbergweg 10-14, 55128 Mainz, Germany

[§]Graduate School of Excellence Materials Science in Mainz (MAINZ), Staudingerweg 9, 55128 Mainz, Germany

Supporting Information

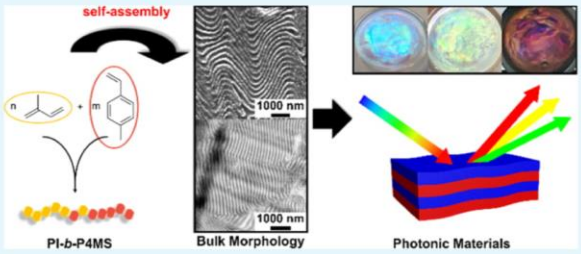

ABSTRACT: Ultrahigh-molecular-weight (UHMW) tapered block copolymers (BCPs) consisting of polyisoprene-*block*-poly(4-methylstyrene) featuring overall molar masses in the range of 1101−2033 kg mol^{-1} (M_w) are synthesized via a convenient one-step anionic copolymerization protocol. The obtained UHMW BCPs are investigated by differential scanning calorimetry, size exclusion chromatography, and ^{1}H NMR spectroscopy. Microphase separation for the UHMW BCPs in the bulk state is investigated by transmission electron microscopy (TEM) measurements and scanning electron microscopy (SEM), revealing well-ordered lamellar and spherical domains with large domain sizes in the range of 100−200 nm. Excellent order and periodicity are observed for lamellar morphologies over large film areas of 90 × 120 μm. Because of this high order of the underlying domains and the different refractive indices of the block segments, vivid structural colors can be observed in the bulk state. Structural colors of BCP films are investigated by angle-dependent UV/vis measurements, revealing intensive reflection colors according to Bragg's law of diffraction. The optical characteristics are directly correlated to TEM and SEM results. Moreover, colored BCP films featuring spherical domains for one block segment with domain sizes of 97−122 nm revealed blue structural colors stemming from disordered particle scattering.

KEYWORDS: *anionic polymerization, block copolymers, self-assembly, morphology, photonic materials, Bragg diffraction*

INTRODUCTION

The formation of highly functional, complex structures and materials at the nanoscale by the principle of self-assembly is well-established in Nature. In this context, specialized optical materials are abundant in different organisms for light harvesting, light manipulation, and light management for a manifold of biologically relevant applications.[1−3] Both natural and artificial photonic materials with structural colors resulting from diffraction and interference have attracted a great deal of attention as potential candidates for various optoelectronic applications.[4−6] A periodic variation of the refractive indices on a length scale on the order of the wavelength of light creates constructive interference, leading to a partial photonic band gap. For polymers, which feature a refractive index of around 1.5, the underlying periodic structures require dimensions of at least 120 nm or larger to show photonic properties in the visible light range. As a result, sharp peaks in reflectivity lead to vivid colors despite the absence of optical absorption. The physical laws and simplified concepts that form the basis for structural colored materials based on particle and layered systems are well-described in the literature. The principles are depicted in a simplified manner in Figure 1.[7−9]

A convenient strategy for the preparation of materials featuring such structural colors is the self-assembly of monodisperse spherical polymer or hybrid colloids forming photonic crystals (Figure 1a).[8,10−12] Good optical performance

Received: February 16, 2018
Accepted: May 8, 2018
Published: May 8, 2018

DOI: 10.1021/acsami.8b02848
ACS Appl. Mater. Interfaces 2018, 10, 18202−18212

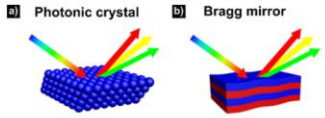

Figure 1. Schematic description of the interplay of visible light with a photonic crystal (a) and a Bragg mirror based on lamellae stacks (b).

with iridescent reflection colors caused by Bragg diffraction of visible light is obtained after colloidal crystallization. This optical feature for three-dimensional (3D) photonic band gap materials has been forecast in the pioneering work of Yablonovitch.[13] Such materials may also consist of stimuli-responsive polymers showing switchable optical properties.[14−21] Other recent strategies for the preparation of one-dimensional photonic crystals focus on brush block copolymers (BCPs) and blends thereof[22−25] or sterically demanding dendronized polymers.[26] In general, diBCPs consisting of two polymer segments covalently connected are capable of self-organizing into a variety of ordered structures comprising spheres in a matrix, lamellae, hexagonally packed cylinders, and double gyroid morphologies at the nanoscale. BCPs are therefore excellent materials to create periodically nanostructured soft matter in the bulk state or in selective solvents for applications in fields as diverse as nanolithography, drug delivery, and separation technologies.[27−33] Moreover, the self-assembly of BCPs has been used as an excellent platform to generate photonic crystals.[19,34] For this purpose, ultrahigh-molecular-weight (UHMW) BCPs are required to attain periodic and sufficiently large domain spacing in the range of the wavelength of visible light. However, the self-assembly of UHMW polymer chains is very complex and typically necessitates long annealing times for their self-assembly. This issue can be overcome to a certain extent by blending the high-molar mass BCPs with low-molecular-weight homopolymers or by focusing on BCP photonic gels, where one or both block segments are (selectively) swollen and thus rather flexible. The Thomas group developed one-dimensionally periodic BCP photonic lamellar gels, which respond with vivid color change upon treatment with different counterions,[35] mechanical stress,[36,37] selective solvents,[38,39] or electrical field.[40] The same group showed the potential for such BCP gels to prepare photonic displays.[41,42] Photo-responsive BCP photonic gel films exhibiting strong reflective multicolors in the visible light range upon near-UV radiation have been reported by Ahn et al.[43] Mesophase-separated olefin BCPs that are capable of changing reflective and transmitted colors upon solvent and temperature change were reported by Hustad et al.[44] Very recently, bulky dendritic BCPs were designed and synthesized for the preparation of 3D printable photonic crystals.[45] Here, a major advantage was the thermally induced self-assembly during filament extrusion of the BCPs. The combination of segments with a high and a low glass-transition temperature is present in polystyrene-*block*-polyisoprene (PS-*b*-PI). Yoon et al. prepared PS-*b*-PI BCPs (M_n = 590 kg mol^{-1}) as a narrow spectral-band selective feedback element to construct a laser cavity.[46] In a subsequent work, the same group presented highly oriented thin-film microdomain patterns of even larger PS-*b*-PI UHMW BCPs (M_n = 1150 kg mol^{-1}) for the creation of photonic films.[39,47] In general, the optical properties of organic photonic structures can be further tuned by incorporation of inorganic, high refractive components according to Bragg's law of diffraction.[48−51]

In addition to issues associated with the self-assembly of BCP architectures, the synthesis of UHMW BCPs remains challenging, as it necessitates precise control over block length and block constitution. Well-controlled or living polymerization strategies are the routes of choice for the preparation of well-defined BCPs.[52−55] An elegant approach was recently reported by Motokawa et al. for the formation of poly(methyl methacrylate)-containing BCPs with PS as a second block, using a polymerization-induced microphase separation method for the controlled formation of polymer interdomain spacings.[56] Mapas et al. reported the feasible combination of atom-transfer radical polymerization with a reversible addition fragmentation chain-transfer polymerization for the preparation of amphiphilic UHMW BCPs with molar masses (M_n) in the range of 800−1600 kg mol^{-1} for photonic applications.[57] Compared to these controlled polymerization routes, especially anionic polymerization is still the most common polymerization method for the synthesis of UHMW BCPs for the creation of polymer architectures featuring photonic properties.[35,58−60] However, the use of a very low initiator concentration—typically highly reactive organolithium compounds—for a large excess of monomer and the subsequent addition of a second monomer for BCP formation render termination reactions very likely. This leads to a mixture of the desired BCP and undesired homopolymer precursor impurities (with unknown composition). In the worst case, the entire anionic polymerization can be terminated after the second monomer addition. Therefore, a one-step initiator addition for two monomers at the same time would be favorable. Very recently, Grune et al. developed the statistical living anionic copolymerization of a mixture of isoprene and 4-methylstyrene (4MS) for the formation of tapered BCPs with narrow taper.[61] Capitalizing on the strong reactivity difference of both monomers, well-defined BCPs could be achieved, featuring microphase-separated domains.

In this study, we present an efficient and simple synthetic approach for the formation of linear UHMW BCP films featuring vivid structural colors in the bulk state. For this purpose, PI-*block*-poly(4MS) (PI-*b*-P4MS) BCPs with overall molar masses up to 2033 kg mol^{-1} are synthesized via statistical anionic copolymerization in hydrocarbon solvents in one single step. For molecular and thermal characterization of the tapered BCPs, ^{1}H NMR spectroscopy, size exclusion chromatography (SEC), and differential scanning calorimetry (DSC) are carried out. As a focus of this work, microphase separation of these UHMW BCPs in the bulk state is investigated by transmission electron microscopy (TEM) and scanning electron microscopy (SEM) measurements, revealing well-ordered lamellar and spherical nanodomains in the range of 100−200 nm. Because of the excellent order of the underlying domains, the BCP films display intense structural colors in the bulk state, which are correlated to the respective nanosegregated morphologies.

■ EXPERIMENTAL SECTION

Reagents. All solvents and reagents were purchased from Alfa Aesar, Sigma-Aldrich, Fisher Scientific, ABCR and used as received unless otherwise stated. Deuterated solvents were purchased from Deutero GmbH, Kastellaun, Germany. Cyclohexane (Cy) was distilled from sodium/benzophenone under reduced pressure (cryo-transfer) prior to the addition of 1,1-diphenylethylene and *sec*-butyllithium (*s*-BuLi), followed by a second cryo-transfer. Isoprene (I) and 4MS were

DOI: 10.1021/acsami.8b02848
ACS Appl. Mater. Interfaces 2018, 10, 18202−18212

dried by stirring over calcium hydride (CaH_2) or trioctyl-aluminum, followed by cryo-transfer prior to use in polymerization. All syntheses were carried out under an atmosphere of nitrogen using Schlenk techniques or a glovebox equipped with a Coldwell apparatus. Bulk films with a diameter of 1.5 cm and a thickness of 1−1.5 mm were prepared by solution-casting from tetrahydrofuran (THF) or $CHCl_3$ (as given and discussed in the main section), followed by solvent annealing with $CHCl_3$ or THF at room temperature (RT) in a desiccator for 1 week. Bulk characterization was accomplished by ultramicrotoming the films into thin slices of 50−70 nm, followed by TEM measurements. In the following, the polymers will be classified by subscriptions, indicating the degree of polymerization of the respective block.

Instrumentation. NMR spectra were recorded on a Bruker DRX 300 spectrometer working at 300 MHz (^{1}H NMR). NMR chemical shifts are referenced relative to tetramethylsilane. Standard SEC was performed with a system composed of a 1260 IsoPump—G1310B (Agilent Technologies), a 1260 VW detector—G1314F—at 254 nm (Agilent Technologies), and a 1260 RI detector—G1362A—at 30 °C (Agilent Technologies), with THF as the mobile phase (flow rate 1 mL min^{-1}) on a SDV column set from PSS (SDV 10^3, SDV 10^5, SDV 10^6). Calibration was carried out using PS standards (from Polymer Standard Service, Mainz). For data acquisition and evaluation of the measurements, PSS WinGPC UniChrom 8.2 was used. TEM experiments were carried out with a Zeiss EM 10 electron microscope operating at 60 kV. All shown images were recorded with a slow-scan charge-coupled device camera obtained from TRS (Tröndle) in bright-field mode. Camera control was computer-aided using the ImageSP software from TRS. Additional TEM measurements were carried out with a JEOL JEM-2100F microscope (JEOL, Tokyo, Japan) equipped with a field emission gun operating at a nominal acceleration voltage of 200 kV. The 2100F was operated in a scanning TEM (STEM) mode. The samples were investigated using a JEOL single tilt holder. The energy-dispersive X-ray spectroscopy (EDS) data were collected with an Oxford X-Max 80 TEM Si-drift detector (Oxford Instruments GmbH, Wiesbaden, Germany). SEM measurements were performed on Philips XL30 FEG at an operating voltage of 2−10 kV using a secondary electron detector. Prior to SEM measurements, the polymer samples were coated with Au using a Quorum Q300T D sputter coater. Reflection spectra were recorded using a vis−NIR fiber spectrophotometer (USB 2000, Ocean Optics). For the reflection measurements, a deuterium/tungsten halogen lamp (DT mini 2, Ocean Optics) was used. For determination of the thermal properties of the polymers, DSC was performed with Mettler Toledo DSC-1 in a temperature range from −100 to 150 °C with a heating rate of 10 K min^{-1}.

One-Step Anionic Block Copolymerization of Isoprene and 4MS. *Exemplary Synthesis of a PI-b-P4MS Featuring an Overall Molar Mass of 1101 kg mol^{-1} (PI_{7574}-b-$P4MS_{4951}$).* In an ampule equipped with a stir bar, 790 mg (6.70 mmol, 3367 equiv) neat 4MS and 700 mg (10.28 mmol, 5168 equiv) isoprene (I) were dissolved in 100 mL of dry Cy. Polymerization was initiated by quick addition of 153 μL *s*-BuLi (2 μmol, 0.013 M solution in hexane, 1 equiv) with a syringe. The solution was stirred for 1 week at RT. After adding a small amount of degassed methanol, the polymer was poured into a 10-fold excess of methanol. The polymer was collected by filtration, washed with methanol, dried in vacuum, and stored under argon or nitrogen at −18 °C (yield: 1460 mg, 97.9%).

SEC (vs PS): M_n = 821 000 g mol^{-1}; M_w = 1 101 000 g mol^{-1}; $Đ$ = 1.34.

^{1}H NMR (300 MHz, 300 K, $CDCl_3$, δ in ppm): 7.10−6.75 (br, H_{11}), 6.62−6.19 (br, H_{12}), 5.18−4.99 (br, H_7), 4.76−4.69 (br, H_3), 2.49−1.23 (alkyl).

RESULTS AND DISCUSSION

UHMW Tapered BCP Synthesis. PI-*b*-P4MS BCPs were synthesized in one single step via anionic copolymerization of the corresponding monomer mixtures in hydrocarbon solvents as recently described for low molar mass BCPs.[61] The synthesis is shown in Scheme 1. The copolymerization starts from a mixture of isoprene and 4MS in Cy with *s*-BuLi as an initiator at RT.

Scheme 1. Statistical Anionic Copolymerization of Isoprene and 4MS in Cy with *s*-BuLi as an Initiator at RT[a]

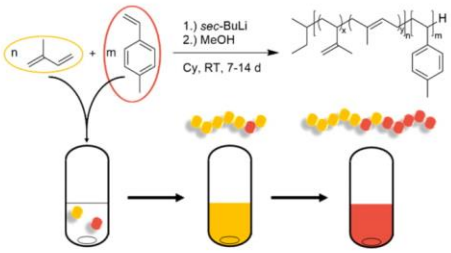

[a]Cy: cyclohexane; RT: room temperature; MeOH: methanol; d: day; yellow/red: colors of the respective carbanion of PI and P4MS.

The obtained BCPs were characterized with respect to their molar masses by SEC measurements (Figures S1−S4). All obtained data comprising M_n, M_w, and dispersity indices, $Đ$, for the investigated PI-*b*-P4MS BCPs within this study are compiled in Table 1. The polymer samples are classified by subscriptions, indicating the degree of polymerization.

Table 1. Molecular Weights and Dispersity Indices of BCPs Synthesized in This Study

	polymer	M_n/kg mol^{-1}	M_w/kg mol^{-1}	$Đ$
1	PI_{7574}-*b*-$P4MS_{4951}$[a,b]	821	1101	1.34
2	PI_{9118}-*b*-$P4MS_{5364}$[a,c]	845	1255	1.48
3	PI_{20011}-*b*-$P4MS_{3798}$[a,d]	1162	1812	1.56
4	PI_{25060}-*b*-$P4MS_{2758}$[a,e]	1446	2033	1.41

[a]Molecular weight determined by SEC (PS standards, THF). [b]Content of 1,4-PI units in the PI block was determined to be 93.5 mol %. [c]Content of 1,4-PI units was determined to be 94.1 mol %. [d]Content of 1,4-PI units was determined to be 95.4 mol %. [e]Content of 1,4-PI units was determined to be 93.3 mol %.

As can be concluded from these results, the molecular weights (M_w) for the BCPs obtained by the one-step anionic copolymerization were in the range of 1101−2033 kg mol^{-1}. A broadened molar mass distribution reflected by the dispersity index values, $Đ$, in the range of 1.34−1.56 could be observed. Because of the increasing viscosity during the polymerization of PI as a first block, stirring of the polymer/monomer mixture was no longer possible despite the low monomer concentration of 1.5 wt % in solution, leading to a diffusion-controlled formation of the P4MS second block. Consequently, this causes a tailing of the molecular mass distribution and therefore an increase of the dispersity. Nevertheless, UHMW BCPs could be prepared with the targeted compositions based on the monomer mixtures employed. To gather first evidence for the formation of a blocklike structure, the thermal properties of the polymers were investigated by DSC measurements (Figure 2a). All obtained data regarding the glass transitions (T_g) of the tapered BCPs are compiled in Table 2.

DSC measurements for all polymers used in this study revealed two distinct glass-transition temperatures in the range

DOI: 10.1021/acsami.8b02848
ACS Appl. Mater. Interfaces 2018, 10, 18202−18212

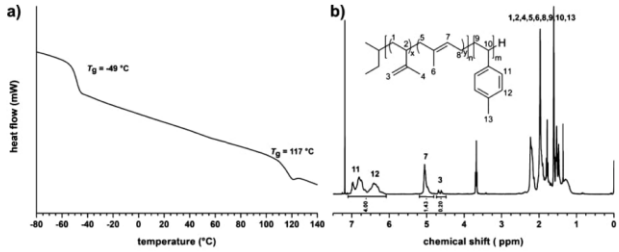

Figure 2. (a) DSC thermogram of PI_{7574}-*b*-$P4MS_{4951}$. The applied heating rate for the DSC run was 10 K min^{-1}. (b) ^1H NMR spectrum of PI_{7574}-*b*-$P4MS_{4951}$ in $CDCl_3$.

Table 2. Characterization of BCPs Used in This Study and the Respective Glass-Transition Temperatures (T_g)

	polymer	$T_{g,PI}$ (°C)[a]	$T_{g,P4MS}$ (°C)[a]
1	PI_{7574}-*b*-$P4MS_{4951}$	−49	117
2	PI_{9118}-*b*-$P4MS_{5364}$	−50	116
3	PI_{20011}-*b*-$P4MS_{3798}$	−53	117
4	PI_{25060}-*b*-$P4MS_{2758}$	−54	116

[a]T_g determined by DSC measurements, given in °C. The applied heating rate for the DSC runs was 10 K min^{-1}.

of −49 to −54 °C for the soft PI block segment and 117 °C for the P4MS block segment, confirming the successful synthesis of tapered, phase-segregated PI-*b*-P4MS BCPs in the statistical copolymerization. These glass-transition temperatures are in accordance with the T_g of PI and P4MS homopolymers with −64 to −69 and 111 °C, respectively.[62−64] The corresponding DSC thermograms of the BCPs are given in Figures S8−S10.

The T_g of PI synthesized by anionic copolymerization in nonpolar solvents leading to a high content of 1,4-PI units (93.5 mol %) is −49 °C, while the higher T_g value corresponds to P4MS, which is in good agreement with the literature.[64] Generally, the PI block segment features a slightly increased T_g of −49 °C compared to the glass transition of pure PI in the literature with −64 to −69 °C.[65,66] This is due to the tapered BCP structure that leads to the incorporation of a certain amount of isolated 4MS moieties in the PI segment[61] and causes a slightly increased glass-transition temperature. As recently reported, the isoprene and 4MS system revealed considerably more disparate reactivity ratios compared to the more common isoprene/styrene system, resulting in tapered BCPs with a steeper gradient.[61] Relying on this previous study, the focus of the present study was the preparation and characterization of UHMW BCPs based on the isoprene/4MS system. To characterize the overall composition and the content of 1,4-PI of the corresponding tapered BCPs, ^1H NMR spectroscopy was used (Figures S5−S7). As an example, the spectrum of PI_{7574}-*b*-$P4MS_{4951}$ is shown in Figure 2b, revealing both the signals for PI and P4MS at 5.18−4.69 and 7.10−6.19 ppm, respectively, which are in good agreement with expectation based on the monomer composition employed. The content of 1,4-PI was found to be in the range of 93−96 mol %, confirmed by the signal area at 4.70−5.20 ppm and is in good agreement with the literature.[62,67−69]

To sum up, SEC, DSC, and ^1H NMR spectroscopy measurements evidence that tapered UHMW BCPs are accessible via a convenient one-step anionic copolymerization. Although molar mass distributions are broadened with $Đ$ values for the polymers in the range of 1.34−1.56, the first evidence for microphase separation was obtained by DSC measurements, showing two distinct glass transitions. In the following, the morphologies of these novel UHMW BCPs will be further investigated with respect to their microphase separation in the bulk state.

Morphology of Tapered BCPs in the Bulk State. The focus of the present study is on the investigation of the structures formed by the one-step UHMW BCPs in the bulk state and their use as potential photonic film materials. Consequently, ordered domains with sizes in the range of visible light according to Bragg's law of diffraction are a fundamental prerequisite. Another key parameter is the difference of the refractive index of the underlying periodically aligned block domains. The morphologies of all prepared PI-*b*-P4MS within this study were investigated by TEM and SEM. For a better comparison and interpretation of the morphologies, all data on molar fraction (x), weight fraction (w), and volume fraction (Φ) obtained by ^1H NMR spectroscopy of the tapered BCPs are compiled in Table 3.

Table 3. Comparison of BCPs Used in This Study with Respect to Molar Ratio (x), Weight Ratio (w), and Volume Ratio (Φ)

	polymer	$x_{PI/P4MS}$	$w_{PI/P4MS}$	$\Phi_{PI/P4MS}$
1	PI_{7574}-*b*-$P4MS_{4951}$[a]	60/40	47/53	50/50
2	PI_{9118}-*b*-$P4MS_{5364}$[a]	63/37	49/51	53/47
3	PI_{20011}-*b*-$P4MS_{3798}$[a]	84/16	75/25	78/22
4	PI_{25060}-*b*-$P4MS_{2758}$[a]	90/10	84/16	86/14

[a]Volume fractions of the block segments were estimated using the densities 0.91[70] and 1.04[71] g cm^{-1} for PI and P4MS, respectively.

First, the morphologies of BCPs having equal compositions with respect to the volume fraction for PI and P4MS were investigated by TEM and SEM measurements, respectively. For this purpose, the PI-*b*-P4MS samples were solution-cast from chloroform ($CHCl_3$) or THF for film preparation in the bulk state with a diameter of 1.5 cm and a thickness of 1 mm. (cf. Experimental Section). To avoid undesired cross-linking reactions or degradation of the unsaturated PI segments, solvent annealing for film preparation was carried out at moderate temperatures, as described in the following. The solvent-cast UHMW BCP films were exposed to a solvent atmosphere of $CHCl_3$ or THF in a desiccator for 1 week, followed by drying in vacuum at RT. For characterization of the

DOI: 10.1021/acsami.8b02848
ACS Appl. Mater. Interfaces 2018, 10, 18202−18212

BCP morphology in the bulk state, the as-prepared films were microtomed from surface to surface (more details are given in Figure S11) at −80 °C into thin slices of 50−70 nm thickness. The collected ultrathin sections were subsequently stained with osmium tetroxide, OsO_4, for selective staining of the PI domains, followed by investigation by TEM measurements.[72] Because of the high electron density after contrasting with OsO_4, the darker appearing domains belong to the PI-containing block segment, while the lighter domains correspond to P4MS. In Figure 3, TEM images of samples PI_{7574}-*b*-$P4MS_{4951}$ (a) and PI_{9118}-*b*-$P4MS_{5364}$ (b) solution cast from $CHCl_3$ after staining are given, clearly revealing a lamellar morphology with large lamellar thickness.

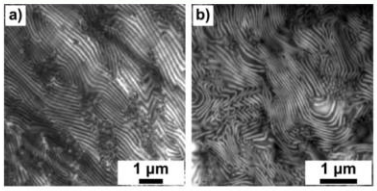

Figure 3. TEM micrographs of the polymers PI_{7574}-*b*-$P4MS_{4951}$ (a) and PI_{9118}-*b*-$P4MS_{5364}$ (b) after ultramicrotoming and contrasting with OsO_4. The bulk UHMW BCP films were solution-cast from $CHCl_3$. Thin sections were obtained after ultramicrotoming at −80 °C. Scale bars correspond to 1 μm.

According to the determined compositions for the polymers given in Table 3, these findings were in excellent agreement with expectation because of the approximately equal volume fractions of PI and P4MS. In the case of PI_{7574}-*b*-$P4MS_{4951}$, the bulk morphology featured a lamellar period, that is, a distance of two lamellae, of about 196 ± 27 nm. The second tapered UHMW BCP sample (PI_{9118}-*b*-$P4MS_{5364}$) revealed lamellar periods of 185 ± 20 nm.

To investigate the influence of the solvent employed for the casting procedure on the microphase separation of UHMW BCPs, films of PI_{7574}-*b*-$P4MS_{4951}$ were solution-cast from THF, which is more selective for P4MS than for PI. This corresponds to the Hansen solubility parameters δ of 19.4, 19.0, 19.4, and 16.65 $MPa^{1/2}$ for THF, $CHCl_3$, P4MS, and PI, respectively.[73,74] The corresponding TEM images after staining with OsO_4 are shown in Figure 4, revealing a lamellar nanostructure. While the morphology and the lamellar period of 185 ± 15 nm are the same as in the case of the chloroform-cast film (Figure 3), the lamellae of the THF-cast film obviously showed increased order in comparison with the chloroform-cast film, which we attribute to the more pronounced selectivity of THF for the P4MS block segment. The UHMW BCP films were prepared as film disks with a diameter of 1.5 cm having film thicknesses of 1−1.5 mm. No correlation between the film thickness and the intensity of the reflection color was observed.

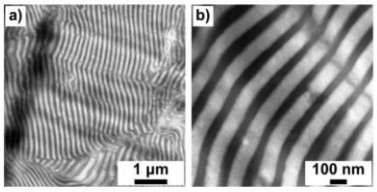

Figure 4. TEM micrographs of the polymer PI_{7574}-*b*-$P4MS_{4951}$ after ultramicrotoming and contrasting with OsO_4. The bulk UHMW BCP film was solution-cast from THF. Thin sections were obtained after ultramicrotoming at −80 °C. Scale bars correspond to 1 μm (a) and 100 nm (b).

To gain an insight into the self-assembled structures over larger BCP film areas, additional SEM measurements of the corresponding films were carried out. For this purpose, the solvent-cast films were frozen in liquid nitrogen, followed by freeze-fracturing (cf. Experimental Section and Figure S11). In Figure 5, SEM images of the cross section for chloroform-cast films of PI_{7574}-*b*-$P4MS_{4951}$ (a,b) and PI_{9118}-*b*-$P4MS_{5364}$ (c,d) are shown, again revealing a lamellar morphology. The lamellar period was determined from the SEM images to be 183 ± 27 nm for PI_{7574}-*b*-$P4MS_{4951}$ and of 193 ± 26 nm for PI_{9118}-*b*-$P4MS_{5364}$, which is in good accordance with the lamellar periods determined by TEM measurements (196 ± 27 and 185 ± 20 nm, respectively).

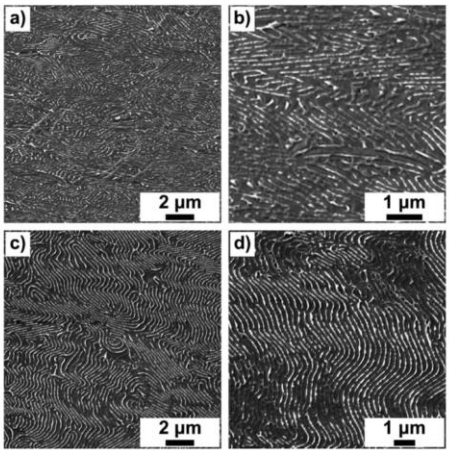

Figure 5. SEM micrographs of the freeze-fractured BCP films for the polymers PI_{7574}-*b*-$P4MS_{4951}$ (a,b) and PI_{9118}-*b*-$P4MS_{5364}$ (c,d). The bulk UHMW BCP films were solution-cast from $CHCl_3$ prior to SEM sample preparation. Scale bars correspond to 2 (a,c) and 1 μm (b,d).

In Figure 6, SEM measurements of the cross section of PI_{7574}-*b*-$P4MS_{4951}$ for the solution-cast film from THF are given. Microphase separation of the corresponding BCPs revealed a lamellar morphology with a lamellar period of 184 ± 16 nm according to the TEM measurements. In contrast to the chloroform-cast film (Figure 5a), a more uniform lamellar morphology in the bulk state can be observed over rather large film areas. While high order of the chloroform-cast film was observed only over a range of a few micrometers, the periodic order in the case of the THF-cast film was observed in a range of 90 × 120 μm (Figure S12). Moreover, the lamellar domains are almost oriented parallel to the surface, which is schematically shown in Figure 6c, not only at the surface itself but also

DOI: 10.1021/acsami.8b02848
ACS Appl. Mater. Interfaces 2018, 10, 18202−18212

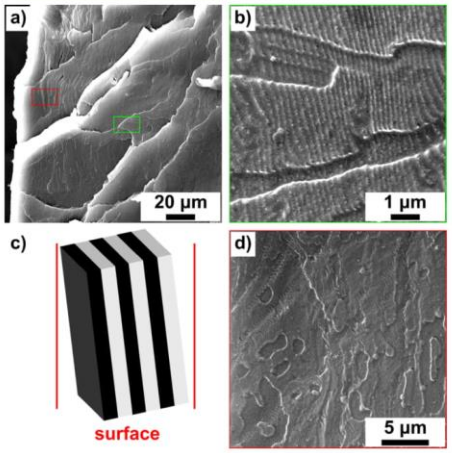

Figure 6. SEM micrographs of the bulk morphology characterization of the cross section for the polymer PI_{7574}-*b*-$P4MS_{4951}$. Micrograph (b) is a zoom-in image of the green box and (d) corresponds to the red box in the overview SEM micrograph (a). The bulk film was solution-cast from THF and freeze-fractured. Scale bars correspond to 20 (a), 1 (b), and 5 μm (d). The schematic illustration (c) shows the orientation of the lamellar domains in relation to the surface, which is indicated by a red line.

inside the bulk film, which is shown in Figure 6b,d. Thus, film casting from block-selective solvents, that is, THF (for P4MS), revealed better order of the nanostructure for the UHMW BCPs consisting of PI and P4MS than in nonselective solvents. Further investigation regarding the self-assembly process as a function of time and various solvents will be part of a future work.

In the following, the morphology of PI-*b*-P4MS BCPs having a significantly different volume ratio of the underlying block segments, that is, a volume ratio of 78 and 86% of PI for PI_{20011}-*b*-$P4MS_{3798}$ and PI_{25060}-*b*-$P4MS_{2758}$, respectively, was investigated by TEM and SEM measurements (samples 3 and 4 in Tables 2 and 3, respectively). The samples were prepared in the same way as described for the symmetric UHMW BCPs. In Figure 7, the corresponding TEM images of PI_{25060}-*b*-$P4MS_{2758}$ are shown, revealing a spherical morphology with an average diameter for the P4MS spheres of approximately 97 ± 10 nm.

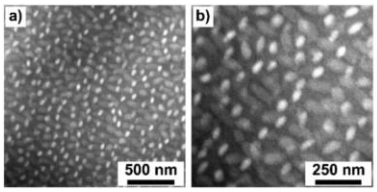

Figure 7. TEM micrographs of the bulk morphology characterization for the polymer PI_{25060}-*b*-$P4MS_{2758}$. Thin sections ultramicrotomed at −80 °C at 50−70 nm thickness. PI domains were stained with OsO_4. Scale bars correspond to 500 (a) and 250 nm (b).

The darker matrix can be assigned to the PI block segment because of the selective staining protocol for the unsaturated block with OsO_4 (see above).[72]

To gain deeper insight into the bulk morphology of PI_{25060}-*b*-$P4MS_{2758}$, the BCP was additionally investigated by TEM in a dark-field mode (STEM) and EDS (Figure S13). The bright matrix is due to the PI-rich block, as evidenced by the increased content of osmium in contrast to the dark appearing spheres, which is also nicely reflected in the corresponding EDS spectra (Figure S13b). However, an exact value for the core-to-core distance could not be determined from the TEM images, as the spherical domains appear to be distorted. This can be explained by the fact that the spherical domains having a size of 97 ± 10 nm are much larger than the microtomed thin slices, which are approximately 50−70 nm in size. For this reason, the spherical domains were cut into round flexible disks. During ultramicrotoming of the bulk polymer films with spherical domains inside a soft matrix, the probability for perfect cutting of spherical objects is reduced, which is a known problem for spherical domains during sample preparation by using ultramicrotomy.[75] As a result, only the largest round slices correspond to the true size of the spherical domains, while outer regions of the cut domains appear smaller (upper or lower part of the spheres). Moreover, as can be concluded from the TEM images, deformation of the spherical domains occurred during sample cutting by ultramicrotomy. Nevertheless, the obtained TEM images confirm microphase separation into rather large spherical domains for the investigated UHMW BCPs.

SEM measurements of the UHMW BCPs PI_{20011}-*b*-$P4MS_{3798}$ and PI_{25060}-*b*-$P4MS_{2758}$ were carried out and given in Figure 8. Interestingly, both investigated polymer samples revealed a mixture of spherical domains and elongated spherical domains stemming from freeze-fracturing. PI_{25060}-*b*-$P4MS_{2758}$ (Figure 8c,d) revealed a spherical morphology with an average sphere

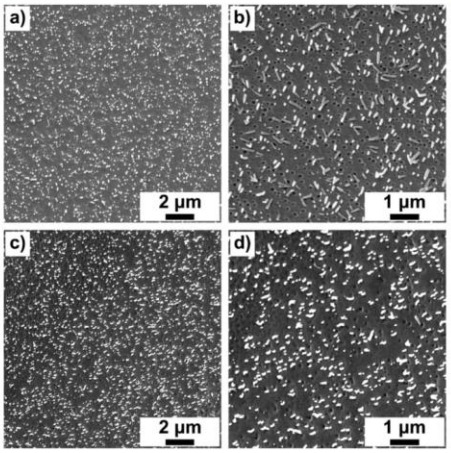

Figure 8. Cross-sectional SEM micrographs of the polymers PI_{20011}-*b*-$P4MS_{3798}$ (a,b) and PI_{25060}-*b*-$P4MS_{2758}$ (c,d). Bulk UHMW BCP films were solution-cast from $CHCl_3$ followed by freeze-fracturing. Scale bars correspond to 2 (a,c) and 1 μm (b,d).

DOI: 10.1021/acsami.8b02848
ACS Appl. Mater. Interfaces 2018, 10, 18202−18212

diameter of about 97 ± 10 nm, while PI_{20011}-*b*-$P4MS_{3798}$ (Figure 8a,b) showed spherical objects of 122 ± 19 nm in size. In summary, TEM images and SEM images for these UHMW BCP samples are similar, showing disordered spherical domains of uniform size.

Optical Properties of the Tapered BCPs. The investigated bulk morphologies as obtained by TEM and SEM measurements for the UHMW BCPs consisting of PI and P4MS proved the existence of periodic, microphase-separated domains, that is, ordered lamellar and disordered spherical structures at the nanoscale. For better comparison, the values for the domain sizes of all samples are compiled in Table 4.

Table 4. Domain Sizes for Lamellar Periods *d* as well as Spherical Diameters *d* and Standard Deviations *σ* Derived from TEM and SEM Measurements

	polymer	d_{TEM} (nm)	σ_{TEM} (nm)	d_{SEM} (nm)	σ_{SEM} (nm)	
1	PI_{7574}-*b*-$P4MS_{4951}$	196[a]	27	183[a]	27	L
		185[b]	15	184[b]	16	L
2	PI_{9118}-*b*-$P4MS_{5364}$	185[a]	20	193[a]	26	L
3	PI_{20011}-*b*-$P4MS_{3798}$			122	19	S
4	PI_{25060}-*b*-$P4MS_{2758}$	97	10	97	12	S

[a]Film was solution-cast from chloroform. [b]Film was solution-cast from THF. The last column gives the corresponding observed morphology from the SEM and TEM images: L (lamellae) and S (spheres in a matrix).

The sizes of the nanodomains determined by TEM were in accordance with the values for the domain sizes obtained by SEM measurements. Self-assembly of these UHMW PI-*b*-P4MS samples leads to microphase-separated domains with ordered domain sizes larger than 100 nm in the bulk state of the BCP films. Because of the size of the underlying BCP domains and according to Bragg's law of diffraction, the BCP films are capable of interacting with visible light. Therefore, excellent structural colors can be observed with the naked eye simply by drying the diluted BCP solutions as shown in Figure 9. All bulk films have a diameter of 1.5 cm and a thickness of 1 mm. Because of the bulk character of these films, there is no correlation between the film thickness and the interaction with light. Because already a few ordered layers suffice to generate structural colors, there is only a dependence of the reflection color on the film thickness in very thin films of our samples but not in bulk films as the ones used in this work.

Freestanding BCP films of PI_{9118}-*b*-$P4MS_{5364}$ (Figure 9d–f) and PI_{7574}-*b*-$P4MS_{4951}$ (Figure 9a–c,g) featured a lamellar morphology, and angle-dependent structural colors could be observed. Because of the increased order over rather larger film areas (Figure 6) and the uniform orientation of the lamellar domains parallel to the surface through the whole film, the THF-cast bulk film of the polymer PI_{7574}-*b*-$P4MS_{4951}$ featured even more brilliant structural colors (Figure 9a–c) in contrast to the chloroform-cast film (Figure 9g). While the BCP films with lamellar morphologies revealed angle-dependent structural colors, the films with spherical nanodomains revealed angle-independent blue structural colors (shown in Figure 9h) for PI_{20011}-*b*-$P4MS_{3798}$ and for PI_{25060}-*b*-$P4MS_{2758}$ (Figure 9i). All shown photonic bulk films were self-assembled by solvent annealing for 1 week. Indeed, already strong reflection colors could be observed after 2–3 days of solvent annealing, albeit

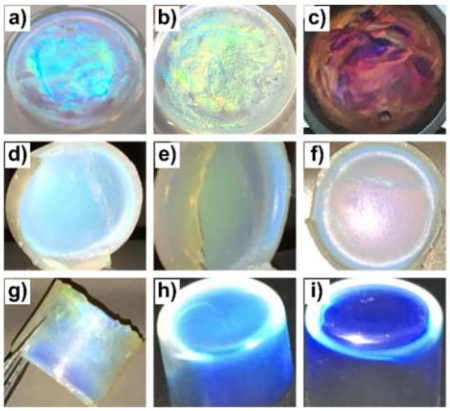

Figure 9. (a–c) Angle-dependent images of the THF-cast bulk UHMW BCP film of sample 1, PI_{7574}-*b*-$P4MS_{4951}$. (d–f) Angle-dependent images of the chloroform-cast bulk film of PI_{9118}-*b*-$P4MS_{5364}$. (g) Image of the chloroform-cast bulk film of PI_{7574}-*b*-$P4MS_{4951}$. (h) Image of the bulk film of PI_{20011}-*b*-$P4MS_{3798}$. (i) Image of the bulk film of PI_{25060}-*b*-$P4MS_{2758}$.

they can be further improved by prolonging the annealing times up to 6–7 days.

For further studies of the optical properties, the structural colors of the freestanding bulk BCP films were measured by UV/vis spectroscopy in the range of 350–800 nm. The corresponding UV/vis spectra of the THF-cast film of the polymer PI_{7574}-*b*-$P4MS_{4951}$ (sample 1, Table 2) are given in Figure 10. First, the reflectance spectrum at an incidence angle

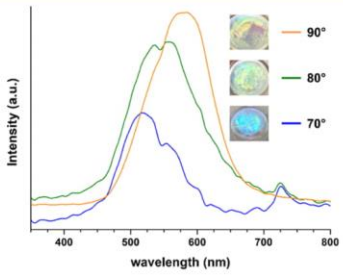

Figure 10. UV/vis spectra of the PI_{7574}-*b*-$P4MS_{4951}$ (sample 1) bulk film measured at a 90° (orange line), 80° (green line), and 70° (blue line) angle. The film was solution-cast from THF.

of 90° was measured by UV/vis spectroscopy, showing a reflection maximum at a wavelength of 580 nm. As shown in Figure 10, the film featured a yellow to orange reflection color in the bulk state at an angle of 90°, which is in good agreement with the measured reflection maximum of 580 nm.

The reflection colors of visible light can be described by Bragg's law of diffraction with the wavelength λ, the incidence angle α, the average refractive index n, and the distance d between parallel lattice planes.

DOI: 10.1021/acsami.8b02848
ACS Appl. Mater. Interfaces 2018, 10, 18202–18212

$$\lambda = 2dn \sin(\alpha)$$

As we can estimate by Bragg's law with an average refractive index n of 1.54 (n_{PI} = 1.51[76] and n_{P4MS} = 1.57[77]), a domain spacing of 188 nm is required for the reflection of visible light with a wavelength of 580 nm at an incident angle of 90°. This condition was fulfilled for the polymer PI_{7574}-*b*-$P4MS_{4951}$ and is in good agreement with the lamellar periods of 185 ± 15 and 184 ± 16 nm, as observed by TEM and SEM measurements, respectively, for the corresponding THF-cast bulk film (Figures 4 and 6). Additional angle-dependent UV/vis spectroscopy measurements were carried out with a goniometer, revealing the reflectance spectra at different viewing angles that are also displayed in Figure 10. By decreasing the incidence angle from 90° over 80° to 70°, the reflection peak followed a blue shift from 580 over 560 up to 520 nm, as shown in the small photographs of the bulk BCP films in Figure 10. These results are also in accordance with the law of Bragg. In summary for the symmetrical BCPs, the UHMW BCPs featuring a lamellar morphology (PI_{9118}-*b*-$P4MS_{5364}$ and PI_{7574}-*b*-$P4MS_{4951}$) revealed excellent angle-dependent reflection colors in the bulk state because of Bragg diffraction (cf. Figure 1b).

Finally, the structural colors of the BCPs exhibiting spherical nanodomains in the bulk state were investigated. The corresponding UV/vis spectra for PI_{20011}-*b*-$P4MS_{3798}$ and PI_{25060}-*b*-$P4MS_{2758}$ are given in Figure 11.

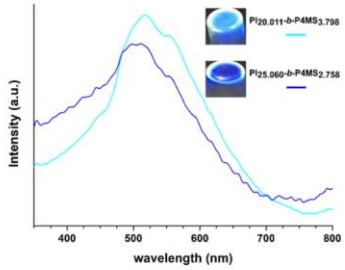

Figure 11. UV/vis spectra of PI_{20011}-*b*-$P4MS_{3798}$ (cyan blue line) and PI_{25060}-*b*-$P4MS_{2758}$ (blue line) bulk films measured at a 45° angle.

As a result of the disorder of the spherical morphology, no angle-dependent reflection color as observed for the lamellar morphology could be recorded at an incidence angle of 90°. Therefore, we measured the UV/vis spectra at an incidence angle of 45°, revealing a peak maximum at a wavelength of 520 nm for PI_{20011}-*b*-$P4MS_{3798}$ and of 510 nm for PI_{25060}-*b*-$P4MS_{2758}$, which is in accordance with the clearly visible blue structural color of the corresponding bulk films (photographs in Figure 11). While the reflection colors for the lamellar morphologies stemmed from classical Bragg diffraction, diffuse scattering of the spherical nanoobjects was the reason for the observed blue color. The spherical domains having a size of 97 and 122 nm act as single scattering centers for the visible light causing a blue structural color, which is also known as Lorenz–Mie-scattering.[78,79]

■ CONCLUSIONS

We have introduced an efficient route for the preparation of UHMW PI-*b*-P4MS tapered BCPs via statistical anionic copolymerization in Cy in a single synthetic step. We take advantage of the highly disparate copolymerization parameters for the isoprene/4MS system in apolar solvents. Molar masses were in the range of 1101–2033 kg mol^{-1}, as determined by SEC measurements. The successful formation of a tapered BCP structure was proven by ^{1}H NMR spectroscopy and DSC measurements, yielding two discrete glass-transition temperatures at −50 °C, which can be assigned to the PI segment, and at 117 °C belonging to the P4MS block segment. Microphase separation and the formation of nanodomains on the order of 100–200 nm in the bulk state were observed for the UHMW BCPs after solvent annealing by TEM measurements after block-selective staining of the PI segment with osmium tetroxide. To study the structure formation of freestanding films in the bulk state in more detail, additional SEM measurements were carried out. In the case of PI_{9118}-*b*-$P4MS_{5364}$ and PI_{7574}-*b*-$P4MS_{4951}$ (Φ_{PI} is 53 and 50%, respectively), lamellar morphologies with lamellar periods of 184–193 nm were observed, while PI_{20011}-*b*-$P4MS_{3798}$ and PI_{25060}-*b*-$P4MS_{2758}$ (Φ_{PI} is 78 and 86%, respectively) revealed spherical nanodomains on the order of 122 and 97 nm, respectively. Well-ordered homogeneous lamellar morphologies were obtained over rather large film areas of 90 × 120 μm featuring intense iridescent structural colors. In contrast to the lamellar nanostructures, the order for spherical domains was found to be lower, yielding angle-independent blue colors because of interaction of single scattering centers with visible light. Photonic properties of the bulk films were investigated by UV/vis measurements, revealing angle-dependent reflection colors because of Bragg diffraction for PI_{7574}-*b*-$P4MS_{4951}$. When decreasing the incidence angle from 90° over 80° to 70°, the reflection peak exhibits a blue shift from 580 nm over 560 up to 520 nm. While the reflection colors for the lamellar morphologies were caused by Bragg diffraction, diffuse scattering of the spherical nanostructures was the mechanism for appearance of the bluish color in the case of the spherical nanodomains. The herein established route for convenient UHMW synthesis of BCPs and film formation thereof enabled tuning of the structural colors of the BCP nanostructures by varying the composition and molecular weight of the tapered UHMW BCPs. Furthermore, these BCPs offer the option to insert functional moieties to generate stimuli-responsive photonic materials via postmodification in the future.[68,69,80]

To sum up, the presented anionic one-step statistical copolymerization represents a valuable strategy for the preparation of UHMW BCP-based photonic materials in the bulk state. In contrast to previously reported photonic structures based on linear BCPs, here, a nonconventional synthetic one-step approach for the generation of UHMW BCPs is reported, rendering additional synthesis steps such as postmodification or change of the polymerization mechanism unnecessary. Furthermore, the herein presented one-pot BCPs feature excellent photonic properties already in the bulk state, despite the absence of solvents, additional swelling of one or both block domains, or the addition of salts or homopolymers. Application of the materials is envisaged as dye- and pigment-free colorants, optical actuators, and switches as well as smart photonic gels.

■ ASSOCIATED CONTENT

Supporting Information

The Supporting Information is available free of charge on the ACS Publications website at DOI: 10.1021/acsami.8b02848.

DOI: 10.1021/acsami.8b02848
ACS Appl. Mater. Interfaces 2018, 10, 18202–18212

Additional data on the anionic polymerization of PI-*b*-P4MS, SEC and DSC measurements for BCPs, ^{1}H NMR spectra of PI-*b*-P4MS, additional SEM measurements of PI_{7574}-*b*-$P4MS_{4951}$ bulk films, schematic illustration for cutting direction, and STEM and corresponding EDS measurements of PI_{25060}-*b*-$P4MS_{2758}$ (PDF)

AUTHOR INFORMATION

Corresponding Author

*E-mail: M.Gallei@MC.tu-darmstadt.de.

ORCID

Holger Frey: 0000-0002-9916-3103

Markus Gallei: 0000-0002-3740-5197

Notes

The authors declare no competing financial interest.

ACKNOWLEDGMENTS

The authors acknowledge the German Research Foundation (DFG GA 2169/1-1) and the "Verband der chemischen Industrie e.V." (VCI) for the financial support of this work. The authors owe Prof. Bernd Stühn (TU Darmstadt, Institute of Condensed Matter Physics) a debt of gratitude for kind discussions. The authors thank Lilia Proskurjakov for help with anionic polymerization procedures and Sebastian Schöttner for STEM and EDS measurements.

REFERENCES

(1) Tadepalli, S.; Slocik, J. M.; Gupta, M. K.; Naik, R. R.; Singamaneni, S. Bio-Optics and Bio-Inspired Optical Materials. *Chem. Rev.* **2017**, *117*, 12705−12763.

(2) Zhao, Y.; Xie, Z.; Gu, H.; Zhu, C.; Gu, Z. Bio-inspired variable structural color materials. *Chem. Soc. Rev.* **2012**, *41*, 3297−3317.

(3) Dumanli, A. G.; Savin, T. Recent advances in the biomimicry of structural colours. *Chem. Soc. Rev.* **2016**, *45*, 6698−6724.

(4) Hynninen, A.-P.; Thijssen, J. H. J.; Vermolen, E. C. M.; Dijkstra, M.; van Blaaderen, A. Self-assembly route for photonic crystals with a bandgap in the visible region. *Nat. Mater.* **2007**, *6*, 202−205.

(5) De La Rue, R. Photonic Crystals: Microassembly in 3D. *Nat. Mater.* **2003**, *2*, 74−76.

(6) González-Urbina, L.; Baert, K.; Kolaric, B.; Pérez-Moreno, J.; Clays, K. Linear and nonlinear optical properties of colloidal photonic crystals. *Chem. Rev.* **2012**, *112*, 2268−2285.

(7) Comoretto, D. *Organic and Hybrid Photonic Crystals*, 1st ed.; Springer International, 2015.

(8) von Freymann, G.; Kitaev, V.; Lotsch, B. V.; Ozin, G. A. Bottom-up assembly of photonic crystals. *Chem. Soc. Rev.* **2013**, *42*, 2528−2554.

(9) Takeoka, Y. Stimuli-responsive opals: colloidal crystals and colloidal amorphous arrays for use in functional structurally colored materials. *J. Mater. Chem. C* **2013**, *1*, 6059−6074.

(10) Li, F.; Josephson, D. P.; Stein, A. Colloidal assembly: the road from particles to colloidal molecules and crystals. *Angew. Chem., Int. Ed.* **2011**, *50*, 360−388.

(11) Galisteo-López, J. F.; Ibisate, M.; Sapienza, R.; Froufe-Pérez, L. S.; Blanco, Á.; López, C. Self-assembled photonic structures. *Adv. Mater.* **2011**, *23*, 30−69.

(12) Gallei, M. Functional Polymer Opals and Porous Materials by Shear-Induced Assembly of Tailor-Made Particles. *Macromol. Rapid Commun.* **2017**, *39*, 1700648.

(13) Yablonovitch, E. Inhibited Spontaneous Emission in Solid-State Physics and Electronics. *Phys. Rev. Lett.* **1987**, *58*, 2059−2062.

(14) Stuart, M. A. C.; Huck, W. T. S.; Genzer, J.; Müller, M.; Ober, C.; Stamm, M.; Sukhorukov, G. B.; Szleifer, I.; Tsukruk, V. V.; Urban, M.; Winnik, F.; Zauscher, S.; luzinov, I.; Minko, S. Emerging applications of stimuli-responsive polymer materials. *Nat. Mater.* **2010**, *9*, 101−113.

(15) Ge, J.; Yin, Y. Responsive photonic crystals. *Angew. Chem., Int. Ed. Engl.* **2011**, *50*, 1492−1522.

(16) Arsenault, A. C.; Míguez, H.; Kitaev, V.; Ozin, G. A.; Manners, I. A Polychromic, Fast Response Metallopolymer Gel Photonic Crystal with Solvent and Redox Tunability: A Step towards Photonic Ink (P-Ink). *Adv. Mater.* **2003**, *15*, 503−507.

(17) Schäfer, C. G.; Gallei, M.; Zahn, J. T.; Engelhardt, J.; Hellmann, G. P.; Rehahn, M. Reversible Light-, Thermo-, and Mechano-Responsive Elastomeric Polymer Opal Films. *Chem. Mater.* **2013**, *25*, 2309−2318.

(18) Scheid, D.; Lederle, C.; Vowinkel, S.; Schäfer, C. G.; Stühn, B.; Gallei, M. Redox- and mechano-chromic response of metallopolymer-based elastomeric colloidal crystal films. *J. Mater. Chem. C* **2014**, *2*, 2583−2590.

(19) Lee, J.-H.; Koh, C. Y.; Singer, J. P.; Jeon, S.-J.; Maldovan, M.; Stein, O.; Thomas, E. L. 25th anniversary article: ordered polymer structures for the engineering of photons and phonons. *Adv. Mater.* **2014**, *26*, 532−569.

(20) Paquet, C.; Kumacheva, E. Nanostructured polymers for photonics. *Mater. Today* **2008**, *11*, 48−56.

(21) Yu, Y.-G.; Chae, C.-G.; Kim, M.-J.; Seo, H.-B.; Grubbs, R. H.; Lee, J.-S. Precise Synthesis of Bottlebrush Block Copolymers from ω-End-Norbornyl Polystyrene and Poly(4-tert-butoxystyrene) via Living Anionic Polymerization and Ring-Opening Metathesis Polymerization. *Macromolecules* **2018**, *51*, 447.

(22) Liberman-Martin, A. L.; Chu, C. K.; Grubbs, R. H. Application of Bottlebrush Block Copolymers as Photonic Crystals. *Macromol. Rapid Commun.* **2017**, *38*, 1700058.

(23) Miyake, G. M.; Piunova, V. A.; Weitekamp, R. A.; Grubbs, R. H. Precisely tunable photonic crystals from rapidly self-assembling brush block copolymer blends. *Angew. Chem., Int. Ed.* **2012**, *51*, 11246−11248.

(24) Miyake, G. M.; Weitekamp, R. A.; Piunova, V. A.; Grubbs, R. H. Synthesis of isocyanate-based brush block copolymers and their rapid self-assembly to infrared-reflecting photonic crystals. *J. Am. Chem. Soc.* **2012**, *134*, 14249−14254.

(25) Sveinbjornsson, B. R.; Weitekamp, R. A.; Miyake, G. M.; Xia, Y.; Atwater, H. A.; Grubbs, R. H. Rapid self-assembly of brush block copolymers to photonic crystals. *Proc. Natl. Acad. Sci. U.S.A.* **2012**, *109*, 14332−14336.

(26) Piunova, V. A.; Miyake, G. M.; Daeffler, C. S.; Weitekamp, R. A.; Grubbs, R. H. Highly ordered dielectric mirrors via the self-assembly of dendronized block copolymers. *J. Am. Chem. Soc.* **2013**, *135*, 15609−15616.

(27) Schacher, F. H.; Rupar, P. A.; Manners, I. Functional Block Copolymers: Nanostructured Materials with Emerging Applications. *Angew. Chem., Int. Ed.* **2012**, *51*, 7898−7921.

(28) Kim, J. K.; Yang, S. Y.; Lee, Y.; Kim, Y. Functional nanomaterials based on block copolymer self-assembly. *Prog. Polym. Sci.* **2010**, *35*, 1325−1349.

(29) Kim, H.-C.; Park, S.-M.; Hinsberg, W. D. Block Copolymer Based Nanostructures: Materials, Processes, and Applications to Electronics. *Chem. Rev.* **2010**, *110*, 146−177.

(30) Lazzari, M.; Liu, G.; Lecommandoux, S. *Block Copolymers in Nanoscience*; Wiley-VCH: Weinheim, 2006.

(31) Staff, R. H.; Gallei, M.; Landfester, K.; Crespy, D. Hydrophobic Nanocontainers for Stimulus-Selective Release in Aqueous Environments. *Macromolecules* **2014**, *47*, 4876−4883.

(32) Schöttner, S.; Schaffrath, H.-J.; Gallei, M. Poly(2-hydroxyethyl methacrylate)-Based Amphiphilic Block Copolymers for High Water Flux Membranes and Ceramic Templates. *Macromolecules* **2016**, *49*, 7286−7295.

(33) Nunes, S. P. Block Copolymer Membranes for Aqueous Solution Applications. *Macromolecules* **2016**, *49*, 2905−2916.

(34) Stefik, M.; Guldin, S.; Vignolini, S.; Wiesner, U.; Steiner, U. Block copolymer self-assembly for nanophotonics. *Chem. Soc. Rev.* **2015**, *44*, 5076−5091.

DOI: 10.1021/acsami.8b02848
ACS Appl. Mater. Interfaces 2018, 10, 18202−18212

(35) Lim, H. S.; Lee, J.-H.; Walish, J. J.; Thomas, E. L. Dynamic Swelling of Tunable Full-Color Block Copolymer Photonic Gels via Counterion Exchange. *ACS Nano* **2012**, *6*, 8933−8939.
(36) Sun, X.; Zhang, J.; Lu, X.; Fang, X.; Peng, H. Mechanochromic photonic-crystal fibers based on continuous sheets of aligned carbon nanotubes. *Angew. Chem., Int. Ed.* **2015**, *54*, 3630−3634.
(37) Chan, E. P.; Walish, J. J.; Urbas, A. M.; Thomas, E. L. Mechanochromic photonic gels. *Adv. Mater.* **2013**, *25*, 3934−3947.
(38) Fan, Y.; Walish, J. J.; Tang, S.; Olsen, B. D.; Thomas, E. L. Defects, Solvent Quality, and Photonic Response in Lamellar Block Copolymer Gels. *Macromolecules* **2014**, *47*, 1130−1136.
(39) Lee, W.; Yoon, J.; Thomas, E. L.; Lee, H. Dynamic Changes in Structural Color of a Lamellar Block Copolymer Photonic Gel during Solvent Evaporation. *Macromolecules* **2013**, *46*, 6528−6532.
(40) Park, T. J.; Hwang, S. K.; Park, S.; Cho, S. H.; Park, T. H.; Jeong, B.; Kang, H. S.; Ryu, D. Y.; Huh, J.; Thomas, E. L.; Park, C. Electrically Tunable Soft-Solid Block Copolymer Structural Color. *ACS Nano* **2015**, *9*, 12158−12167.
(41) Walish, J. J.; Kang, Y.; Mickiewicz, R. A.; Thomas, E. L. Bioinspired Electrochemically Tunable Block Copolymer Full Color Pixels. *Adv. Mater.* **2009**, *21*, 3078−3081.
(42) Kang, H. S.; Lee, J.; Cho, S. M.; Park, T. H.; Kim, M. J.; Park, C.; Lee, S. W.; Kim, K. L.; Ryu, D. Y.; Huh, J.; Thomas, E. L.; Park, C. Printable and Rewritable Full Block Copolymer Structural Color. *Adv. Mater.* **2017**, *29*, 1700084.
(43) Ahn, Y.; Kim, E.; Hyon, J.; Kang, C.; Kang, Y. Photoresponsive block copolymer photonic gels with widely tunable photosensitivity by counter-ions. *Adv. Mater.* **2012**, *24*, OP127.
(44) Hustad, P. D.; Marchand, G. R.; Garcia-Meitin, E. I.; Roberts, P. L.; Weinhold, J. D. Photonic Polyethylene from Self-Assembled Mesophases of Polydisperse Olefin Block Copolymers. *Macromolecules* **2009**, *42*, 3788−3794.
(45) Boyle, B. M.; French, T. A.; Pearson, R. M.; McCarthy, B. G.; Miyake, G. M. Structural Color for Additive Manufacturing: 3D-Printed Photonic Crystals from Block Copolymers. *ACS Nano* **2017**, *11*, 3052−3058.
(46) Yoon, J.; Lee, W.; Thomas, E. L. Optically Pumped Surface-Emitting Lasing Using Self-Assembled Block-Copolymer-Distributed Bragg Reflectors. *Nano Lett.* **2006**, *6*, 2211−2214.
(47) Yoon, J.; Lee, W.; Thomas, E. L. Highly Oriented Thin-Film Microdomain Patterns of Ultrahigh Molecular Weight Block Copolymers via Directional Solidification of a Solvent. *Adv. Mater.* **2006**, *18*, 2691−2694.
(48) Song, D.-P.; Li, C.; Li, W.; Watkins, J. J. Block Copolymer Nanocomposites with High Refractive Index Contrast for One-Step Photonics. *ACS Nano* **2016**, *10*, 1216−1223.
(49) Song, D.-P.; Li, C.; Colella, N. S.; Lu, X.; Lee, J.-H.; Watkins, J. J. Thermally Tunable Metallodielectric Photonic Crystals from the Self-Assembly of Brush Block Copolymers and Gold Nanoparticles. *Adv. Opt. Mater.* **2015**, *3*, 1169−1175.
(50) Huang, Y.; Zheng, Y.; Pribyl, J.; Benicewicz, B. C. A versatile approach to different colored photonic films generated from block copolymers and their conversion into polymer-grafted nanoplatelets. *J. Mater. Chem. C* **2017**, *5*, 9873−9878.
(51) Guldin, S.; Kolle, M.; Stefik, M.; Langford, R.; Eder, D.; Wiesner, U.; Steiner, U. Tunable mesoporous bragg reflectors based on block-copolymer self-assembly. *Adv. Mater.* **2011**, *23*, 3664−3668.
(52) Braunecker, W. A.; Matyjaszewski, K. Controlled/living radical polymerization: Features, developments, and perspectives. *Prog. Polym. Sci.* **2007**, *32*, 93−146.
(53) Boyer, C.; Corrigan, N. A.; Jung, K.; Nguyen, D.; Nguyen, T.-K.; Adnan, N. N. M.; Oliver, S.; Shanmugam, S.; Yeow, J. Copper-Mediated Living Radical Polymerization (Atom Transfer Radical Polymerization and Copper(0) Mediated Polymerization): From Fundamentals to Bioapplications. *Chem. Rev.* **2016**, *116*, 1803−1949.
(54) Keddie, D. J. A guide to the synthesis of block copolymers using reversible-addition fragmentation chain transfer (RAFT) polymerization. *Chem. Soc. Rev.* **2014**, *43*, 496−505.
(55) Ellison, C. J.; Mundra, M. K.; Torkelson, J. M. Impacts of Polystyrene Molecular Weight and Modification to the Repeat Unit Structure on the Glass Transition-Nanoconfinement Effect and the Cooperativity Length Scale. *Macromolecules* **2005**, *38*, 1767−1778.
(56) Motokawa, R.; Taniguchi, T.; Kumada, T.; Iida, Y.; Aoyagi, S.; Sasaki, Y.; Kohri, M.; Kishikawa, K. Photonic Crystals Fabricated by Block Copolymerization-Induced Microphase Separation. *Macromolecules* **2016**, *49*, 6041−6049.
(57) Mapas, J. K. D.; Thomay, T.; Cartwright, A. N.; Ilavsky, J.; Rzayev, J. Ultrahigh Molecular Weight Linear Block Copolymers: Rapid Access by Reversible-Deactivation Radical Polymerization and Self-Assembly into Large Domain Nanostructures. *Macromolecules* **2016**, *49*, 3733−3738.
(58) Grubbs, R. B.; Grubbs, R. H. 50th Anniversary Perspective: Living Polymerization—Emphasizing the Molecule in Macromolecules. *Macromolecules* **2017**, *50*, 6979−6997.
(59) Chiang, Y.-W.; Chou, C.-Y.; Wu, C.-S.; Lin, E.-L.; Yoon, J.; Thomas, E. L. Large-Area Block Copolymer Photonic Gel Films with Solvent-Evaporation-Induced Red- and Blue-Shift Reflective Bands. *Macromolecules* **2015**, *48*, 4004−4011.
(60) Urbas, A.; Sharp, R.; Fink, Y.; Thomas, E. L.; Xenidou, M.; Fetters, L. J. Tunable Block Copolymer/Homopolymer Photonic Crystals. *Adv. Mater.* **2000**, *12*, 812−814.
(61) Grune, E.; Johann, T.; Appold, M.; Wahlen, C.; Blankenburg, J.; Leibig, D.; Müller, A. H. E.; Gallei, M.; Frey, H. Tapered Block Copolymers with Narrow Taper: A Fundamental Study Reveals that one Methyl Group Makes the Difference. *Macromolecules* **2018**, *51*, 3527−3537.
(62) Gotro, J. T.; Graessley, W. W. Model hydrocarbon polymers: rheological properties of linear polyisoprenes and hydrogenated polyisoprenes. *Macromolecules* **1984**, *17*, 2767−2775.
(63) Widmaier, J. M.; Meyer, G. C. Glass Transition Temperature of Anionic Polyisoprene. *Macromolecules* **1981**, *14*, 450−452.
(64) Chikhaoui-Grioune, D.; Benaboura, A.; Jérome, R. Synthesis and characterization of novel vinyl copolymers containing N-vinyl-phthalimide: Comonomers reactivity ratios and thermal stability. *Eur. Polym. J.* **2007**, *43*, 3849−3855.
(65) Peinemann, K.-V.; Abetz, V.; Simon, P. F. W. *Nat. Mater.* **2007**, *6*, 992.
(66) Laforest, N.; Bas, C.; De Baerdemaeker, J.; Dauwe, C. Modeling the time and temperature dependence of the oPs formation probability in polystyrene and its derivatives. *J. Polym. Sci., Part B: Polym. Phys.* **2009**, *47*, 2063−2073.
(67) Worsfold, D. J.; Bywater, S. Anionic Polymerization of Isoprene. *Can. J. Chem.* **1964**, *42*, 2884−2892.
(68) Rüttiger, C.; Appold, M.; Didzoleit, H.; Eils, A.; Dietz, C.; Stark, R. W.; Stühn, B.; Gallei, M. Structure Formation of Metallopolymer-Grafted Block Copolymers. *Macromolecules* **2016**, *49*, 3415−3426.
(69) Appold, M.; Rüttiger, C.; Kuttich, B.; Stühn, B.; Gallei, M. Polyvinylpyridine-Grafted Block Copolymers by an Iterative All-Anionic Polymerization Strategy. *Macromol. Chem. Phys.* **2018**, *219*, 1700187.
(70) Wu, L.; Cochran, E. W.; Lodge, T. P.; Bates, F. S. Consequences of Block Number on the Order-Disorder Transition and Viscoelastic Properties of Linear (AB)n Multiblock Copolymers. *Macromolecules* **2004**, *37*, 3360−3368.
(71) Brandrup, J. I.; Edmund, E. A.; Grulke, H.; Abe, A.; Bloch, D. R. *Polymer Handbook*; John Wiley & Sons, 1999.
(72) Kato, K. Osmium Tetroxide Fixation of Rubber Latices. *J. Polym. Sci., Polym. Phys. Ed.* **1966**, *4*, 35−38.
(73) Mark, J. E. *Physical Properties of Polymers Handbook*; Springer, 2007.
(74) Yu, X.; Wang, X.; Wang, H.; Li, X.; Gao, J. Prediction of solubility parameters for polymers by a QSPR model. *QSAR Comb. Sci.* **2006**, *25*, 156−161.
(75) Gleinser, W.; Maier, D.; Schneider, M.; Weese, J.; Friedrich, C.; Honerkamp, J. Estimation of Sphere-Size Distributions in Two-Phase Polymeric Materials from Transmission Electron Microscopy Data. *J. Appl. Polym. Sci.* **1994**, *53*, 39−50.

DOI: 10.1021/acsami.8b02848
ACS Appl. Mater. Interfaces 2018, 10, 18202−18212

(76) Urbas, A.; Fink, Y.; Thomas, E. L. One-Dimensionally Periodic Dielectric Reflectors from Self-Assembled Block Copolymer-Homopolymer Blends. *Macromolecules* **1999**, *32*, 4748−4750.
(77) Jeon, S.-J.; Chiappelli, M. C.; Hayward, R. C. Photocrosslinkable Nanocomposite Multilayers for Responsive 1D Photonic Crystals. *Adv. Funct. Mater.* **2016**, *26*, 722−728.
(78) Retsch, M.; Schmelzeisen, M.; Butt, H.-J.; Thomas, E. L. Visible mie scattering in nonabsorbing hollow sphere powders. *Nano Lett.* **2011**, *11*, 1389−1394.
(79) Jia, L.; Thomas, E. L. Optical forces and optical torques on various materials arising from optical lattices in the Lorentz-Mie regime. *Phys. Rev. B: Condens. Matter Mater. Phys.* **2011**, *84*, 125128.
(80) Appold, M.; Mari, C.; Lederle, C.; Elbert, J.; Schmidt, C.; Ott, I.; Stühn, B.; Gasser, G.; Gallei, M. Multi-stimuli responsive block copolymers as a smart release platform for a polypyridyl ruthenium complex. *Polym. Chem.* **2017**, *8*, 890−900.

DOI: 10.1021/acsami.8b02848
ACS Appl. Mater. Interfaces 2018, 10, 18202−18212

A3 List of Publications

1. Grune, E.; Bareuther, J.; Blankenburg, J.; Appold, M.; Shaw, L.; Floudas, G.; Müller, A. H. E.; Hutchings, L. R.; Gallei, M.; Frey, H, "Towards bio-based tapered block copolymers: the behaviour of myrcene in the statistical anionic copolymerisation", *to be submitted.*

2. Grune, E.; Wahlen, C.; Appold, M.; Frey, H.; Floudas G., "Tapered multiblock copolymers based on isoprene and 4-methylstyrene: Does a steep gradient make a difference?", *to be submitted.*

3. Grune, E.; Appold, M.; Müller, A. H. E.; Gallei, M.; Frey, H., "Anionic Copolymerisation Enables the Scalable Synthesis of Alternating (AB) n Multiblock Copolymers with High Molecular Weight in n Steps", *ACS Macro Lett.* **2018**, 7, 807–810.

4. Grune, E.; Johann, T.; Appold, M.; Wahlen, C.; Blankenburg, J.; Leibig, D.; Müller, A. H. E.; Gallei, M.; Frey, H. One-Step Block Copolymer Synthesis versus Sequential Monomer Addition: A Fundamental Study Reveals That One Methyl Group Makes a Difference, *Macromolecules* **2018**, *51*, 3527–3537.

5. Appold, M.; Grune, E.; Frey, H.; Gallei, M. One-Step Anionic Copolymerisation Enables Formation of Linear Ultrahigh-Molecular-Weight Block Copolymer Films Featuring Vivid Structural Colors in the Bulk State, *ACS Applied Materials & Interfaces* **2018**, *10*, 18202–18212.

6. Rieger, E.; Blankenburg, J.; Grune, E.; Wagner, M.; Landfester, K.; Wurm, F. R. Controlling the Polymer Microstructure in Anionic Polymerization by Compartmentalization. *Angew. Chemie Int. Ed.* **2018**, *57*, 2483–2487.

7. Leibig, D.; Morsbach, J.; Grune, E.; Herzberger, J.; Müller, A. H.E.; Frey, H. Die lebende anionische Polymerisation. *Chem. Unserer Zeit* **2017**, *51*, 254–263.

A4 Curriculum Vitae